



**Politecnico  
di Torino**

Polytechnic of Turin

Master's Degree in Mechanical Engineering  
2023/2024  
Session of October 2024

**Study of the dynamic response of composite laminates for the  
evaluation of the material elastic constants**

Relatore & Correlatori:  
Ciardiello Raffaele  
Boursier Niutta Carlo  
Paolino Davide Salvatore

Candidato:  
Robert Cosmin Jugaru  
S296186

## Abstract

The following study investigates the dynamic response and mechanical elastic properties of four different composite materials: flax fiber with epoxy resin, carbon fiber with epoxy resin, and two types of glass fiber composites — one with an inorganic resin and the other with a 30% organic resin component. The primary objective is to characterize the elastic moduli and damping coefficients of these composites at varying temperatures. Utilizing the Impulse Excitation Technique (IET), the natural frequencies of the composites were measured and analyzed according to the ASTM E1876-21 standard to evaluate the longitudinal modulus  $E_1$  and the shear modulus  $G_{12}$ .

To enhance the accuracy of these evaluations, the coefficients of thermal expansion (CTEs) in three directions were also evaluated by directly measuring strains of each composite during a typical thermal expansion. This allowed for the separation of the thermal effects on the composite expansions from the mechanical properties, ensuring precise determination of the moduli under thermal variations.

Additionally, the study examines the impact of 70 °C distilled water aging on the mechanical properties of the composites. Specimens were submerged in distilled water for 7 and 13 days in accordance with the ASTM D570 standard, followed by a reevaluation of their mechanical properties. The study revealed significant insights into the changes in elastic moduli and damping coefficients due to both temperature variations and aging in water.

The results of this research provide a comprehensive understanding of the dynamic behavior and durability of these composite materials, contributing to their potential applications in various engineering fields, particularly the automotive one.

## INDEX

<b>Abstract</b> .....	<b>2</b>
<b>1. Dynamics and modal analysis</b> .....	<b>10</b>
<b>2. Signal processing</b> .....	<b>14</b>
The logarithmic decrement method .....	16
-3 dB method .....	17
<b>3. Finite element method/analysis (FEM)</b> .....	<b>19</b>
Numerical Errors .....	27
Time integration methods.....	34
Advantages and disadvantages of both time integration methods.....	36
<b>4. Composites materials</b> .....	<b>36</b>
Advantages .....	37
Disadvantages.....	38
Fibres characteristics.....	38
Matrix characteristics .....	39
Advantages .....	39
Disadvantages.....	39
Hooke’s Law for 3D Orthotropic Lamina .....	40
Fundamental material properties.....	43
Laminate.....	49
From displacement field to Strain field.....	50
From strain filed to stress field .....	51
Thermal stresses and strains in a laminate .....	54
<b>Composites lamination: vacuum bag method</b> .....	<b>57</b>
Types of composites .....	60
<b>5. Evaluation of specimen mechanical properties</b> .....	<b>61</b>
Settings of the software .....	62
Results of the thin glass fibre with epoxy 30% natural resin .....	64
Results of the thick glass fibre with epoxy resin .....	67
Results of the carbon fibre with epoxy resin .....	69
Results of the flax fibre with epoxy resin.....	71
General trend of the elastic moduli in the experimental case.....	73
.....	74
<b>6. Evaluation of thermal expansion of composites</b> .....	<b>75</b>
From strains to CTE .....	78

<b>7. FEM models.....</b>	<b>80</b>
Modal analysis.....	80
Results of the modal analysis and comparison with the experimental results.....	84
Thermal model .....	87
Results of the thermal analysis and comparison with the experimental results .....	93
Coupled analysis – Modal and Thermal models with temperature dependency of the elastic moduli .....	94
Results of the elastic moduli temperature dependent analysis and comparison with the experimental results .....	97
Validation of the numerical model.....	99
Limits of the model.....	102
<b>8. Aging of composites .....</b>	<b>108</b>
Seven days aging – mass variation .....	109
Seven days aging – external aspect and geometry.....	110
Seven days aging – elastic moduli and damping coefficient .....	114
Thirteen days aging – mass variation.....	123
Thirteen days aging – external aspect and geometry .....	124
Thirteen days aging – elastic moduli and damping coefficient .....	129
<b>9. Conclusions .....</b>	<b>139</b>
<b>Appendix .....</b>	<b>141</b>
<b>Bibliography .....</b>	<b>142</b>

## Table of figures

Figure 1: Impulse response functions with damping ratio from 0 to 1.....	11
Figure 2: Form of the impulse force in time (above) and its Fourier Transform in frequency domain (below).....	11
Figure 3: Shifting of the realizations to avoid leakage error .....	15
Figure 4: Free response of a damped system.....	16
Figure 5: Receptance peak reduced of 3 dB .....	17
Figure 6: Infinitesimal continuum showing components of tension and virtual displacements .....	20
Figure 7: Truss element .....	23
Figure 8: From distorted general coordinate system to natural coordinate system .....	28
Figure 9: The concept of Jacobian used to pass from the derivative of shape functions in general coordinates to the derivative of shape functions in natural coordinates. ....	29
Figure 10: Integration points inside a quadratic element of four nodes .....	32
Figure 11: Approximation of the u through its derivative .....	34
Figure 12: Physical and Mechanical properties comparison between Composites and metals .....	38
Figure 13: Three material axes of a lamina .....	41
Figure 14: Lamina representation under tension along direction 1 .....	44
Figure 15: Lamina representation under tension along direction 2 .....	45
Figure 16: Lamina representation under tension along direction 1 with width variation for the evaluation of Poisson's ratio.....	45
Figure 17: Lamina representation under tension along direction 2 for the evaluation of minor Poisson's ratio.....	46
Figure 18: Lamina under shear tension for the evaluation of the shear modulus.....	46
Figure 19: Lamina under thermal load in direction 1 .....	47
Figure 21: Global and material coordinates of a composite. ....	49
Figure 22: Infinitesimal element under bending with direct effect on the displacement $u(x,y,z)$ . ....	50
Figure 23: Laminate's N-th Lamina and distances from the midplane. ....	52
Figure 24: Layup Layers.....	57
Figure 25: Layers covered by the sealed vacuum bag.....	58
Figure 26: Mixing the resin with the hardener.....	58
Figure 27: Curing oven (left) and final result of the lamination (right).....	59
Figure 28: Carbon and Flax fibers (left) epoxy infusion resin (right) .....	60
Figure 29: Impulse excitation machine RFDA-HT 1600 IMCE .....	61
Figure 30: Block diagram of the machine.....	61
Figure 31: Characteristics of the specimen and mode to be calculated .....	62
Figure 32: Sampling frequency and possible filters for the signal .....	62
Figure 33: Trigger time repeated impulses and max points to calculate the FFT.....	63
Figure 34: General window of results.....	63
Figure 35: Spectrum of Thin glass in flexural configuration.....	64
Figure 36: Spectrum of Thin glass in torsional configuration .....	65
Figure 37: Spectrum of thick glass in flexural configuration .....	67
Figure 38: Spectrum of thick glass in torsional configuration.....	68
Figure 39: Spectrum of Carbon in flexural configuration .....	69
Figure 40: Spectrum of carbon in torsional configuration.....	70
Figure 41: Spectrum of flax in flexural configuration.....	71
Figure 42: Spectrum of flax in torsional configuration .....	72

Figure 43: Strain gages installed on the specimens .....	75
Figure 44: Strain gage installed along the thickness.....	75
Figure 45: Wheatstone bridge circuit.....	76
Figure 46: Wheatstone bridge.....	77
Figure 47: Connector (left) and acquisition system Quantum X (right).....	77
Figure 48: General window of the Catman software.....	77
Figure 49: Meshed geometry in LS-Dyna using shell elements.....	80
Figure 50: Card of the part composite .....	81
Figure 51: Material card for an elastic orthotropic material.....	81
Figure 52: Control card for implicit dynamics analysis using Newmark time integration.....	82
Figure 53: card for setting the number of modes to be calculated.....	82
Figure 54: card used for the choice of the initial time step.....	83
Figure 55: control card used to set the non-linear solution and solver .....	83
Figure 56: control card used to set the type of solver .....	84
Figure 57: First 8 modes for carbon composite .....	85
Figure 58: Meshed geometry in LS-Dyna using solid elements.....	87
Figure 59: card for defining the temperature curve (left) and card for initial temperature set (right) .....	88
Figure 60: Temperature profile (in this case 40 Celsius).....	88
Figure 61: Material card for orthotropic material used for thermal expansion.....	89
Figure 62: Material card for thermal properties.....	89
Figure 63: Control card for setting the coupled structural thermal analysis.....	90
Figure 64: control card used to set the non-linear solution and solver .....	90
Figure 65: control card used to set the time-step .....	91
Figure 66: control card to set the thermal time-step .....	91
Figure 67: control card for setting the non-linear thermal solver .....	92
Figure 68: control card for controlling the divergence of the non-linear problem .....	92
Figure 69: thermal expansion in the three directions.....	93
Figure 70: card needed to define the eigenvalues curve.....	95
Figure 71: Curve of eigenvalues to be computed .....	95
Figure 72: Material card for orthotropic temperature dependent materials.....	96
Figure 73: control card needed to set the curve of eigenvalues that will be eventually calculated .....	96
Figure 74: control accuracy to improve the convergence.....	97
Figure 75: First mode at 25C (left) and at 80C (right) with frequency reduction .....	97
Figure 76: Second mode at 25C (left) and at 80C (right) with frequency reduction.....	98
Figure 77: Composites prepared for aging.....	108
Figure 78: : thin glass thickness and aspect variation, conditioned (left), wet (right), reconditioned (below) .....	110
Figure 79: thick glass thickness and aspect variation, conditioned (left), wet (right), reconditioned (below) .....	111
Figure 80: : carbon fibre thickness and aspect variation, conditioned (left), wet (right), reconditioned (below) .....	112
Figure 81: : flax thickness and aspect variation, conditioned (left), wet (right), reconditioned (below) .....	113
Figure 82: flax aspect variation, conditioned (left), wet (right), reconditioned (below) .....	114
Figure 83: thin glass thickness and aspect variation, conditioned (left), wet (right), reconditioned (below) .....	125
Figure 84: thick glass thickness and aspect variation, conditioned (left), wet (right), reconditioned (below) .....	126

Figure 85: carbon thickness and aspect variation, conditioned (left), wet (right), reconditioned (below) ..... 127

Figure 86: flax thickness and aspect variation, conditioned (left), wet (right), reconditioned (below) ..... 128

Figure 87: flax aspect variation, conditioned (left), wet (right), reconditioned (below) ..... 128

## Table of tables

Table 1: Sampling points and weight for Gauss quadrature [-1, 1] .....	32
Table 2: general mechanical properties of fibers .....	39
Table 3: Thin glass fiber composite first and second natural frequencies at different temperature .....	64
Table 4: Thin glass fiber composite elastic moduli at different temperatures .....	66
Table 5: percentage variation of elastic moduli and damping coefficient with respect to the room temperature values .....	66
Table 6: Thick glass fibers composite first and second natural frequencies and damping at different temperature .....	67
Table 7: Thick glass fiber composite elastic moduli at different temperature .....	68
Table 8: percentage variation of elastic moduli and damping coefficient with respect to the room temperature values .....	68
Table 9: Carbon fiber composite first and second natural frequencies and damping coefficient at different temperatures .....	69
Table 10: Carbon fiber composite elastic moduli at different temperatures .....	70
Table 11: : percentage variation of elastic moduli and damping coefficient with respect to the room temperature values .....	70
Table 12: Flax fibers composite first and second natural frequencies and damping at different temperature .....	71
Table 13: Flax fiber composite elastic moduli at different temperatures .....	72
Table 14: : percentage variation of elastic moduli and damping coefficient with respect to the room temperature values .....	72
Table 15: CTE coefficients of four types of composites .....	79
Table 16: comparison of CTE of alumina from experiments and from literature .....	79
Table 17: comparison of CTE of composites from experiments and from literature .....	79
Table 18: Comparison between experimental and numerical natural frequencies at different temperature for thin glass .....	86
Table 19: Comparison between experimental and numerical natural frequencies at different temperature for thick glass .....	86
Table 20: Comparison between experimental and numerical natural frequencies at different temperature for carbon .....	87
Table 21: Comparison between experimental and numerical natural frequencies at different temperature for flax .....	87
Table 22: Comparison between experimental and numerical results of thermal expansion for thin glass .....	94
Table 23: Comparison between experimental and numerical results of thermal expansion for thick glass .....	94
Table 24: Comparison between experimental and numerical results of thermal expansion carbon .....	94
Table 25: Comparison between experimental and numerical results of thermal expansion flax .....	94
Table 26: Comparison between experimental and numerical results of modal analysis with thermal dependency .....	98
Table 27: Validation and comparison of intermediate temperatures .....	99
Table 28: Comparison of experimental natural freq. and from the linear interpolation .....	101
Table 30: Increase in weight and soluble matter .....	109
Table 31: Geometry variation for thin glass .....	111



Table 32: Geometry variation of thick glass.....	112
Table 33: Geometry variation of carbon.....	113
Table 34: Geometry variation of flax.....	114
Table 37: Geometry variation thin glass.....	125
Table 38: Geometry variation thick glass.....	126
Table 39: Geometry variation of carbon.....	127
Table 40: Geometry variation of flax.....	129

## 1. Dynamics and modal analysis

In this study, the dynamic behavior of the composite materials was analyzed using the Impulse Excitation Technique (IET). This method involves subjecting the specimen to an impulse-like force to investigate its natural frequencies and mode shapes. The general formulation of the equation of motion for a linear time-invariant system is provided in Equation (1.0) [1].

$$m\ddot{x} + c\dot{x} + kx = f(t) \quad (1.0)$$

Here,  $m$  represents the mass of the system,  $c$  is the damping coefficient,  $k$  is the system's stiffness, and  $f(t)$  is the time-dependent force. In the initial phase of this study, only the mass of the composite is known, with the other parameters being determined through the Fast Fourier Transform (FFT) of the testing machine's data. Before proceeding, it is important to clarify the concept of an impulse. An impulse is an idealized mathematical concept that is challenging to achieve in practical experiments. However, with appropriate approximations, it can be effectively utilized. Mathematically, an impulse is a function that approaches infinity at a specific time  $t_0$  and is zero at all other points. This model is based on the unit-impulse function,  $\delta(t)$  defined by:

$$\begin{cases} \delta = 0 & (\text{for } t \neq t_0) \\ \delta = \infty & (\text{for } t = t_0) \end{cases} \quad \int_{-\infty}^{+\infty} \delta(t) dt = 1 \quad (1.1)$$

The impulse excitation can thus be expressed by:  $F = f_0 \delta(t)$  where  $\delta$  is expressed in  $[s^{-1}]$  And  $f_0$  has the dimensions of an impulse  $[Ns]$ .

Usually for a single degree of freedom the response of the system depends on the initial conditions of the system such as: initial displacement and initial velocity (see eq 1.2).

$$x(t) = \frac{f_0}{m \omega_n} h(t) \quad (1.2)$$

Where  $\omega_n$  is the natural frequency of the system and  $h(t)$  is the so-called impulse response function and is define as follows:

$$h(t) = \frac{1}{1 - \zeta^2} e^{-\zeta \omega_n t} * \sin(\omega_n \sqrt{1 - \zeta^2} t) \quad (1.3)$$

Here  $\zeta$  is the damping ratio and  $h(t)$  is defined for  $\zeta < 1$ . The response can be seen in the graph of figure (1.0).

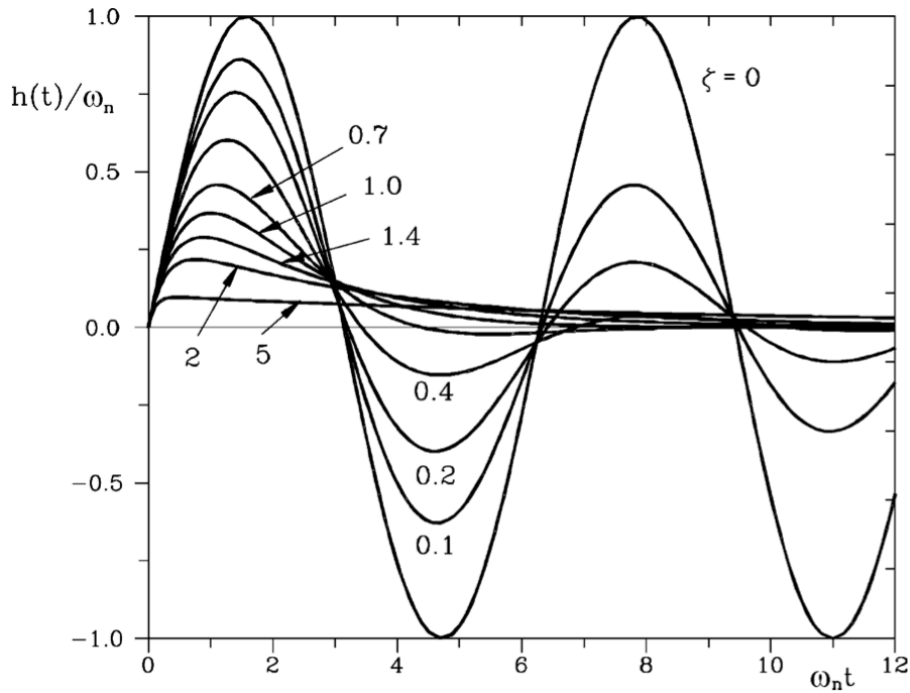


Figure 1: Impulse response functions with damping ratio from 0 to 1.

The idea behind an impulse excitation is to find a way to excite all the frequencies of the system with the same intensity or at least to be able to see the first main important mode shapes. In fact, the spectrum of an ideal impulse is a constant horizontal line (with value  $f_0$ ) that excites all the frequencies in the same way (figure n). In the real case the situation is far from the ideal one and can be represented by figure 2 [2] [3].

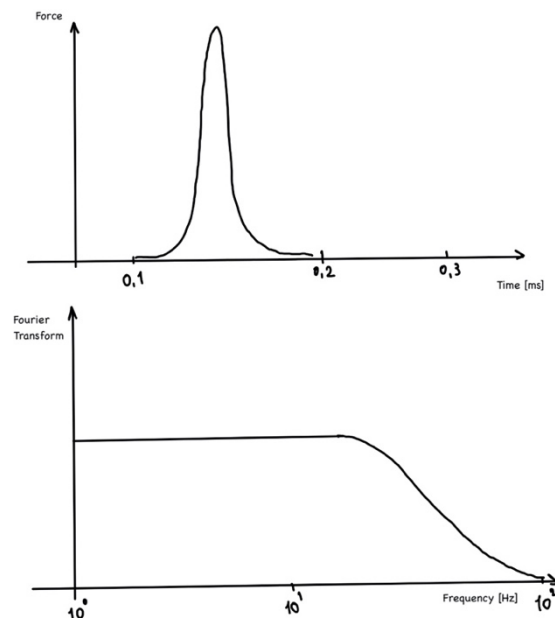


Figure 2: Form of the impulse force in time (above) and its Fourier Transform in frequency domain (below).

The impulse does not go to infinite and moreover does not excite all the frequencies with the same intensity, but it decreases after a certain frequency.

So, the higher the frequency that we want to excite, the faster it goes to zero, thus its effect on the specimen is limited to the first instants of the impulse. In the first instants all the modes are excited, so we see high oscillations of  $x(t) = 0$ , after a while, due to damping, their oscillations decrease following an exponential law. The higher the frequency of the mode that we want to analyze the faster it will decay.

The bases of the modal analysis and the analytical approach of Euler-Bernoulli beam and Timoshenko beam.

Any multi degree of freedom system can be studied as a single degree of freedom if it respects the modal analysis hypothesis: the system has to be linear, time invariant and no force must be applied on its boundary, also damping is neglected. The central idea is to split the different degrees of freedom of the system and consider them independent from each other, in order to study them separately as single degree of freedom systems and at the end use the superpositions effect (thanks to linearity) and sum each contribution to get the total effect.

We start from the homogeneous equation of motion, because as it has been stated before, there must be no force applied on the system  $f(t) = 0$ .

$$[m]\ddot{x} + [c]\dot{x} + [k]x = 0 \quad (1.4)$$

$[m]$ ,  $[c]$ ,  $[k]$  are matrices:  $[m]$  is diagonal and positive defined,  $[c]$  should be symmetric and  $[k]$  is again symmetric and positive defined.

The variable  $x$  can be seen as a harmonic motion so easily substituted with a combination of different harmonics (synchronous motion):

$$x = x_0 e^{i\omega t} \quad (1.5)$$

$$\dot{x} = i\omega x_0 e^{i\omega t} \quad (1.6)$$

$$\ddot{x} = -\omega^2 x_0 e^{i\omega t} \quad (1.7)$$

After the substitution, the exponential part can be simplified being valid for any instant of time. Leading to:

$$-\omega^2 x_0 [m] + i\omega x_0 [c] + x_0 [k] = 0 \quad (1.8)$$

Consider the hypothesis of no damping, so  $[c]=0$ . The result of the eigenvalue problem gives the natural frequencies of the system, that are in number equal to the  $n$  number of degrees of freedom, and the mode shapes.

So, to study the natural frequencies of the system one can start from:

$$\det([k] - \omega^2 [m]) = 0 \quad (1.9)$$

Imposing the determinant equal to zero, gives us the  $n$  eigenvalues ( $\omega^2$ ) while the natural frequencies are  $\sqrt{\omega^2}$ . The so-called mode shapes are the different shapes that the structure can undergo while excited at the specific eigenvalue used to obtain the eigenvector.

$$([k] - \omega^2 [m])\{x_0\} = 0 \quad (1.10)$$

Here  $\{x_0\}$  is the eigenvector and the matrix made of all the eigenvectors is the modal matrix  $[\phi]$ . Due to the fact that the determinant of the matrix  $([k] - \omega^2[m])$  is lower than  $n$ , the eigenvectors are linearly dependent on each other. So, in order to obtain the eigenvectors, we need to impose the value of one of them and the others will be scaled accordingly.

Up to this point, the system degrees of freedom have not yet been decoupled. To achieve decoupling, we will employ a mathematical technique known as modal transformation, utilizing the concepts of mass-orthogonality (m-orthogonality) and stiffness-orthogonality (k-orthogonality). The new variable introduced by the modal transformation is referred to as the modal coordinate  $\eta$ , which is related to the original coordinate  $x$  as follows:

$$\{x\} = [\phi]\{\eta\} \quad (1.11)$$

The modal matrix  $[\phi]$  is invariant in time so during the derivation it is behaving like a constant. So, by substituting in the equation of motion the following result is obtained:

$$[m][\phi]\{\ddot{\eta}\} + [c][\phi]\{\dot{\eta}\} + [k][\phi]\{\eta\} = \{f\} \quad (1.12)$$

By pre-multiplying by  $[\phi]^T$ :

$$[\phi]^T[m][\phi]\{\ddot{\eta}\} + [\phi]^T[c][\phi]\{\dot{\eta}\} + [\phi]^T[k][\phi]\{\eta\} = [\phi]^T\{f\} \quad (1.13)$$

If we consider the m and k orthogonality, and we normalize the eigenvectors by dividing each eigenvector by the square root of the modal mass we get the following equations:

$$\{\varphi_r\}^T [m] \{\varphi_r\} = M_r \quad (\text{modal mass}) \quad (1.14)$$

$$\{\varphi_r\}^T [k] \{\varphi_r\} = K_r \quad (\text{modal stiffness}) \quad (1.15)$$

$$\{\phi_r\} = \frac{\{\varphi_r\}}{\sqrt{M_r}} \quad (1.16)$$

$$\{\phi_r\}^T [m] \{\phi_r\} = [I] \quad (\text{identity matrix}) \quad (1.17)$$

$$\{\phi_r\}^T [k] \{\phi_r\} = \text{diag}(\omega_r^2) \quad (1.18)$$

Leading to the final formulation in modal coordinates:

$$[I]\{\ddot{\eta}\} + [\text{diag}(2\zeta_r\omega_r)]\{\dot{\eta}\} + [\text{diag}(\omega_r^2)]\{\eta\} = \{\Gamma\} \quad (1.19)$$

So, from each equation of the system we can get a SDOF system that has its single contribution to the total effect (superposition of effects).

It can be shown that by performing an inverse transformation the equations can pass from modal coordinate, back to real coordinate in order to see the real effects. Leading to:

$$\{x\} = [\phi] \{\eta\} \quad (1.20)$$

$$\{x\} = \sum_r^n \{\phi_r\} \{\eta_r\} = \sum_r^n \{\phi_r\} e^{-\zeta_r \omega_r t} (A_r \cos(\omega_{d,r} t) + B_r \sin(\omega_{d,r} t)) \quad (1.21)$$

Where  $A_r$  and  $B_r$  are functions that depend on the initial conditions:

$$A_r = \frac{\{\phi_r\}[M]\{x_0\}}{m_r} \quad (1.22)$$

$$B_r = \frac{\{\phi_r\}[M][\{\dot{x}_0\} + \zeta_r \omega_r \{x_0\}]}{m_r \omega_{d,r}} \quad (1.23)$$

## 2. Signal processing

Once the equation of motion  $x(t)$  is defined, performing a Fast Fourier Transform (FFT) allows us to transition from the time domain to the frequency domain. This transformation enables the identification of the system's natural frequencies, which correspond to the peaks observed in the FFT [4].

To transition from an analog signal to a digital one, the machine discretizes the sampling points. This requires defining the sampling period  $dt$  or the sampling frequency  $f_s$ . Accurately determining the appropriate sampling frequency can be challenging without prior knowledge of the system's characteristic frequencies. A practical approach is to initially sample at very high frequencies (if the equipment permits), and once the frequency range of interest is identified, gradually reduce the sampling frequency.

However, there are important limitations to consider, one of which is Shannon's Theorem. According to this theorem, to avoid "aliasing" errors in the data, the following condition must be met:

$$f_s \geq 2f_{max} \quad (2.0)$$

So, the sampling frequency must be at least twice the maximum frequency willing to study.

Another important aspect of the signal processing is to understand the process of passing from a Fourier Transform to a Discrete Fourier Transform (DFT) and in the end to a Fast Fourier Transform.

The Fourier Transform definition is as follows:

$$F(t) = \int_{-\infty}^{+\infty} f(t)e^{-i\Omega t} dt \quad (2.1)$$

Then being the system discretized we pass to a digital from so we perform the DFT:

$$F_k = \frac{1}{N} \sum_{n=0}^{N-1} f_n e^{-i2\pi \frac{kn}{N}} \quad (2.2)$$

The last step is the Fast Fourier Transform (FFT): which gets born thanks to Cooley and Tuckey that invented a new algorithm from which the signals could be processed in real time, with a computational time proportional to  $\frac{N}{2} \log_2 N$ . From here comes the necessity for N to be a power of two. So, in order to obtain this, software add a number of zeros to the sampling points vector (called “zero padding” operation) to make it a power of two. Speeding up the results up to real time.

By using the DFT though, another type of error (called “leakage”) comes out due to the hypothesis of having a periodic signal, which in most cases it is not true. This error can be avoided by performing a “windowing” before the DFT. By multiplying the series by a so-called window, it is imposed a periodicity to the temporal signal (also called realizations). It is obvious that this procedure is introducing amplitude errors in the first and last part of the signal due to the window itself. To avoid this last error, it is performed an overlap. This overlap consists in translating the realization  $x(t)_{k+1}$  back on the realization  $x(t)_k$  so having the last point of  $x(t)_k$  not coincident with the first point of the  $x(t)_{k+1}$ . (figure n, a and b)

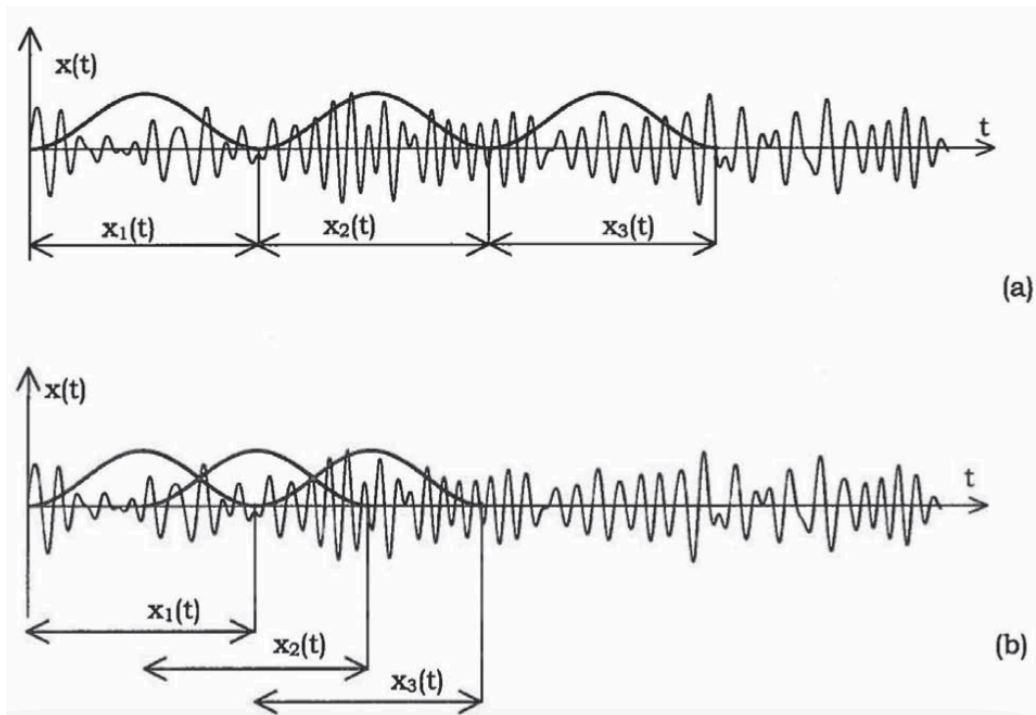


Figure 3: Shifting of the realizations to avoid leakage error

## The logarithmic decrement method

The logarithmic decrement method is a technique used to determine the damping ratio  $\zeta$  of an underdamped system, typically a mechanical or electrical oscillatory system. This method is particularly useful when the system is exhibiting free oscillations.

When a system oscillates with damping, the amplitude of the oscillations decreases over time. The logarithmic decrement  $\delta$  quantifies how much the amplitude decreases between successive peaks in the oscillation.

The free response of a damped system has the form:

$$x(t) = e^{-\xi\omega_n t}(a \cos(\omega_d t) + b \sin(\omega_d t)) \quad (2.3)$$

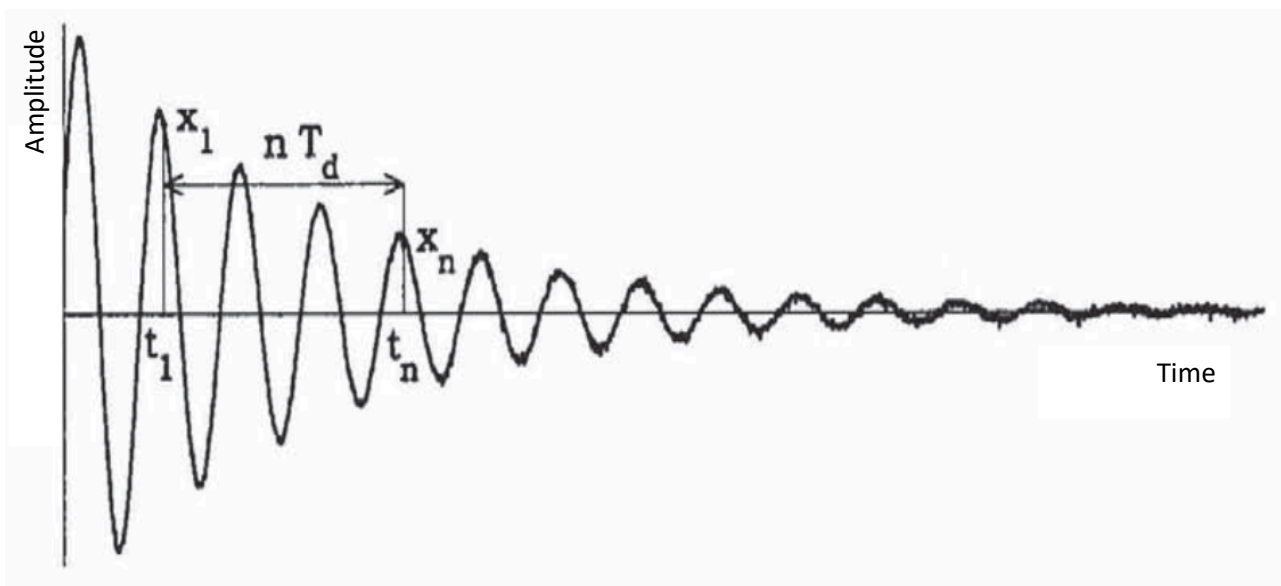


Figure 4: Free response of a damped system

If from the peak  $x_1$  at time  $t_1$  one moves an  $n$  integer periods, an amplitude  $x_n$  is reached at a time  $t_n$ . The natural logarithm of the amplitudes represents the logarithmic decrement  $\delta$ , if it is considered also the periodicity of the harmonic function, it can be stated:

$$\delta = \ln \frac{x_1}{x_n} = \xi \omega_n n T_d = \xi \omega_n n \frac{2\pi}{\omega_d} = \xi \omega_n n \frac{2\pi}{\omega_n \sqrt{1 - \xi^2}} \quad (2.4)$$

The known values that are coming from the measurement are  $x_1$  and  $x_n$  so it can be concluded that the damping factor is:

$$\xi = \frac{\delta}{\sqrt{4n^2\pi^2 + \delta^2}} \quad (2.5)$$



### -3 dB method

The N dB method is a useful approach for determining the damping ratio of a system by analyzing its frequency response. The method involves identifying the frequency points where the system's response drops by a certain amount in decibels (dB) from its peak value. The starting point of this method is the formula of the modulus of the receptance of a system with viscous damping.

$$|\alpha(\Omega)| = \frac{1/k}{\sqrt{\left(1 - \frac{\Omega^2}{\omega_n^2}\right)^2 + \left(\frac{2\xi\Omega}{\omega_n}\right)^2}} \quad (2.6)$$

By using the curve of the receptance  $|\alpha(\Omega)|$  the maximum value can be read at  $\omega_r = \omega_n\sqrt{1 - 2\xi^2}$ , once at this point one has to consider a decrease of 3 decibel and trace a horizontal line on the curve of  $|\alpha(\Omega)|$  that will intersect it in two points that have an amplitude decrease of  $10^{\frac{3}{20}} \cong \sqrt{2}$  with respect to the maximum.

Since the power dissipated in a viscous damped system is proportional to the amplitude of the oscillation squared, this means that the two points identified are points of half power with respect to the maximum power.

Generally speaking, it is possible to decrease of any N dB and obtain points of reduced amplitude with respect to the maximum of a factor  $\sqrt{n}$  with  $20\log\sqrt{n} = N$ .

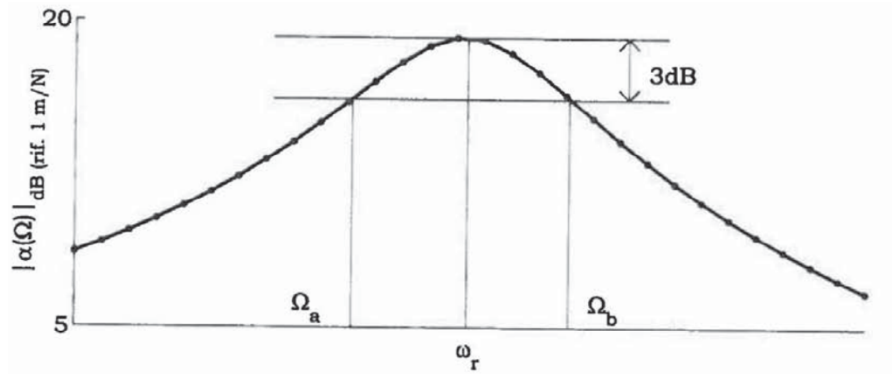


Figure 5: Receptance peak reduced of 3 dB

The value of the receptance at the peak is obtained as follows:

$$|\alpha| = \left| \frac{x_0}{F_0} \right| = \frac{1/k}{\sqrt{(2\xi)^2}} = \frac{1/k}{\beta} = \frac{1}{m \omega_n^2 \beta} \quad (2.7)$$

Where  $\beta$  is the loss factor, in the end it can be obtained that at resonance

$$|x_0| = \frac{F_0/m}{\omega_n^2 \beta} \quad (2.8)$$

The difference between the peak amplitude and the two points should be:

$$20\log|x_0|_{res} - 20\log|x_0|_{A,B} = N \quad (2.9)$$

Leading to

$$\frac{20}{20} \log \frac{|x_0|_{res}}{|x_0|_{A,B}} = \frac{N}{20} \quad (2.10)$$

$$\frac{|x_0|_{res}}{|x_0|_{A,B}} = 10^{\frac{N}{20}} = n \quad (2.11)$$

$$\frac{1/k}{\sqrt{(1-r^2)^2 + (2\xi r)^2}} = \frac{1/k}{2\xi\sqrt{1-\xi^2}\sqrt{n}} \quad (2.12)$$

Where r is the ratio of  $\Omega/\omega_n$

$$r^4 - 2r^2(1 - 2\xi^2) + 1 - 4n\xi^4(1 - \xi^2) \quad (2.13)$$

Equation that has zeros:

$$r_{a,b}^2 = 1 - 2\xi^2 \pm 2\xi\sqrt{(1-\xi^2)(n-1)} \quad (2.14)$$

Subtracting the two roots and remembering that  $\omega_r = \omega_n\sqrt{1-2\xi^2}$ , moreover  $r_b^2 > r_a^2$ , it can be obtained:

$$\frac{\xi\sqrt{1-\xi^2}}{1-2\xi^2} = \frac{1}{\sqrt{n-1}} \cdot \frac{\Omega_b + \Omega_a}{2\omega_r} \cdot \frac{\Omega_b - \Omega_a}{2\omega_r} \quad (2.15)$$

$$\xi = \frac{1}{\sqrt{n-1}} \cdot \frac{\Omega_b - \Omega_a}{2\omega_r} \quad (2.16)$$

If  $n = \sqrt{3}$  we get

$$\xi = \frac{\Omega_b - \Omega_a}{2\omega_r} \quad (2.17)$$

### 3. Finite element method/analysis (FEM)

The Finite Element Method (FEM) is a numerical technique employed to solve differential equations that model physical phenomena such as heat transfer, structural mechanics, fluid dynamics, and electromagnetism. FEM simplifies complex systems by dividing them into smaller, more manageable elements or subdomains, facilitating the approximation of solutions to these differential equations [5].

In the following sections, a general approach to applying FEM for structural mechanics will be outlined, focusing primarily on static and dynamic problems.

We will examine the key differential equations used in the mechanical context to address these systems and derive the fundamental matrices: the stiffness matrix and the mass matrix. Additionally, for dynamic problems, we will also consider the damping matrix, circulatory matrix, and gyroscopic matrix.

The three principal partial differential equations governing equilibrium are:

$$\sum_{i=1}^3 \frac{\partial \sigma_{ij}}{\partial x_i} + \phi_j = \rho_j \quad (j = 1,2,3) \quad (3.0)$$

Where the variation of the stress in the different directions are the forces acting on the boundary and the second term  $\phi_j$  are the volume forces. According to the position (it will be explained in detail later on) this equilibrium equation can be equal to zero or equal to a quality called residual (which is an error).

Next set of equations are made by six partial differential equations of compatibility which define the deformations:

$$\varepsilon_{ii} = \frac{\partial u_i}{\partial x_i} \quad (3.1)$$

$$\gamma_{ij} = \frac{\partial u_i}{\partial x_j} + \frac{\partial u_j}{\partial x_i} \quad (i, j = 1,2,3) \quad (3.2)$$

In the end there are other six algebraic equations called constitutive laws of the material (written in matrix form):

$$\{\sigma\} = [E] \{\varepsilon\} \quad (3.3)$$

Given these three sets of equations, the Finite Element Method (FEM) transitions from differential equations to a numerical solution in integral form over a finite domain. The core concept of FEM is to discretize a continuum system by introducing approximation functions. This involves converting the differential equations into a numerical functional over the

discretized domain. By substituting the approximation functions into the integral functional, the problem is reduced to a matrix problem, which can be efficiently solved using a computer.

A critical aspect of FEM is the choice of functional. In structural mechanics, different approaches can lead to the same results, with some methods being more efficient depending on the problem type. In statics, the primary functional used is the principle of virtual work, whereas in dynamics, the Lagrange equations are predominantly employed. Both methods yield the same results and are considered energetic methods, as the energetic functional is essentially a scalar quantity, simplifying its handling. Additionally, variational methods such as the Galerkin and Rayleigh-Ritz methods are used to evaluate functionals. The following sections will provide detailed descriptions of the first two methods.

The principle of virtual work states that, for a continuum with infinitesimal volume elements  $dx$ ,  $dy$ , and  $dz$ , and a field of forces and stresses in equilibrium, the virtual internal work (resulting from the stresses and strains) is equal to the virtual external work (resulting from the forces and displacements) when a virtual displacement and strain field are applied. (See Figure 6).

$$L_i = L_e \quad (3.4)$$

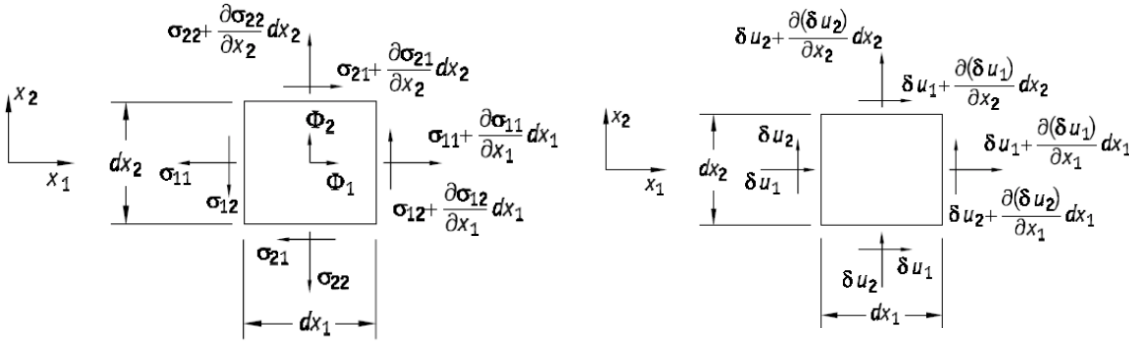


Figure 6: Infinitesimal continuum showing components of tension and virtual displacements

The virtual work in all the points of the structure of the continuum mechanics is a scalar given by the multiplication of the components of the tension and the virtual components of the displacement.

$$\sum_{k=1}^3 \left[ -\sigma_{ik} \delta u_k dA_i + \left( \sigma_{ik} + \frac{\partial \sigma_{ik}}{\partial x_i} dx_i \right) \left( \delta u_k + \frac{\partial}{\partial x_i} (\delta u_k) dx_i \right) dA_i \right] \quad (3.5)$$

Leading to the sum of the three directions:

$$\sum_{i=1}^3 \sum_{k=1}^3 \left( \frac{\partial \sigma_{ik}}{\partial x_i} \delta u_k + \sigma_{ik} \frac{\partial}{\partial x_i} (\delta u_k) \right) dV \quad (3.6)$$

From here it can be seen that the six compatibility equations are coming from the second term:

$$\begin{aligned}
\sum_{i=1}^3 \sum_{k=1}^3 \sigma_{ik} \delta \frac{\partial u_k}{\partial x_i} &= \\
&= \sigma_{11} \delta \varepsilon_{11} \sigma_{22} \delta \varepsilon_{22} + \sigma_{33} \delta \varepsilon_{33} + (\sigma_{12} \delta \frac{\partial u_2}{\partial x_1} + \sigma_{21} \delta \frac{\partial u_1}{\partial x_2} + \sigma_{13} \delta \frac{\partial u_3}{\partial x_1} \\
&+ \sigma_{31} \delta \frac{\partial u_1}{\partial x_3} + \sigma_{23} \delta \frac{\partial u_3}{\partial x_2} + \sigma_{32} \delta \frac{\partial u_2}{\partial x_3}
\end{aligned} \tag{3.7}$$

It is obtained a form of a scalar product:

$$\sum_{i=1}^3 \sum_{k=1}^3 \sigma_{ik} \delta \frac{\partial u_k}{\partial x_i} = \{\sigma\}^T \{\delta \varepsilon\} = \{\delta \varepsilon^T\} \{\sigma\} \tag{3.8}$$

While from the first term it can be obtained the differential equations of equilibrium:

$$\sum_{i=1}^3 \sum_{k=1}^3 \frac{\partial \sigma_{ik}}{\partial x_i} \delta u_k = \sum_{k=1}^3 \left( \frac{\partial \sigma_{1k}}{\partial x_1} + \frac{\partial \sigma_{2k}}{\partial x_2} + \frac{\partial \sigma_{3k}}{\partial x_3} \right) \delta u_k \tag{3.9}$$

$$\sum_{i=1}^3 \sum_{k=1}^3 \frac{\partial \sigma_{ik}}{\partial x_i} \delta u_k = - \sum_{k=1}^3 \phi_k \delta u_k = -\{\phi\}^T \{\delta u\} = -\{\delta u\}^T \{\phi\} \tag{3.10}$$

Leading to the final formulation:

$$\sum_{i=1}^3 \sum_{k=1}^3 \left( \frac{\partial \sigma_{ik}}{\partial x_i} \delta u_k + \sigma_{ik} \frac{\partial}{\partial x_i} (\delta u_k) \right) dV = (\{\delta \varepsilon^T\} \{\sigma\} - \{\delta u\}^T \{\phi\}) dV \tag{3.11}$$

Now it can be considered also the contribution of the virtual external work of the force acting on the boundary:

$$\sum_{k=1}^3 \int t_k \delta u_k dA = \int (t_1 \delta u_1 + t_2 \delta u_2 + t_3 \delta u_3) dA = \int \{\delta u\}^T \{t\} dA \tag{3.12}$$

By rewriting the virtual work equation from (3.4) one gets:

$$\int \{\delta \varepsilon^T\} \{\sigma\} dV = \int \{\delta u\}^T \{\phi\} dV + \int \{\delta u\}^T \{t\} dA \tag{3.13}$$

So, from the principle of virtual works it can be obtained one single integral equation that contains both the compatibility equations and the equilibrium equations.

$$\int \{\delta u\}^T \{t\} dA = \int \{\delta \varepsilon\}^T \{\sigma\} dV - \int \{\delta u\}^T \{\phi\} dV \quad (3.14)$$

At this stage, the only remaining step is to substitute the shape functions, or approximation functions, into the integral formulation to obtain the matrix formulation or matrix problem.

The selection of shape functions is influenced by the physical properties of the system. Shape functions are typically polynomials characterized by various coefficients, and, like all polynomials, they have an order. The coefficients of these polynomials are determined by the geometric characteristics of the element, while the polynomial order is based on the number of nodes used to describe the element. The most commonly used formulation is expressed by the following equation:

$$\{u\} = [n]\{s\} \quad (3.15)$$

Where  $\{u\}$  are the generic displacements in the element,  $[n]$  is the shape function and  $\{s\}$  are the displacements of the nodes.

To pass from here to strains and stress it is enough to derive the displacements  $\{u\}$ :

$$\{\varepsilon\} = [\partial]\{u\} = [\partial][n]\{s\} = [b]\{s\} \quad (3.16)$$

$$\{\sigma\} = [E](\{\varepsilon\} - \{\varepsilon_0\}) + \{\sigma_0\} \quad (3.17)$$

Since at the beginning the principle of virtual works assigned a displacement field, this implies that equilibrium will not be satisfied at each point: leading us back to the idea of residual.

$$\sum_{i=1}^3 \frac{\partial \sigma_{ij}}{\partial x_i} + \phi_j = \rho_j \quad (3.18)$$

$\rho_j$  is present in each point of the element, but not in the nodes where it is zero (so the equilibrium will be respected there because the solution is exact). The idea of residual is that of an error introduced in the model being every FEM model stiffer than the reality. So, it is a like saying how much stiffer is the system with respect to the reality. Another point of view of the residual is to imagine a continuum object forced to fit in a frame, from where it can be concluded that basically all FEM models are wrong, being just approximations. Although thanks to numerical integrations techniques results are quite impressive.

Let's see how the choice of the elements might change the interpolation shape function. By increasing the number of divisions so increasing the number of nodes of discretization we are basically decreasing the residual error of the model. Another way of decreasing the residual

error is to change the type of element and use one which has more nodes per element, increasing in this way the grade of the polynomial. When the number of nodes or elements (which correspond also to the n degrees of freedom of the model) tends to infinite, the model converges to the exact solution. Or stated in another way: if  $\rho_j$  tends to zero in all points, the model has converged to the exact solution.

If an element was a certain number of nodes, it means the shape function will have an equal number of coefficients. While for the degree of the polynomial, it is connected with the number of nodes per element.

At this point, the previous formulations of  $\{u\}$  and  $\{\varepsilon\}$  might be replaced in the integral formulation to pass to the matrix formulation:

$$\{\varepsilon\} = [\partial]\{u\} = [\partial][n]\{s\} = [b]\{s\} \quad (3.19)$$

$$\int \{\delta u\}^T \{t\} dA = \int \{\delta \varepsilon\}^T \{\sigma\} dV - \int \{\delta u\}^T \{\phi\} dV \quad (3.20)$$

$$\begin{aligned} & \{\delta s\}^T \int [n]^T \{t^*\} dA - \{\delta s\}^T \int [n]^T \{\rho\} dV + \{\delta s\}^T \int [n]^T \{t_0\} dA \\ & + \{\delta s\}^T \int [n]^T \{\phi\} dV = \{\delta s\}^T \int [b]^T [E] [b] dV \{s\} \end{aligned} \quad (3.21)$$

$\{\delta s\}$  is virtual for any value, that allows us to simplify it and write all in a stiffness matrix formulation:

$$\{f\} + \{f_e\}_{t_0} + \{f_e\}_\phi = [k]\{s\} \quad (3.22)$$

Where  $\{f\}$  are the nodal loads  $\{f_e\}_{t_0}$  are the surface loads,  $\{f_e\}_\phi$  are the body forces and  $[k]$  is the stiffness matrix.

Let us see some examples of shape function and element: truss element which has two nodes, and it was one degree of freedom per node (figure n).

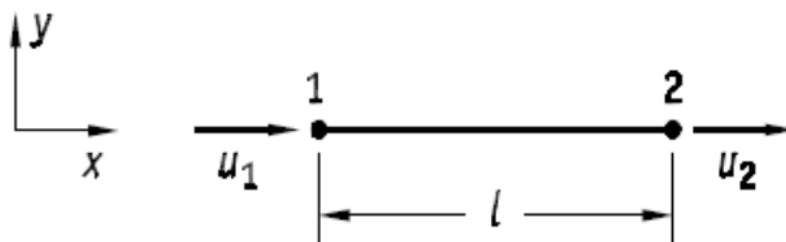


Figure 7: Truss element

A general procedure for finding the shape functions can be seen for this type of element:

$$\{u\} = [P]\{a\} \quad (3.23)$$

$$\{s\} = [A]\{a\} \quad (3.24)$$

$$\{a\} = [A]^{-1}\{s\} \quad (3.25)$$

$$\{u\} = [P][A]^{-1}\{s\} = [n]\{s\} \quad (3.26)$$

Which for the truss element becomes:

$$u_1 = \begin{bmatrix} 1 & x_1 \end{bmatrix} \begin{Bmatrix} a_1 \\ a_2 \end{Bmatrix} \quad (3.27)$$

$$u_2 = \begin{bmatrix} 1 & x_2 \end{bmatrix} \begin{Bmatrix} a_1 \\ a_2 \end{Bmatrix} \quad (3.28)$$

By imposing the boundary conditions of the coordinates:  $x_1 = 0$  and  $x_2 = l$

$$u = a_1 + a_2x \quad (3.29)$$

$$\begin{Bmatrix} u_1 \\ u_2 \end{Bmatrix} = \begin{bmatrix} 1 & 0 \\ 1 & l \end{bmatrix} \begin{Bmatrix} a_1 \\ a_2 \end{Bmatrix} \quad (3.30)$$

At this point the relation  $\{a\} = [A]^{-1}\{s\}$  :

$$\begin{Bmatrix} a_1 \\ a_2 \end{Bmatrix} = \begin{bmatrix} 1 & 0 \\ 1 & l \end{bmatrix}^{-1} \begin{Bmatrix} u_1 \\ u_2 \end{Bmatrix} \quad (3.31)$$

The last passage becomes:

$$\{u\} = [P][A]^{-1}\{s\} = [n]\{s\} \quad (3.32)$$

$$\{u\} = \begin{bmatrix} 1 & x \end{bmatrix} \frac{1}{l} \begin{bmatrix} l & 0 \\ -1 & 1 \end{bmatrix} \begin{Bmatrix} u_1 \\ u_2 \end{Bmatrix} = \begin{bmatrix} 1 - \frac{x}{l} & \frac{x}{l} \end{bmatrix} \begin{Bmatrix} u_1 \\ u_2 \end{Bmatrix} \quad (3.33)$$

$$\{u\} = [n_1 \ n_2]\{s\} = \begin{bmatrix} 1 - \frac{x}{l} & \frac{x}{l} \end{bmatrix} \{s\} \quad (3.34)$$

In order to pass to the strains, it is enough to derivate the shape functions:

$$\{\varepsilon\} = [\partial][n]\{s\} = [b]\{s\} \quad (3.35)$$

$$\varepsilon_{xx} = \frac{d}{dx} [n_1 \ n_2]\{s\} = \begin{bmatrix} \frac{1}{l} & \frac{1}{l} \end{bmatrix} \{s\} \quad (3.36)$$



And the last passage to express stiffness matrix becomes:

$$[k] = \int [b]^T [E] [b] dV \quad (3.37)$$

$$[k] = \int \begin{bmatrix} -\frac{1}{l} \\ 1 \\ \frac{1}{l} \end{bmatrix} E \begin{bmatrix} -\frac{1}{l} & \frac{1}{l} \end{bmatrix} dV \quad (3.38)$$

$$[k] = \frac{EA}{l} \begin{bmatrix} 1 & -1 \\ -1 & 1 \end{bmatrix} \quad (3.39)$$

With the conclusion of this example, we can emphasize a critical aspect of continuum discretization: achieving more accurate results necessitates a high-quality discretization. This can be accomplished either by increasing the number of nodes or by elevating the degree of the polynomial shape functions, as previously discussed.

In dynamic problems, it is also essential to consider the mass matrix and the damping matrix. These matrices can be evaluated using either the principle of virtual work or the Lagrange method. Both approaches will be presented in the following sections.

Recalling:

$$\begin{aligned} \{\delta u\}^T \{f\} + \int \{\delta u\}^T \{t_0\} dA \\ + \int \{\delta u\}^T \{\phi\} dV \\ = \int \{\delta \epsilon\}^T \{\sigma\} dV + \int \{\delta u\}^T \rho \{\ddot{u}\} dV + \int \{\delta u\}^T c_s \{\dot{u}\} dV \end{aligned} \quad (3.40)$$

Where the last two terms are the dynamic internal work and dynamic internal damping:

$$\int \{\delta u\}^T \rho \{\ddot{u}\} dV + \int \{\delta u\}^T c_s \{\dot{u}\} dV \quad (3.41)$$

Introducing the shape function:  $\{u\} = [n]\{s\}$

Leading to the formulation:

$$\begin{aligned}
\{\delta s\}^T \{f\} + \{\delta s\}^T \int [n]^T \{t_0\} dA + \{\delta s\}^T \int [n]^T \{\phi\} dV \\
= \{\delta s\}^T \int [b]^T [E] [b] dV \{s\} + \{\delta s\}^T \int \rho [n]^T [n] dV \{\ddot{s}\} \\
+ \{\delta s\}^T \int c_s [n]^T [n] dV \{\dot{s}\}
\end{aligned} \tag{3.42}$$

Being the right-hand side of the equation (in order) the stiffness matrix, mass matrix and damping matrix.

$$[k]\{s\} + [m]\{\ddot{s}\} + [c]\{\dot{s}\} = \{f\} + \{f_e\}_{t_0} + \{\{f_e\}_\phi\} \tag{3.43}$$

Some matrixes can be obtained if instead of the virtual works we would have used the Lagrange equation:

$$\frac{d}{dt} \left( \frac{\partial T}{\partial \dot{x}_i} \right) - \frac{\partial T}{\partial x_i} + \frac{\partial U}{\partial x_i} = Q_i \tag{3.44}$$

Where T is the kinetic energy, U is the potential energy, Q the external force and x the general coordinate. The equation of Q can be obtained from the derivation of the virtual work with respect to the virtual displacement:

$$Q_i = \frac{\partial \delta L}{\partial \delta x_i} \tag{3.45}$$

From this Q external force, it can be extrapolated the dissipative forces:

$$\tilde{F} = \frac{1}{2} \dot{x}^T C \dot{x} + \dot{x}^T H x \tag{3.46}$$

$$\frac{\partial \tilde{F}}{\partial \dot{x}_i} = c_i \dot{x}_i + h_i x_i \tag{3.47}$$

With [H] being the circulatory matrix typical of rotating systems on lubricated bearing. The term T kinetic energy has three components, one depending on the square of the velocity, one depending linearly on the velocity and on independent from it. The potential energy is formed by two terms, one dependent on the square of the displacement and the other independent from it. From the kinetic terms derived according to the equation of Lagrange can be obtained the matrixes G and  $K_g$  also called  $M_g$  to remind the fact that it comes from the kinetic energy (so responsible of the mass matrix).

The final complete formulation for any dynamic system is:

$$[M]\{\ddot{x}\} + ([G] + [C])\{\dot{x}\} + ([k] + [M_g] + [H])\{x\} = Q \tag{3.48}$$

The stiffness formulation comes from the potential energy:

$$U = \frac{1}{2} \int \varepsilon^T \sigma dV = \frac{1}{2} \{s\}^T \left( \int [b]^T [E] [b] dV \right) \{s\} \quad (3.49)$$

$$[k] = \int [b]^T [E] [b] dV \quad (3.50)$$

While the mass from kinetic energy:

$$T = \frac{1}{2} \int \rho \dot{u}^T \dot{u} dV = \frac{1}{2} \{\dot{s}^T\} \left( \int \rho [n]^T [n] dV \right) \{\dot{s}\} \quad (3.51)$$

$$[M] = \int \rho [n]^T [n] dV \quad (3.52)$$

Which basically is the same formulation obtained before by using the virtual work approach.

## Numerical Errors

Let us describe in the following the three main types of errors that we can have in a FEM model.

- The discretization error or residual given by the discretization of the mesh and the degree of the polynomial shape functions.
- The distortion of the elements or better the non-regular form of the elements.
- The error due to numerical integration affecting the matrices of the system.

It is very important to mention also that the errors may be local or global. For example, the residual is a global error.

While the first type of error may be reduced by increasing the number of nodes (or elements) the second one might need to be analyzed in more depth to understand its critical points. This idea starts from a basic question: does the shape or distortion of the elements affect the stiffness matrix and can we have problems in calculating it? The answer is clearly yes.

Starting from the polynomial shape functions it was been found a way to describe a distorted element but in another coordinate system. The procedure is called conformal mapping, practically it is possible to describe the polynomial shape function in natural coordinate. In natural coordinate the shape function must be non-dimensional and limited between -1 and 1 as a weight function. Maximum 1 in correspondence of the described node and 0 in all the other nodes.

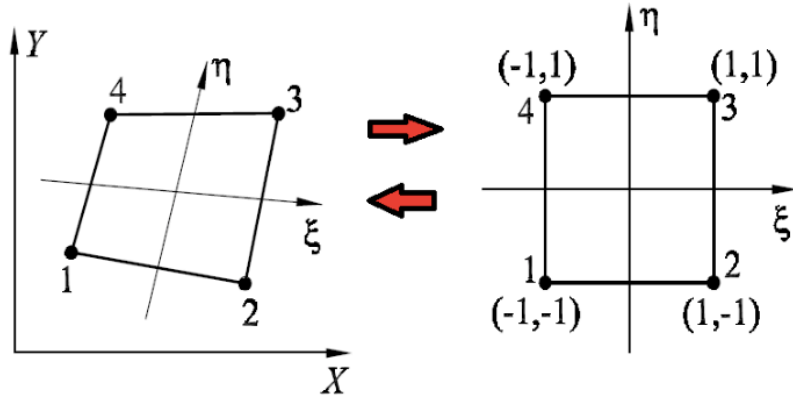


Figure 8: From distorted general coordinate system to natural coordinate system

The equation describing the conformal mapping are:

$$x = \sum_{i=1}^n n_i(\xi, \eta, \zeta) x_i \quad (3.53)$$

$$y = \sum_{i=1}^n n_i(\xi, \eta, \zeta) y_i \quad (3.54)$$

$$z = \sum_{i=1}^n n_i(\xi, \eta, \zeta) z_i \quad (3.55)$$

Where  $n_i(\xi, \eta, \zeta)$  are the shape functions in natural coordinates. Also, the displacements can be expressed using a conformal mapping:

$$u = \sum_{i=1}^m n_i(\xi, \eta, \zeta) u_i \quad (3.56)$$

$$v = \sum_{i=1}^m n_i(\xi, \eta, \zeta) v_i \quad (3.57)$$

$$w = \sum_{i=1}^m n_i(\xi, \eta, \zeta) w_i \quad (3.58)$$

If  $m = n$  it is said isoperimetric formulation, having the same number of parameters for the geometry field and for the displacement field. Moreover, also the strains can be represented with this method:

$$\varepsilon_{xx} = \sum_{i=1}^n \frac{\partial n_i}{\partial x} u_i \quad (3.59)$$

$$\varepsilon_{yy} = \sum_{i=1}^n \frac{\partial n_i}{\partial y} v_i \quad (3.60)$$

$$\gamma_{xy} = \sum_{i=1}^n \left( \frac{\partial n_i}{\partial y} u_i + \frac{\partial n_i}{\partial x} v_i \right) \quad (3.61)$$

Expressing the shape function derivative in function of the natural coordinates

$$\begin{Bmatrix} \frac{\partial n_i}{\partial \xi} \\ \frac{\partial n_i}{\partial \eta} \end{Bmatrix} = \begin{bmatrix} \frac{\partial x}{\partial \xi} & \frac{\partial y}{\partial \xi} \\ \frac{\partial x}{\partial \eta} & \frac{\partial y}{\partial \eta} \end{bmatrix} \begin{Bmatrix} \frac{\partial n_i}{\partial x} \\ \frac{\partial n_i}{\partial y} \end{Bmatrix} \quad (3.62)$$

This formulation leads to the Jacobian matrix that describes how the general coordinates change in function of the natural coordinates. Moreover, the Jacobian matrix [J] is used to pass from the derivative of the shape functions in general coordinates to the derivative of shape functions in natural coordinates.

$$\begin{Bmatrix} \frac{\partial n_i}{\partial \xi} \\ \frac{\partial n_i}{\partial \eta} \end{Bmatrix} = [J] \begin{Bmatrix} \frac{\partial n_i}{\partial x} \\ \frac{\partial n_i}{\partial y} \end{Bmatrix} \quad (3.63)$$

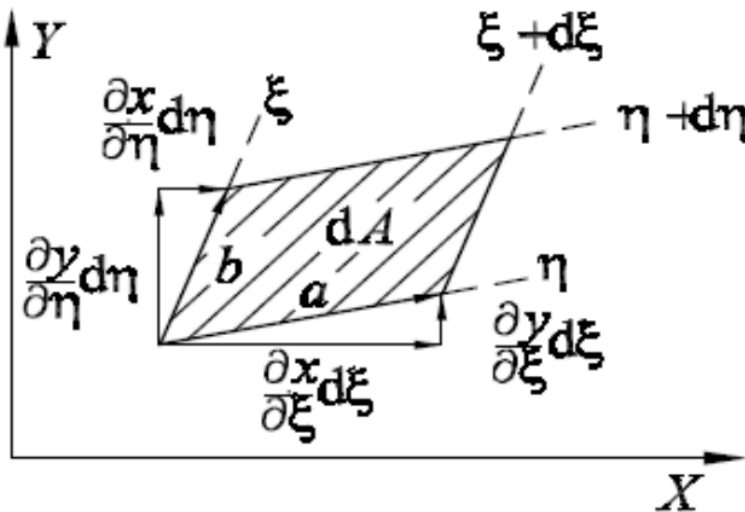


Figure 9: The concept of Jacobian used to pass from the derivative of shape functions in general coordinates to the derivative of shape functions in natural coordinates.

Conformal mapping requires to evaluate the correspondence of  $dA$  (see Figure 9) integration domain in natural coordinates.

$$\{a\} = \begin{Bmatrix} \frac{\partial x}{\partial \xi} \\ \frac{\partial y}{\partial \xi} \end{Bmatrix} d\xi \quad (3.64)$$

$$\{b\} = \begin{Bmatrix} \frac{\partial x}{\partial \eta} \\ \frac{\partial y}{\partial \eta} \end{Bmatrix} d\eta \quad (3.65)$$

$$dA = \{a\} \cdot \{b\} = \left( \frac{\partial x}{\partial \xi} \frac{\partial y}{\partial \eta} - \frac{\partial y}{\partial \xi} \frac{\partial x}{\partial \eta} \right) d\xi d\eta \quad (3.66)$$

So,  $dA$  can be expressed:

$$dA = \{a\} \cdot \{b\} = \det[J] d\xi d\eta \quad (3.67)$$

And now finally connecting it with the formulation of stiffness:

$$[k] = \int [b]^T [E] [b] dV \quad (3.68)$$

$$[k] = \int [b]^T [E] [b] dA h \quad (\text{in a 2D formulation}) \quad (3.69)$$

$$[k] = h \int_{-1}^1 \int_{-1}^1 [b]^T [E] [b] \det[J] d\xi d\eta \quad (3.70)$$

The stiffness matrix of each element of the model is numerically integrated in natural coordinates and related to the physical domain by means of Jacobian transformation:

$$[k] = \sum_{i=1}^m \sum_{j=1}^m w_i w_j [b]^T_{ij} [E] [b]_{ij} \det[J]_{ij} h \quad (3.71)$$

Where  $w_i$  and  $w_j$  are the weight functions of the numerical integration.

In conclusion it is clear how the distortion of the element can affect the stiffness matrix, the more the element is distorted the more the determinant of  $J$  will have a value close to zero or also zero. In the absurd case in which the  $\det(J)$  is zero or negative (so we have a negative

stiffness) the stiffness matrix can't be calculated. When the  $\det(J)$  is equal to one, it means that the element is not distorted at all. Distortion can be a global error or more often a local error.

Let us see now the error coming out of the numerical integration of the stiffness matrix. Numerical integration is a global error.

$$\int f(x, y, z) dx dy dz = \sum_{i=1}^{m_i} \sum_{j=1}^{m_j} \sum_{k=1}^{m_k} w_i w_j w_k f(x_i, y_j, z_k) + e \quad (3.72)$$

One of the most used numerical integration methods is called: Gauss-Legendre. This type of method locates the sampling points so that for a given number of them, greatest accuracy is achieved.

$$\int_a^b f(x) dx = \int_a^b F(x) dx + e \quad (3.73)$$

$$F(x) = \sum_{i=1}^m f(x_i) l_i(x) + P(x)(a_0 + a_1 x + a_2 x^2 + \dots + a_{n-1} x^{n-1}) \quad (3.74)$$

Where  $l_i(x)$  is the so-called Lagrange function while the integral of it  $\int_a^b l_i(x) dx = w_i$

$$P(x) = (x - x_1)(x - x_2) \dots (x - x_m) \quad (3.75)$$

$P(x)$  is called the Legendre polynomial.

$$\int_a^b F(x) dx = \sum_{i=1}^m f(x_i) \int_a^b l_i(x) dx + \sum_{i=1}^{m-1} a_i \int_a^b x^i P(x) dx \quad (3.76)$$

To find the best integration points in order to minimize the integration error (called also optimal points or Barlow points) it must be imposed that the integral of the Legendre polynomial must be zero:

$$\int_a^b x^i P(x) dx = 0 \quad (3.77)$$

Also called minimization technique: finding the best points of estimating the function inside the element. Moreover, the optimal points are calculated in the natural domain. Leading to:

$$\int_a^b F(x) dx = \sum_{i=1}^m f(x_i^*) \int_a^b l_i(x) dx \quad (3.78)$$

Meaning that with  $m$  sampling points a function of order  $(2m-1)$  can be exactly integrated. For example, we can exactly integrate a function of order 5 with only 3 points. In table n it can be seen the values of the integration points (optimal points) in natural coordinate and the values of the wight functions depending on the number of sampling points.

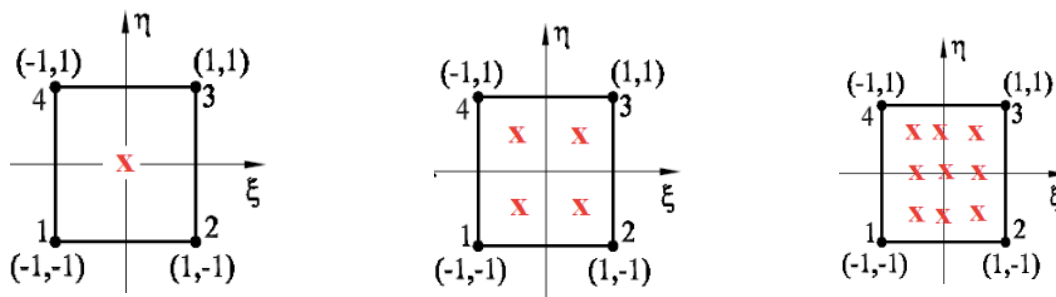


Figure 10: Integration points inside a quadratic element of four nodes

$m$	$\xi_i$	$\eta_i$	$w_i$
1	0	0	2
2	$\pm 1/\sqrt{3}$	$\pm 1/\sqrt{3}$	1
3	0	0	8/9
	$\pm\sqrt{0.6}$	$\pm\sqrt{0.6}$	5/9

Table 1: Sampling points and weight for Gauss quadrature  $[-1, 1]$

$$[k] = \sum_{i=1}^m \sum_{j=1}^m w_i w_j [b]_{ij}^T [E] [b]_{ij} \det[J]_{ij} h \quad (3.79)$$

As it can be seen from the formula, the wight functions directly affect the stiffness matrix, so the choice of the integration points is extremely important to correctly estimate the stiffness matrix.

Moreover, the choice of the integration points of the stiffness matrix could affect the elastic energy of the system, introducing spurious modes or hidden mechanism (zero-energy deformation mode) or better it can be seen as a new rigid motion that doesn't exist in reality.



$$U \propto [k^*] \int h \det[J] d\xi d\eta \quad (3.80)$$

A general formula of understanding if spurious modes are introduced in the system is by evaluating the next formula:

$$M = GN - L - rn \quad (3.81)$$

If  $M \leq 0$  no spurious modes are present. Or if  $rn \geq GN - L$ .

G: number of nodal d.o.f.

N: number of element nodes

L: number of rigid modes d.o.f.

r: rank of matrix [E]

n: number of integration points

Another valuable test for verifying spurious modes is examining the eigenvalues of the stiffness matrix. The eigenvalues of the stiffness matrix are proportional to the potential energy associated with different deformation modes. Therefore, an eigenvalue test can serve as an effective measure of element quality, as it can identify zero-energy modes, which indicate potential issues with the discretization or element formulation.

The element strain energy is:

$$U = \frac{1}{2} \{s\}^T [k] \{s\} \quad (3.82)$$

The eigenproblem:

$$[k] \{\phi\} = \lambda \{\phi\} \quad (3.83)$$

Each eigenvalue  $\lambda_i$  of [k] is twice the element strain energy  $U_i$  when normalized nodal displacement  $\{\phi_i\}$  are imposed:

$$\{\phi_i\}^T [k] \{\phi_i\} = 2U_i = \lambda_i \quad (3.84)$$

$\lambda_i = 0$  when the corresponding  $\{\phi_i\}$  represent rigid body motion.

If the number of zero eigenvalues is greater than, d.o.f. of rigid body motion, spurious rigid body motion will be present. In fact, zero-energy deformation modes also yield zero eigenvalues combination of zero-energy mode and rigid body mode.

## Time integration methods

Equations are verified only at discrete value of time and usually at very time step  $\Delta t$ . A law is assumed for displacement, velocity, and acceleration in the time interval  $\Delta t$ . For this reason, some direct integration methods are born. The most know two are classified as Explicit and Implicit methods.

- Explicit methods (central difference method): Solution at time  $t$  is written and solution at time  $t + \Delta t$  is obtained by using the finite difference expressions for displacement, velocity, and acceleration. This method is conditionally stable and can be solved directly.

$$u(t_{n+1}) = u(t_n) + \Delta t f(t_n, u(t_n)) \quad (3.85)$$

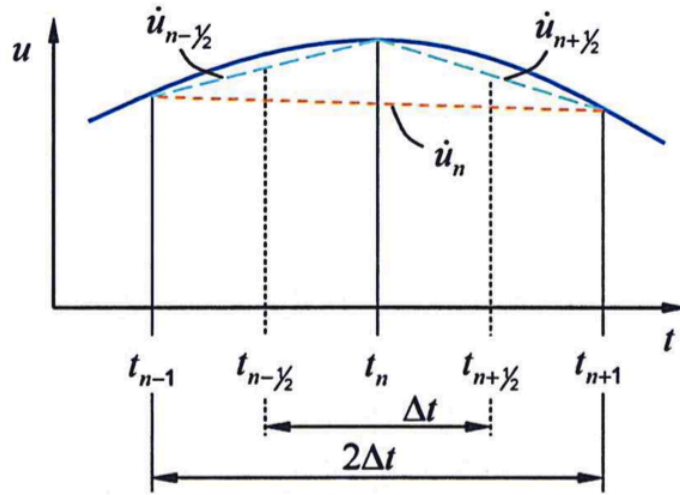


Figure 11: Approximation of the  $u$  through its derivative

$$Mu_{n+1}'' + Cu_{n+1}' + Ku_{n+1} = P_{n+1}(t) \quad (3.86)$$

Approximation of velocity and acceleration becomes:

$$\dot{u}_n = \frac{1}{2\Delta t} (u_{n+1} - u_{n-1}) \quad (3.87)$$

$$\ddot{u}_n = \frac{1}{\Delta t^2} (u_{n+1} - 2u_n + u_{n-1}) \quad (3.88)$$

$$\left(M + \frac{1}{2}\Delta t C\right) u_{n+1} = (\Delta t^2)P_n - [(\Delta t^2)K - 2M]u_n - \left(M - \frac{\Delta t}{2}C\right) u_{n-1} \quad (3.89)$$

- Implicit methods (Houbolt, Wilson- $\theta$ , Newmark): equilibrium equation is written at time  $t+\Delta t$ . Displacement vector is a function of displacement at time  $t$  (know), and velocities and acceleration at time  $t+\Delta t$  (unknow). Implicit methods are unconditionally stable, but it has to be solved iteratively.

$$u(t_{n+1}) = u(t_n) + \Delta t f(t_{n+1}, u(t_{n+1})) \quad (3.90)$$

$$Mu_{n+1}'' + Cu_n + Ku_n = P_n(t) \quad (3.91)$$

An important observation is that the cost of a direct integration is directly proportional to the number of time steps required for the solution. The time step  $\Delta t$  must be small enough to obtain accuracy in the solution and avoid divergence problems, but it must not be smaller than necessary. Stability of an integration method means that the initial condition for the equations with a large value of  $\Delta t/T$  must not be amplified artificially. Accuracy errors in the integration method can be measured in terms of period elongation or amplitude decay.

The general condition for stability in explicit is to have a convergence criterion:

$$\Delta t \leq \frac{2}{\max(\text{eigenvalue})} \quad (3.92)$$

While for implicit it's enough  $\Delta t > 0$  but an opportune time step has to be chosen to yield an accurate and effective solution and avoid period elongations or amplitude decay.

Another equivalent method of evaluating the time-step  $\Delta t$  is determined by the smallest element of the mesh:

$$\Delta t \leq f * \min\left(\frac{h}{c}\right) \quad (3.93)$$

The time-step size is limited so that a stress wave cannot travel farther than the smallest element characteristic length in a single time-step. This is called the Courant-Friedrichs-Lewy (CFL) condition.

- $h$  is the characteristic length of a finite element. In explicit analysis, having uniform element size is very important, because the time-step size is controlled by the smallest element.
- $c$  is the sound speed in the material.
- $f$  is a safety factor, usually equal to or smaller than 1.

## Advantages and disadvantages of both time integration methods

### Explicit

- Computational fast
- Robust, even for strong nonlinear problems
- Conditionally stable
- Expensive to conduct long durations
- To control equilibrium the energy balance must be controlled

### Implicit

- The method is unconditionally stable
- Can be used for static simulations
- Relatively inexpensive for long durations
- Often requires large amount of memory
- Can have problems with strong non-linear models

The two methods are used for different applications. The explicit time integration is used for high-rate dynamic analysis, car crash, impact/penetration problems, explosives. While the implicit time integration is used for low-rate dynamic analysis, static simulations, eigenvalue analyses, spring-back, gravity loading, preload.

## 4. Composites materials

A composite material is a material made from two or more constituent materials with significantly different physical or chemical properties that, when combined, produce a material with characteristics different from those of the individual components. In simpler terms, composites are created by blending two or more materials to achieve desired properties that may not be achievable with any single material alone.

One of the most common types of composite materials is fibre-reinforced composites, where fibres—often made of materials like carbon, glass, or aramid—are embedded within a matrix material, typically a polymer resin. The fibres provide strength and stiffness, while the matrix holds them in place and transfers loads between them. This combination results in a material that is lightweight, strong, and tailored to specific applications.

The applications of composite materials are vast and varied, spanning industries from aerospace and automotive to construction and sports equipment. Here are some notable examples:

- Aerospace: Composite materials revolutionized the aerospace industry by offering lightweight alternatives to traditional metals. Aircraft components like wings,

fuselages, and empennages are now commonly constructed using carbon fiber composites, reducing weight and improving fuel efficiency.

- Automotive: In the automotive sector, composites are used to manufacture components such as body panels, chassis parts, and interior trim. Carbon fibre reinforced polymers (CFRP) are particularly popular in high-performance vehicles for their strength-to-weight ratio and corrosion resistance.
- Marine: Composite materials find extensive use in the marine industry due to their resistance to corrosion and ability to withstand harsh environments. They are used in boat hulls, decks, masts, and other structural components, offering durability and performance benefits over traditional materials like wood or metal.
- Wind Energy: Wind turbine blades benefit greatly from composite construction. Fiberglass and carbon fibre composites are used to create lightweight yet durable blades that efficiently capture wind kinetic energy. Composites enable longer blades, increasing the energy output of wind turbines.
- Sporting Goods: From tennis rackets to golf clubs and bicycle frames, composite materials have become synonymous with high-performance sporting goods. Their ability to be precisely engineered for specific stiffness, strength, and weight characteristics makes them ideal for enhancing athletic performance.
- Construction: In the construction industry, composites are used in a variety of applications, including bridges, panels, and reinforcement materials. Composite materials offer advantages such as corrosion resistance, high strength, and ease of installation, making them appealing for both new construction and rehabilitation projects.

## Advantages

Composites are engineered materials. We can engineer them specifically to meet our needs on a case-to-case basis. In general, following properties can be improved by using composite materials.

- Strength
- Modulus
- Weight
- Vibration damping
- Thermal stability
- Acoustical insulation o Fatigue
- Aesthetics
- Resistance to wear
- Resistance to corrosion

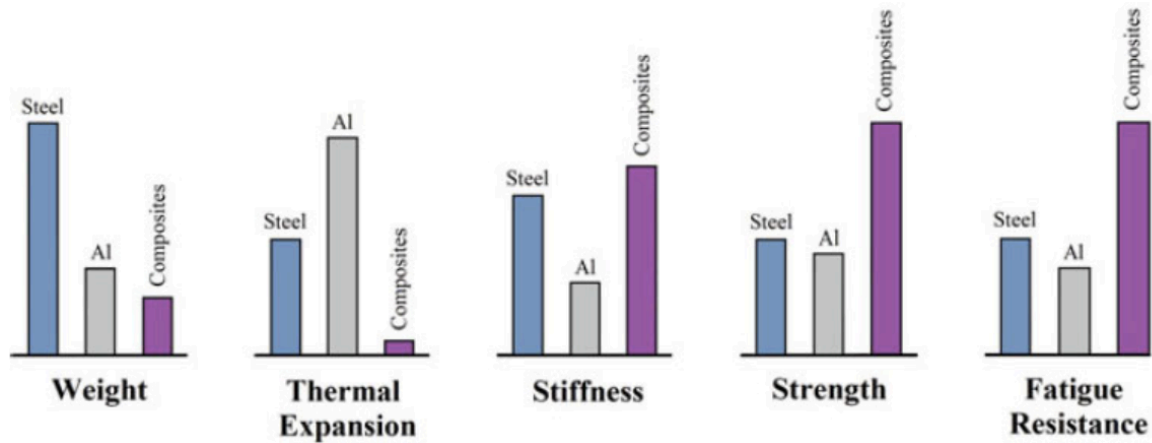


Figure 12: Physical and Mechanical properties comparison between Composites and metals

## Disadvantages

Like all things in nature, composites materials have their limitations as well. Some of the important ones are:

- Anisotropy: Many composites have direction dependent material properties. This makes them more difficult to understand, analyse and engineer, compared to isotropic materials.
- Non-homogenous: Further, these materials by definition are not homogenous. Hence their material properties vary from point-to-point. This factor as well makes them difficult to model and analyse.
- Costly: Composite materials are in general expensive. Thus, they are used only in applications where their benefits outweigh their costs.
- Residual thermal stresses: Laminated composites come in with residual thermal stresses because they get fabricated at high temperatures, and then cooled. Such a process locks in thermal stresses into the structure.
- Moisture effects: Laminated composites are also sensitive to moisture, and their performance varies significantly when exposed to moisture for long periods of time.

## Fibres characteristics

Fibres are significantly stronger than bulk materials because:

- They have a far more “perfect” structure, i.e. their crystals are aligned along the fibre axis.
- There are fewer internal defects, especially in direction normal to fibre orientation, and hence there are lesser number of dislocations.

As it can be seen from the table the difference in the bulk and fibres strength is significant.

Fibre	Specific Gravity	E modulus (GPa)	Bulk tensile strength (MPa)	Fibre tensile strength (MPa)
Al	2.7	78	140-620	620
Ti alloy/fibre	4.5	115	1040	1900
Stell	7.8	210	340-1200	4100
E-glass	2.54	72	70-210	3500
S-glass	2.48	86	70-210	4600
Carbon	1.41	190	Very low	2100-2500

Table 2: general mechanical properties of fibers

## Matrix characteristics

The matrix has different functions in the composite:

- Transmit force between fibers
- Arrest cracks from spreading between fibers
- Do not carry most of the load
- Hold fibers in proper orientation
- Protect fibers from environment

Moreover, the matrix should also sustain interlaminar shear stress, be tough, resist to environmental moisture and temperature conditions.

Most widely used matrix materials are: Epoxies, Polyesters, vinylesters, PEEK, PPS, nylon, polycarbonate, polyacetals, polyamides, polyether imides, polystyrene, silicones.

## Advantages

- Relatively low cost
- Easy to process
- Low density
- Superior chemical resistance

## Disadvantages

- Low strength
- Low modulus
- Limited range for operating temperature
- Sensitivity to UV radiation, specific solvents, and occasionally humidity

## Hooke's Law for 3D Orthotropic Lamina

The stress tensor comprises nine different components: normal stresses, which can be either compressive or tensile, and shear stresses, which arise from torsional moments or pure shear forces. Similarly, the strain tensor also has nine components: three are normal strains, and the remaining six are shear strains. Initially, this would suggest 81 independent elastic constants to relate stresses and strains according to Hooke's Law. However, by applying the reciprocity theorem of stresses and strains and leveraging the symmetry of the stiffness matrix (as described by Schwarz's theorem), the number of independent elastic constants is reduced to 36 [6].

$$\sigma_{ij} = \sigma_{ji} \quad (4.0)$$

$$\gamma_{kl} = \gamma_{lk} \quad (4.1)$$

$$C_{ij} = C_{ji} \quad (4.2)$$

$$\frac{\partial^2 \eta}{\partial \varepsilon_i \partial \varepsilon_j} = \frac{\partial^2 \eta}{\partial \varepsilon_j \partial \varepsilon_i} \quad (4.3)$$

$$\begin{Bmatrix} \sigma_1 \\ \sigma_2 \\ \sigma_3 \\ \tau_{23} \\ \tau_{31} \\ \tau_{12} \end{Bmatrix} = \begin{bmatrix} C_{11} & C_{12} & C_{13} & C_{14} & C_{15} & C_{16} \\ C_{21} & C_{22} & C_{23} & C_{24} & C_{25} & C_{26} \\ C_{31} & C_{32} & C_{33} & C_{34} & C_{35} & C_{36} \\ C_{41} & C_{42} & C_{43} & C_{44} & C_{45} & C_{46} \\ C_{51} & C_{52} & C_{53} & C_{54} & C_{55} & C_{56} \\ C_{61} & C_{62} & C_{63} & C_{64} & C_{65} & C_{66} \end{bmatrix} \begin{Bmatrix} \varepsilon_1 \\ \varepsilon_2 \\ \varepsilon_3 \\ \gamma_{23} \\ \gamma_{31} \\ \gamma_{12} \end{Bmatrix} \quad (4.4)$$

Only 21 of these 36 constants are independent constants:

$$\begin{Bmatrix} \sigma_1 \\ \sigma_2 \\ \sigma_3 \\ \tau_{23} \\ \tau_{31} \\ \tau_{12} \end{Bmatrix} = \begin{bmatrix} C_{11} & C_{12} & C_{13} & C_{14} & C_{15} & C_{16} \\ C_{21} & C_{22} & C_{23} & C_{24} & C_{25} & C_{26} \\ C_{31} & C_{32} & C_{33} & C_{34} & C_{35} & C_{36} \\ C_{41} & C_{42} & C_{43} & C_{44} & C_{45} & C_{46} \\ C_{51} & C_{52} & C_{53} & C_{54} & C_{55} & C_{56} \\ C_{61} & C_{62} & C_{63} & C_{64} & C_{65} & C_{66} \end{bmatrix} \begin{Bmatrix} \varepsilon_1 \\ \varepsilon_2 \\ \varepsilon_3 \\ \gamma_{23} \\ \gamma_{31} \\ \gamma_{12} \end{Bmatrix} \quad (4.5)$$

Composites are not isotropic material, so their properties are not the same in all directions, but they are orthotropic, meaning that properties are constants only along the material axis thank to the existence of three planes of material symmetry.

Having an orthotropic material, the number of constants are decreasing to 9:



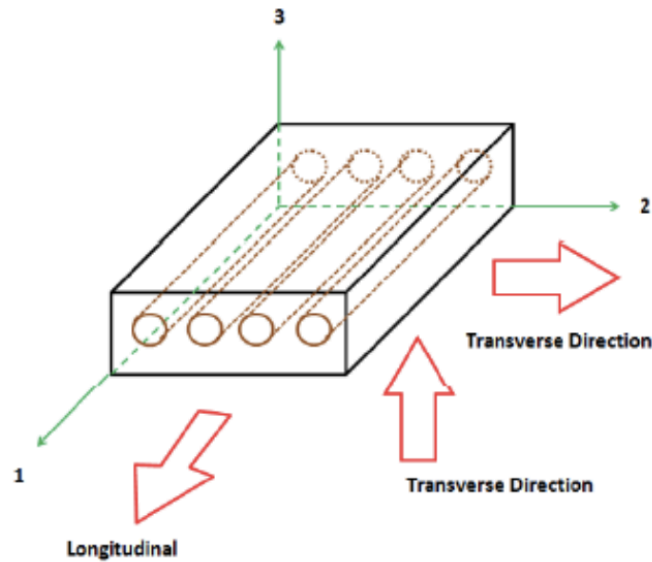
$$[C] = \begin{bmatrix} C_{11} & C_{12} & C_{13} & 0 & 0 & 0 \\ C_{12} & C_{22} & C_{23} & 0 & 0 & 0 \\ C_{13} & C_{23} & C_{33} & 0 & 0 & 0 \\ 0 & 0 & 0 & C_{44} & 0 & 0 \\ 0 & 0 & 0 & 0 & C_{55} & 0 \\ 0 & 0 & 0 & 0 & 0 & C_{66} \end{bmatrix} \quad (4.6)$$

As it is known, if the stiffness matrix exists we can also write the inverse of it: the compliance matrix [S].

$$[S] = \begin{bmatrix} S_{11} & S_{12} & S_{13} & 0 & 0 & 0 \\ S_{12} & S_{22} & S_{23} & 0 & 0 & 0 \\ S_{13} & S_{23} & S_{33} & 0 & 0 & 0 \\ 0 & 0 & 0 & S_{44} & 0 & 0 \\ 0 & 0 & 0 & 0 & S_{55} & 0 \\ 0 & 0 & 0 & 0 & 0 & S_{66} \end{bmatrix} \quad (4.7)$$

$$[S] = \begin{bmatrix} \frac{1}{E_1} & \frac{-\nu_{12}}{E_1} & \frac{-\nu_{13}}{E_1} & 0 & 0 & 0 \\ \frac{-\nu_{21}}{E_2} & \frac{1}{E_2} & \frac{-\nu_{23}}{E_2} & 0 & 0 & 0 \\ \frac{-\nu_{31}}{E_3} & \frac{-\nu_{32}}{E_3} & \frac{1}{E_3} & 0 & 0 & 0 \\ 0 & 0 & 0 & \frac{1}{G_{23}} & 0 & 0 \\ 0 & 0 & 0 & 0 & \frac{1}{G_{31}} & 0 \\ 0 & 0 & 0 & 0 & 0 & \frac{1}{G_{12}} \end{bmatrix} \quad (4.8)$$

Another important point to keep in mind is that even if the composite are orthotropic, there is a transversely isotropic plane (plane 2-3).



In direction 2 and 3, elastic properties are direction independent: leading to another reduction of the elastic constants from 9 to 5.

$$[C] = \begin{bmatrix} C_{11} & C_{12} & C_{12} & 0 & 0 & 0 \\ C_{12} & C_{22} & C_{23} & 0 & 0 & 0 \\ C_{12} & C_{23} & C_{22} & 0 & 0 & 0 \\ 0 & 0 & 0 & \frac{C_{22} - C_{23}}{2} & 0 & 0 \\ 0 & 0 & 0 & 0 & C_{55} & 0 \\ 0 & 0 & 0 & 0 & 0 & C_{55} \end{bmatrix} \quad (4.9)$$

A lamina may be assumed to have only two dimensions as its thickness is very small compared to its in-plane dimensions. The plane stress conditions are:  $\sigma_3 = \tau_{23} = \tau_{31} = 0$ . Allowing to have in this way 6 independent constants. In case the composite is transversely isotropic, they will be 5.

$$\begin{Bmatrix} \sigma_1 \\ \sigma_2 \\ \tau_{12} \end{Bmatrix} = \begin{bmatrix} Q_{11} & Q_{12} & 0 \\ Q_{12} & Q_{22} & 0 \\ 0 & 0 & Q_{66} \end{bmatrix} \begin{Bmatrix} \varepsilon_1 \\ \varepsilon_2 \\ \gamma_{12} \end{Bmatrix} \quad (4.10)$$

## Fundamental material properties

For transversely isotropic composites, there are five fundamental material strength parameters and five elastic constants that are crucial for describing the behavior of a lamina. To summarize, for transversely isotropic unidirectional materials, you need to specify five distinct material strength parameters in the principal material directions, as well as five elastic constants.

- Longitudinal tensile strength  $\sigma_{Ltu}$
- Transverse tensile strength  $\sigma_{Ttu}$
- Longitudinal compressive strength  $\sigma_{Lcu}$
- Transverse compressive strength  $\sigma_{Tcu}$
- In-plane shear strength  $\tau_u$
- Longitudinal modulus  $E_1$
- Transverse modulus  $E_2$
- Major Poisson's ratio  $\nu_{12}$
- Shear modulus  $G_{12}$
- Transverse Poisson's ratio  $\nu_{23}$

These properties can be expressed either as volume fractions, or as mass fractions. While mass fractions are easier to obtain during fabrication of composites, volume fractions are handier in theoretical analyses.

Volume fraction of matrix  $V_m$  and fiber  $V_f$  are given by the ratio of volumes:

$$V_m = \frac{v_m}{v_c} \quad (4.11)$$

$$V_f = \frac{v_f}{v_c} \quad (4.12)$$

Then the mass fraction of matrix  $M_m$  and fiber  $M_f$  are:

$$M_m = \frac{m_m}{m_c} = \frac{\rho_m}{\rho_c} V_m \quad (4.13)$$

$$M_f = \frac{m_f}{m_c} = \frac{\rho_f}{\rho_c} V_f \quad (4.14)$$

The density of the composite is obtained as a rule of mixture:

$$\rho_c = \rho_m \frac{v_m}{v_c} + \rho_f \frac{v_f}{v_c} = \rho_m V_m + \rho_f V_f \quad (4.15)$$

In real cases, there is also a volume fraction of voids in the composites  $V_v$  :

$$V_v = \frac{v_v}{v_{ce}} \quad (4.16)$$

Where  $v_{ce}$  is the empirical (with voids) composite volume. Leading to an empirical and a theoretical composites density:

$$\begin{cases} \rho_{ce} = \frac{m_c}{v_{ce}} \\ \rho_{ct} = \frac{m_c}{v_{ct}} \end{cases} \quad (4.17)$$

It can be seen that the longitudinal modulus  $E_1$  can be obtained also by a rule of mixture, considering the composite as a spring in parallel model, having two stiffnesses, one of the matrix, and one of the fibre. Both are undergoing the same strain when deformed but the stresses are different.

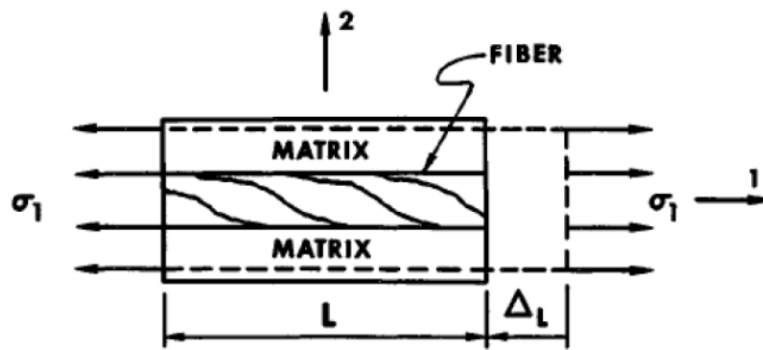


Figure 14: Lamina representation under tension along direction 1

$$\varepsilon = \varepsilon_c = \varepsilon_f = \varepsilon_m \quad (4.18)$$

$$\sigma_1 = \sigma_f V_f + \sigma_m V_m \quad (4.19)$$

$$E_L = E_1 = E_f V_f + E_m V_m \quad (4.20)$$

The rule of mixtures indicates that the load carried by fibers can be increased by either enhancing the fiber stiffness or by raising the fiber volume fraction. However, experimental data reveal that targeting fiber volume fractions above 80% becomes impractical. This is due to challenges such as poor fiber wetting and inadequate matrix impregnation between the fibers.

Regarding the transverse modulus  $E_2$ : it can be evaluated by considering the model of tow spring in series. They undergo the same load but different strains due to the difference in stiffness.

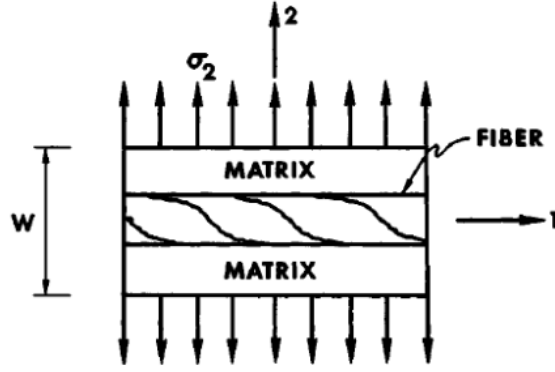


Figure 15: Lamina representation under tension along direction 2

$$\sigma_2 = \sigma_c = \sigma_f = \sigma_m \quad (4.21)$$

$$\varepsilon_2 = \varepsilon_{2,c} = \varepsilon_{2,f}V_f + \varepsilon_{2,m}V_m \quad (4.22)$$

$$\frac{1}{E_2} = \frac{1}{E_T} = \frac{V_f}{E_f} + \frac{V_m}{E_M} \quad (4.23)$$

According to experiments this rule of mixture is not so accurate, for this reason a correction is introduced by Halpin-Tsai:

$$\frac{E_2}{E_m} = \frac{1 + \zeta\eta V_f}{1 - \eta V_f} \quad (4.24)$$

Where  $\zeta$  is a parameter that accounts for packing, fiber geometry and loading conditions. It is 2 for fibers with square and round cross-sections.

Another important parameter is the major Poisson's ratio (obtained with another rule of mixture):  $\nu_{12}$

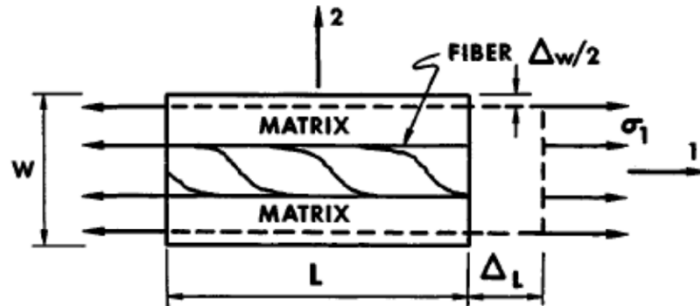
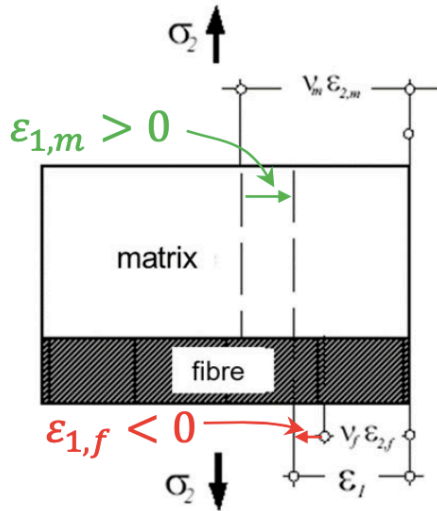


Figure 16: Lamina representation under tension along direction 1 with width variation for the evaluation of Poisson's ratio.

$$\varepsilon_T = \frac{\Delta W}{w} = \frac{\Delta W_f + \Delta W_m}{w} = \frac{-\nu_f \varepsilon_L W_f - \nu_m \varepsilon_L W_m}{w} \quad (4.25)$$

$$\nu_{12} = \nu_{LT} = \frac{-\varepsilon_T}{\varepsilon_L} = \nu_f V_f + \nu_m V_m \quad (4.26)$$

For the minor Poisson's ratio, it's important to consider the differing behaviors of the two materials under load. The matrix tends to contract more, while the fiber tends to contract less. Although the final deformation is uniform, this difference in behavior results in the matrix being subjected to tensile stress, while the fiber experiences compressive stress.



$$\varepsilon_{1,f} = \varepsilon_1 + \nu_f \varepsilon_{2,f} < 0 \quad (4.27)$$

$$\varepsilon_{1,m} = \varepsilon_1 + \nu_m \varepsilon_{2,m} > 0 \quad (4.28)$$

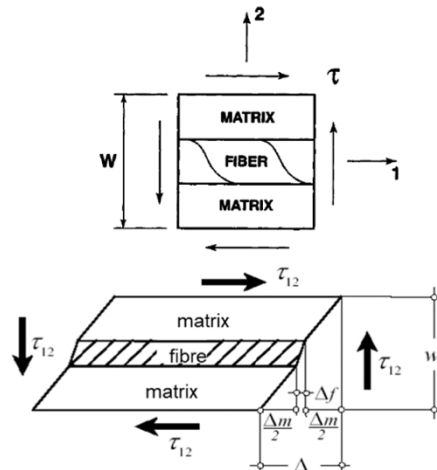
$$\sigma_2 = \sigma_{2,f} = \sigma_{2,m} \quad (4.29)$$

$$\sigma_{1,f} V_f + \sigma_{1,m} V_m = 0 \quad (4.30)$$

$$\frac{\nu_{21}}{E_2} = \frac{\nu_{12}}{E_1} \quad (4.31)$$

Figure 17: Lamina representation under tension along direction 2 for the evaluation of minor Poisson's ratio.

Next in line is the shear modulus  $G_{12}$ , it is evaluated in the same way as the model of series springs explained previously. So, the springs undergo the same load, but due to their different stiffness they deform differently. From here another rule of mixture will come out:



$$\tau_{12} = \tau_c = \tau_f = \tau_m \quad (4.32)$$

$$\gamma_c = \gamma_f V_f + \gamma_m V_m \quad (4.33)$$

$$\frac{1}{G_{12}} = \frac{1}{G_{LT}} = \frac{V_m}{G_m} + \frac{V_f}{G_f} \quad (4.34)$$

Figure 18: Lamina under shear tension for the evaluation of the shear modulus

A more accurate formulation is provided by Halpin-Tsai:

$$\frac{G_{12}}{G_m} = \frac{1 + \eta V_f}{1 - \eta V_f} \quad (4.35)$$

Another important material constant is the longitudinal CTE (coefficient of thermal expansion): During the thermal expansion of a composite, the different parts of it tend to react differently, the matrix would like to expand more while the fibre would like to expand less. The final deformation is the same, but the conditions of stress are different, the matrix is under compression while the fibre is under tension. These equations are valid for a unidirectional lamina.

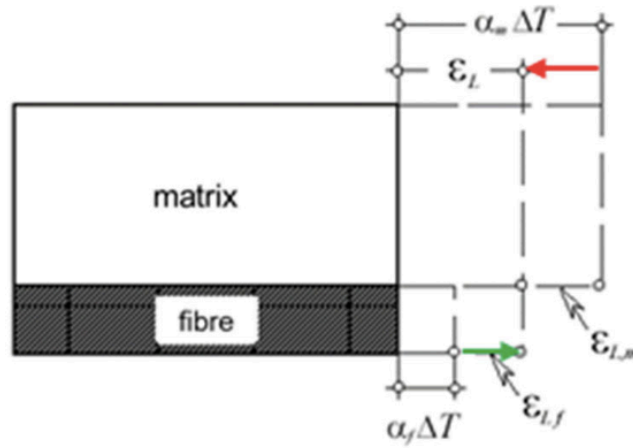


Figure 19: Lamina under thermal load in direction 1

The strains are:

$$\varepsilon_{1,f,\Delta T} = \varepsilon_1 - \alpha_f \Delta T > 0 \quad (4.36)$$

$$\varepsilon_{1,m,\Delta T} = \varepsilon_1 - \alpha_m \Delta T < 0 \quad (4.37)$$

The stresses are:

$$\sigma_{1,f} V_f + \sigma_{(1,m)} V_m = 0 \quad (4.38)$$

The rule of mixture describing the longitudinal CTE:

$$\alpha_1 = \alpha_L = \alpha_f \frac{E_f V_f}{E_1} + \alpha_m \frac{E_m V_m}{E_1} \quad (4.39)$$

The CTE in the transversal direction can be evaluated starting from physical considerations (as before). During the expansion of the composite the matrix would like to expand more

while the fibre would like to expand less. In terms of stresses the matrix is under compression and the fibre is under tension.

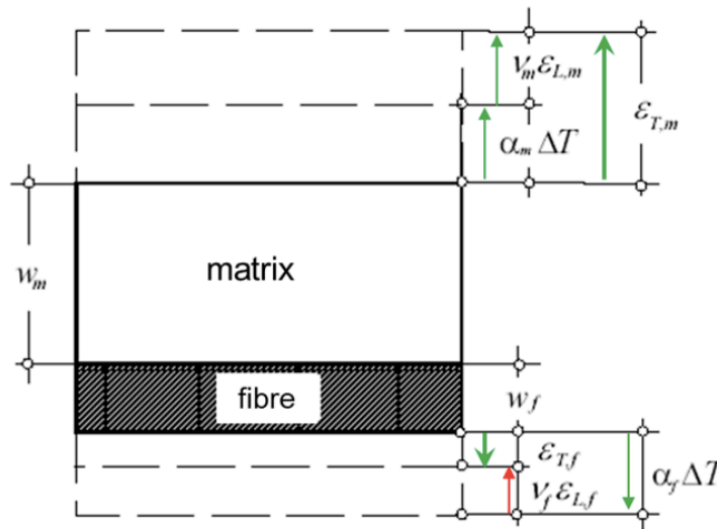


Figure 20: Laminate under thermal load in direction 2

The situation is more complex in this case, in order to understand what's happening it must be considered the strains of fibre and of the matrix separately:

Strain in fibre due to thermal dilatation of fibre

$$\varepsilon_{2,f,\Delta T} = \alpha_f \Delta T > 0 \quad (4.40)$$

The dilatation in direction two will induce a reduction of dimension in direction one described by the Poisson's ratio:

$$\varepsilon_{2,f,\nu_f} = -\nu_f \varepsilon_{1,f,\Delta T} < 0 \quad (4.41)$$

So, the total strain of the fibre is:

$$\varepsilon_{2,f} = \alpha_f \Delta T - \nu_f \varepsilon_{1,f,\Delta T} > 0 \quad (4.42)$$

Which is positive (so fibres in tension) only if  $\varepsilon_{2,f,\Delta T} > \varepsilon_{2,f,\nu_f}$

For the matrix the situation is analogous, the only difference is that the strain that comes from Poisson's ratio in this case is positive.

$$\varepsilon_{2,m,\Delta T} = \alpha_m \Delta T > 0 \quad (4.43)$$

$$\varepsilon_{2,m,\nu_f} = -\nu_m \varepsilon_{1,m,\Delta T} > 0 \quad (4.44)$$

$$\varepsilon_{2,m} = \alpha_m \Delta T - \nu_m \varepsilon_{1,m,\Delta T} > 0 \quad (4.45)$$

In this case the matrix is in tension. The transversal coefficient CTE is given by:



$$\alpha_2 = \alpha_T = (1 + \nu_f)\alpha_f V_f + (1 + \nu_m)\alpha_m V_m - \nu_{12}\alpha_1 \quad (4.46)$$

## Laminate

A laminate is composed of multiple laminae, stacked and bonded together. Each lamina within the stack may possess different properties. To predict the response of a laminate, the first step is to develop stress-strain relations for a composite plate. The primary assumptions regarding the properties of each lamina are as follows: it is elastic, orthotropic, and homogeneous; the adhesive bond between two adjacent layers is perfect, meaning it has zero thickness and no shear deformation (i.e., laminae cannot slip over one another). Additionally, the displacements across the laminate are assumed to be continuous.

To transform from a global coordinate system  $x,y,z$ , to the material coordinate system, a transformation matrix  $[T]$  is required. For the stresses:

$$\begin{Bmatrix} \sigma_1 \\ \sigma_2 \\ \tau_{12} \end{Bmatrix} = [T] \begin{Bmatrix} \sigma_x \\ \sigma_y \\ \tau_{xy} \end{Bmatrix} \quad (4.47)$$

Where  $[T]$  is:

$$[T] = \begin{bmatrix} \cos^2 \theta & \sin^2 \theta & 2 \sin \theta \cos \theta \\ \sin^2 \theta & \cos^2 \theta & -2 \sin \theta \cos \theta \\ -\sin \theta \cos \theta & \sin \theta \cos \theta & \cos^2 \theta - \sin^2 \theta \end{bmatrix} \quad (4.48)$$

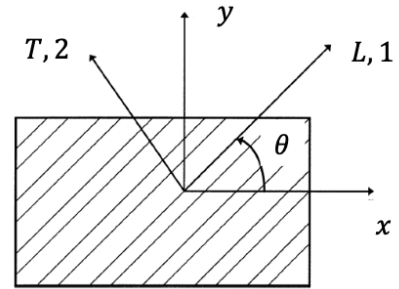


Figure 21: Global and material coordinates of a composite.

$$\begin{Bmatrix} \sigma_x \\ \sigma_y \\ \tau_{xy} \end{Bmatrix} = [T]^{-1} \begin{Bmatrix} \sigma_1 \\ \sigma_2 \\ \tau_{12} \end{Bmatrix} \quad (4.49)$$

For the strains:

$$\begin{Bmatrix} \varepsilon_1 \\ \varepsilon_2 \\ \gamma_{12} \end{Bmatrix} = [R][T][R]^{-1} \begin{Bmatrix} \varepsilon_x \\ \varepsilon_y \\ \gamma_{xy} \end{Bmatrix} \quad (4.50)$$

With  $[R]$ :

$$[R] = \begin{bmatrix} 1 & 0 & 0 \\ 0 & 1 & 0 \\ 0 & 0 & 2 \end{bmatrix} \quad (4.51)$$

In case the stresses in x,y,z directions must be evaluated starting from the strains in x,y,z the stiffness matrix [Q] will be modified as follows.

$$\begin{Bmatrix} \sigma_1 \\ \sigma_2 \\ \tau_{12} \end{Bmatrix} = [Q] \begin{Bmatrix} \varepsilon_1 \\ \varepsilon_2 \\ \gamma_{12} \end{Bmatrix} \quad (4.52)$$

$$[T]^{-1} \begin{Bmatrix} \sigma_1 \\ \sigma_2 \\ \tau_{12} \end{Bmatrix} = [T]^{-1}[Q] \begin{Bmatrix} \varepsilon_1 \\ \varepsilon_2 \\ \gamma_{12} \end{Bmatrix} \quad (4.53)$$

$$\begin{Bmatrix} \sigma_x \\ \sigma_y \\ \tau_{xy} \end{Bmatrix} = [T]^{-1}[Q] \begin{Bmatrix} \varepsilon_1 \\ \varepsilon_2 \\ \gamma_{12} \end{Bmatrix} = [T]^{-1}[Q][R][T][R]^{-1} \begin{Bmatrix} \varepsilon_x \\ \varepsilon_y \\ \gamma_{xy} \end{Bmatrix} = [\bar{Q}] \begin{Bmatrix} \varepsilon_x \\ \varepsilon_y \\ \gamma_{xy} \end{Bmatrix} \quad (4.54)$$

$[\bar{Q}]$  is fully populated:

$$[\bar{Q}] = \begin{bmatrix} \bar{Q}_{11} & \bar{Q}_{12} & \bar{Q}_{16} \\ \bar{Q}_{12} & \bar{Q}_{22} & \bar{Q}_{26} \\ \bar{Q}_{16} & \bar{Q}_{26} & \bar{Q}_{66} \end{bmatrix} \quad (4.55)$$

Particular attention must be dedicated to the terms  $Q_{16}$  and  $Q_{26}$  which couple normal and shear responses, present in orthotropic lamina when loading direction and material axes are not coincident, application of normal stresses produces normal as well as shear strains. These two terms are also known as cross-coupling stiffness coefficients.

From displacement field to Strain field

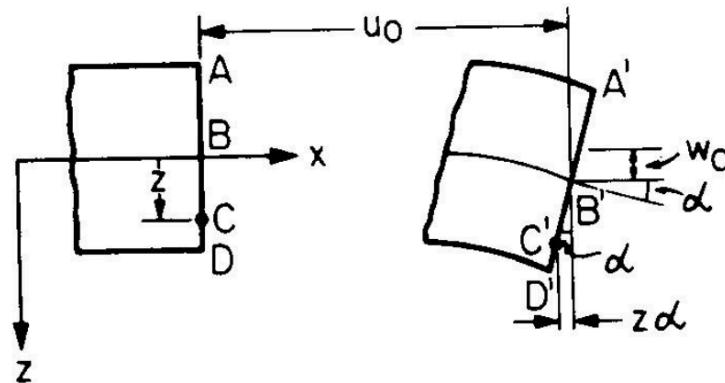


Figure 22: Infinitesimal element under bending with direct effect on the displacement  $u(x,y,z)$ .

$$u(x, y, z) = u_0(x, y) - \alpha(x, y) \cdot z \quad (4.56)$$

$$w(x, y) = w_0(x, y) \quad (4.57)$$

$$\alpha(x, y) = \frac{\partial w(x, y)}{\partial x} = \frac{\partial w_0(x, y)}{\partial x} \quad (4.58)$$

$$u(x, y, z) = u_0(x, y) - z \frac{\partial w_0(x, y)}{\partial x} \quad (4.59)$$

$$v(x, y, z) = v_0(x, y) - z \frac{\partial w_0(x, y)}{\partial y} \quad (4.60)$$

It is known that the strains are nothing but the variation of the displacement in the different directions:

$$\varepsilon_x = \frac{\partial u(x, y, z)}{\partial x} = \frac{\partial u_0(x, y)}{\partial x} - z \frac{\partial^2 w_0(x, y)}{\partial x^2} \quad (4.61)$$

$$\varepsilon_y = \frac{\partial v(x, y, z)}{\partial y} = \frac{\partial v_0(x, y)}{\partial y} - z \frac{\partial^2 w_0(x, y)}{\partial y^2} \quad (4.62)$$

$$\gamma_{xy} = \frac{\partial u(x, y, z)}{\partial y} + \frac{\partial v(x, y, z)}{\partial x} = \frac{\partial u_0(x, y)}{\partial y} + \frac{\partial v_0(x, y)}{\partial x} - 2z \frac{\partial^2 w_0(x, y)}{\partial x \partial y} \quad (4.63)$$

Leading to obtain two contributions, the first one is the membrane strain while the other one is the k curvature due to bending.

$$\begin{Bmatrix} \varepsilon_x \\ \varepsilon_y \\ \gamma_{xy} \end{Bmatrix} = \begin{Bmatrix} \varepsilon_x^0 \\ \varepsilon_y^0 \\ \gamma_{xy}^0 \end{Bmatrix} + z \begin{Bmatrix} k_x \\ k_y \\ k_{xy} \end{Bmatrix} \quad (4.64)$$

From strain field to stress field

The stress in one layer is given by:

$$\begin{Bmatrix} \sigma_x \\ \sigma_y \\ \tau_{xy} \end{Bmatrix} = \begin{bmatrix} \overline{Q_{11}} & \overline{Q_{12}} & \overline{Q_{16}} \\ \overline{Q_{12}} & \overline{Q_{22}} & \overline{Q_{26}} \\ \overline{Q_{16}} & \overline{Q_{26}} & \overline{Q_{66}} \end{bmatrix} \begin{Bmatrix} \varepsilon_x^0 \\ \varepsilon_y^0 \\ \gamma_{xy}^0 \end{Bmatrix} + z \begin{bmatrix} \overline{Q_{11}} & \overline{Q_{12}} & \overline{Q_{16}} \\ \overline{Q_{12}} & \overline{Q_{22}} & \overline{Q_{26}} \\ \overline{Q_{16}} & \overline{Q_{26}} & \overline{Q_{66}} \end{bmatrix} \begin{Bmatrix} k_x \\ k_y \\ k_{xy} \end{Bmatrix} \quad (4.65)$$

The stresses are evaluated from the resultant forces and moments along the thickness of the layers of the laminate. At the same time stress are also evaluated as the result of the stiffness matrix and strains.

$$\begin{Bmatrix} N_x \\ N_y \\ N_{xy} \end{Bmatrix} = \sum_{j=1}^N \int_{h_{j-1}}^{h_j} \begin{Bmatrix} \sigma_x \\ \sigma_y \\ \tau_{xy} \end{Bmatrix} dz \quad (4.66)$$

$$\begin{Bmatrix} M_x \\ M_y \\ M_{xy} \end{Bmatrix} = \sum_{j=1}^N \int_{h_{j-1}}^{h_j} \begin{Bmatrix} \sigma_x \\ \sigma_y \\ \tau_{xy} \end{Bmatrix} z dz \quad (4.67)$$

So, it can be shown the connection between the forces, moments, and stresses (eq. 4.68 and 4.69):

$$\begin{Bmatrix} N_x \\ N_y \\ N_{xy} \end{Bmatrix} = \sum_{j=1}^N \int_{h_{j-1}}^{h_j} \begin{bmatrix} \overline{Q_{11}} & \overline{Q_{12}} & \overline{Q_{16}} \\ \overline{Q_{12}} & \overline{Q_{22}} & \overline{Q_{26}} \\ \overline{Q_{16}} & \overline{Q_{26}} & \overline{Q_{66}} \end{bmatrix} \begin{Bmatrix} \varepsilon_x^0 \\ \varepsilon_y^0 \\ \gamma_{xy}^0 \end{Bmatrix} dz + \sum_{j=1}^N \int_{h_{j-1}}^{h_j} \begin{bmatrix} \overline{Q_{11}} & \overline{Q_{12}} & \overline{Q_{16}} \\ \overline{Q_{12}} & \overline{Q_{22}} & \overline{Q_{26}} \\ \overline{Q_{16}} & \overline{Q_{26}} & \overline{Q_{66}} \end{bmatrix} \begin{Bmatrix} k_x \\ k_y \\ k_{xy} \end{Bmatrix} z dz$$

$$\begin{Bmatrix} M_x \\ M_y \\ M_{xy} \end{Bmatrix} = \sum_{j=1}^N \int_{h_{j-1}}^{h_j} \begin{bmatrix} \overline{Q_{11}} & \overline{Q_{12}} & \overline{Q_{16}} \\ \overline{Q_{12}} & \overline{Q_{22}} & \overline{Q_{26}} \\ \overline{Q_{16}} & \overline{Q_{26}} & \overline{Q_{66}} \end{bmatrix} \begin{Bmatrix} \varepsilon_x^0 \\ \varepsilon_y^0 \\ \gamma_{xy}^0 \end{Bmatrix} z dz + \sum_{j=1}^N \int_{h_{j-1}}^{h_j} \begin{bmatrix} \overline{Q_{11}} & \overline{Q_{12}} & \overline{Q_{16}} \\ \overline{Q_{12}} & \overline{Q_{22}} & \overline{Q_{26}} \\ \overline{Q_{16}} & \overline{Q_{26}} & \overline{Q_{66}} \end{bmatrix} \begin{Bmatrix} k_x \\ k_y \\ k_{xy} \end{Bmatrix} z^2 dz$$

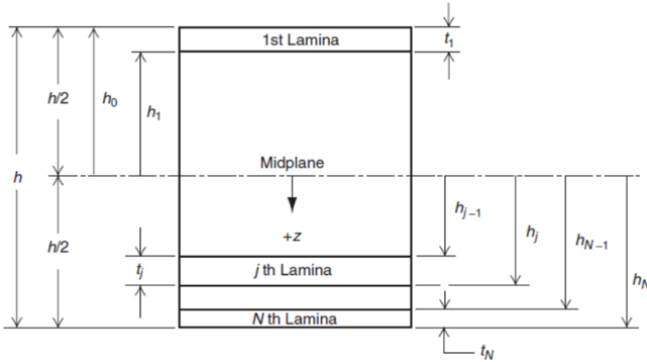


Figure 23: Laminate's N-th Lamina and distances from the midplane.

$$\int_{h_{j-1}}^{h_j} dz = h_j - h_{j-1} \quad (4.70)$$

$$\int_{h_{j-1}}^{h_j} z dz = \frac{h_j^2 - h_{j-1}^2}{2} \quad (4.71)$$

$$\int_{h_{j-1}}^{h_j} z^2 dz = \frac{h_j^3 - h_{j-1}^3}{3} \quad (4.72)$$

Obtaining (4.73 and 4.74):

$$\begin{Bmatrix} N_x \\ N_y \\ N_{xy} \end{Bmatrix} = \sum_{j=1}^N (h_j - h_{j-1}) \begin{bmatrix} \overline{Q_{11}} & \overline{Q_{12}} & \overline{Q_{16}} \\ \overline{Q_{12}} & \overline{Q_{22}} & \overline{Q_{26}} \\ \overline{Q_{16}} & \overline{Q_{26}} & \overline{Q_{66}} \end{bmatrix} \begin{Bmatrix} \varepsilon_x^0 \\ \varepsilon_y^0 \\ \gamma_{xy}^0 \end{Bmatrix} + \sum_{j=1}^N \frac{h_j^2 - h_{j-1}^2}{2} \begin{bmatrix} \overline{Q_{11}} & \overline{Q_{12}} & \overline{Q_{16}} \\ \overline{Q_{12}} & \overline{Q_{22}} & \overline{Q_{26}} \\ \overline{Q_{16}} & \overline{Q_{26}} & \overline{Q_{66}} \end{bmatrix} \begin{Bmatrix} k_x \\ k_y \\ k_{xy} \end{Bmatrix}$$

$$\begin{Bmatrix} M_x \\ M_y \\ M_{xy} \end{Bmatrix} = \sum_{j=1}^N \frac{h_j^2 - h_{j-1}^2}{2} \begin{bmatrix} \overline{Q_{11}} & \overline{Q_{12}} & \overline{Q_{16}} \\ \overline{Q_{12}} & \overline{Q_{22}} & \overline{Q_{26}} \\ \overline{Q_{16}} & \overline{Q_{26}} & \overline{Q_{66}} \end{bmatrix} \begin{Bmatrix} \varepsilon_x^0 \\ \varepsilon_y^0 \\ \gamma_{xy}^0 \end{Bmatrix} + \sum_{j=1}^N \frac{h_j^3 - h_{j-1}^3}{3} \begin{bmatrix} \overline{Q_{11}} & \overline{Q_{12}} & \overline{Q_{16}} \\ \overline{Q_{12}} & \overline{Q_{22}} & \overline{Q_{26}} \\ \overline{Q_{16}} & \overline{Q_{26}} & \overline{Q_{66}} \end{bmatrix} \begin{Bmatrix} k_x \\ k_y \\ k_{xy} \end{Bmatrix}$$

$$\begin{Bmatrix} N_x \\ N_y \\ N_{xy} \end{Bmatrix} = \begin{bmatrix} A_{11} & A_{12} & A_{16} \\ A_{12} & A_{22} & A_{26} \\ A_{16} & A_{26} & A_{66} \end{bmatrix} \begin{Bmatrix} \varepsilon_x^0 \\ \varepsilon_y^0 \\ \gamma_{xy}^0 \end{Bmatrix} + \begin{bmatrix} B_{11} & B_{12} & B_{16} \\ B_{12} & B_{22} & B_{26} \\ B_{16} & B_{26} & B_{66} \end{bmatrix} \begin{Bmatrix} k_x \\ k_y \\ k_{xy} \end{Bmatrix} \quad (4.75)$$

$$\begin{Bmatrix} M_x \\ M_y \\ M_{xy} \end{Bmatrix} = \begin{bmatrix} B_{11} & B_{12} & B_{16} \\ B_{12} & B_{22} & B_{26} \\ B_{16} & B_{26} & B_{66} \end{bmatrix} \begin{Bmatrix} \varepsilon_x^0 \\ \varepsilon_y^0 \\ \gamma_{xy}^0 \end{Bmatrix} + \begin{bmatrix} D_{11} & D_{12} & D_{16} \\ D_{12} & D_{22} & D_{26} \\ D_{16} & D_{26} & D_{66} \end{bmatrix} \begin{Bmatrix} k_x \\ k_y \\ k_{xy} \end{Bmatrix} \quad (4.76)$$

Shortly written as:

$$\begin{Bmatrix} N \\ M \end{Bmatrix} = \begin{bmatrix} A & B \\ B & D \end{bmatrix} \begin{Bmatrix} \varepsilon^0 \\ k \end{Bmatrix} \quad (4.77)$$

Considerations about extensional matrix [A]:

- For a given resultant force, mid-plane strains decrease as elements of this matrix increase in magnitude.
- Magnitude of extensional stiffness increases directly in proportion to the thickness of each layer, since  $(h_j - h_{j-1})$  equals thickness of  $k_{th}$  lamina.
- If terms  $A_{16}$  and  $A_{26}$  are different from zero means an extensional force will generate not only extensional strain but shear strain as well; similarly shear forces will generate not only shear strain in the laminate but extensional strain as well.

Considerations about coupling matrix [B]:

- If the magnitude of this matrix is non-zero, then a composite laminate will exhibit bending and twisting, even if external moment on it is perfectly zero; also the composite will exhibit extensional and shear strains even if external forces on it are zero.
- Laminates are carefully engineered to ensure that all elements of B are zero.

Considerations about bending matrix [D]:

- The bigger the magnitude of [D] the lower the curvature generate by a unit bending moment.

- Terms  $D_{16}$  and  $D_{26}$  couple bending and twisting. If either of these terms is non-zero, then, a pure moment will generate not only bending curvature but twist curvature as well; vice-versa for a pure torque.

### Thermal stresses and strains in a laminate

Mechanical and thermal strains in the  $j$ -th lamina are the sum of the two contributions:

$$\begin{Bmatrix} \varepsilon_x \\ \varepsilon_y \\ \gamma_{xy} \end{Bmatrix} = \begin{Bmatrix} \varepsilon_x \\ \varepsilon_y \\ \gamma_{xy} \end{Bmatrix}^M + \begin{Bmatrix} \varepsilon_x \\ \varepsilon_y \\ \gamma_{xy} \end{Bmatrix}^{\Delta T} \quad (4.78)$$

$$\begin{Bmatrix} \varepsilon_x \\ \varepsilon_y \\ \gamma_{xy} \end{Bmatrix} = \begin{Bmatrix} \varepsilon_x^0 \\ \varepsilon_y^0 \\ \gamma_{xy}^0 \end{Bmatrix} + z \begin{Bmatrix} k_x \\ k_y \\ k_{xy} \end{Bmatrix} \quad (4.79)$$

$$\begin{Bmatrix} \varepsilon_x \\ \varepsilon_y \\ \gamma_{xy} \end{Bmatrix}^{\Delta T} = [R][T]^{-1}[R]^{-1} \begin{Bmatrix} \varepsilon_1 \\ \varepsilon_2 \\ \gamma_{12} \end{Bmatrix}^{\Delta T} = [R][T]^{-1}[R]^{-1} \begin{Bmatrix} \alpha_1 \\ \alpha_2 \\ 0 \end{Bmatrix} \Delta T = \begin{Bmatrix} \alpha_x \\ \alpha_y \\ \alpha_{xy} \end{Bmatrix} \Delta T \quad (4.80)$$

$$\begin{Bmatrix} \varepsilon_x \\ \varepsilon_y \\ \gamma_{xy} \end{Bmatrix}^M = \begin{Bmatrix} \varepsilon_x^0 \\ \varepsilon_y^0 \\ \gamma_{xy}^0 \end{Bmatrix} + z \begin{Bmatrix} k_x \\ k_y \\ k_{xy} \end{Bmatrix} - \Delta T \begin{Bmatrix} \alpha_x \\ \alpha_y \\ \alpha_{xy} \end{Bmatrix} \quad (4.81)$$

From the strains the passage to the stresses is straightforward:

$$\begin{Bmatrix} \sigma_x \\ \sigma_y \\ \gamma_{xy} \end{Bmatrix}^M = \begin{bmatrix} \overline{Q_{11}} & \overline{Q_{12}} & \overline{Q_{16}} \\ \overline{Q_{12}} & \overline{Q_{22}} & \overline{Q_{26}} \\ \overline{Q_{16}} & \overline{Q_{26}} & \overline{Q_{66}} \end{bmatrix} \left( \begin{Bmatrix} \varepsilon_x^0 \\ \varepsilon_y^0 \\ \gamma_{xy}^0 \end{Bmatrix} + z \begin{Bmatrix} k_x \\ k_y \\ k_{xy} \end{Bmatrix} - \Delta T \begin{Bmatrix} \alpha_x \\ \alpha_y \\ \alpha_{xy} \end{Bmatrix} \right) \quad (4.82)$$

Mechanical force in the laminate if only the  $\Delta T$  is applied are zero so we can express the thermal forces in the laminate can be expressed as:

$$\begin{Bmatrix} N_x \\ N_y \\ N_{xy} \end{Bmatrix}^{\Delta T} = \Delta T \sum_{j=1}^N \begin{bmatrix} \overline{Q_{11}} & \overline{Q_{12}} & \overline{Q_{16}} \\ \overline{Q_{12}} & \overline{Q_{22}} & \overline{Q_{26}} \\ \overline{Q_{16}} & \overline{Q_{26}} & \overline{Q_{66}} \end{bmatrix} \begin{Bmatrix} \alpha_x \\ \alpha_y \\ \alpha_{xy} \end{Bmatrix} (h_j - h_{j-1}) \quad (4.83)$$

Coupling with strains:

$$\begin{Bmatrix} N_x \\ N_y \\ N_{xy} \end{Bmatrix}^{\Delta T} = \begin{bmatrix} A_{11} & A_{12} & A_{16} \\ A_{12} & A_{22} & A_{26} \\ A_{16} & A_{26} & A_{66} \end{bmatrix} \begin{Bmatrix} \varepsilon_x^0 \\ \varepsilon_y^0 \\ \gamma_{xy}^0 \end{Bmatrix} + \begin{bmatrix} B_{11} & B_{12} & B_{16} \\ B_{12} & B_{22} & B_{26} \\ B_{16} & B_{26} & B_{66} \end{bmatrix} \begin{Bmatrix} k_x \\ k_y \\ k_{xy} \end{Bmatrix} \quad (4.84)$$

The mechanical moments in the laminate if only  $\Delta T$  is applied are zero so the thermal moments in the laminate are:

$$\begin{Bmatrix} M_x \\ M_y \\ M_{xy} \end{Bmatrix}^{\Delta T} = \Delta T \sum_{j=1}^N \begin{bmatrix} \overline{Q_{11}} & \overline{Q_{12}} & \overline{Q_{16}} \\ \overline{Q_{12}} & \overline{Q_{22}} & \overline{Q_{26}} \\ \overline{Q_{16}} & \overline{Q_{26}} & \overline{Q_{66}} \end{bmatrix} \begin{Bmatrix} \alpha_x \\ \alpha_y \\ \alpha_{xy} \end{Bmatrix} \frac{h_j^2 - h_{j-1}^2}{2} \quad (4.85)$$

Coupling with strains:

$$\begin{Bmatrix} M_x \\ M_y \\ M_{xy} \end{Bmatrix}^{\Delta T} = \begin{bmatrix} B_{11} & B_{12} & B_{16} \\ B_{12} & B_{22} & B_{26} \\ B_{16} & B_{26} & B_{66} \end{bmatrix} \begin{Bmatrix} \varepsilon_x^0 \\ \varepsilon_y^0 \\ \gamma_{xy}^0 \end{Bmatrix} + \begin{bmatrix} D_{11} & D_{12} & D_{16} \\ D_{12} & D_{22} & D_{26} \\ D_{16} & D_{26} & D_{66} \end{bmatrix} \begin{Bmatrix} k_x \\ k_y \\ k_{xy} \end{Bmatrix} \quad (4.86)$$

So, the thermal strains in the laminate can be expressed as:

$$\begin{Bmatrix} \varepsilon^0 \\ k \end{Bmatrix}^{\Delta T} = \begin{bmatrix} A^* & B^* \\ B^* & D^* \end{bmatrix} \begin{Bmatrix} N \\ M \end{Bmatrix}^{\Delta T} \quad (4.87)$$

$$\begin{bmatrix} A^* & B^* \\ B^* & D^* \end{bmatrix} = \begin{bmatrix} A & B \\ B & D \end{bmatrix}^{-1} \quad (4.88)$$

$$\begin{Bmatrix} \varepsilon_x \\ \varepsilon_y \\ \gamma_{xy} \end{Bmatrix}^{\Delta T} = \begin{Bmatrix} \varepsilon_x^0 \\ \varepsilon_y^0 \\ \gamma_{xy}^0 \end{Bmatrix}^{\Delta T} + \begin{Bmatrix} k_x \\ k_y \\ k_{xy} \end{Bmatrix}^{\Delta T} \quad (4.89)$$

The residual thermal strains and stresses in the j-th lamina is given by the subtraction of the actual strains of the j-th lamina and the free stains that would have happened in the lamina if it would be free to expand.

$$\begin{Bmatrix} \varepsilon_x \\ \varepsilon_y \\ \gamma_{xy} \end{Bmatrix}_j^{\Delta T_{res}} = \begin{Bmatrix} \varepsilon_x \\ \varepsilon_y \\ \gamma_{xy} \end{Bmatrix}_j^{\Delta T} - \Delta T \begin{Bmatrix} \alpha_x \\ \alpha_y \\ \alpha_{xy} \end{Bmatrix}_j \quad (4.90)$$

$$\begin{Bmatrix} \sigma_x \\ \sigma_y \\ \tau_{xy} \end{Bmatrix}_j^{\Delta T_{res}} = \begin{bmatrix} \overline{Q_{11}} & \overline{Q_{12}} & \overline{Q_{16}} \\ \overline{Q_{12}} & \overline{Q_{22}} & \overline{Q_{26}} \\ \overline{Q_{16}} & \overline{Q_{26}} & \overline{Q_{66}} \end{bmatrix}_j \begin{Bmatrix} \varepsilon_x \\ \varepsilon_y \\ \gamma_{xy} \end{Bmatrix}_j^{\Delta T_{res}} \quad (4.91)$$



## Composites lamination: vacuum bag method

The vacuum bag infusion technique is a popular technique for fabricating high-quality composite laminates. This method involves placing the fiber fabric layup into a vacuum bag to obtain the vacuum and then carrying out the resin infusion.

A description of the manufacturing processes used to fabricate the laminates used in the work is provided below:

- Depending on the thickness needed, an appropriate number of fiber layers should be cut according to the dimensions of the mold.
- Clean the mold, ensuring that the mold surface is clean, smooth, and free from any debris.
- Apply a mold release agent to ensure the laminate can be easily removed from the mold once cured.
- Layup Layers (Figure 24): Lay the composite fabric onto the mold, layer by layer, according to the design specifications. In this case we had 2x2 woven configuration for all composites.

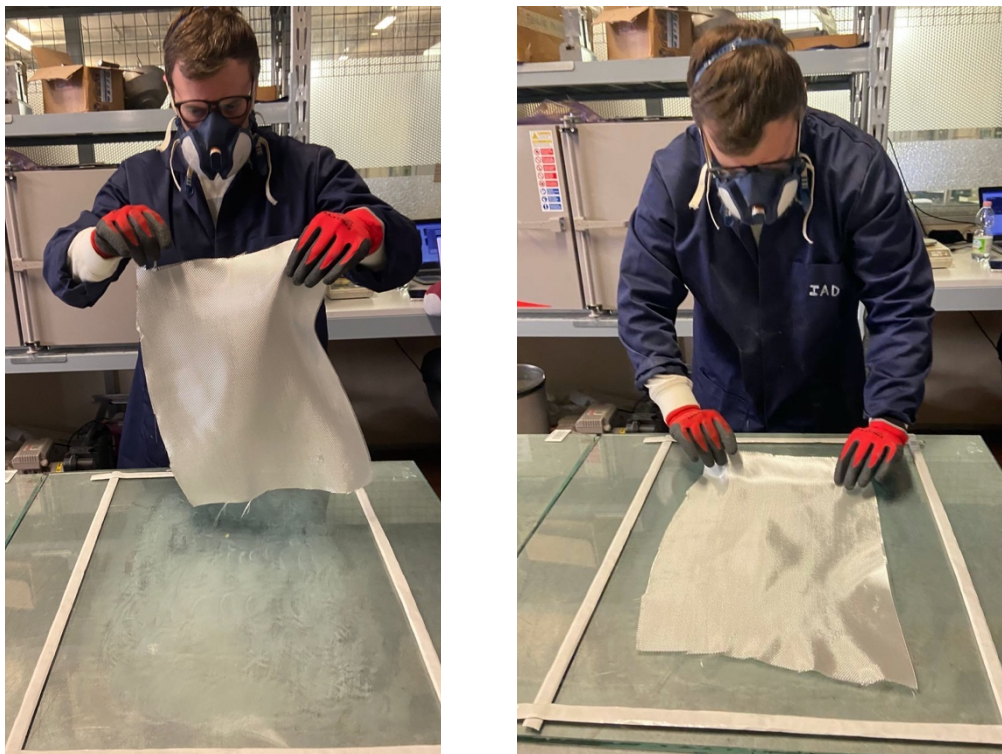


*Figure 24: Layup Layers*

- Flow mesh: Place the mesh cloth over the release fabric. This material allows air and resin to flow from inlet to outlet valves.
- Apply sealant tape around the perimeter of the mold, ensuring there are no gaps.

- Cut the vacuum bag film to size and place it over the entire layup and mold. Press the edges of the bag onto the sealant tape to create an airtight seal.
- Attach the vacuum port to the bag and connect it to the vacuum pump using tubes (Figure 25)

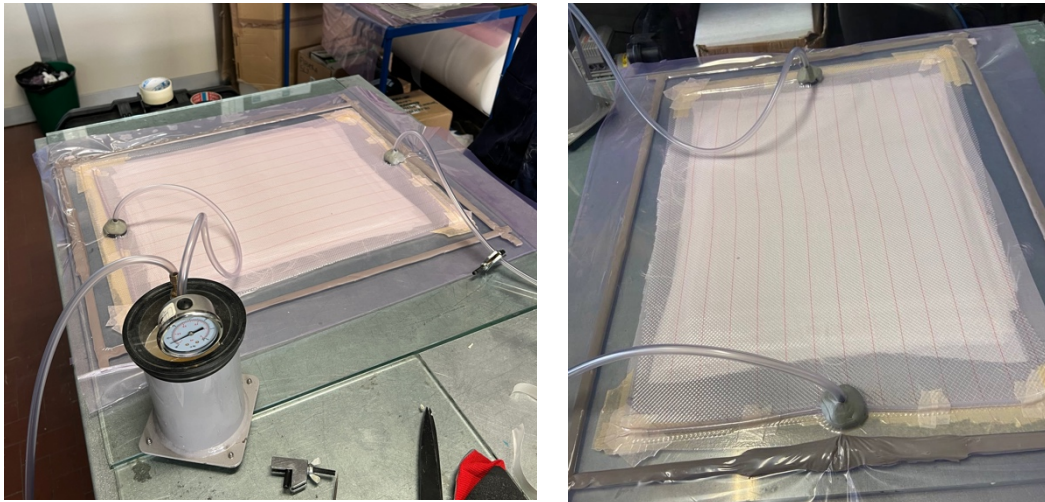


*Figure 25: Layers covered by the sealed vacuum bag*

- Evacuate Air: Turn on the vacuum pump and evacuate the air from the vacuum bag, monitoring the vacuum gauge to ensure proper vacuum pressure is achieved.
- Monitor for 5-10 min that the vacuum gauge pressure does not change, in order to understand if the bag has some leakages due to the sealant or it's damaged.
- Mix the resin with the hardener according to the specifications of the producer and by using the vacuum pump eliminate any possible air trapped inside during the mixing process (Figure 26).



*Figure 26: Mixing the resin with the hardener*

- From one side of the bag use one of the tubes to blow the resin inside the bag wetting the fibers.
- Cure the Laminate: allow the laminate to cure as per the resin manufacturer's instructions. This may involve room temperature curing or elevated temperature curing in an oven. For this thesis a room temperature curing of 24 h plus a 4h at 90 °C has been implemented.
- Remove the Vacuum Bag and demold the part: once the laminate is fully cured, carefully remove the vacuum bag, breather cloth, and demold the part. The oven curing can start at this point.



*Figure 27: Curing oven (left) and final result of the lamination (right)*

After the curing process the composite is ready to be cut according to the dimensions needed for the tests. In the case of this thesis the composites had general dimensions of 150x30x(3.5-4) mm.

## Types of composites

In this thesis, four types of composites were laminated using the vacuum technique method:

- Woven glass fiber with 30% natural epoxy resin
- Woven glass fiber with a traditional epoxy resin.
- Woven carbon fiber with traditional epoxy resin
- Woven flax fiber with traditional epoxy resin

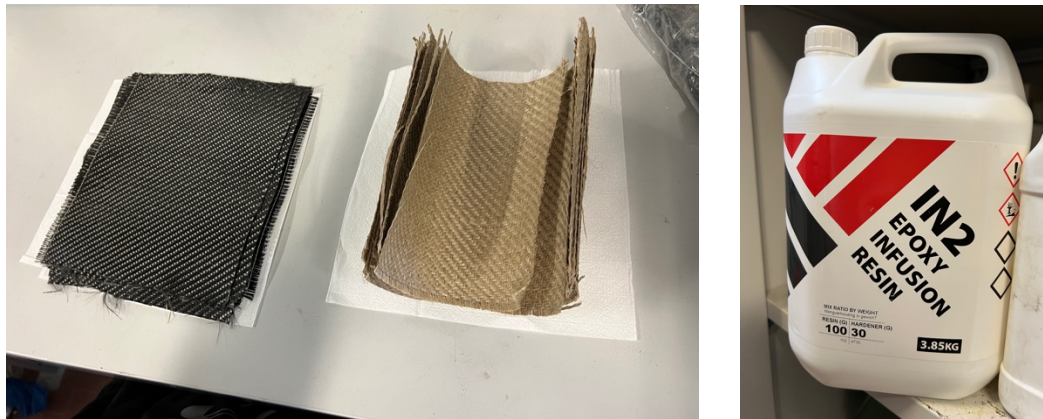


*Figure 28: Carbon and Flax fibers (left) epoxy infusion resin (right)*

In this study the theoretical geometry of each specimen after the cutting process using the sand water jet machine is  $150 \times 30 \times (3.5 \div 4)$  mm.

## 5. Evaluation of specimen mechanical properties

The four types of composites have been tested in the RFDA-HT1600 machine. Each specimen was located on two supports depending on the configuration tested: flexural or torsional. Under the specimen there was located an impulse device that hits the specimen exciting it and making it vibrate or better exciting all its modes (or most of them). Above the specimen, a special microphone is located, for detecting and capturing the vibrations of the specimen [7].

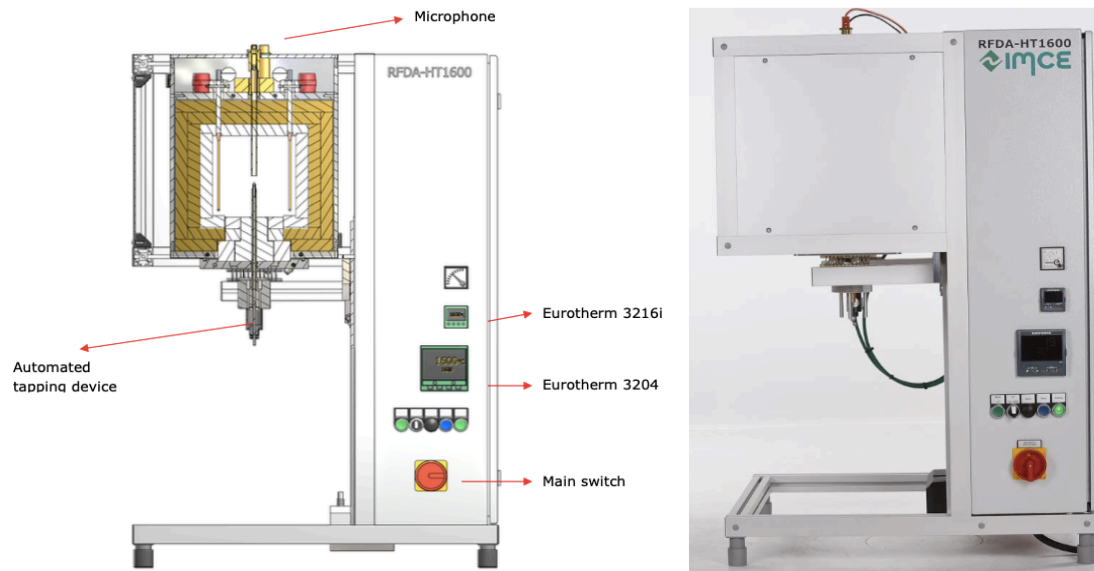


Figure 29: Impulse excitation machine RFDA-HT 1600 IMCE

The tests have been performed at different temperatures: 25°C, 40°C, 60°C, 80°C thanks to the Eurotherm programs of the machine.

The general block diagram followed by the machine and acquisition system is illustrated in figure 31.

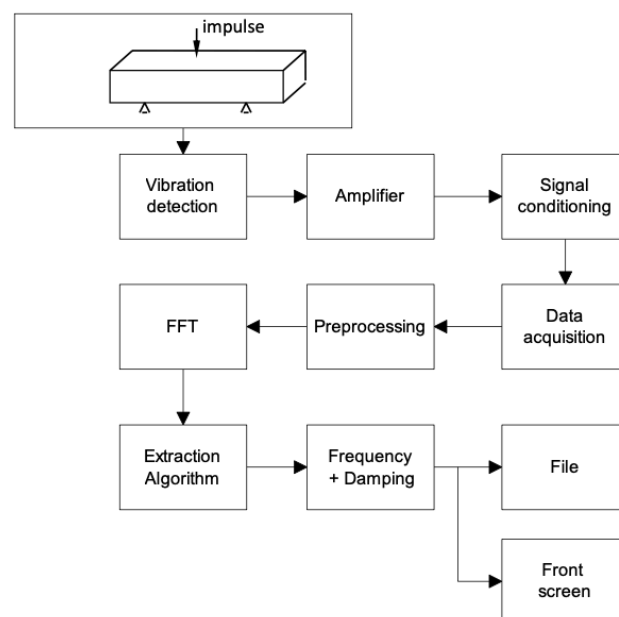


Figure 30: Block diagram of the machine

## Settings of the software

In the software of the machine, it is possible to set the specific parameters of the specimen and of the acquisition system. First information to insert are: the mass of the specimen, the geometry, the distance of the nodes, the Poisson's ratio and the modes tested: flexural or torsional (Figure 31).

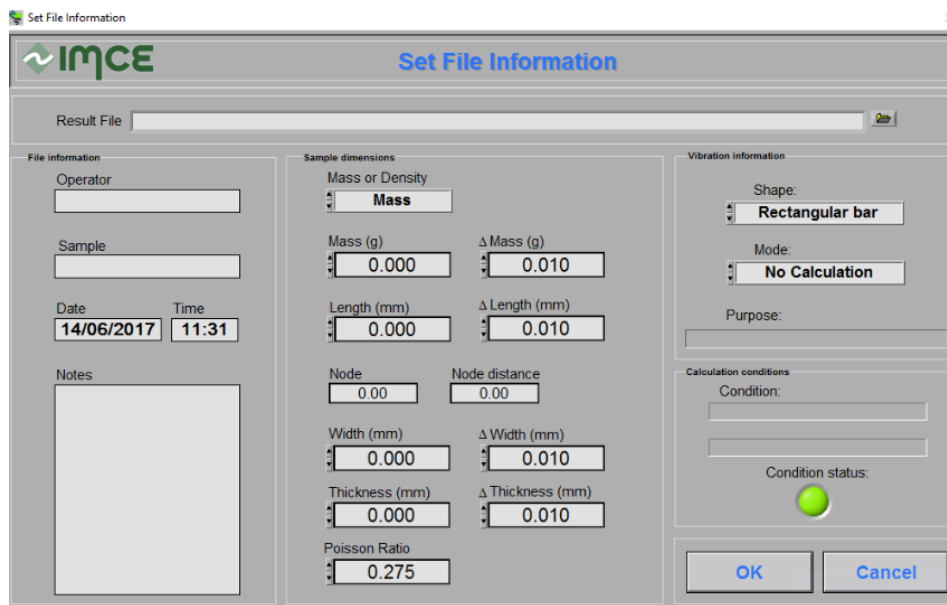


Figure 31: Characteristics of the specimen and mode to be calculated

For the acquisition system there are some specific settings; i) the sampling rate, depending on the biggest natural frequency needed to be evaluated; ii) the channel to be used for the acquisition; iii) the maximum measured time; iv) the trigger level in volts; v) the interval of time after which another impulse will take place; vi) the power of the impulse. In case one is interested in some portions of the signal, there is the possibility of inserting a filter having (according to the type of filter) low or high cut-off frequency.

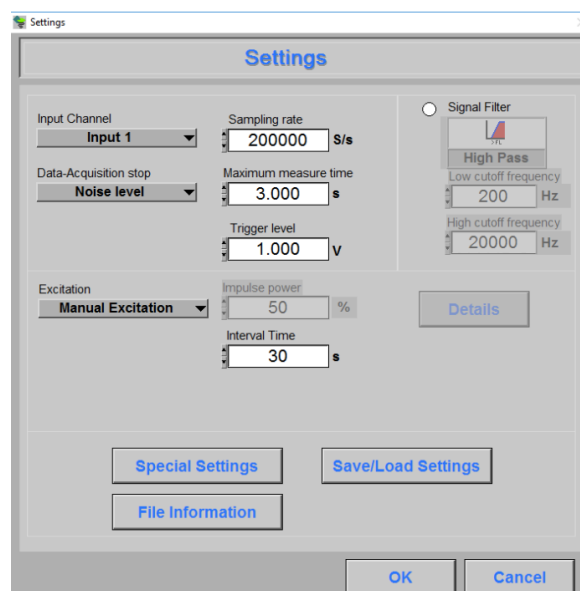


Figure 32: Sampling frequency and possible filters for the signal

Other special settings regard the number of points used for the FFT (fast Fourier transform) or the upper and lower limit of the signal in percentage used to evaluate the FFT.

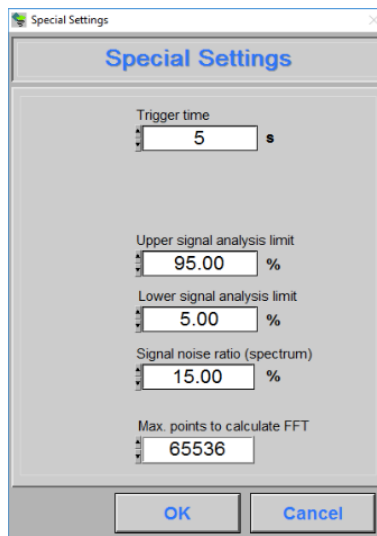


Figure 33: Trigger time repeated impulses and max points to calculate the FFT

The results of the test are the graph of the signal decay, the FFT graph (spectrum) showing all the peaks representing the natural frequencies of the structure, the loss rate and the damping coefficient. The software also calculates the modulus (E or G), depending on the configuration that has been chosen.

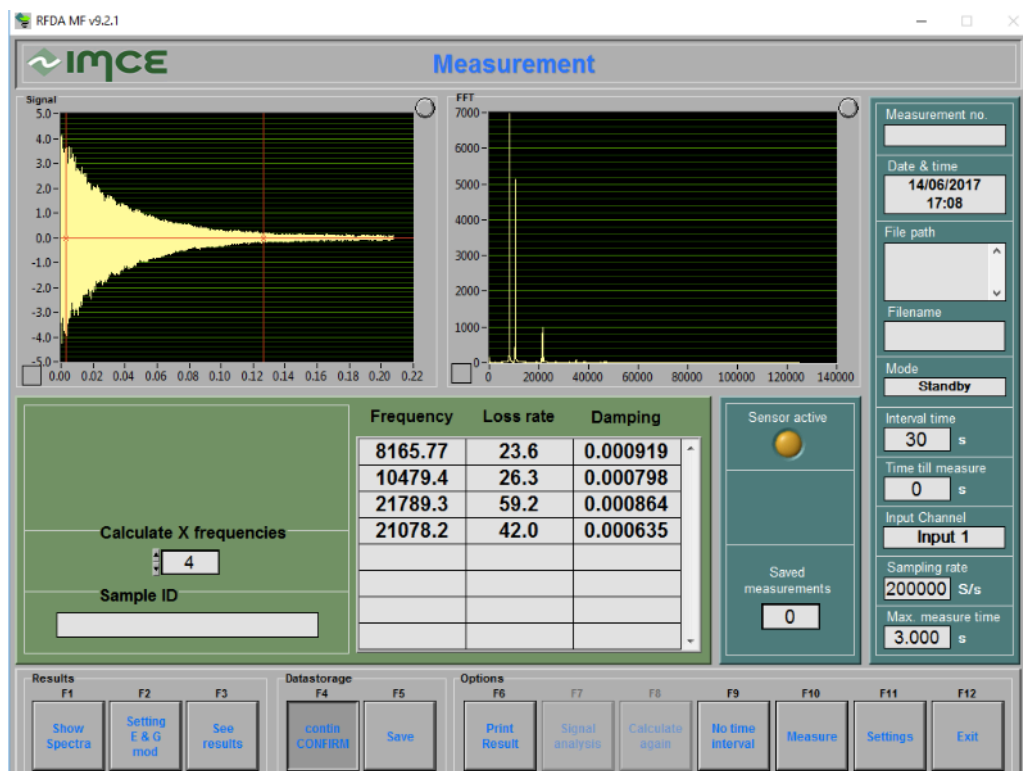


Figure 34: General window of results

## Results of the thin glass fibre with epoxy 30% natural resin

After performing the impulse excitation tests at different temperatures on the composite in flexural and torsional configuration it was possible to calculate according to the standard ASTM E1876-21, the elastic modulus  $E_1$  and  $G_{12}$ .

In table 3 it can be seen the natural frequencies and damping coefficient at the different temperatures.

Table 3: Thin glass fiber composite first and second natural frequencies at different temperature

Natural flexural frequency (Hz)	Natural torsional frequency (Hz)	Damping coefficient (flexural)	Damping coefficient (torsional)	Temperature (°C)
571.35	1092.6	0.0262	0.0359	25
567.68	1059.67	0.0291	0.0306	40
559.15	994.24	0.0246	0.04	60
505.72	728.33	0.1349	0.06	80

In figure 35 and 36 it can be observed a typical spectrum in flexural and torsional configuration having on the abscissa the frequency in Hz and on the ordinate the amplitude in a linear scale.

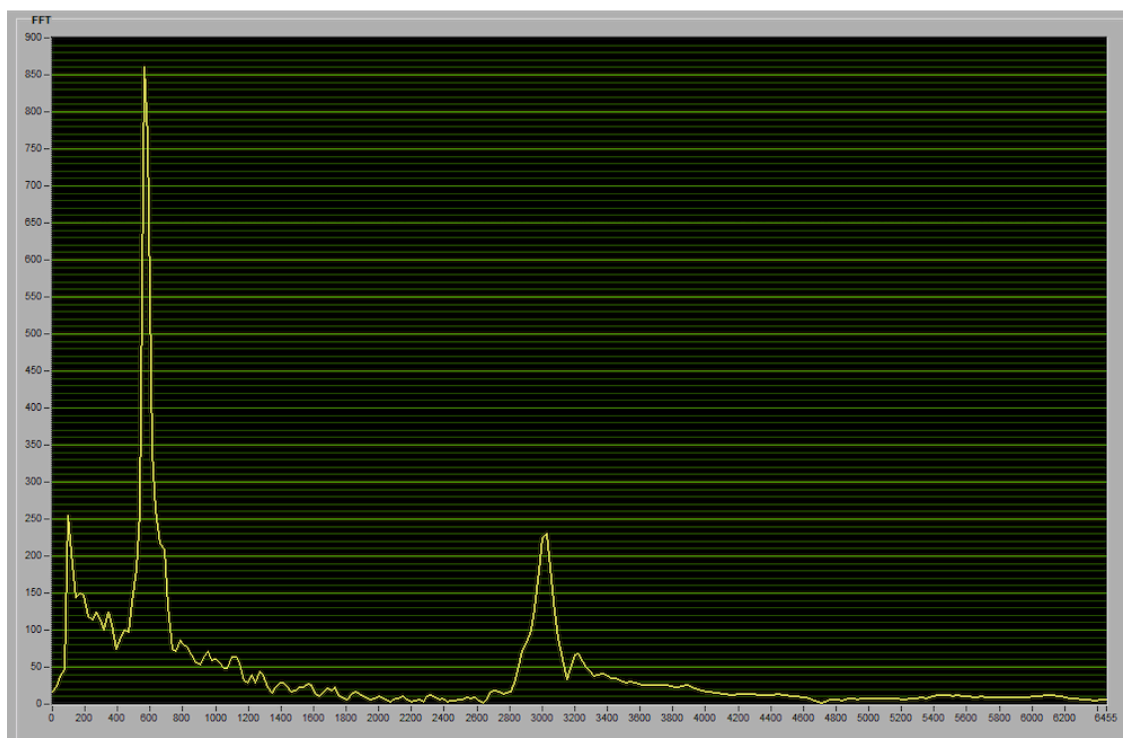


Figure 35: Spectrum of Thin glass in flexural configuration



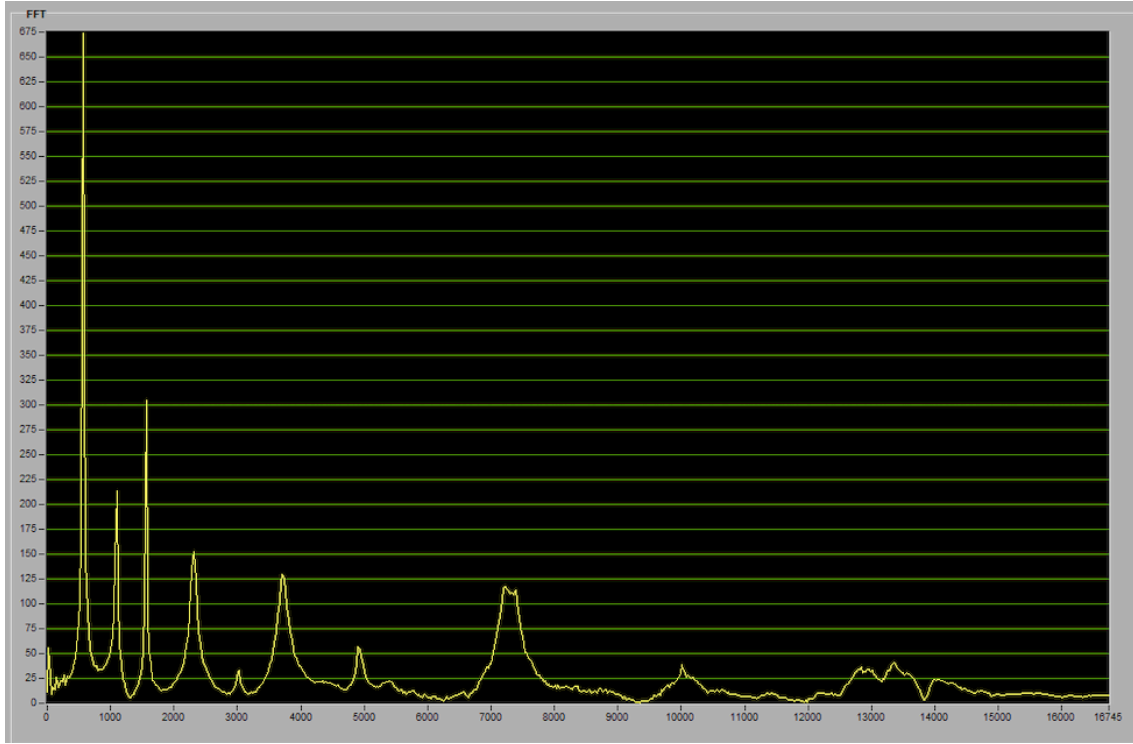


Figure 36: Spectrum of Thin glass in torsional configuration

It can be calculated, starting from the natural frequencies and geometry of the specimen, the elastic modulus  $E_1$  and shear modulus  $G_{12}$  according to the formulas [8]:

$$E = 0.9465 \left( \frac{m f_f^2}{b} \right) \left( \frac{L^3}{t^3} \right) T_1 \quad (5.0)$$

Where  $T_1$  is a correction factor that if  $L/t > 20$ , it is equal to:

$$T_1 = \left[ 1 + 6.585 \left( \frac{t}{L} \right)^2 \right] \quad (5.1)$$

$$G = \frac{4 L m f_t^2}{b t} R \quad (5.2)$$

Where R is a correction factor:

$$R = \left[ \frac{(1 + \left(\frac{b}{t}\right)^2)}{4 - 2.521 \frac{t}{b} \left(1 - \frac{1.991}{e^{\frac{b}{t}} + 1}\right)} \right] \left[ 1 + \frac{0.00851 n^2 b^2}{L^2} \right] - 0.060 \left(\frac{nb}{L}\right)^{\frac{3}{2}} \left(\frac{b}{t} - 1\right)^2 \quad (5.3)$$

Where each parameter is:

E = Young modulus [GPa]

G= shear modulus [GPa]

m = mass [g]

$f_s$  or  $f_t$  = flexural or torsional natural frequency [Hz]

b = width of sample [mm]

L = length of sample [mm]

t = thickness of sample [mm]

n = order of the resonance

In table 4 it can be seen the results of this equations:

Table 4: Thin glass fiber composite elastic moduli at different temperatures

Elastic modulus $E_1$ (GPa)	Shear modulus $G_{12}$ (GPa)	Temperature (°C)
21.47	3.27	25
21.15	3.07	40
20.46	2.69	60
16.69	1.44	80

In order to have a better overview on what it's happening, it can be seen in table 5 the increase or decrease in percentage of the elastic modulus  $E_1$ , shear modulus  $G_{12}$  and the damping coefficients [9] [10] [11].

Table 5: percentage variation of elastic moduli and damping coefficient with respect to the room temperature values

Elastic modulus $E_1$ variation %	Shear modulus $G_{12}$ variation %	Damping coefficient % (flexural)	Damping coefficient % (torsional)	Temperature (°C)
-1.49%	-6.13%	11.29%	-14.65%	40
-4.69%	-17.6%	-5.87%	11.42%	60
-22.26%	-55.89%	414.76%	67.13%	80

## Results of the thick glass fibre with epoxy resin

Starting again from the measurements of the natural frequencies in different configurations (flexural or torsional) it was possible to evaluate the elastic modulus  $E_1$  and shear modulus  $G_{12}$ . Let us see again in table n the values of natural frequencies and damping coefficients.

Table 6: Thick glass fibers composite first and second natural frequencies and damping at different temperature

Natural flexural frequency (Hz)	Natural torsional frequency (Hz)	Damping coefficient (flexural)	Damping coefficient (torsional)	Temperature (°C)
668.58	1338.26	0.00934	0.03067	25
664.49	1312.16	0.00812	0.02763	40
647.60	1243.89	0.01210	0.06485	60
606.87	1215.81	0.05306	0.05580	80

In figure 37 and 38 it can be observed a typical spectrum in flexural and torsional configuration having on the abscissa the frequency in Hz and on the ordinate the amplitude in a linear scale.

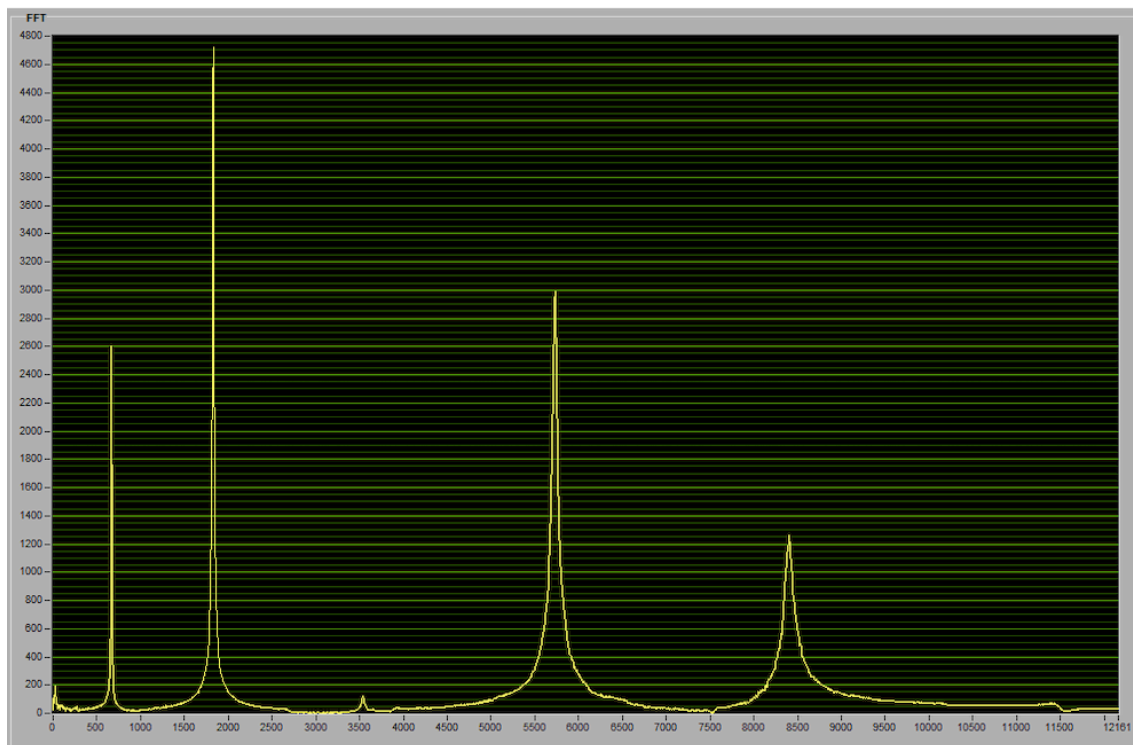


Figure 37: Spectrum of thick glass in flexural configuration

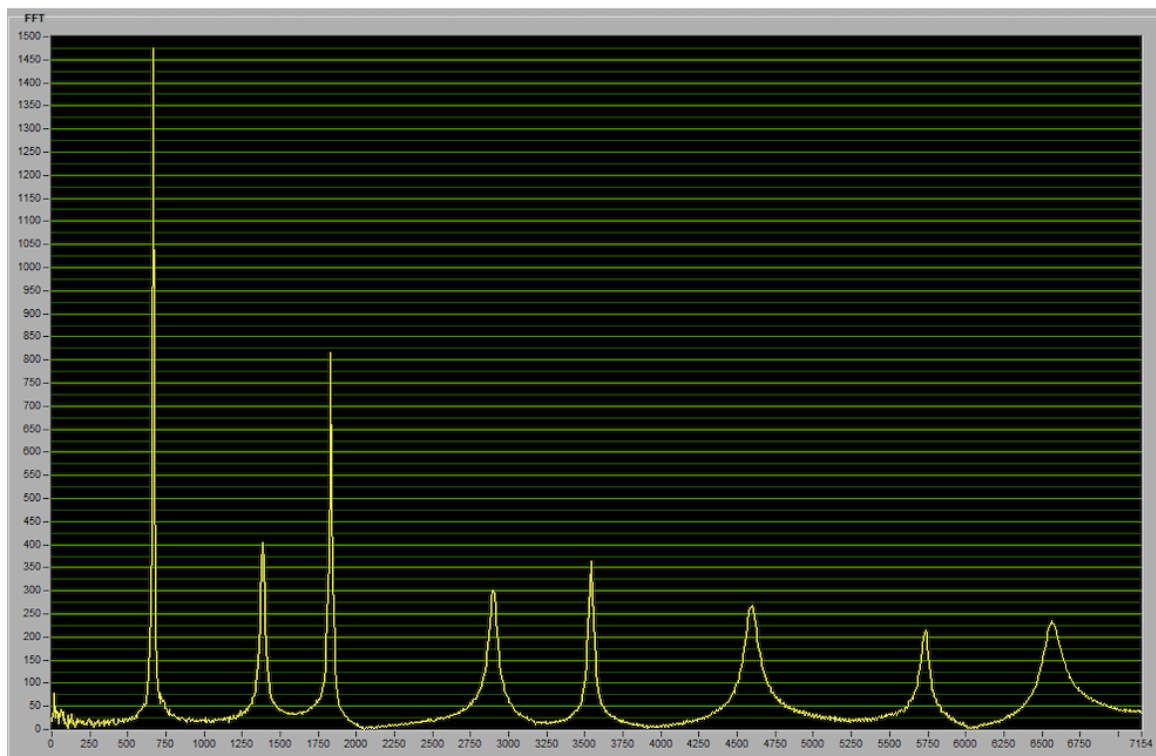


Figure 38: Spectrum of thick glass in torsional configuration

Using the same formulas of the standard, in table n it can be seen the results of  $E_1$  and  $G_{12}$ :

Table 7: Thick glass fiber composite elastic moduli at different temperature

Elastic modulus $E_1$ (GPa)	Shear modulus $G_{12}$ (GPa)	Temperature (°C)
22.24	3.62	25
21.92	3.47	40
20.75	3.11	60
18.15	2.96	80

In order to have a better overview on what it's happening, it can be seen in table n the increase or decrease in percentage of the elastic modulus  $E_1$ , shear modulus  $G_{12}$  and the damping coefficients.

Table 8: percentage variation of elastic moduli and damping coefficient with respect to the room temperature values

Elastic modulus $E_1$ variation %	Shear modulus $G_{12}$ variation %	Damping coefficient % (flexural)	Damping coefficient % (torsional)	Temperature (°C)
-1.47%	-4.09%	-13.06%	-9.91%	40
-6.73%	-14.07%	29.55%	111.44%	60
-18.38%	-18.20%	468.09%	81.94%	80

## Results of the carbon fibre with epoxy resin

Starting again from the measurements of the natural frequencies in different configurations (flexural or torsional) it was possible to evaluate the elastic modulus  $E_1$  and shear modulus  $G_{12}$ . Let us see again in table n the values of natural frequencies and damping coefficients.

Table 9: Carbon fiber composite first and second natural frequencies and damping coefficient at different temperatures

Natural flexural frequency (Hz)	Natural torsional frequency (Hz)	Damping coefficient (flexural)	Damping coefficient (torsional)	Temperature (°C)
1042.80	1388.77	0.0188	0.0222	25
1041.64	1357.02	0.0130	0.0296	40
1032.78	1314.08	0.0147	0.0382	60
1003.84	1308.93	0.0340	0.0398	80

In figure 39 and 40 it can be observed a typical spectrum in flexural and torsional configuration having on the abscissa the frequency in Hz and on the ordinate the amplitude in a linear scale.

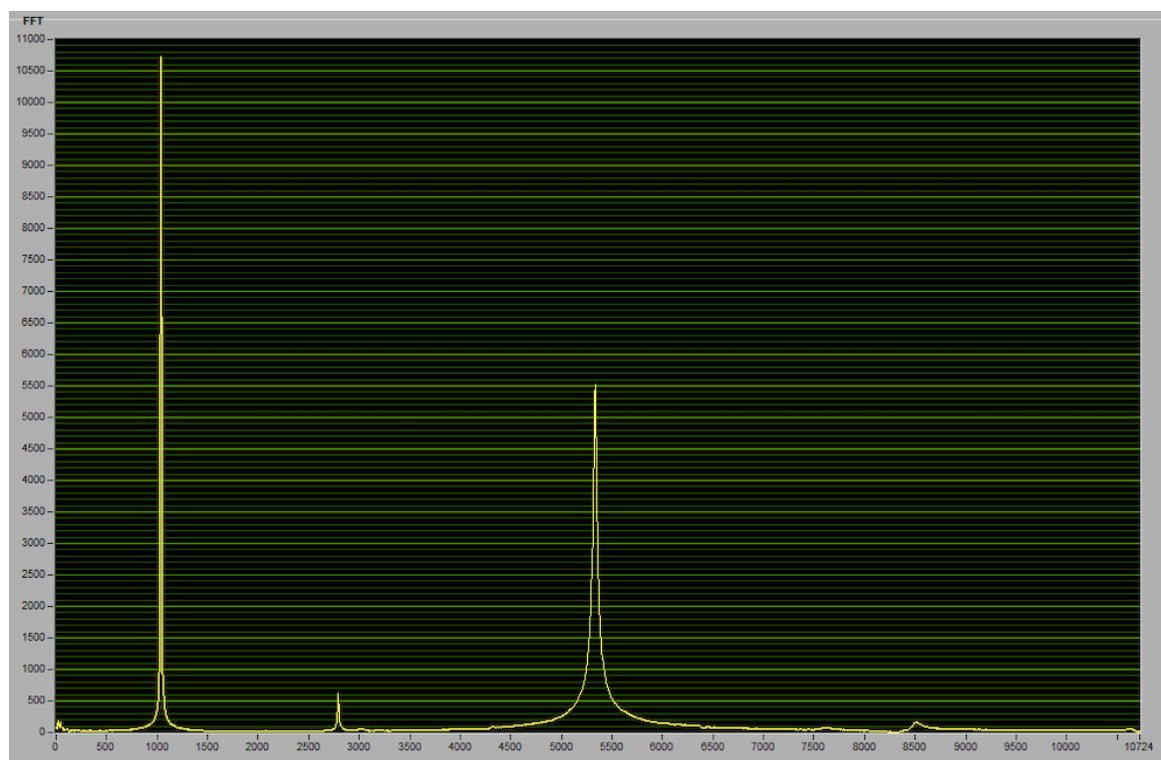


Figure 39: Spectrum of Carbon in flexural configuration

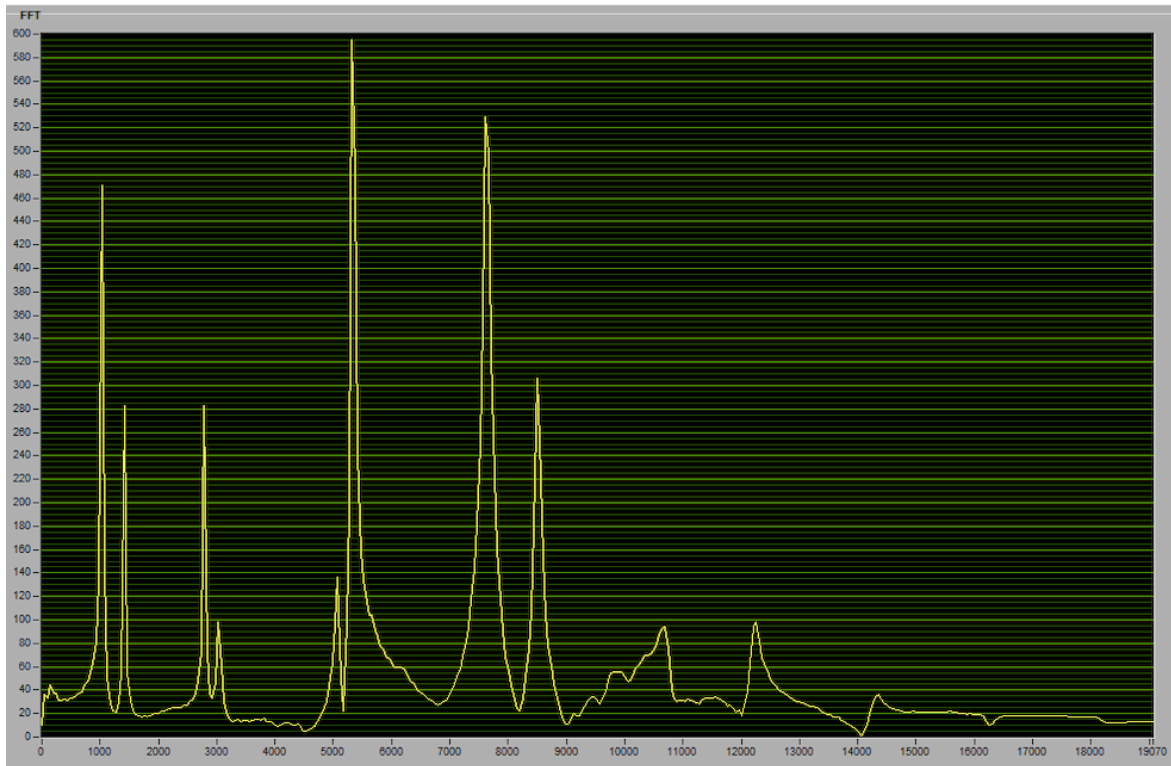


Figure 40: Spectrum of carbon in torsional configuration

Using the same formulas of the standard, in table n it can be seen the results of  $E_1$  and  $G_{12}$ :

Table 10: Carbon fiber composite elastic moduli at different temperatures

Elastic modulus $E_1$ (GPa)	Shear modulus $G_{12}$ (GPa)	Temperature (°C)
45.13	3.22	25
44.91	3.06	40
44.02	2.86	60
41.43	2.83	80

In order to have a better overview on what it's happening, it can be seen in table n the increase or decrease in percentage of the elastic modulus  $E_1$ , shear modulus  $G_{12}$  and the damping coefficients.

Table 11: : percentage variation of elastic moduli and damping coefficient with respect to the room temperature values

Elastic modulus $E_1$ variation %	Shear modulus $G_{12}$ variation %	Damping coefficient % (flexural)	Damping coefficient % (torsional)	Temperature (°C)
-0.51%	-4.78%	10.17%	32.85%	40
-2.47%	-10.94%	24.57%	71.36%	60
-8.19%	-11.94%	188.17%	78.95%	80

## Results of the flax fibre with epoxy resin

Using the measurements of the natural frequencies in different configurations (flexural or torsional) it was possible to evaluate the elastic modulus  $E_1$  and shear modulus  $G_{12}$ . Let us see again in table n the values of natural frequencies and damping coefficients.

Table 12: Flax fibers composite first and second natural frequencies and damping at different temperature

Natural flexural frequency (Hz)	Natural torsional frequency (Hz)	Damping coefficient (flexural)	Damping coefficient (torsional)	Temperature (°C)
534.37	962.02	0.0230	0.0388	25
521.24	923.64	0.0246	0.0330	40
488.49	825.07	0.0462	0.0427	60
380.26	679.10	0.0859	0.0678	80

In figure 41 and 42 it can be observed a typical spectrum in flexural and torsional configuration having on the abscissa the frequency in Hz and on the ordinate the amplitude in a linear scale.

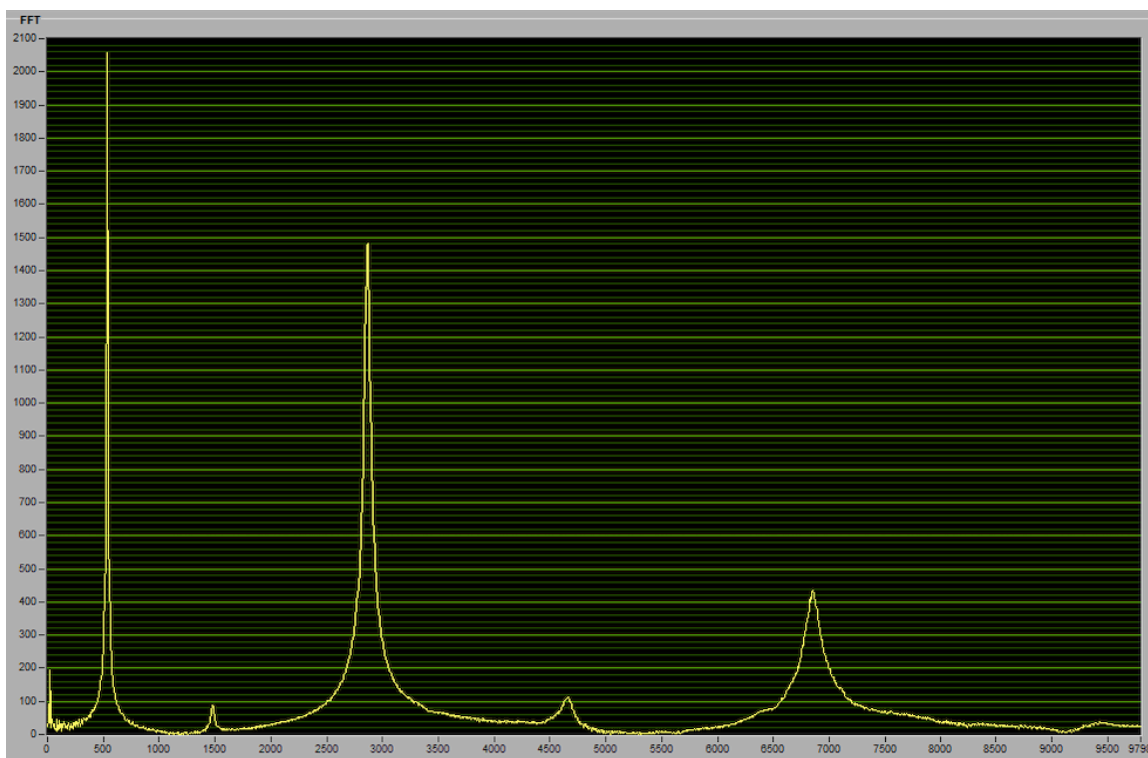


Figure 41: Spectrum of flax in flexural configuration

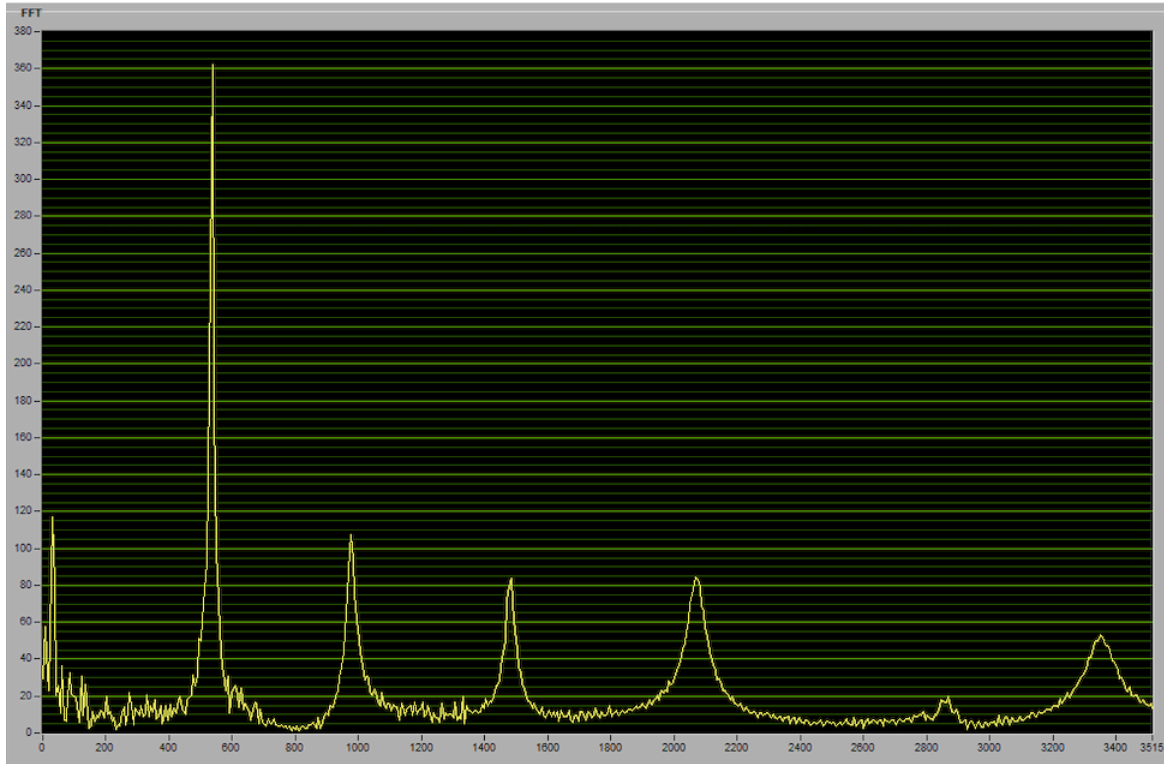


Figure 42: Spectrum of flax in torsional configuration

Using the same formulas of the standard, in table n it can be seen the results of  $E_1$  and  $G_{12}$ :

Table 13: Flax fiber composite elastic moduli at different temperatures

Elastic modulus $E_1$ (GPa)	Shear modulus $G_{12}$ (GPa)	Temperature (°C)
10.69	1.38	25
10.14	1.27	40
8.85	1.01	60
5.33	0.68	80

In order to have a better overview on what it's happening, it can be seen in table n the increase or decrease in percentage of the elastic modulus  $E_1$ , shear modulus  $G_{12}$  and the damping coefficients.

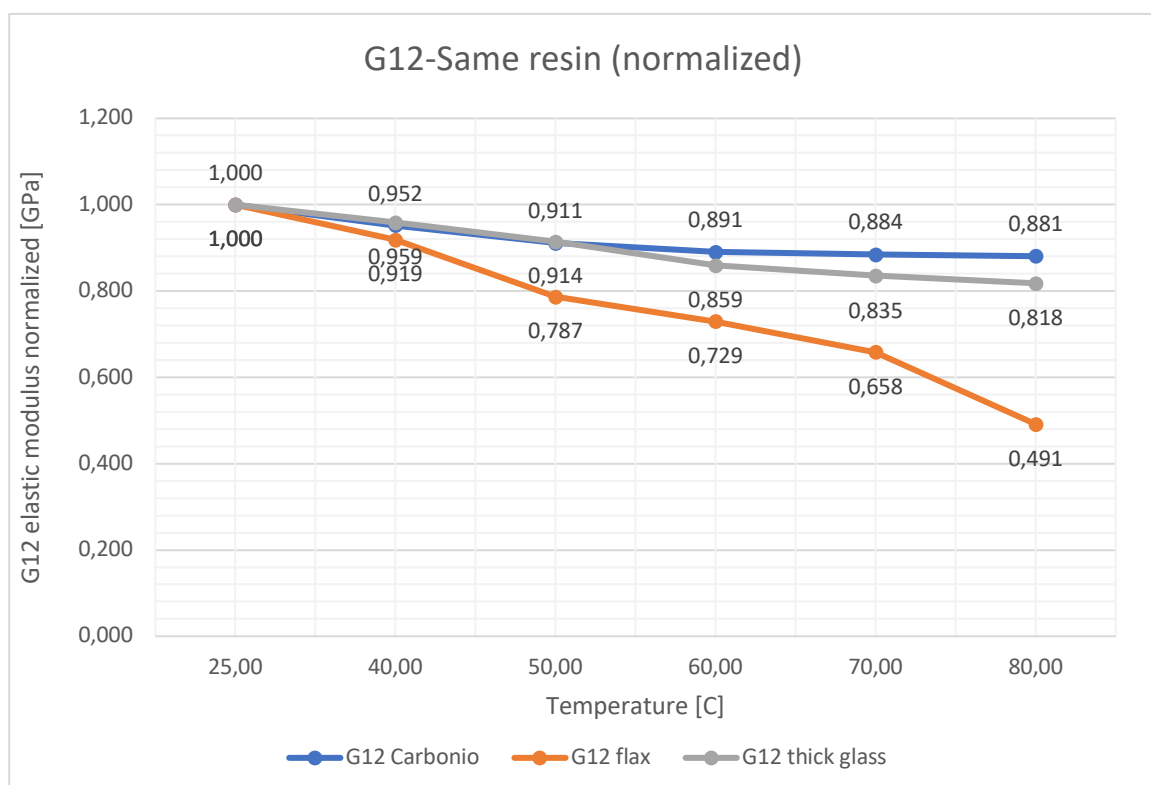
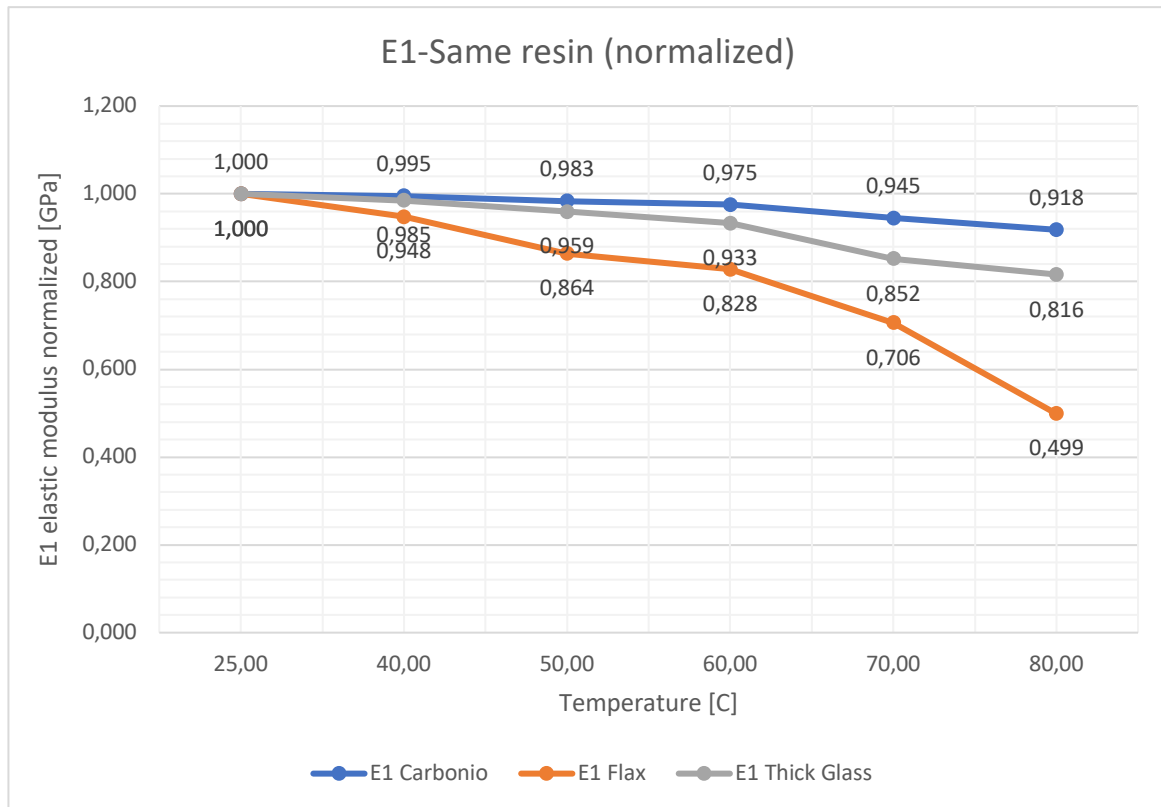
Table 14: : percentage variation of elastic moduli and damping coefficient with respect to the room temperature values

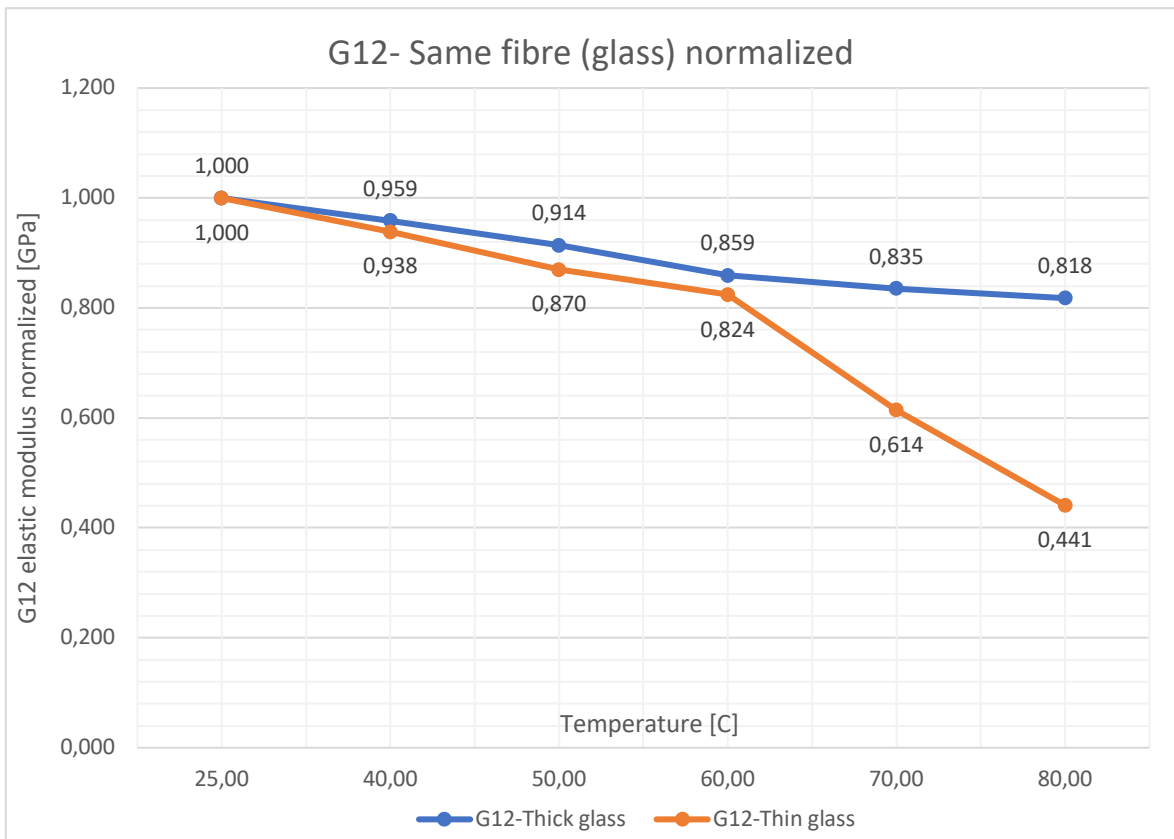
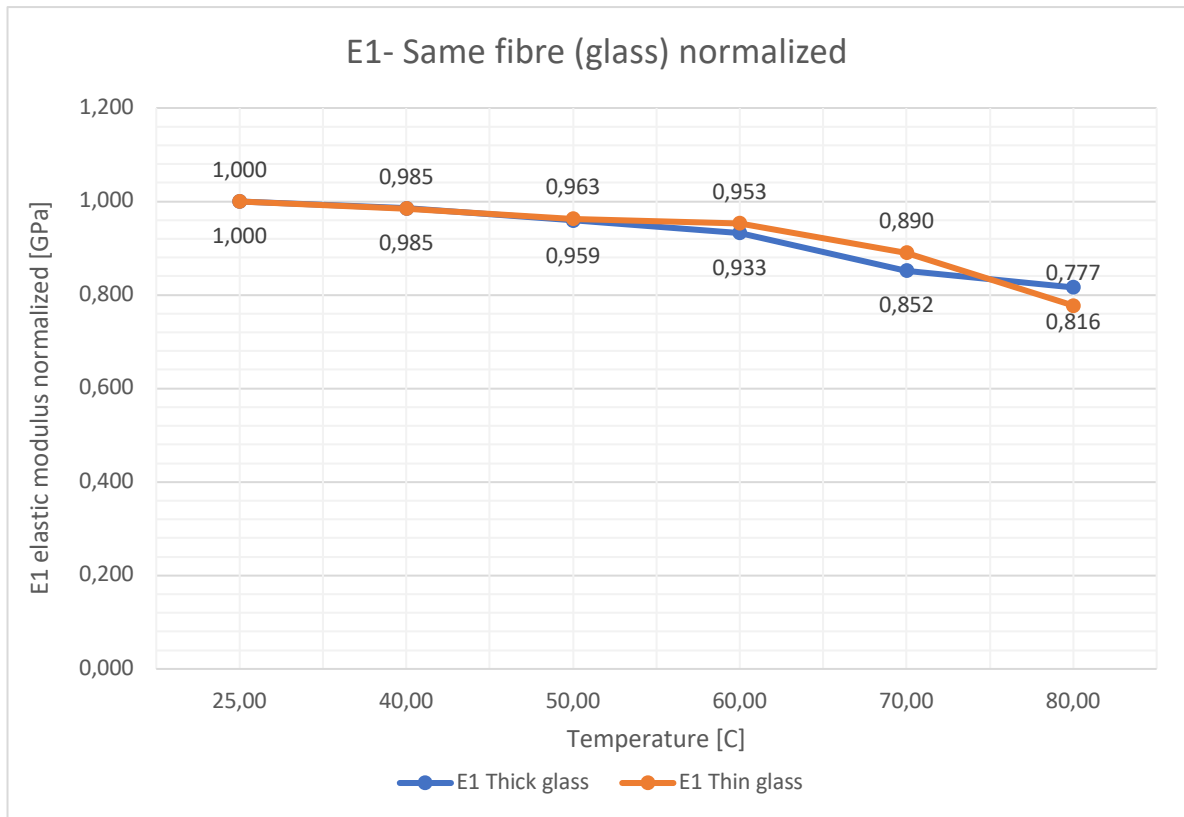
Elastic modulus $E_1$ variation %	Shear modulus $G_{12}$ variation %	Damping coefficient % (flexural)	Damping coefficient % (torsional)	Temperature (°C)
-5.19%	-8.14%	6.96%	-15.01%	40
-17.23%	-27.10%	100.87%	9.97%	60
-50.14%	-50.56%	273.48%	74.56%	80



## General trend of the elastic moduli in the experimental case

In this section four graphs will be presented in order to have a general idea of the trend in function of the temperature of the elastic moduli E1 and G12. The graphs have been divided in two categories, same fibre and same resin having the normalized value of E1 and G12 at temperature 25°C.





## 6. Evaluation of thermal expansion of composites

Considering the conditions presented previously (specimen exposed to thermal gradients) in which the composites were tested, it seemed more than logic to evaluate the natural frequencies independently from the thermal expansions. So, all the results seen before (in terms of  $E_1$  and  $G_{12}$ ) have been evaluated considering first the thermal expansions of the composites, then the variation of their geometry.

In order to evaluate the thermal expansions of each composite, it has been installed two strain gages located on the surface of the specimen with an orientation of 0 and 90 degrees to evaluate the coefficients of thermal expansion  $\alpha_{11}$  and  $\alpha_{22}$  (in direction 1 and respectively 2). The tests were performed at 60°C in the oven [12].

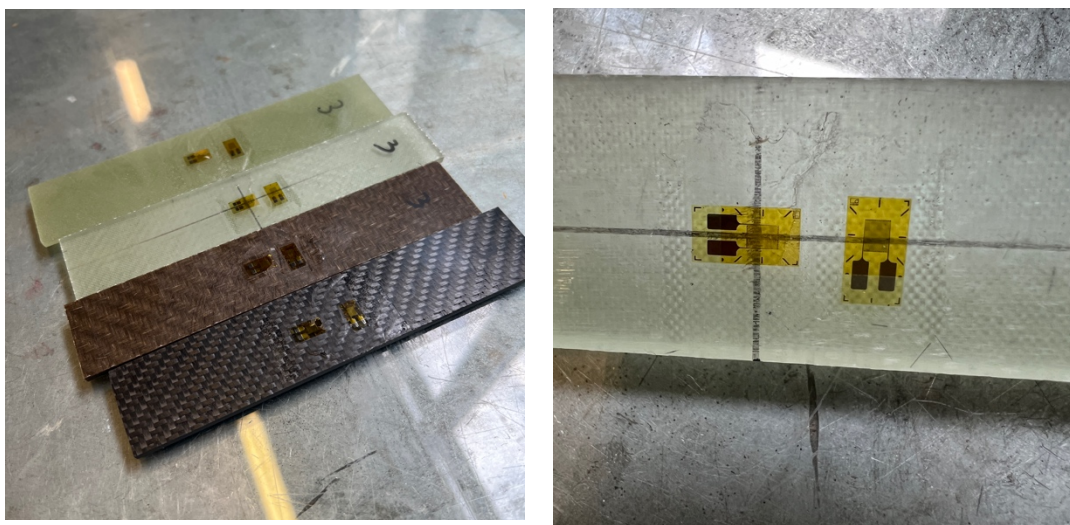


Figure 43: Strain gages installed on the specimens

For the direction 3, so in order to evaluate  $\alpha_{33}$ , another type of strain gage (smaller with respect to the first one) has been installed along the thickness of each specimen (Figure 45).

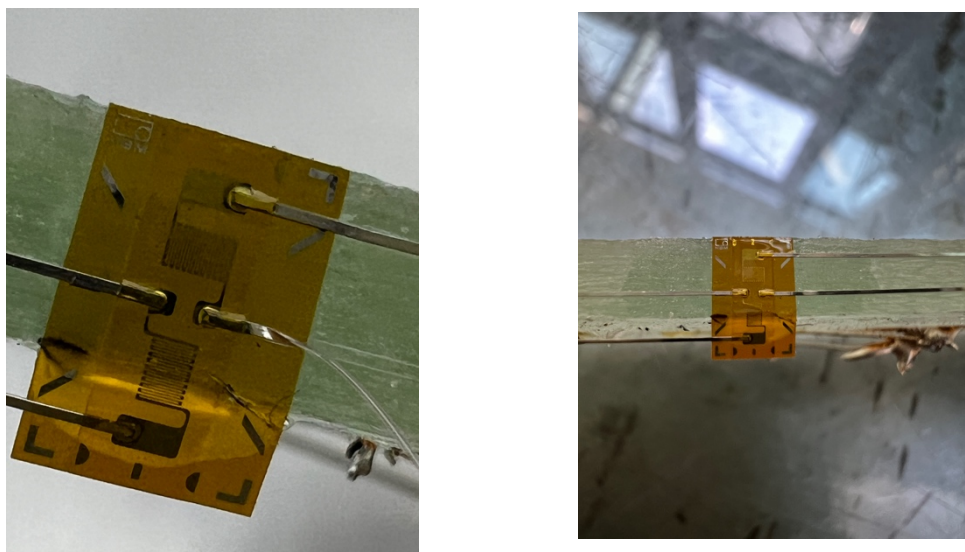


Figure 44: Strain gage installed along the thickness

Each strain gage was connected to the acquisition board (Quantum X HBM) through a one quarter Wheatstone bridge connection using the software Catman to change the parameters of the strain gauge.

The Wheatstone bridge circuit in its simplest form consists of four resistive elements (figure 45), or bridge arms ( $R_1$ ,  $R_2$ ,  $R_3$ ,  $R_4$ ), connected in a series-parallel arrangement, with an excitation voltage source. The connection points formed by (adjacent) pairs of bridge arms and the leadwires from the excitation voltage source are input corners of the bridge; and those formed by pairs of bridge arms and the signal ( $V_0$ ) measurement leads are output corners. It is worth noting for this discussion that each input corner is adjacent to each output corner, and each bridge arm is connected between two adjacent corners.

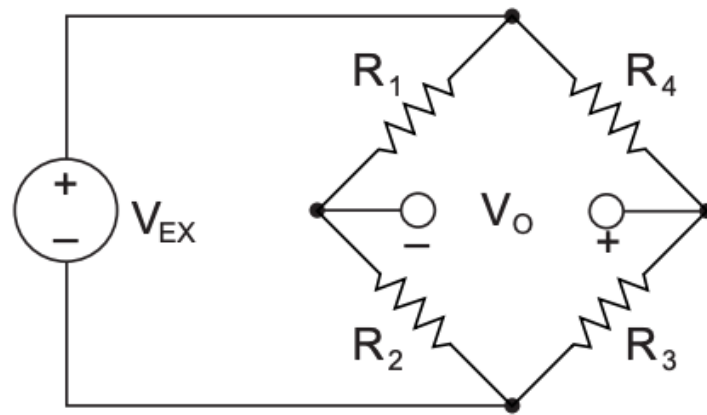


Figure 45: Wheatstone bridge circuit

The output voltage of the bridge will be  $V_0$ :

$$V_0 = \left[ \frac{R_3}{R_3 + R_4} - \frac{R_2}{R_1 + R_2} \right] \cdot V_{EX} \quad (6.0)$$

Any change in resistance in any arm of the bridge will result in a nonzero output voltage. Therefore, if we replace  $R_4$  with an active strain gauge, any changes in the strain gauge resistance will unbalance the bridge and produce a nonzero output voltage. If the nominal resistance of the strain gauge is designated as  $R_G$ , then the strain-induced change in resistance,  $\Delta R$ , can be expressed as  $\Delta R = R_G \cdot GF \cdot \varepsilon$  (where  $\varepsilon$  is the strain and  $GF$  the gage factor). Assuming that  $R_1 = R_2$  and  $R_3 = R_G$  (figure 46), the bridge equation above can be rewritten to express  $\frac{V_0}{V_{EX}}$  as a function of strain. Note the presence of the  $1/(1+GF \cdot \varepsilon/2)$  term that indicates the nonlinearity of the quarter-bridge output with respect to strain.

$$\frac{V_0}{V_{EX}} = -\frac{GF \cdot \varepsilon}{4} \left( \frac{1}{1 + GF \cdot \frac{\varepsilon}{2}} \right) \quad (6.1)$$

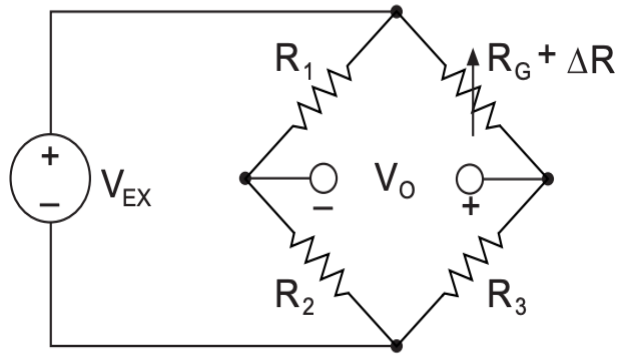


Figure 46: Wheatstone bridge

From a practical point of view the wires were located into the connector as it is shown in Figure 47 and connected to the quantum x acquisition system in the appropriate channel.

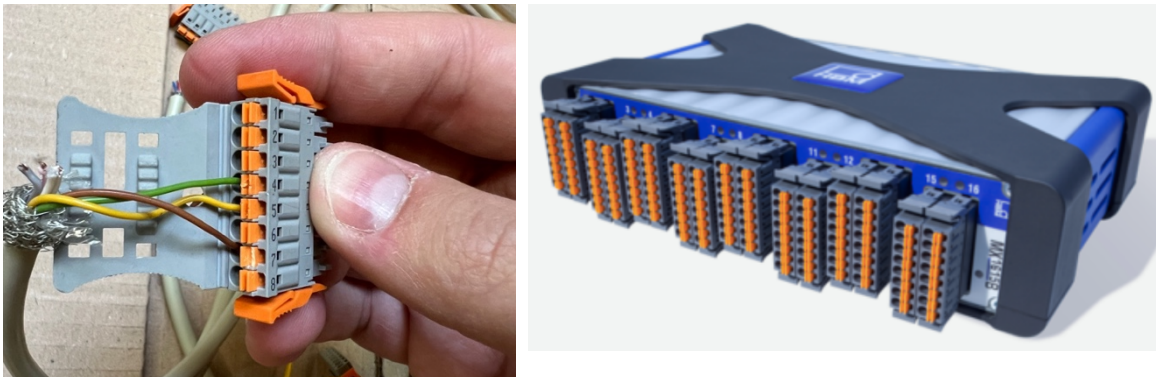


Figure 47: Connector (left) and acquisition system Quantum X (right)

The same procedure has been performed for both strain gauges. Moreover, together with the strain gauges, on the specimen, was mounted also a thermocouple in order to monitor the temperature of the composite. Both strain gages and thermocouple could be configurate in the Catman software (Figure 48).

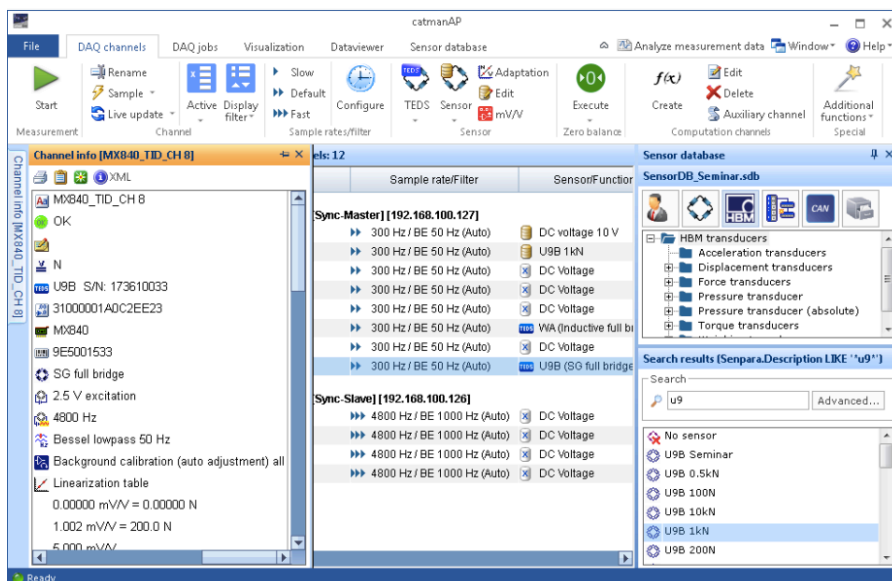


Figure 48: General window of the Catman software

In the software Catman it was possible, if the temperature was provided (using a thermocouple), to automatically compensate the strain of the strain gage due to temperature by giving as input the four constants:  $a_0$ ,  $a_1$ ,  $a_2$  and  $a_3$  (see data sheet of the strain gage in the appendix).

Other parameters that must be provided when performing the configuration in the software of the strain gauges are gage factor, excitation voltage, CTE of the strain gage and the reference temperature (which in this case was always 25 °C).

The sampling frequency for this type of measurement was set at 1 Hz.

### From strains to CTE

In order to pass from the strains, measured with the strain gages, to the coefficients of thermal expansion, it has been used a formula given by the technical sheet of the strain gage (eq. 6.2)

$$\varepsilon(T) = \varepsilon_{measured} - (a_0 + a_1T + a_2T^2 + a_3T^3) - (\alpha_m - \alpha_{SG})(T - T_{ref}) \quad (6.2)$$

The term  $\varepsilon_{measured}$  is the strain measured by the strain gage to which we compensate the expansion of the strain gage, so subtracting the coefficients “a”. The coefficient of thermal expansion  $\alpha_{SG}$  of the strain gage is given by the technical sheet while the unknown is the  $\alpha_m$  of the measured material. In order to find the value of the last one ( $\alpha_m$ ), we need to hypothesize the value of  $\alpha_m$  material using two different values and see if the value of the  $\varepsilon$  measured stays more or less constant. It has been done this test with  $\alpha_m$  material equal to zero and one. The measured strain remained constant. Thanks to this it was possible to compute the values of CTE using the following equations. Moreover  $\varepsilon(T)$  is the equation of the total strain (including the strain coming from mechanical loads, not only thermal).

From eq.6.2 considering the fact that we have no mechanical load applied we can pass to eq. 6.3.

$$0 = \varepsilon_{measured} - (a_0 + a_1T + a_2T^2 + a_3T^3) - (\alpha_m - \alpha_{SG})(T - T_{ref}) \quad (6.3)$$

From this point it is straight forward to obtain  $\alpha$  of the material:

$$(\alpha_m - \alpha_{SG}) \cdot \Delta T = \varepsilon_{measured} - (a_0 + a_1T + a_2T^2 + a_3T^3) \quad (6.4)$$

$$\alpha_m = \alpha_{SG} + \frac{\varepsilon_{measured} - (a_0 + a_1T + a_2T^2 + a_3T^3)}{\Delta T} \quad (6.5)$$

The values obtained for the four types of composites are listed in the following table:

Table 15: CTE coefficients of four types of composites

CTE	Flax	Carbon	Thick glass	Thin glass
$\alpha_1$	$7.61 \cdot 10^{-6}$	$4.85 \cdot 10^{-6}$	$13.29 \cdot 10^{-6}$	$14.58 \cdot 10^{-6}$
$\alpha_2$	$7.92 \cdot 10^{-6}$	$6.12 \cdot 10^{-6}$	$15.48 \cdot 10^{-6}$	$14.97 \cdot 10^{-6}$
$\alpha_3$	$97.25 \cdot 10^{-6}$	$61.6 \cdot 10^{-6}$	$70.45 \cdot 10^{-6}$	$56.11 \cdot 10^{-6}$

In order to confirm the results, some additional tests have been performed on an isotropic material with known value of CTE. The material tested was alumina, an aluminum oxide. The value of alumina CTE was certified according to some lab experiments involving the use of a dilatometer while the values obtained in this study were obtained in the same way previously discussed (by installing a strain gage).

The value of CTE obtained according to the tests and from literature are listed in the following table.

Table 16: comparison of CTE of alumina from experiments and from literature

CTE	From strain gage tests	From literature
$\alpha$	$5.67 \cdot 10^{-6}$	$(4.22 \div 9.2) \cdot 10^{-6}$

Also for the four composites the value of CTE was in the range according to the values available in literature.

Table 17: comparison of CTE of composites from experiments and from literature

CTE in literature	Flax	Carbon	Thick glass	Thin glass
$\alpha_1$	$(7 \div 10) \cdot 10^{-6}$	$(3.6 \div 5) \cdot 10^{-6}$	$(13 \div 18) \cdot 10^{-6}$	$(13 \div 18) \cdot 10^{-6}$
$\alpha_2$	$(7 \div 10) \cdot 10^{-6}$	$(3.6 \div 5) \cdot 10^{-6}$	$(13 \div 18) \cdot 10^{-6}$	$(13 \div 18) \cdot 10^{-6}$
$\alpha_3$	$(50 \div 100) \cdot 10^{-6}$	$(40 \div 60) \cdot 10^{-6}$	$(40 \div 70) \cdot 10^{-6}$	$(40 \div 70) \cdot 10^{-6}$

## 7. FEM models

In this study three types of simulations have been performed in order to study and compare from a numerical point of view the physics of the experimental test performed on the composites. All three models have been created in LS Dyna ANSYS using the student version of the software [13].

### Modal analysis

This type of model is needed in order to evaluate the natural frequencies and the mode shapes of the system studied.

Starting from the bases, the first step to be considered is the creation of the geometry of the model, the evaluation of the constrains (in case they are needed) the choice of the size of the mesh and the type of elements used. It is purely theoretical because each specimen has been cut using the sand water machine so the geometries might vary slightly, so in each simulation the real dimensions has been used (see Figure 49).

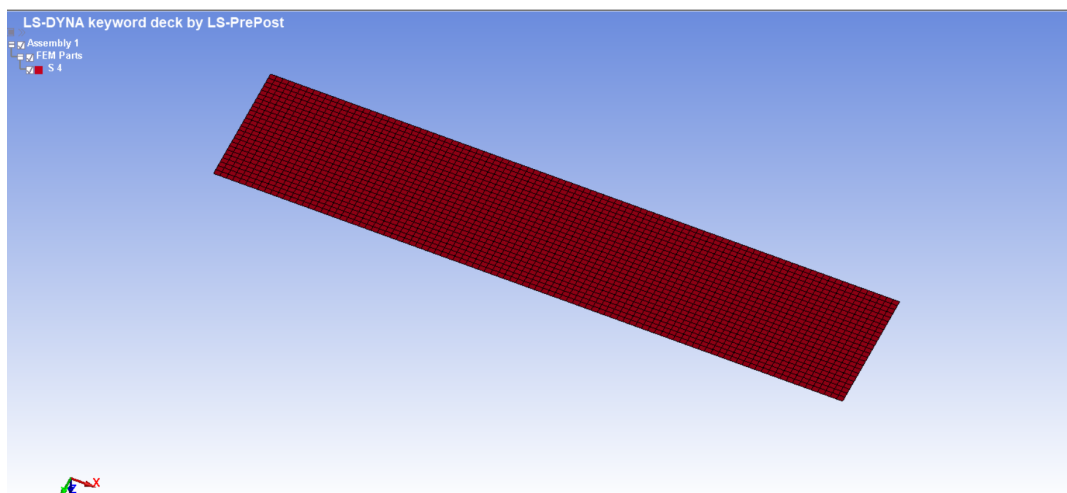


Figure 49: Meshed geometry in LS-Dyna using shell elements

The model had no constraints, due to the principal hypothesis of the modal analysis, the body should be free. The optimal size of the shell elements involved is of 1 mm although this wasn't the initial size. In order to understand which was the best size a convergence analysis have been performed.

The second step is to set the part as a composite (using an option of LS Dyna) and set the number of layers, with their thickness and angle orientation (figure 50).



Keyword Input Form

NewID Draw RefBy Pick Add Accept Delete Default Done 4

Use \*Parameter  Comment (Subsys: 1 ThinGlass.k) Setting

\*PART\_COMPOSITE\_(TITLE) (1)

1 TITLE  
Composite

OPTC IRPL  
OPTCARD 0

2 PID ELFORM SHRF NLOC MAREA HGID ADPOPT THSHEL  
4 16 0.0 0.0 0.0 0 0 0

Repeated Data by Button and List

3 MID THICK1 B1 TMID1 MID2 THICK2 B2 TMID2  
1 0.1765 0.0 0 1 0.1765 0.0 0

	MID	THICK1	B1	TMID1	MID2	THICK2	B2	TMID2
1	1	0.1765	0.0	0	1	0.1765	0.0	0
2	1	0.1765	0.0	0	1	0.1765	0.0	0
3	1	0.1765	0.0	0	1	0.1765	0.0	0
4	1	0.1765	0.0	0	1	0.1765	0.0	0
5	1	0.1765	0.0	0	1	0.1765	0.0	0
6	1	0.1765	0.0	0	1	0.1765	0.0	0
7	1	0.1765	0.0	0	1	0.1765	0.0	0

Total Card: 1 Smallest ID: 4 Largest ID: 4 Total deleted card: 0

Figure 50: Card of the part composite

This option allows us to consider the real number of layers with their thickness (see THICK1 and THICK2) and the angle between each fiber layer (see B1 and B2). Another aspect needed is the selection of a material card (see MID1 and MID2).

The material card used for this type of simulation was the “002” of LS Dyna, orthotropic elastic. There was no need for a more complex card at least for this simulation considering that the displacements during the application of the impulse were very small. Accordingly, the composite was not undergoing any damage or failure.

Keyword Input Form

NewID MatDB RefBy Pick Add Accept Delete Default Done 1

Use \*Parameter  Comment (Subsys: 1 Carbon.k) Setting

\*MAT\_ORTHOTROPIC\_ELASTIC\_(TITLE) (002) (1)

TITLE

1 MID RO EA EB EC PRBA PRCA PRCB  
1 1.385e-09 4.513e+04 4.500e+04 5000.0000 0.2000000 0.2000000 0.1000000

2 GAB GBC GCA AOPT G SIGF  
3217.0000 3200.0000 2800.0000 2.0 0.0 0.0

3 XP YP ZP A1 A2 A3 MACF JHIS  
0.0 0.0 0.0 1.0000000 0.0 0.0 1 0

4 V1 V2 V3 D1 D2 D3 BETA REF  
0.0 0.0 0.0 0.0 0.0 0.0 0.0 0.0

COMMENT:

Total Card: 1 Smallest ID: 1 Largest ID: 1 Total deleted card: 0

Figure 51: Material card for an elastic orthotropic material

In this material card it is possible to insert the density of the composite, the six elastic moduli and the three Poisson's moduli. Moreover, it is also possible to define the material axes which in this case was globally orthotropic with material axes determined by vectors A and D.

The next step is to set the different controls of the simulation: they will be responsible of the results of the simulation. In this simulation the dynamics of the composites have been evaluated in an implicit way.

Keyword Input Form

Use \*Parameter  Comment

(Subsys: 1 Carbon.k)

\*CONTROL\_IMPLICIT\_DYNAMICS (1)

1	IMASS	GAMMA	BETA	TDYBIR	TDYDTH	TDYBUR	IRATE	ALPHA
	1	0.5000000	0.2500000	0.0	1.000e+28	1.000e+28	0	0.0

Repeated Data by Button and List

2	PSID	ANGLE
		90

COMMENT:

IMASS:=Implicit analysis type:  
 LT.0: curve ID=(-IMASS) used to control amount of implicit dynamic effect applied to the analysis. TDYBIR, TDYDTH and TDYBUR are ignored with this option  
 EQ.0: static analysis  
 EQ.1: dynamic analysis using Newmark time integration.  
 EQ.2: dynamic analysis by modal superposition following the solution of the eigenvalue problem.  
 EQ.3: dynamic analysis by modal superposition using the eigenvalue solution in d3eigv files that are in the runtime directory.

Figure 52: Control card for implicit dynamics analysis using Newmark time integration

The analysis uses a Newmark time integration also known as the Newmark-beta method, that is a numerical technique used in structural dynamics to integrate the equations of motion. It is widely used for solving linear and non-linear second-order ordinary differential equations in the context of dynamic analysis, particularly for structures subjected to time-varying loads.

The following control card is the one responsible of the evaluation of the number of modes of the structure. (Figure 54)

Keyword Input Form

Use \*Parameter  Comment

(Subsys: 1 Carbon.k)

\*CONTROL\_IMPLICIT\_EIGENVALUE (1)

1	NEIG	CENTER	LFLAG	LFTEND	RFLAG	RHTEND	EIGMTH	SHFACL
	80	0.0	0	0.0	0	0.0	2	0.0

2	ISOLID	IBEAM	ISHELL	ITSHELL	MSTRES	EVDUMP	MSTRSCL
	0	0	0	0	0	0	0.0010000

3	ROTSCL	EIGMSCL
	0.001	0

COMMENT:

Figure 53: card for setting the number of modes to be calculated

Number of modes extracted are set in the NEIG option. To compute the eigenvalues the Block Shift-and-Invert Lanczos method is used (see EIGMTH). It is an advanced numerical technique used for extracting a few eigenvalues and corresponding eigenvectors of large, sparse matrices. This method is particularly useful in structural dynamics, computational physics, and other fields requiring efficient computation of eigenvalues. It reduces the matrix to a tridiagonal form, from which eigenvalues are easier to compute. The block method instead of working with single vectors, works with blocks of vectors, enhancing numerical stability and convergence for multiple eigenvalues. This is particularly useful when multiple eigenvalues are needed or when dealing with nearly degenerate eigenvalues.

In the control implicit general card, it can be set the type of analysis that in this case was implicit, it can be chosen with the flag IMFLAG that is a switching flag allowing the user to choose between different explicit and implicit analysis.

Keyword Input Form

Use \*Parameter  Comment

Clear Accept Delete Default Done

(Subsys: 1 Carbon.k) Setting

\*CONTROL\_IMPLICIT\_GENERAL (1)

1	IMFLAG	DT0	IMFORM	NSBS	IGS	CNSTN	FORM	ZERO_V
	1	0.0010000	2	1	2	0	0	0

COMMENT:

IGS:= Geometric (initial stress) stiffness flag  
EQ,2: ignore(default)  
EQ,1: include  
LT,0: include on part set |IGS|

Figure 54: card used for the choice of the initial time step

Still in this material card, also the initial time step can be set for the analysis (see DT0). Another type of control implemented in the model is “control implicit solution”, in this card it can be set the solution method, which in this case was a non-linear one.

Keyword Input Form

Use \*Parameter  Comment

Clear Accept Delete Default Done

(Subsys: 1 Carbon.k) Setting

\*CONTROL\_IMPLICIT\_SOLUTION (1)

1	NSOLVR	ILMIT	MAXREF	DCTOL	ECTOL	RCTOL	LSTOL	ABSTOL
	12	0	0	0.0	0.0	0.0	0.0	1.000e-10
2	DNORM	DIVERG	ISTIF	NLPRINT	NLNORM	D3ITCTL	CPCHK	
	2	1	1	0	2.0000000	0	0	
3	DMTOL	EMTOL	RMTOL	NTTOL	MRTOL	RTTOL	RRTOL	
	0.0	0.0	0.0	0.0	0.0	0.0	0.0	
4	ARCCTL	ARCDIR	ARCLEN	ARCMTH	ARCDMP	ARCPST	ARCALE	ARCTJM
	0	0	0.0	1	2	0.0	0.0	0.0
5	LSMTD	LSDIR	JRAD	SRAD	AWGT	SRED		
	4	2	0.0	0.0	0.0	0.0		

COMMENT:

EQ,6: Nonlinear with BFGS updates + arclength,  
EQ,7: Nonlinear with Broyden updates + arclength,  
EQ,8: Nonlinear with DFP updates + arclength,  
EQ,9: Nonlinear with Davidon updates + arclength.  
EQ,12: Nonlinear with BFGS updates. This solver incorporates different line search and integration schemes as compared to obsolete NSOLVR=2. Inclusion of an arc length method is optional and is invoked by setting ARCMTH=3.

Figure 55: control card used to set the non-linear solution and solver

Moreover, in this card it can be decided also the convergence method. In this study the default method has been used, so the energy method using sum of translational rotational degrees of freedom.

Last but not the least is the solver control, called “control implicit solver” used in order to choose the solver method, in this study is a linear equation solver parallel multi-frontal sparse solver. The parallel multi-frontal sparse solver is an advanced solver for efficiently handling large, sparse systems of linear equations by decomposing the problem into smaller dense submatrices, leveraging parallel processing to achieve high performance and scalability. It is particularly well-suited for the computational demands of implicit finite element analysis.

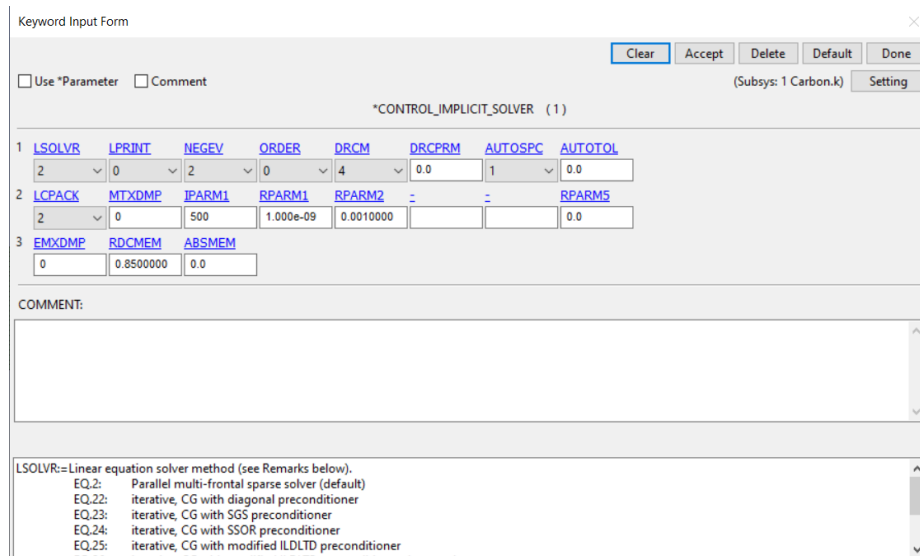
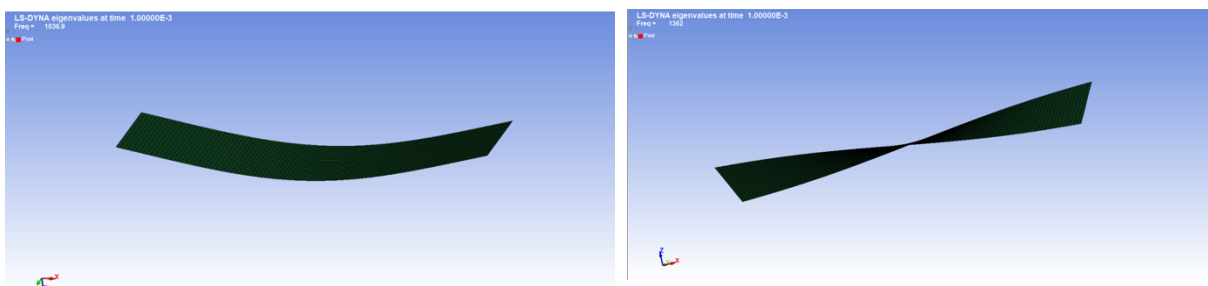


Figure 56: control card used to set the type of solver

## Results of the modal analysis and comparison with the experimental results

In the next figures it will be illustrated the graphical results of the modal analysis of one type of composite analyzed in this study (carbon fiber with epoxy resin). The first six mode shapes are not illustrated because they are just rigid body motion, being the structure free to move.



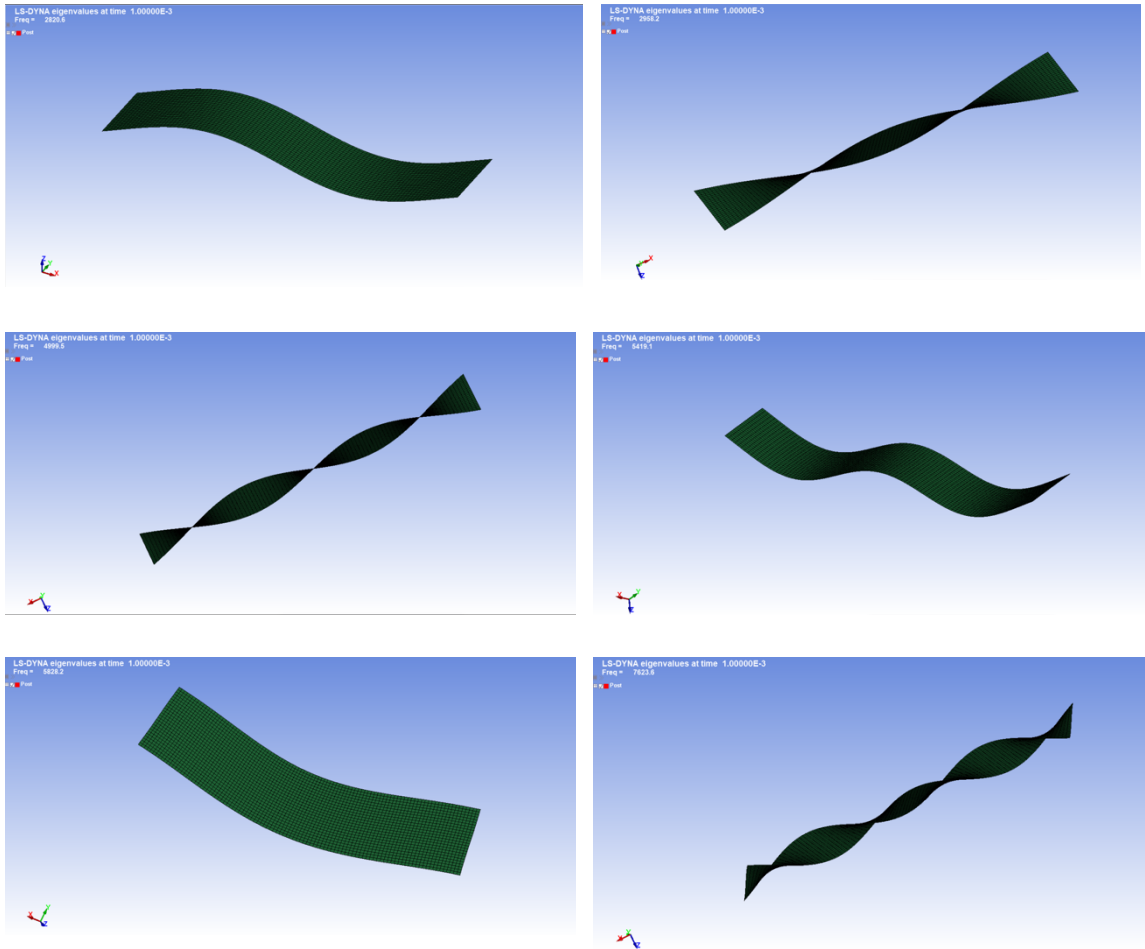
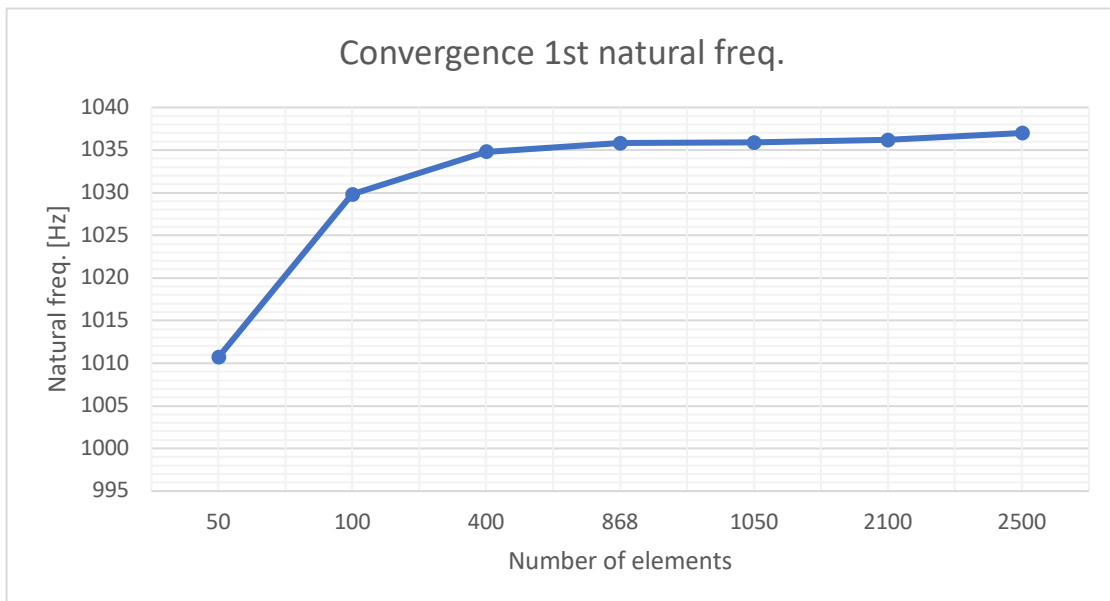
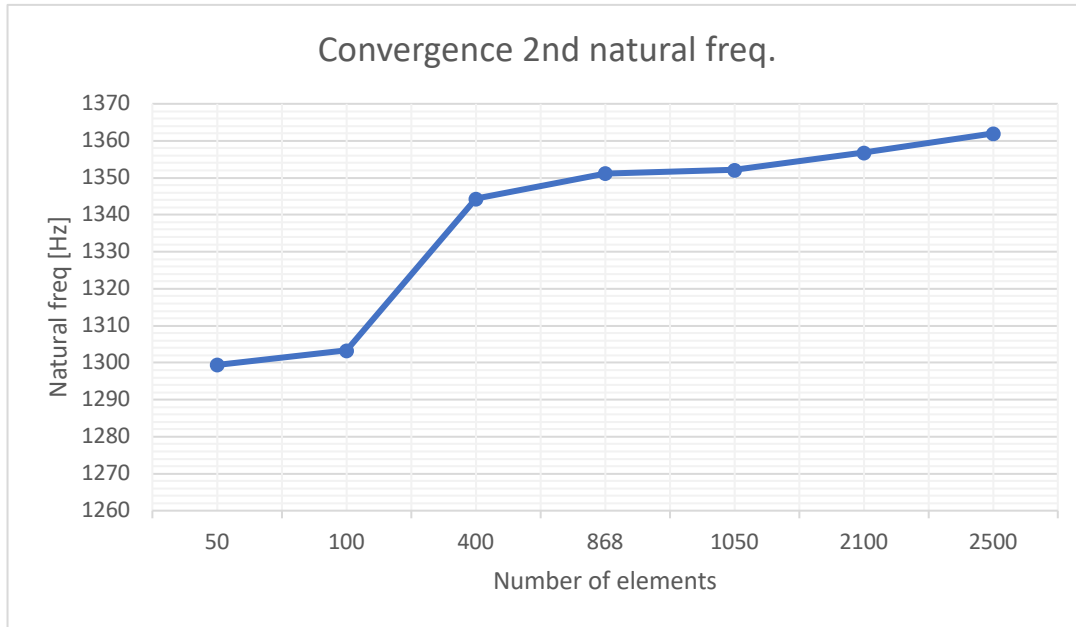


Figure 57: First 8 modes for carbon composite

In order to understand how many elements were needed in the modal analysis, a convergence analysis on the first two natural frequencies has been performed (here are illustrated the two natural freq. of carbon composite).





The comparison of the experimental and numerical results can be seen in the following tables. Each frequency has been analyzed at the four different temperatures of the study and the percentage difference between the experimental and numerical results have been also computed. These results are obtained by manually changing the moduli, so we need a more complex model to fully describe the physics of the problem.

Table 18: Comparison between experimental and numerical natural frequencies at different temperature for thin glass

Thin glass with epoxy resin 30% natural						
1 <sup>st</sup> natural freq. [Hz] experimental	1 <sup>st</sup> natural freq. [Hz] numerical	2 <sup>nd</sup> natural freq. [Hz] experimental	2 <sup>nd</sup> natural freq. [Hz] numerical	Difference in % of 1 <sup>st</sup> freq.	Difference in % of 2 <sup>nd</sup> freq.	Temperature [°C]
571.35	570.83	1092.60	1050.40	0.091%	3.862%	25
567.68	566.92	1059.67	1019.50	0.134%	3.791%	40
559.15	558.26	994.24	956.41	0.159%	3.805%	60
505.72	504.42	728.33	706.45	0.256%	3.004%	80

Table 19: Comparison between experimental and numerical natural frequencies at different temperature for thick glass

Thick glass with epoxy resin						
1 <sup>st</sup> natural freq. [Hz] experimental	1 <sup>st</sup> natural freq. [Hz] numerical	2 <sup>nd</sup> natural freq. [Hz] experimental	2 <sup>nd</sup> natural freq. [Hz] numerical	Difference in % of 1 <sup>st</sup> freq.	Difference in % of 2 <sup>nd</sup> freq.	Temperature [°C]
668.58	667.37	1338.25	1296.40	0.181%	3.127%	25
664.49	663.19	1312.15	1271.50	0.196%	3.098%	40
647.60	646.14	1243.89	1206.20	0.225%	3.030%	60
606.87	605.53	1215.80	1177	0.221%	3.191%	80

Table 20: Comparison between experimental and numerical natural frequencies at different temperature for carbon

Carbon fiber with epoxy resin						
1 <sup>st</sup> natural freq. [Hz] experimental	1 <sup>st</sup> natural freq. [Hz] numerical	2 <sup>nd</sup> natural freq. [Hz] experimental	2 <sup>nd</sup> natural freq. [Hz] numerical	Difference in % of 1 <sup>st</sup> freq.	Difference in % of 2 <sup>nd</sup> freq.	Temperature [°C]
1042.80	1037	1388.77	1362	0.556%	1.928%	25
1041.64	1035.60	1357.02	1331.70	0.580%	1.866%	40
1032.78	1026.90	1314.08	1291.20	0.569%	1.741%	60
1003.84	998.50	1308.93	1285.30	0.532%	1.805%	80

Table 21: Comparison between experimental and numerical natural frequencies at different temperature for flax

Flax fiber with epoxy resin						
1 <sup>st</sup> natural freq. [Hz] experimental	1 <sup>st</sup> natural freq. [Hz] numerical	2 <sup>nd</sup> natural freq. [Hz] experimental	2 <sup>nd</sup> natural freq. [Hz] numerical	Difference in % of 1 <sup>st</sup> freq.	Difference in % of 2 <sup>nd</sup> freq.	Temperature [°C]
534.37	527.66	962.02	922.70	1.256%	4.087%	25
521.24	514.71	923.64	886.73	1.253%	3.996%	40
488.49	482.13	825.07	794.10	1.302%	3.754%	60
380.26	375.36	679.14	650.24	1.289%	4.255%	80

## Thermal model

This model is needed in order to simulate the thermal expansion of the composite specimen at different temperature, in particular 40, 60 and 80 °C.

The first step as previously seen for the modal analysis is the definition of the geometry of the model (which is the same as in the model analysis). In this case study, the geometry has been modeled with solid elements fully integrated quadratic 8 nodes with nodal rotation. While in terms of constraints, the structure was free to move as in the experimental case. The results of the simulations are the expansions of the specimen in the three directions x,y,z.

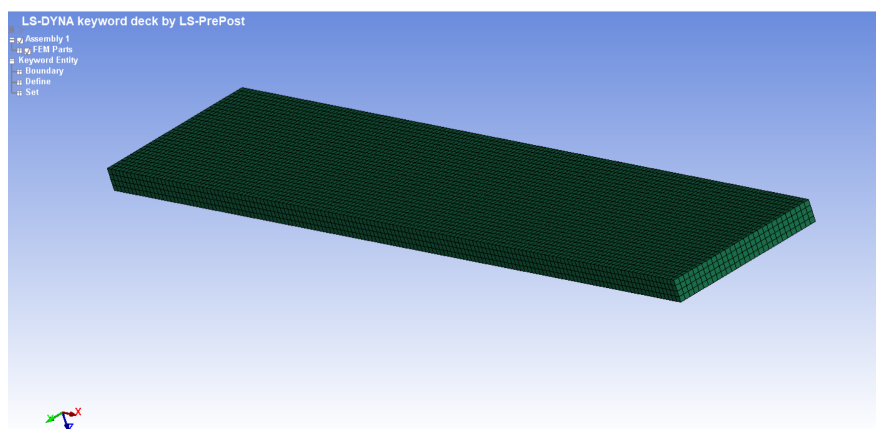


Figure 58: Meshed geometry in LS-Dyna using solid elements

Let us see the only boundary given for this model which is the initial temperature. In order to see the expansion of the specimen the model need an initial temperature and a final one. The initial temperature has been given using a boundary condition able to select all the nodes of the structure and set an initial temperature of 25°C.

To set the final temperature a curve has been defined, giving the profile of temperature needed to be followed by the simulation.

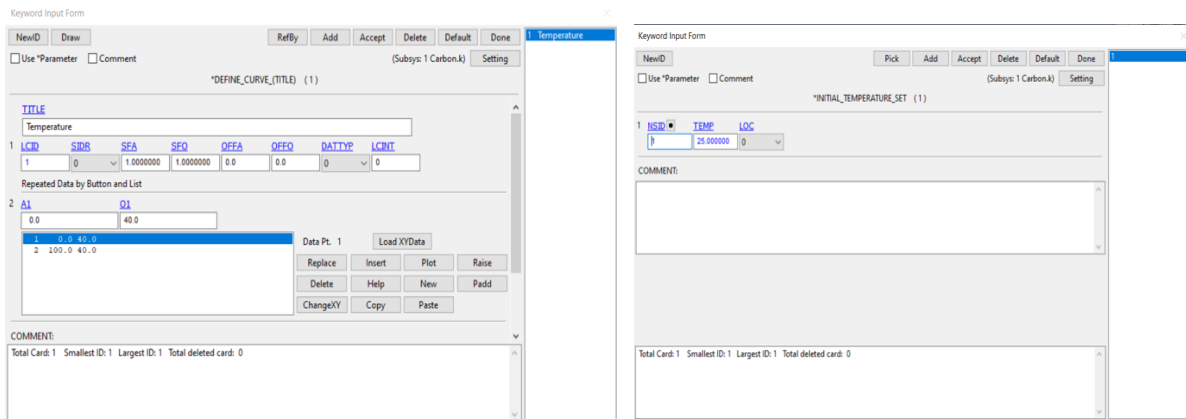


Figure 59: card for defining the temperature curve (left) and card for initial temperature set (right)

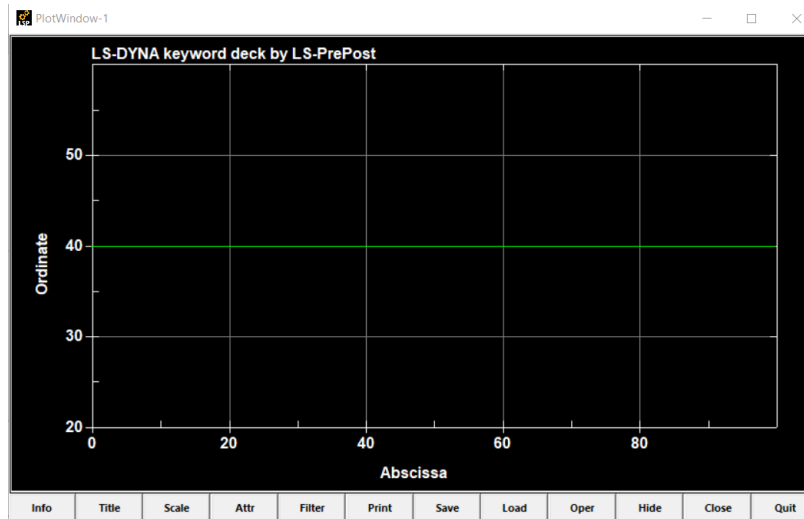


Figure 60: Temperature profile (in this case 40 Celsius)

Regarding the material, in this simulation the material card is completely different from the one used in the modal analysis. The material card is the orthotropic thermal 021. It needs as input the density of the composite, the six elastic moduli, the three coefficients of thermal



expansion (CTEs) and the three coefficients of Poisson's. Another aspect is the definition of two unitary vectors (see A1 and D2) used in the definition of the material axes (in this case globally orthotropic).

Figure 61: Material card for orthotropic material used for thermal expansion

For this thermal model it is necessary also a card for the material thermal properties. Some of the properties required by the thermal material card are: the thermal density, which in this case is equal to the structural one (see TRO), the phase change temperature (not so relevant for this study, so it has been set to 1000°C (temperature never reached in the simulation), the latent heat, and the most important, the heat capacity (see HC) and the thermal conductivity in the three directions x,y,z (see K1, K2, K3).

Figure 62: Material card for thermal properties

One of the most important aspects to consider in simulation is the solution imposed to the solver, in this case the analysis is a coupled one, thermal and structural (see SOLN). It can be set in the “control solution”.

Keyword Input Form

Use \*Parameter Comment (Subsys: 1 Carbon.k) Setting

\*CONTROL\_SOLUTION (1)

1	SOLN	NLQ	ISNAN	LCINT	LCACC	NDCFE	NOCOP
	2	0	0	100	0	1	0

COMMENT:

SOLN:=Analysis solution procedure:  
 EQ:0: Structural analysis only,  
 EQ:1: Thermal analysis only,  
 EQ:2: Coupled structural thermal analysis.

Figure 63: Control card for setting the coupled structural thermal analysis

Beside this solution the simulation needs the usual implicit solution needed for the non-linear analysis (see NSOLVR 12).

Keyword Input Form

Use \*Parameter Comment (Subsys: 1 Carbon.k) Setting

\*CONTROL\_IMPLICIT\_SOLUTION (1)

1	NSOLVR	ILMIT	MAXREF	DCTOL	ECTOL	RCTOL	LSTOL	ABSTOL
	12	11	15	0.0010000	0.0100000	1.000e+10	0.9000000	1.000e-10

2	DNORM	DIVERG	ISTJF	NLPRINT	NLNORM	D3ITCTL	CPCHK
	2	1	1	0	4.0000000	0	0

3	DMTOL	EMTOL	RMTOL	NITOL	NRTOL	RTTOL	RRTOL
	0.0	0.0	0.0	0.0	0.0	0.0	0.0

4	ARCCTL	ARCDIR	ARCLEN	ARCMTH	ARCDMP	ARCPST	ARCALE	ARCTJM
	0	0	0.0	1	2	0.0	0.0	0.0

5	LSMTD	LSDJR	JRAD	SRAD	AWGT	SRED
	4	2	0.0	0.0	0.0	0.0

COMMENT:

NSOLVR:=Solution method for implicit analysis:  
 EQ:-1: Multistep linear,  
 EQ:1: Linear,  
 EQ:6: Nonlinear with BFGS updates + arclength,  
 EQ:7: Nonlinear with Broyden updates + arclength,  
 EQ:8: Nonlinear with DFP updates + arclength,

Figure 64: control card used to set the non-linear solution and solver

The next important step is the evaluation of the time-step. Being a coupled simulation, the time-step of the structural part must, at least at the beginning of the simulation, match the time-step

of the thermal part. For the structural part the time-step can be set in the “control implicit general” (see DT0).

Keyword Input Form

Use \*Parameter  Comment

Clear Accept Delete Default Done

(Subsys: 1 Carbon.k) Setting

\*CONTROL\_IMPLICIT\_GENERAL (1)

1	IMFLAG	DT0	IMFORM	NSBS	IGS	CNSTN	FORM	ZERO_V
1	1	0.1000000	2	1	2	0	0	0

COMMENT:

DT0:=Initial time step size for implicit analysis. See Remarks 2 and 5.  
 LT0: eliminate negative principal stresses in geometric(initial stress) stiffness.Initial time step is |DT0|.

Figure 65: control card used to set the time-step

The time-step of the thermal part can be set in “control thermal timestep”. Moreover, in this control it can be set also the time integration parameter to a fully implicit or a Crank-Nicholson scheme, which is an implicit of second order. For this study the last one has been used (see TIP).

Keyword Input Form

Use \*Parameter  Comment

Clear Accept Delete Default Done

(Subsys: 1 Carbon.k) Setting

\*CONTROL\_THERMAL\_TIMESTEP (1)

1	TS	TIP	ITS	TMIN	TMAX	DTEMP	TSCP	LCTS
1	1	0.5000000	0.1000000	0.0	0.0	1.0000000	0.5000000	0

COMMENT:

TIP:=Time integration parameter:  
 Default is 0.5 - Crank-Nicholson scheme (default),  
 EQ 1.0: fully implicit.

Figure 66: control card to set the thermal time-step

Next step to follow is the implementation of the type of analysis needed in the thermal model. In this study it has been performed a transient analysis (see AYPE) of a non-linear problem (see PTYPE) set by using “control thermal solver”.

Keyword Input Form

Clear Accept Delete Default Done

Use \*Parameter  Comment (Subsys: 1 Carbon.k) Setting

\*CONTROL\_THERMAL\_SOLVER ( 1)

1	ATYPE	PTYPE	SOLVER	:	GPT	EQHEAT	FWORK	SBC
	1	1	11		8	1.0000000	1.0000000	0.0

Active optional cards  
 None  Opt1  Opt12

2	MSGVL	MAXITR	ABSTOL	RELTOL	OMEGA	UNUSED	UNUSED	TSE
	0	500	1.0e-10	1.0E-06	0.0			1.0

3	MXDMP	DTVE	VARDEN	:	NCYCL
	0	0	0		1

COMMENT:

PTYPE= Thermal problem type: (see \*CONTROL\_THERMAL\_NONLINEAR if no-zero)  
EQ.0: linear problem,  
EQ.1: nonlinear problem with material properties evaluated at gauss point temperature,  
EQ.2: nonlinear problem with material properties evaluated at element average temperature.

Figure 67: control card for setting the non-linear thermal solver

Another control needed for the transient problem is the divergence control parameter set in the card “control thermal nonlinear” (see DCP=0.5).

Keyword Input Form

Clear Accept Delete Default Done

Use \*Parameter  Comment (Subsys: 1 Carbon.k) Setting

\*CONTROL\_THERMAL\_NONLINEAR ( 1)

1	REFMAX	TOL	DCP	LUMPBC	THLSTL	NLTHPR	PHCHPN
	100	1.000e-04	0.5000000	0	0.0	0	100.000000

COMMENT:

Figure 68: control card for controlling the divergence of the non-linear problem

## Results of the thermal analysis and comparison with the experimental results

In the following figures it is illustrated the graphical results of the thermal analysis in terms of x,y,z displacements caused by the thermal expansion. The numerical results are compared with the analytical ones obtained by using the values of the three coefficients of thermal expansions that have been calculated from the experimental strains.

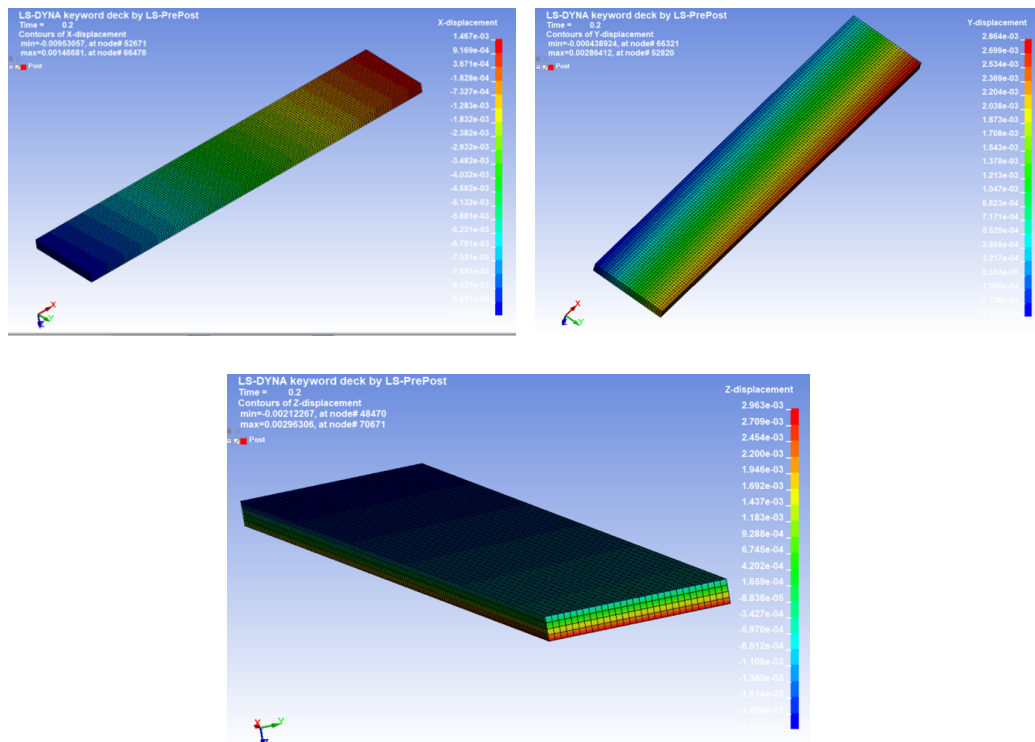


Figure 69: thermal expansion in the three directions

The analytical relations used for the comparison with the numerical results are:

$$\Delta L = L_0 \cdot \alpha_x \cdot \Delta T \quad (7.0)$$

$$\Delta b = b_0 \cdot \alpha_y \cdot \Delta T \quad (7.1)$$

$$\Delta t = t_0 \cdot \alpha_z \cdot \Delta T \quad (7.2)$$

Where  $L_0$ ,  $b_0$ , and  $t_0$  are respectively the initial length, the initial width, and the initial thickness. This increment in dimensions is to be added to the initial value of the geometry considered. In the following tables can be seen the final values of L, b and t after the thermal expansion.

Table 22: Comparison between experimental and numerical results of thermal expansion for thin glass

Thin glass with epoxy resin 30% natural									
Analytical [mm]			Numerical [mm]			Difference in %			Temp [°C]
L	b	t	L	b	t	L	b	t	
150.372	30.566	3.533	150.372	30.567	3.533	0	0.003	0	40
150.416	30.576	3.537	150.416	30.576	3.538	0	0	0.028	60
150.460	30.585	3.541	150.461	30.588	3.542	0.0007	0.0098	0.028	80

Table 23: Comparison between experimental and numerical results of thermal expansion for thick glass

Thick glass with epoxy resin									
Analytical [mm]			Numerical [mm]			Difference in %			Temp [°C]
L	b	t	L	b	t	L	b	t	
148.969	29.447	4.014	148.969	29.447	4.014	0	0	0	40
149.009	29.456	4.019	149.009	29.456	4.021	0	0	0.049	60
149.048	29.465	4.025	149.049	29.466	4.026	0.00067	0.0034	0.025	80

Table 24: Comparison between experimental and numerical results of thermal expansion carbon

Carbon with epoxy resin									
Analytical [mm]			Numerical [mm]			Difference in %			Temp [°C]
L	b	t	L	b	t	L	b	t	
149.111	29.303	3.964	149.111	29.303	3.965	0	0	0.0252	40
149.125	29.306	3.968	149.125	29.307	3.972	0	0.0034	0.1	60
149.140	29.310	3.973	149.140	29.312	3.973	0	0.0068	0	80

Table 25: Comparison between experimental and numerical results of thermal expansion flax

Flax with epoxy resin									
Analytical [mm]			Numerical [mm]			Difference in %			Temp [°C]
L	b	t	L	b	t	L	b	t	
149.227	29.333	3.875	149.227	29.334	3.876	0	0.0034	0.0258	40
149.250	29.338	3.883	149.250	29.338	3.883	0	0	0	60
149.272	29.343	3.891	149.273	29.346	3.892	0.0007	0.0102	0.0257	80

### Coupled analysis – Modal and Thermal models with temperature dependency of the elastic moduli

The goal of this type of simulation is to underline the temperature dependency of the elastic moduli through the change in natural frequencies. This simulation performs three simulations in one; i) a first a modal analysis at room temperature; ii) a thermal simulation that modifies the geometry of the specimen and iii) in the end another modal analysis that accounts for the variation of the elastic moduli and specimen dimensions in the computation of natural frequencies.

Being a combination of the two previous simulations, in the following pages it will be discussed only the new parts added to the simulation.

The type of element used is the same of the thermal simulation (solid elements).

In addition to the curve of the temperature profile, a new curve has been defined. This curve is needed in order to set the initial and final modal analysis. Basically, it is just an horizontal line, but the idea behind it is to start a modal analysis at the first point of the curve (in this case at time equal zero) and one at the last point of the curve (in this case time 0.2 seconds) which corresponds also at the end of the thermal analysis.

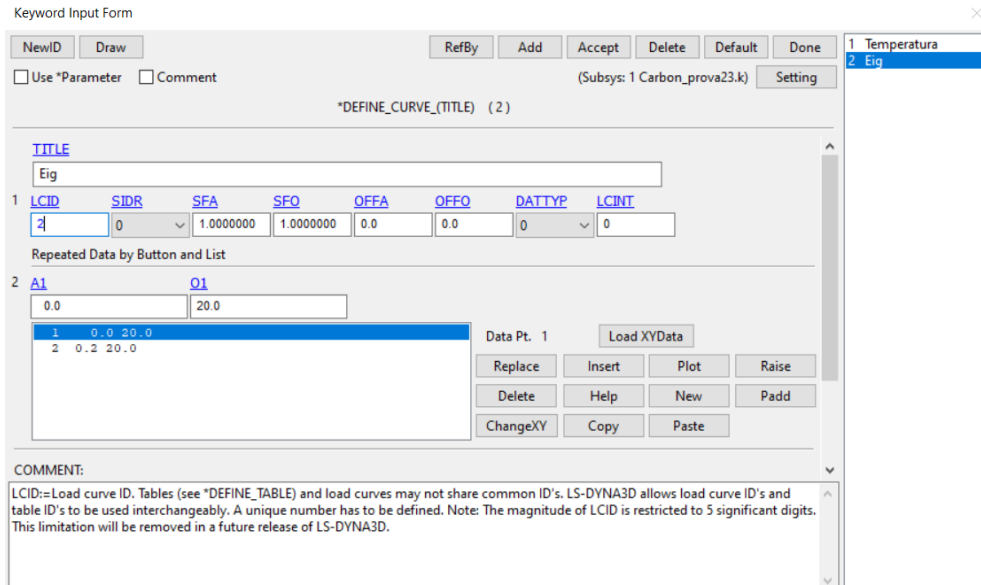


Figure 70: card needed to define the eigenvalues curve

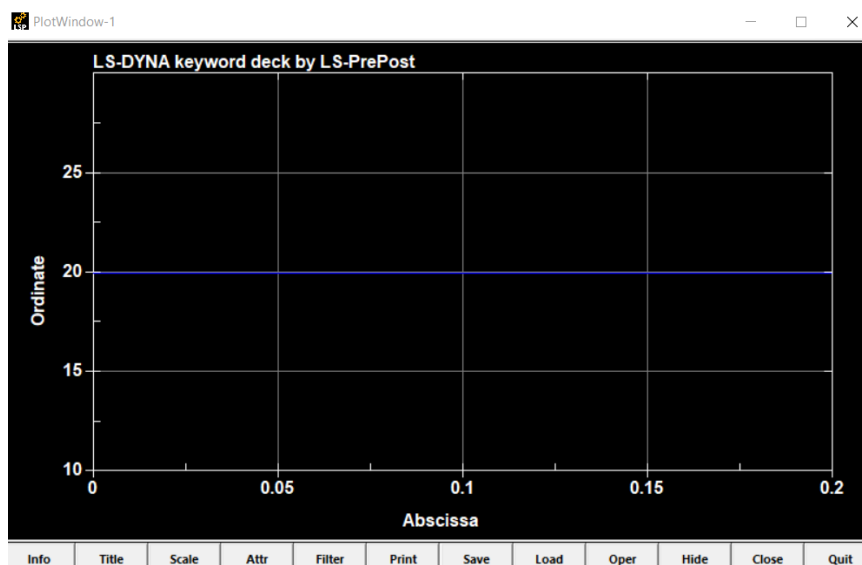


Figure 71: Curve of eigenvalues to be computed

The value of the ordinates of the graph sets the number of modes needed to be extracted (in this case was 20 modes).

Another new aspect of this simulation is the material card. This new material card is called “temperature dependent orthotropic” and as the name suggests it allows the user to insert different points that are temperature dependent. At each temperature can be set: the six elastic moduli, the three Poisson’s ratios and the three coefficients of thermal expansion (CTEs).

Keyword Input Form

MatDB RefBy Pick Add Accept Delete Default Done **1 Composite\_T\_depend**

Use \*Parameter  Comment (Subsys: 1 Carbon\_prova23.k) Setting

\*MAT\_TEMPERATURE\_DEPENDENT\_ORTHOTROPIC\_(TITLE) (023) (1)

**TITLE**  
Composite\_T\_dependent

1	MID	RO	AOPT	REF	MACE
	1	1.385e-09	2.0000000	0.0	1

2	XP	YP	ZP	A1	A2	A3
	0.0	0.0	0.0	1.0000000	0.0	0.0

3	V1	V2	V3	D1	D2	D3	BETA
	0.0	0.0	0.0	0.0	1.0000000	0.0	0.0

Repeated Data by Button and List

4	EAI	EBI	ECI	PRBAI	PRCAI	PRCBI
	45130.0	45000.0	5000.0	0.2	0.2	0.1

5	AAI	ABI	ACI	GABI	GBCI	GCAI	TI
	4.84700E-6	6.12600E-6	6.16000E-5	3217.0	3200.0	2800.0	25.0

1	45130.0	45000.0	5000.0	0.2	0.2	0.1	4.84700E-6	6.12600E-6	6.16000E-5	3217.0	3200.0	2800.0	25.0
2	44905.0	44000.0	5000.0	0.2	0.2	0.1	4.84700E-6	6.12600E-6	6.16000E-5	3217.0	3200.0	2800.0	25.0
3	44017.0	44000.0	4800.0	0.2	0.2	0.1	4.84700E-6	6.12600E-6	6.16000E-5	3217.0	3200.0	2800.0	25.0
4	41435.0	41000.0	4500.0	0.2	0.2	0.1	4.84700E-6	6.12600E-6	6.16000E-5	3217.0	3200.0	2800.0	25.0

Data Pt. 1

Replace Insert  
Delete Help

Total Card: 1 Smallest ID: 1 Largest ID: 1 Total deleted card: 0

Figure 72: Material card for orthotropic temperature dependent materials

As for the thermal model, also in this simulation is needed the same thermal orthotropic card that provides the thermal properties of the composite.

In the control cards the only difference for the modal analysis is the number of modes to be extracted. In the modal analysis implicit eigenvalue card the NEIG was responsible of the extraction of n number of modes. Now the card gets the curve shown before in order to extract the modes, the value of the ordinates are the modes to be extracted while the abscissa values are the two moments in time when the modal analysis is performed.

Keyword Input Form

Clear Accept Delete Default Done

Use \*Parameter  Comment (Subsys: 1 Carbon\_prova23.k) Setting

\*CONTROL\_IMPLICIT\_EIGENVALUE (1)

1	NEIG	CENTER	LFLAG	LFTEND	RFLAG	RHTEND	EIGMTH	SHFSCL
	-2	0.0	0	-1.000e+29	0	1.000e+29	2	0.0

2	ISOLID	IBEAM	ISHELL	IT_SHELL	MSTRES	EVDUMP	MSTRSCL
	0	0	0	0	0	0	0.0010000

3	ROTSCL	EIGMSCL
	0.001	0

COMMENT:

NEIG:=Number of eigenvalues to extract. This must be specified. The other parameters below are optional.  
LT.0: curve ID = (-NEIG) used for intermittent eigenvalue analysis

Figure 73: control card needed to set the curve of eigenvalues that will be eventually calculated



The other control card added in this simulation is the accuracy card. This card is used to increase the accuracy of the simulation especially in this case of solid elements used for an orthotropic material that undergoes significant deformations. In the “control accuracy” can be set an option called “INN” to value 4. This option has no effect on solid elements of isotropic elements, but only anisotropic material subjected to significant deformation.

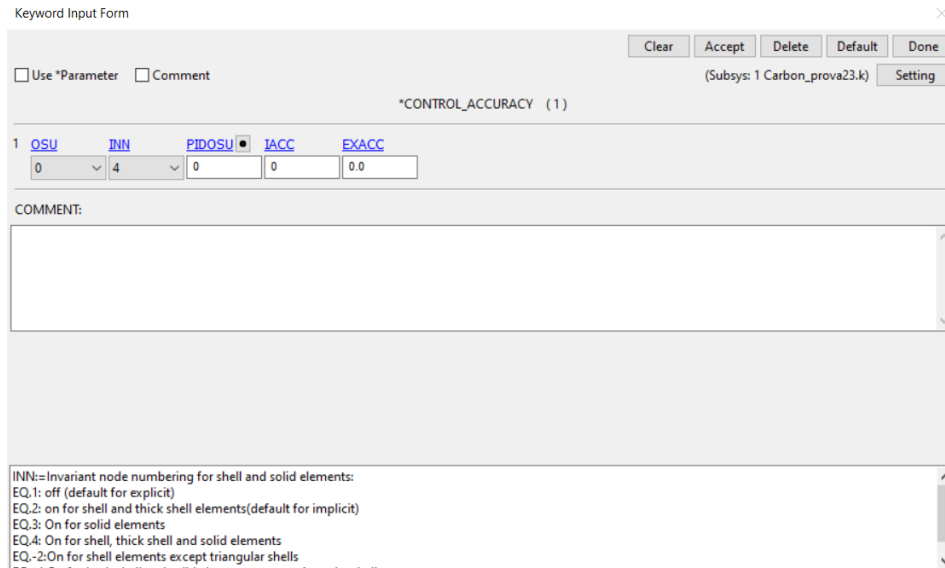


Figure 74: control accuracy to improve the convergence

## Results of the elastic moduli temperature dependent analysis and comparison with the experimental results

In this section it will be illustrated the graphical and numerical results of the most important simulation performed in this study. The characteristic length of the solid elements was 1 mm, having in total 17284 elements. Particular attention has been dedicated also to the distortion index of the model, being connected with the determinant of the Jacobian matrix, in this case the distortion index had values between 0.999 and 1 which means that the elements were not distorted.

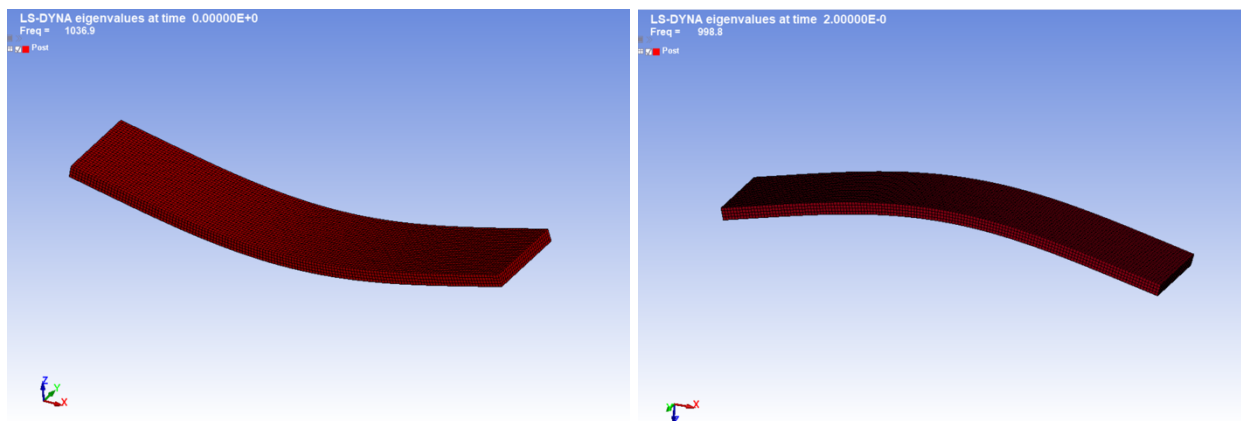


Figure 75: First mode at 25C (left) and at 80C (right) with frequency reduction

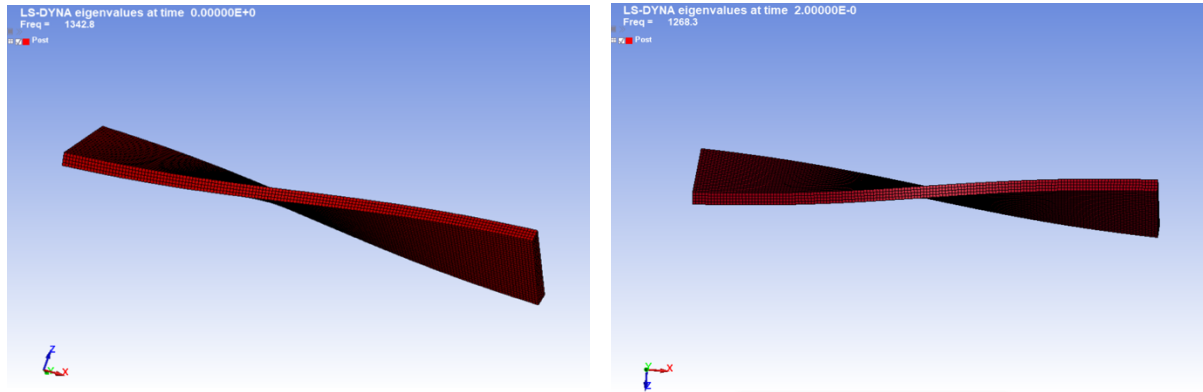


Figure 76: Second mode at 25C (left) and at 80C (right) with frequency reduction

Table 26: Comparison between experimental and numerical results of modal analysis with thermal dependency

Thin glass fiber with epoxy resin 30% natural						
1 <sup>st</sup> natural freq. experimental [Hz]	1 <sup>st</sup> natural freq. numerical [Hz]	2 <sup>nd</sup> natural freq. experimental [Hz]	2 <sup>nd</sup> natural freq. numerical [Hz]	%Diff. on the 1 <sup>st</sup> natural freq.	%Diff. on the 2 <sup>nd</sup> natural freq.	Temperature [°C]
571.4	570.6	1092.6	1038.1	0.14%	4.9%	25
567.7	566.6	1059.7	1001.3	0.19%	5.5%	40
559.2	558.5	994.2	944.5	0.13%	5%	60
505.7	505.1	728.3	701.2	0.12%	3.7%	80

Thick glass fiber with epoxy resin						
1 <sup>st</sup> natural freq. experimental [Hz]	1 <sup>st</sup> natural freq. numerical [Hz]	2 <sup>nd</sup> natural freq. experimental [Hz]	2 <sup>nd</sup> natural freq. numerical [Hz]	%Diff. on the 1 <sup>st</sup> natural freq.	%Diff. on the 2 <sup>nd</sup> natural freq.	Temperature [°C]
668.6	667.2	1338.3	1273.4	0.21%	4.85%	25
664.5	663.4	1312.2	1251.1	0.16%	4.65%	40
647.6	647.1	1243.2	1191.4	0.08%	4.16%	60
606.8	606.8	1215.8	1161.9	0%	4.43%	80

Carbon fiber with epoxy resin						
1 <sup>st</sup> natural freq. experimental [Hz]	1 <sup>st</sup> natural freq. numerical [Hz]	2 <sup>nd</sup> natural freq. experimental [Hz]	2 <sup>nd</sup> natural freq. numerical [Hz]	%Diff. on the 1 <sup>st</sup> natural freq.	%Diff. on the 2 <sup>nd</sup> natural freq.	Temperature [°C]
1042.8	1036.9	1388.7	1342.8	0.56%	3.31%	25
1041.6	1035.8	1357	1314.9	0.55%	3.10%	40
1032.7	1027.2	1314	1275	0.53%	2.97%	60
1003.8	998.8	1308.9	1268.3	0.49%	3.10%	80

Flax fiber with epoxy resin						
1 <sup>st</sup> natural freq. experimental [Hz]	1 <sup>st</sup> natural freq. numerical [Hz]	2 <sup>nd</sup> natural freq. experimental [Hz]	2 <sup>nd</sup> natural freq. numerical [Hz]	%Diff. on the 1 <sup>st</sup> natural freq.	%Diff. on the 2 <sup>nd</sup> natural freq.	Temperature [°C]
534.4	534.1	962	923.1	0.056%	4.04%	25
521.2	521.1	923.6	887.3	0.019%	3.93%	40

488.5	488.3	825	794.9	0.041%	3.65%	60
380.3	379.8	679.1	648.4	0.13%	4.52%	80

## Validation of the numerical model

In this section of the study, the numerical model will be validated thanks to some simulations performed at intermediate temperature, in particular at 50 and 70°C. The results of the experimental tests and numerical results will be compared in order to understand if the model is reflecting the reality and how is the model interpolating between the given parameters. As a reminder, in the material card 23 it has been implemented 4 points with mechanical properties at 25, 40, 60, and 80°C. So, to get the values at 50 and 70°C the software will interpolate between the given points.

Table 27: Validation and comparison of intermediate temperatures

Thin glass fiber with epoxy resin 30% natural						
1 <sup>st</sup> natural freq. experimental [Hz]	1 <sup>st</sup> natural freq. numerical [Hz]	2 <sup>nd</sup> natural freq. experimental [Hz]	2 <sup>nd</sup> natural freq. numerical [Hz]	%Diff. on the 1 <sup>st</sup> natural freq.	%Diff. on the 2 <sup>nd</sup> natural freq.	Temperature [°C]
561.6	562.6	1020.9	973.5	0.17%	4.64%	50
538.7	532.5	858.8	832.4	1.15%	3.07%	70

Thick glass fiber with epoxy resin						
1 <sup>st</sup> natural freq. experimental [Hz]	1 <sup>st</sup> natural freq. numerical [Hz]	2 <sup>nd</sup> natural freq. experimental [Hz]	2 <sup>nd</sup> natural freq. numerical [Hz]	%Diff. on the 1 <sup>st</sup> natural freq.	%Diff. on the 2 <sup>nd</sup> natural freq.	Temperature [°C]
656.2	655.4	1282.4	1221.7	0.12%	4.73%	50
619.6	627.4	1228	1176.8	1.35%	4.16%	70

Carbon fiber with epoxy resin						
1 <sup>st</sup> natural freq. experimental [Hz]	1 <sup>st</sup> natural freq. numerical [Hz]	2 <sup>nd</sup> natural freq. experimental [Hz]	2 <sup>nd</sup> natural freq. numerical [Hz]	%Diff. on the 1 <sup>st</sup> natural freq.	%Diff. on the 2 <sup>nd</sup> natural freq.	Temperature [°C]
1036.3	1031.6	1328.3	1295.2	0.45%	2.49%	50
1017.7	1013.2	1310.8	1271.7	0.44%	2.98%	70

Flax fiber with epoxy resin						
1 <sup>st</sup> natural freq. experimental [Hz]	1 <sup>st</sup> natural freq. numerical [Hz]	2 <sup>nd</sup> natural freq. experimental [Hz]	2 <sup>nd</sup> natural freq. numerical [Hz]	%Diff. on the 1 <sup>st</sup> natural freq.	%Diff. on the 2 <sup>nd</sup> natural freq.	Temperature [°C]
498.4	505	856	842.5	1.32%	1.57%	50
451.9	437.6	784.9	725.9	3.16%	7.51%	70

As it can be observed in the table the difference in percentage for the first natural frequency is quite accurate for the first natural frequency being in almost all the cases under 3%, the big

difference is observed on the second natural frequency where it reaches also 7.5% for the flax. For this reason, it is necessary to see and understand how is the software interpolating in this particular material card.

In the implementation for three-dimensional continua a total Lagrangian formulation is used. In this approach the material law that relates second Piola-Kirchhoff stress  $S$  to the Green-St. Venant strain  $E$  is:

$$S = C \cdot E = T^T C_1 T \cdot E \quad (7.3)$$

Where  $T$  is the transformation matrix

$$T = \begin{bmatrix} l_1^2 & m_1^2 & n_1^2 & & & & l_1 m_1 & m_1 n_1 & n_1 l_1 \\ l_2^2 & m_2^2 & n_2^2 & & & & l_2 m_2 & m_2 n_2 & n_2 l_2 \\ l_3^2 & m_3^2 & n_3^2 & & & & l_3 m_3 & m_3 n_3 & n_3 l_3 \\ 2l_1 l_2 & 2m_1 m_2 & 2n_1 n_2 & (l_1 m_2 + l_2 m_1) & (m_1 n_2 + m_2 n_1) & (n_1 l_2 + n_2 l_1) & & & \\ 2l_2 l_3 & 2m_2 m_3 & 2n_2 n_3 & (l_2 m_3 + l_3 m_2) & (m_2 n_3 + m_3 n_2) & (n_2 l_3 + n_3 l_2) & & & \\ 2l_3 l_1 & 2m_3 m_1 & 2n_3 n_1 & (l_3 m_1 + l_1 m_3) & (m_3 n_1 + m_1 n_3) & (n_3 l_1 + n_1 l_3) & & & \end{bmatrix} \quad (7.4)$$

$l_i, m_i, n_i$  are the direction cosines.

The material axis  $x'_i$  is given by:

$$x'_i = l_i x_1 + m_i x_2 + n_i x_3 \quad \text{for } i = 1, 2, 3 \quad (7.5)$$

The temperature dependent constitutive matrix  $C_1$  is defined in terms of the material axes as

$$C_1^{-1} = \begin{bmatrix} \frac{1}{E_{11}(T)} & -\frac{\nu_{21}(T)}{E_{22}(T)} & -\frac{\nu_{31}(T)}{E_{33}(T)} & & & & & & \\ & \frac{1}{E_{22}(T)} & -\frac{\nu_{32}(T)}{E_{33}(T)} & & & & 0 & 0 & 0 \\ -\frac{\nu_{12}(T)}{E_{11}(T)} & & & & & & 0 & 0 & 0 \\ \frac{\nu_{13}(T)}{E_{11}(T)} & -\frac{\nu_{23}(T)}{E_{22}(T)} & \frac{1}{E_{33}(T)} & & & & 0 & 0 & 0 \\ & & & & & & & & \\ & & & & & & \frac{1}{G_{12}(T)} & 0 & 0 \\ & 0 & 0 & 0 & & & & & \\ & 0 & 0 & 0 & & & 0 & \frac{1}{G_{23}(T)} & 0 \\ & 0 & 0 & 0 & & & 0 & 0 & \frac{1}{G_{31}(T)} \end{bmatrix} \quad (7.6)$$

Since C1 is symmetric

$$\frac{\nu_{12}}{E_{11}} = \frac{\nu_{21}}{E_{22}} \quad (7.7)$$

The vector of Green-St. Venant strain components is:

$$E^T = [E_{11} \ E_{22} \ E_{33} \ E_{12} \ E_{23} \ E_{31}] \quad (7.8)$$

The local strains are integrated in time in the following form:

$$\varepsilon_{aa}^{n+1} = \varepsilon_{aa}^n + \alpha_a \left( T^{n+\frac{1}{2}} \right) [T^{n+1} - T^n] \quad (7.9)$$

$$\varepsilon_{bb}^{n+1} = \varepsilon_{bb}^n + \alpha_b \left( T^{n+\frac{1}{2}} \right) [T^{n+1} - T^n] \quad (7.10)$$

$$\varepsilon_{cc}^{n+1} = \varepsilon_{cc}^n + \alpha_c \left( T^{n+\frac{1}{2}} \right) [T^{n+1} - T^n] \quad (7.11)$$

Where alfa is the coefficient of thermal expansion.

Due to this formulation the natural frequencies, which are strictly connected to the stiffness of the structure (that is now temperature dependent) and to the changing geometry (due to thermal expansion), are not actually linearly interpolated.

The results of a linear interpolation at 50 and 70°C are illustrated and compared with the experimental results in the table n.

Table 28: Comparison of experimental natural freq. and from the linear interpolation

Thin glass fiber with epoxy resin 30% natural						
1 <sup>st</sup> natural freq. experimental [Hz]	1 <sup>st</sup> natural freq. linear interpolation [Hz]	2 <sup>nd</sup> natural freq. experimental [Hz]	2 <sup>nd</sup> natural freq. linear interpolation [Hz]	%Diff. on the 1 <sup>st</sup> natural freq.	%Diff. on the 2 <sup>nd</sup> natural freq.	Temperature [°C]
561.6	563.5	1020.9	1026.9	0.34%	0.59%	50
538.7	532.5	858.8	861.3	1.15%	0.29%	70

Thick glass fiber with epoxy resin						
1 <sup>st</sup> natural freq. experimental [Hz]	1 <sup>st</sup> natural freq. linear interpolation [Hz]	2 <sup>nd</sup> natural freq. experimental [Hz]	2 <sup>nd</sup> natural freq. linear interpolation [Hz]	%Diff. on the 1 <sup>st</sup> natural freq.	%Diff. on the 2 <sup>nd</sup> natural freq.	Temperature [°C]
656.2	656.1	1282.4	1277.7	0.015%	0.37%	50
619.6	627.2	1228	1229.5	1.23%	0.12%	70

Carbon fiber with epoxy resin						
1 <sup>st</sup> natural freq. experimental [Hz]	1 <sup>st</sup> natural freq. linear interpolation [Hz]	2 <sup>nd</sup> natural freq. experimental [Hz]	2 <sup>nd</sup> natural freq. linear interpolation [Hz]	%Diff. on the 1 <sup>st</sup> natural freq.	%Diff. on the 2 <sup>nd</sup> natural freq.	Temperature [°C]
1036.3	1037.5	1328.3	1335.5	0.11%	0.54%	50
1017.7	1018.2	1310.8	1311.4	0.05%	0.05%	70

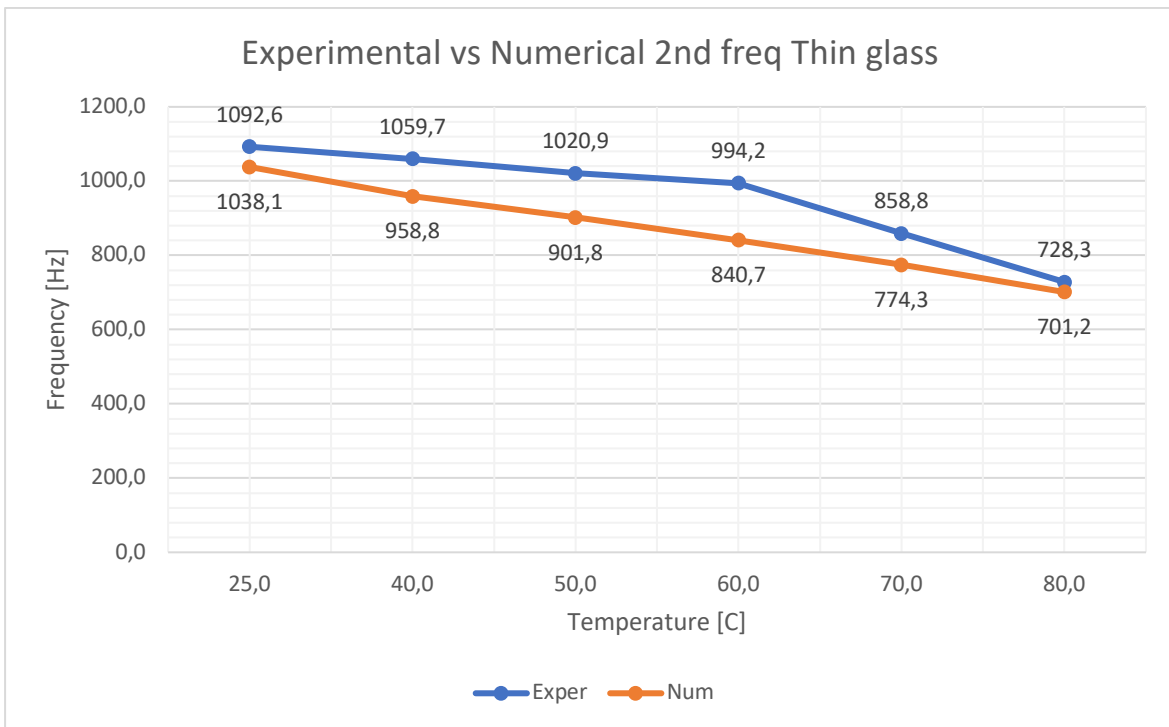
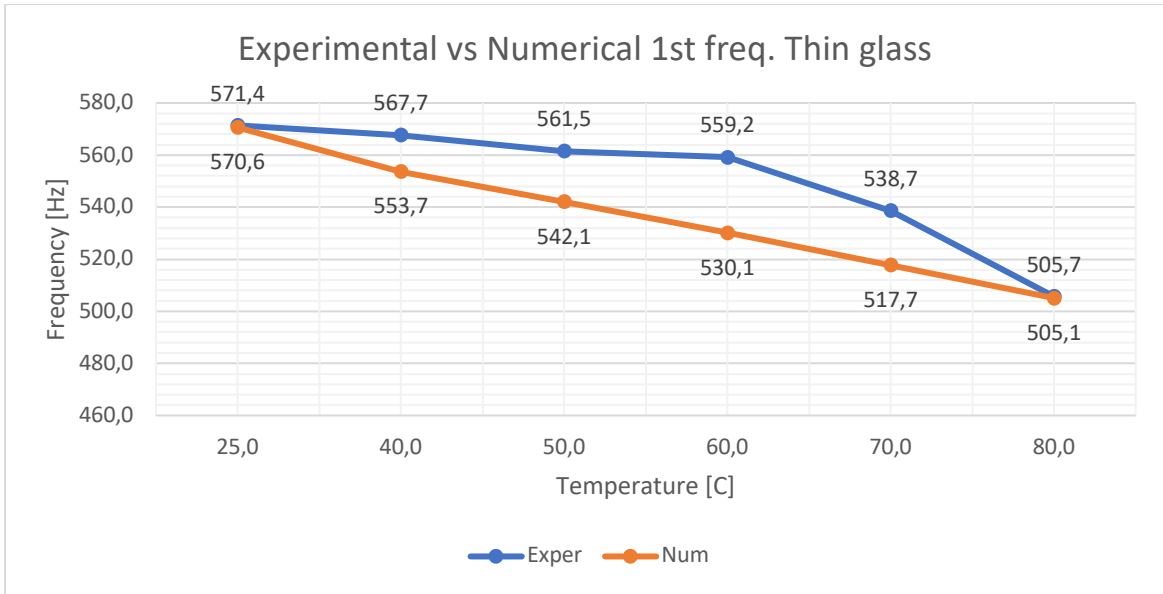
Flax fiber with epoxy resin						
1 <sup>st</sup> natural freq. experimental [Hz]	1 <sup>st</sup> natural freq. linear interpolation [Hz]	2 <sup>nd</sup> natural freq. experimental [Hz]	2 <sup>nd</sup> natural freq. linear interpolation [Hz]	%Diff. on the 1 <sup>st</sup> natural freq.	%Diff. on the 2 <sup>nd</sup> natural freq.	Temperature [°C]
498.4	504.8	856	874.3	1.28%	2.14%	50
451.9	434.3	784.9	752.1	3.89%	4.17%	70

The conclusion of this comparison is that, if it is compared also with the previous results where the software performed its own interpolation, by using a simple linear interpolation the results are better, especially considering the second natural frequency, where the difference is around 4%, significantly better than the previous result of 7%.

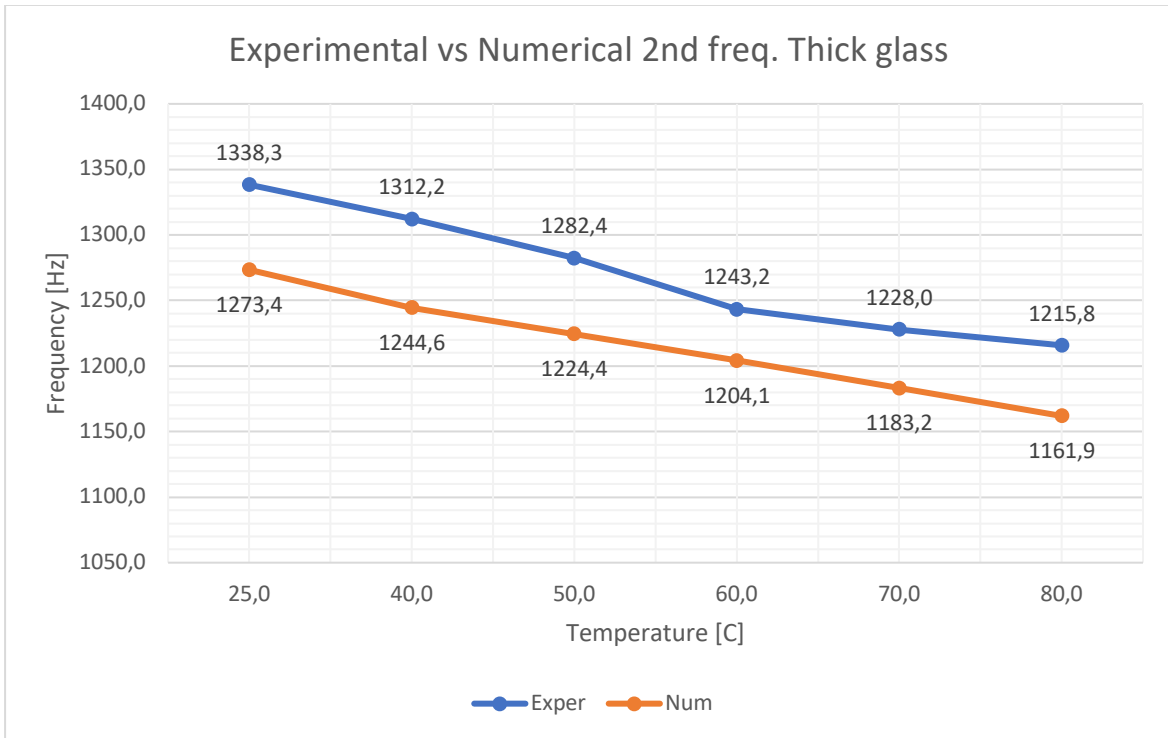
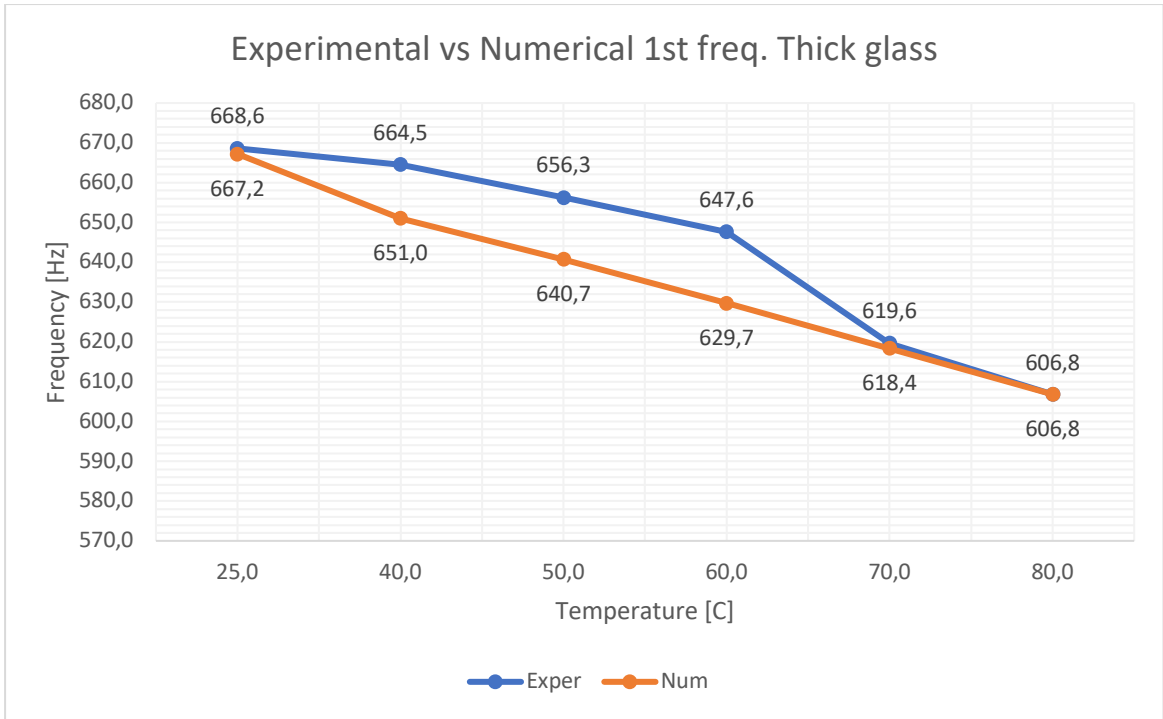
### Limits of the model

In this sub-section it will be shown how the model is behaving in a more extreme situation, in particular, the model will have in input only two points out of four, at 25 and 80°C (at the extremes of our testing). The general trend of the experimental frequencies will be compared with the results of interpolation of LS-Dyna.

Let's see the trend of the first and second natural frequency for thin glass.

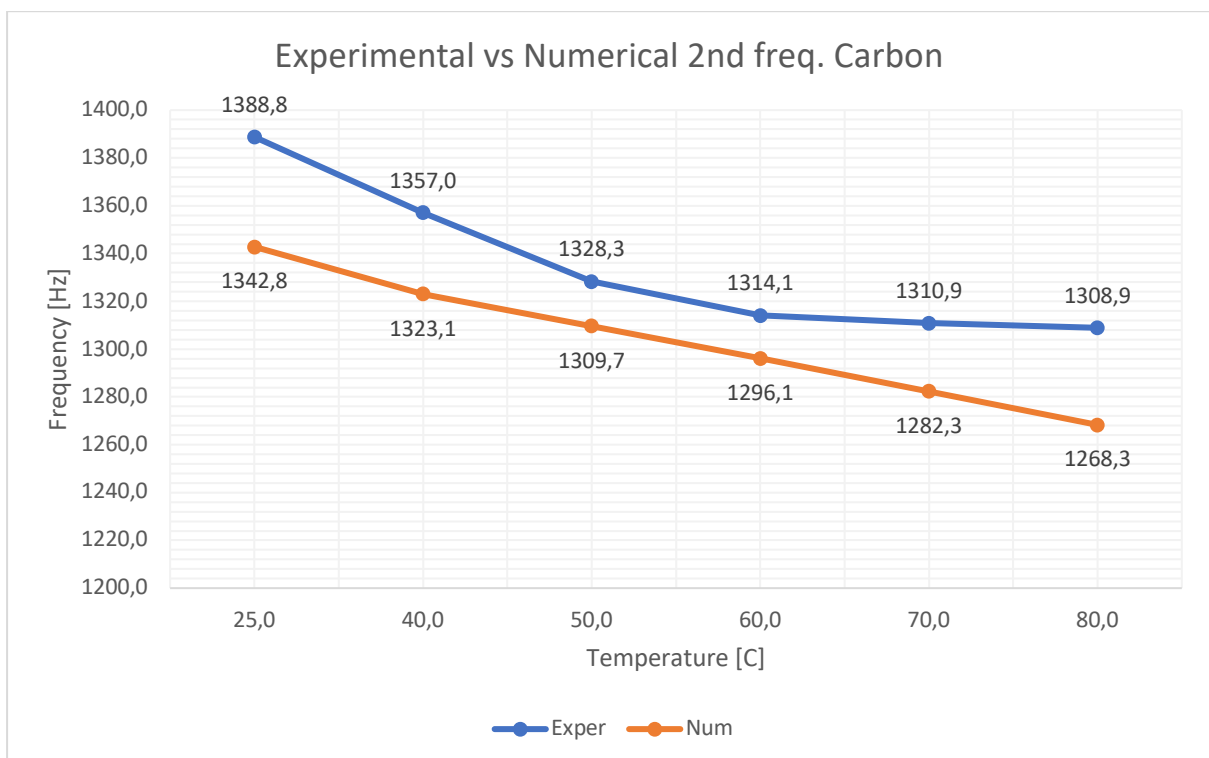
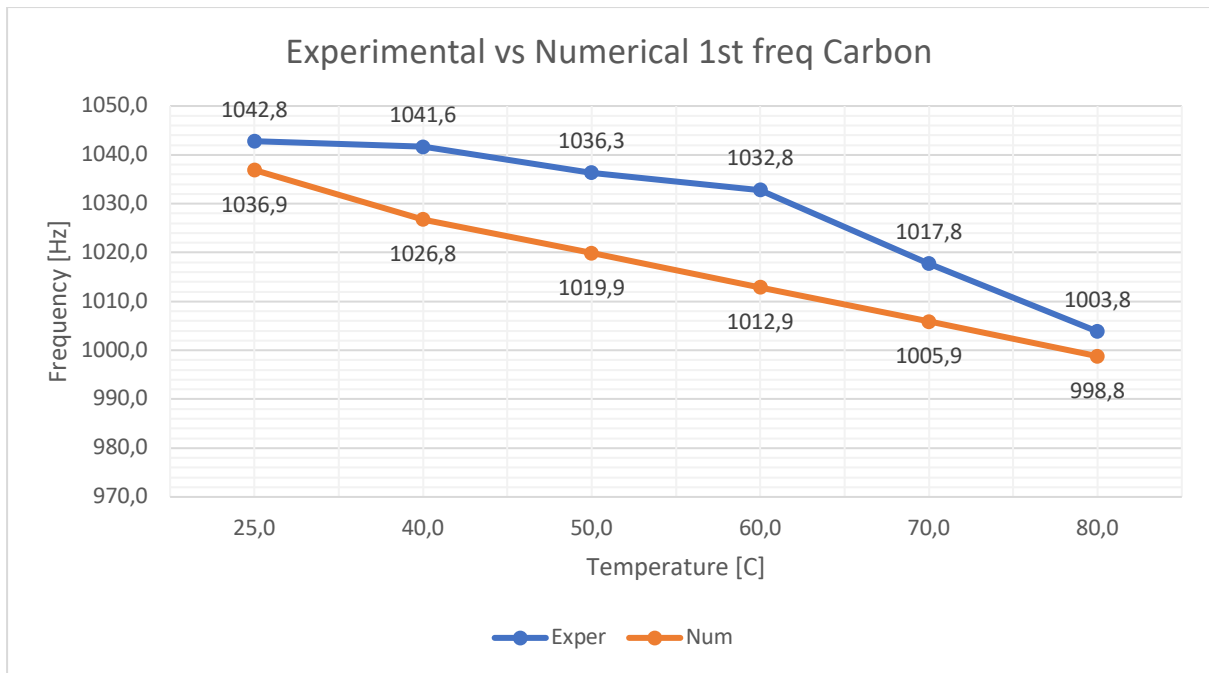


Same graphs can be plot for thick glass composite:

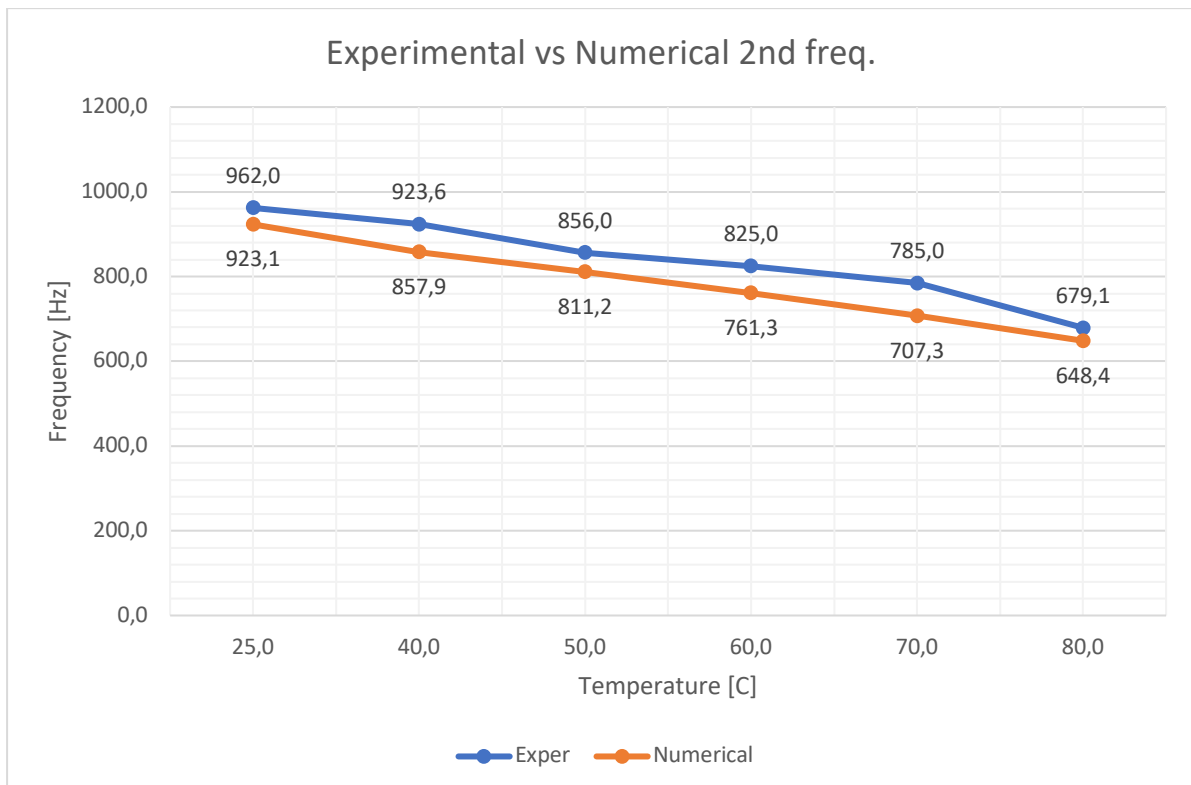
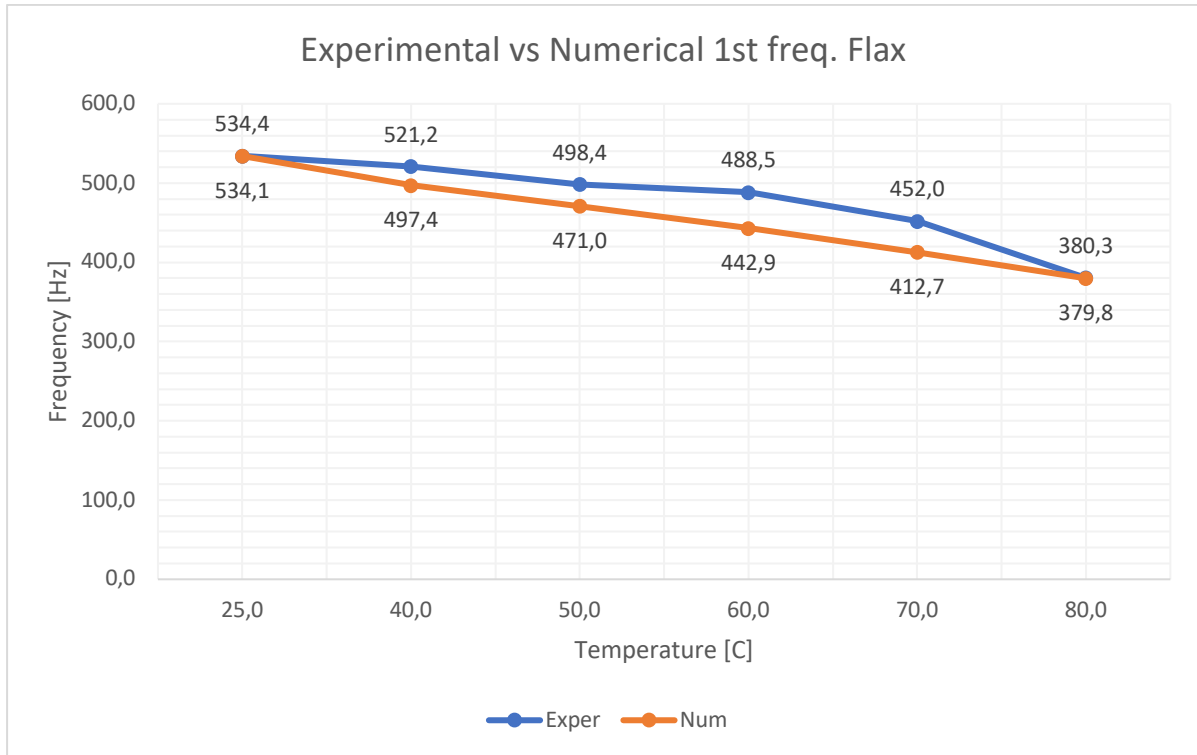


Let's see the carbon fiber composite:





Last but not the least, the flax composite:



The obvious conclusion is that the model behaves quite linear in both approximations, first and second natural frequency, moreover it is always underestimating the natural frequency

with respect to the real values. So the model considers the composites less stiff compared with the reality when the model is let free to interpolate having only two points.

## 8. Aging of composites

This section describes a process of aging applied to composites in order to understand how well are, the composites tested, reacting to extreme conditions. Considering that a lot of composites undergo an aging process during their life, especially in the automotive field, it might be interesting to see how their mechanical properties will be affected.

In this procedure of aging the four types of composites have been immersed in distilled water at 70°C in the oven. In total eight specimens (two by two identical) have been tested; the only difference was the immersion time. Four of them have been immersed for seven days while the other four composites for thirteen days.

Before immersion each composite has been measured, weighted, and subsequently conditioned for 16h at 70°C in order to reduce to minimum the humidity level present inside of it. After one week the first set of composites was taken out, measured, weighted, and afterward reconditioned for other 16h at 70°C. After the reconditioning, they were measured and weighted again and tested at the IET machine in the same range of temperatures used for the other tests seen before. The same procedure was used for the other four composites after thirteen days of aging.

In order to understand the increase in weight between the state wet and after the conditioning of 16h as well as the solubility of the resin, the standard ASTM D570-22 has been used [14].

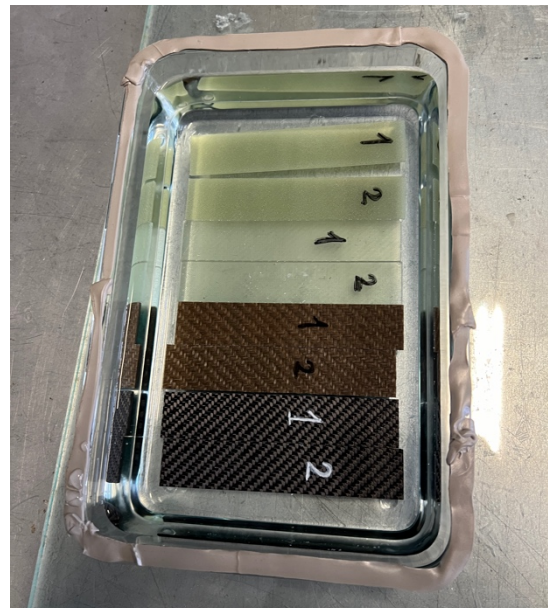
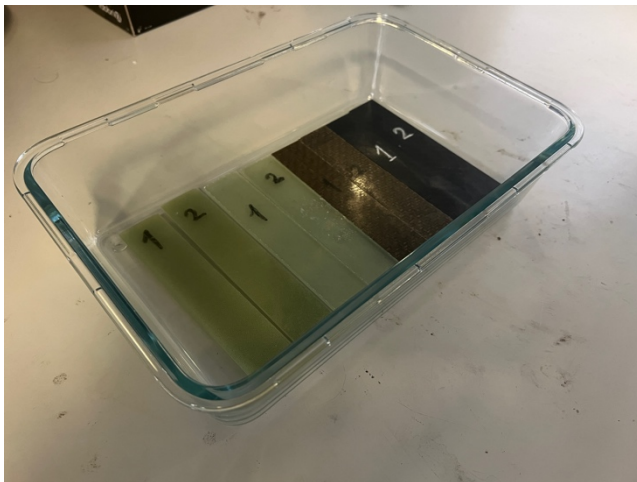
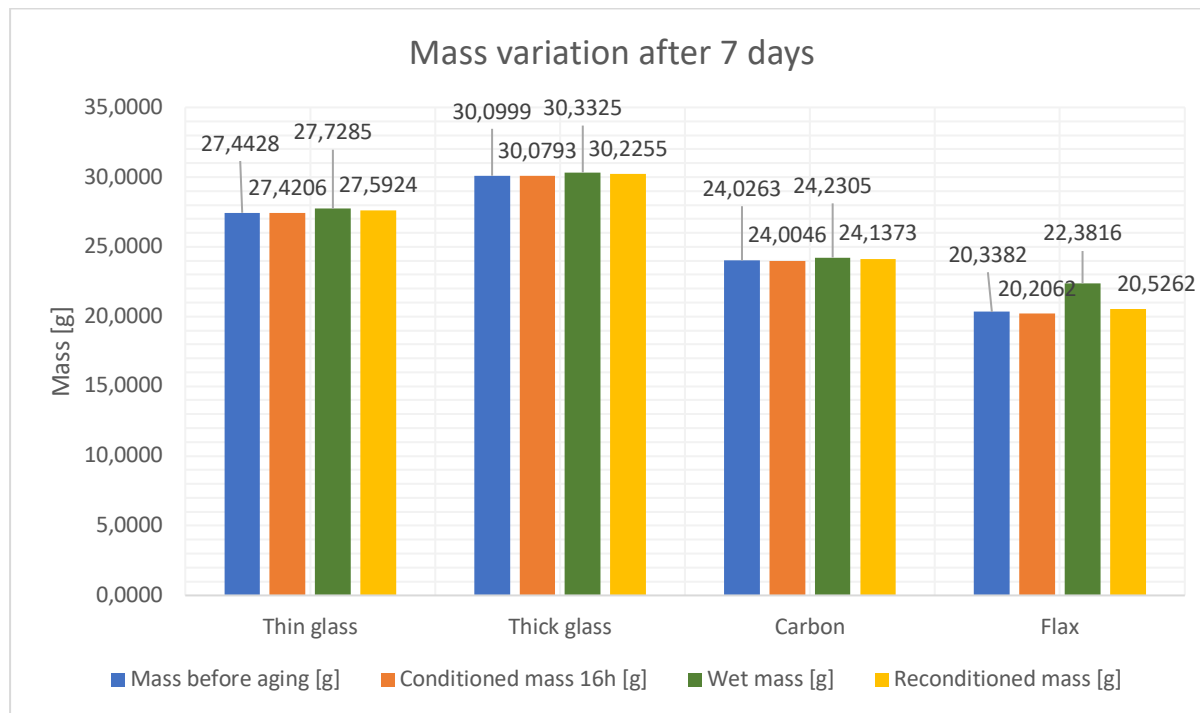


*Figure 77: Composites prepared for aging*

## Seven days aging – mass variation

In the following table it is shown the difference in mass of each composite (of the first set of four), before aging, after conditioning, after aging and after reconditioning.



By using the standard ASTM D570-22 and the equations suggested it is possible to calculate the percentage of increase weight between the conditioned mass and the wet mass. Moreover, it is possible to understand the percentage of soluble matter lost in the reconditioning.

$$\text{Increase in weight \%} = \frac{\text{wet weight} - \text{conditioned weight}}{\text{conditioned weight}} \times 100 \quad (8.0)$$

$$\text{Soluble matter lost \%} = \frac{\text{conditioned weight} - \text{reconditioned weight}}{\text{conditioned weight}} \times 100 \quad (8.1)$$

Table 29: Increase in weight and soluble matter

Composites	Thin glass	Thick glass	Carbon	Flax
Increase in weight %	1.12%	0.84%	0.94%	10.77%
Soluble matter lost%	-0.63%	-0.49%	-0.55%	-1.58%

As it can be seen from table 30, the flax exhibits the biggest increase in weight due to its fibers that absorb the water much easier with respect to the other types of fibers.

For what concerns the solubility of the resin in water, no matter is actually lost, it can be seen the negative values that mean an increase in weight between the conditioning and reconditioning, so even with 16h in the oven, the composites retained a small percentage of humidity.

### Seven days aging – external aspect and geometry

A special microscope has made it possible to assess the external appearance of the composites and detect any changes in color. For each specimen it will be shown three conditions: before aging, after seven days wet and after seven days of aging reconditioned. Depending on the type of composite, in most of the cases if there was no variation of the external aspect, the study is focused mainly on the thickness variation.

For the thin glass for example, there are no external variations, the color of the composite stays invariant the only variation is along the thickness. The composite is thicker after the reconditioning with respect to the initial geometry conditioned.

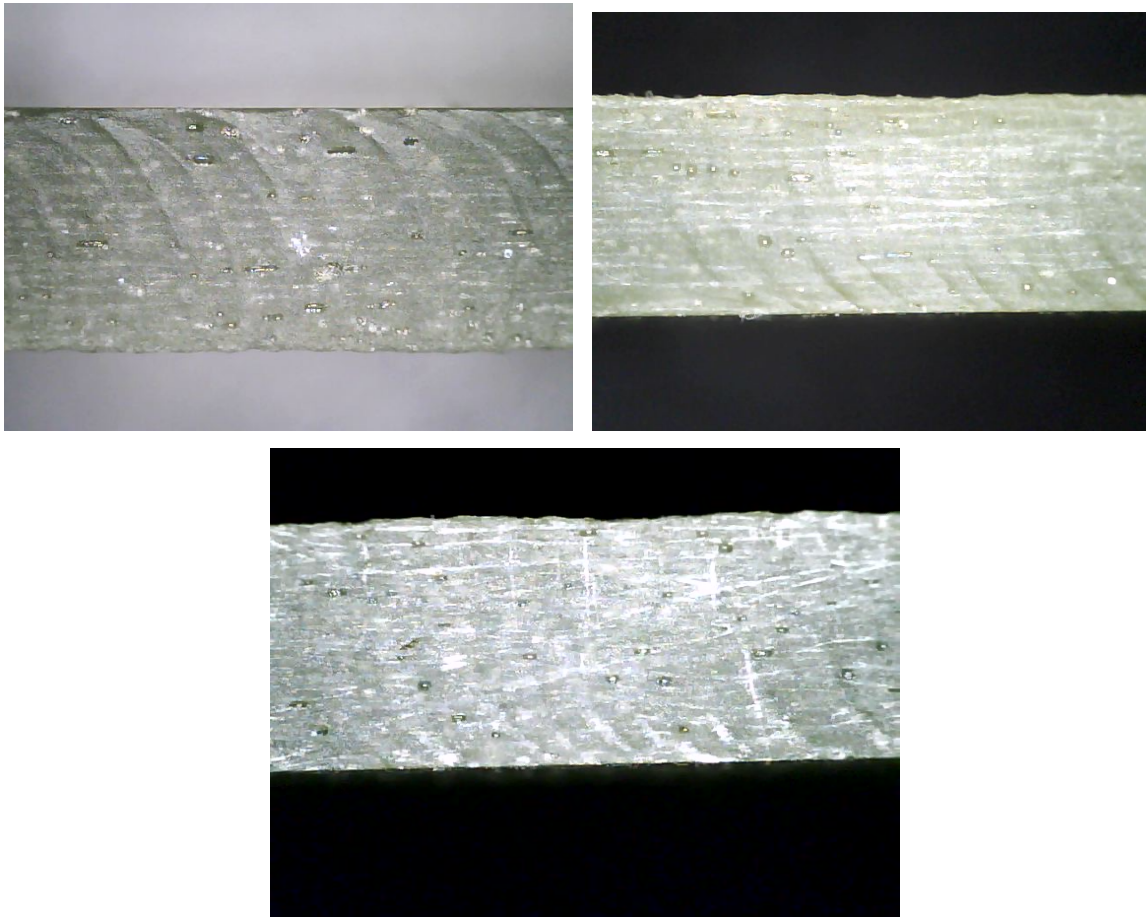


Figure 78: : thin glass thickness and aspect variation, conditioned (left), wet (right), reconditioned (below)

Table 30: Geometry variation for thin glass

Thin Glass Geometry				
	Conditioned	Wet	Reconditioned	%Increase between cond. and recond.
L [mm]	150.31	150.34	150.31	0%
b [mm]	30.56	30.56	30.56	0%
t [mm]	3.55	3.62	3.585	0.98%

For the thick glass composite the situation is similar as for the thin glass, the only important variation of geometry is along the thickness. The external aspect and color remain constant during the aging.

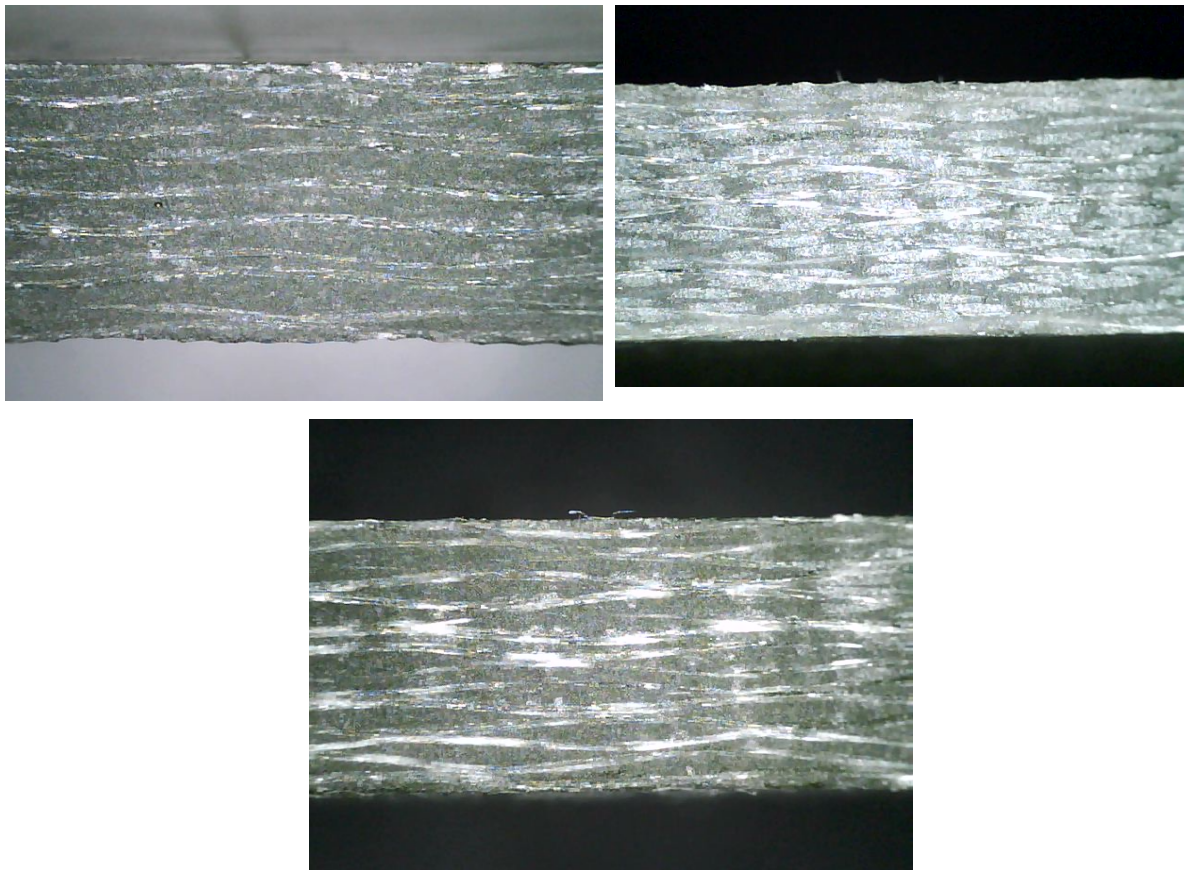


Figure 79: thick glass thickness and aspect variation, conditioned (left), wet (right), reconditioned (below)

Table 31: Geometry variation of thick glass

Thick Glass Geometry				%Increase between cond. and recond.
	Conditioned	Wet	Reconditioned	
L [mm]	148.94	148.94	148.94	0%
b [mm]	29.44	29.44	29.44	0%
t [mm]	4.01	4.05	4.00	-0,25%

For the Carbon composite the same aspects considered for the previous two composites are valid. The carbon doesn't suffer the humidity, similarly to the glass fibers. Due to small porosity inside the composite, water might get trapped insides and might seem that the composite is retaining some water.

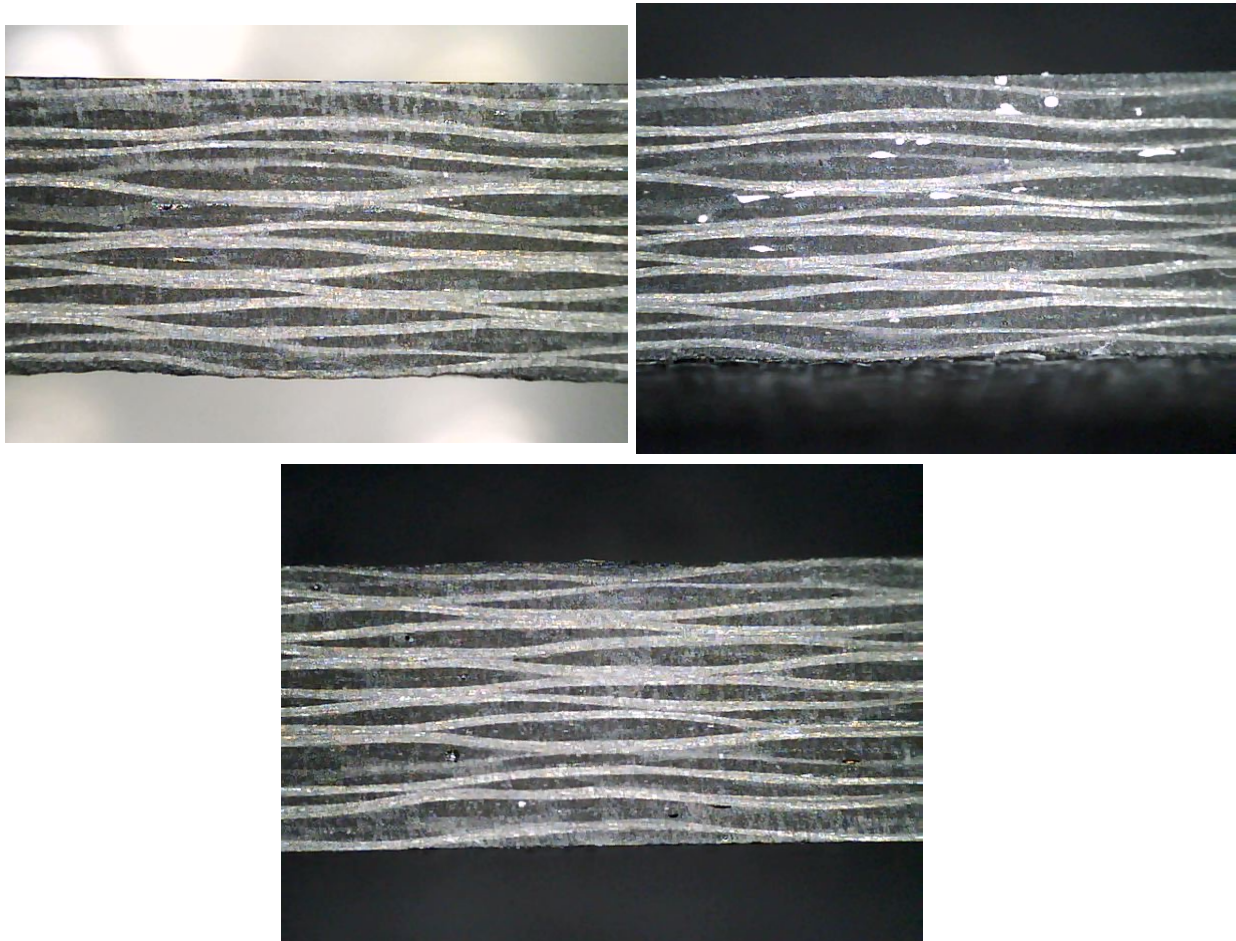


Figure 80: : carbon fibre thickness and aspect variation, conditioned (left), wet (right), reconditioned (below)



Table 32: Geometry variation of carbon

Carbon Geometry				%Increase between cond. and recond.
	Conditioned	Wet	Reconditioned	
L [mm]	149.10	149.10	149.10	0%
b [mm]	29.30	29.30	29.30	0%
t [mm]	3.96	4.035	4.00	1%

The most affected composite was the flax, due to the ability of linen fibers of absorbing humidity the thickness of the composites was significantly affected. The external aspect was affected too, the color of the composites changed passing from a light green to an almost dark yellow color. The fibers had absorbed the water becoming darker, having an almost black color on the surface of the composite.

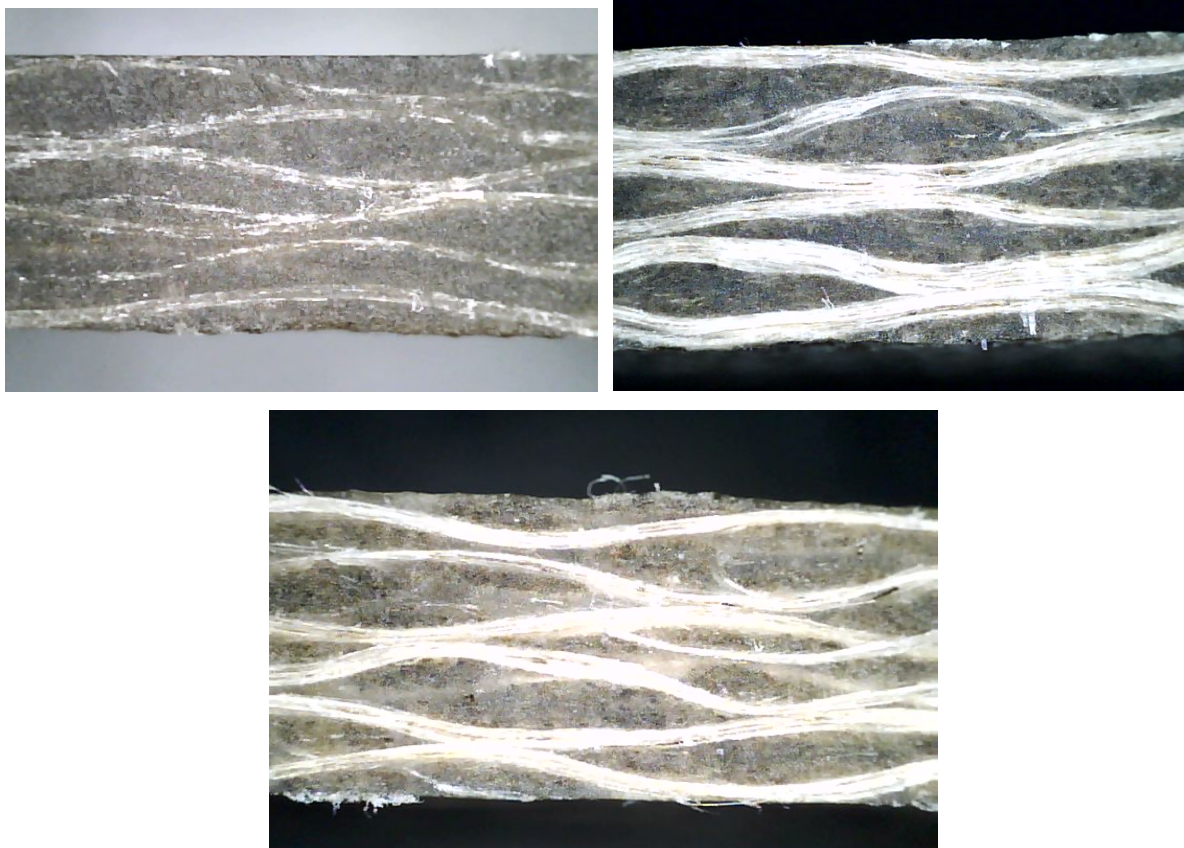
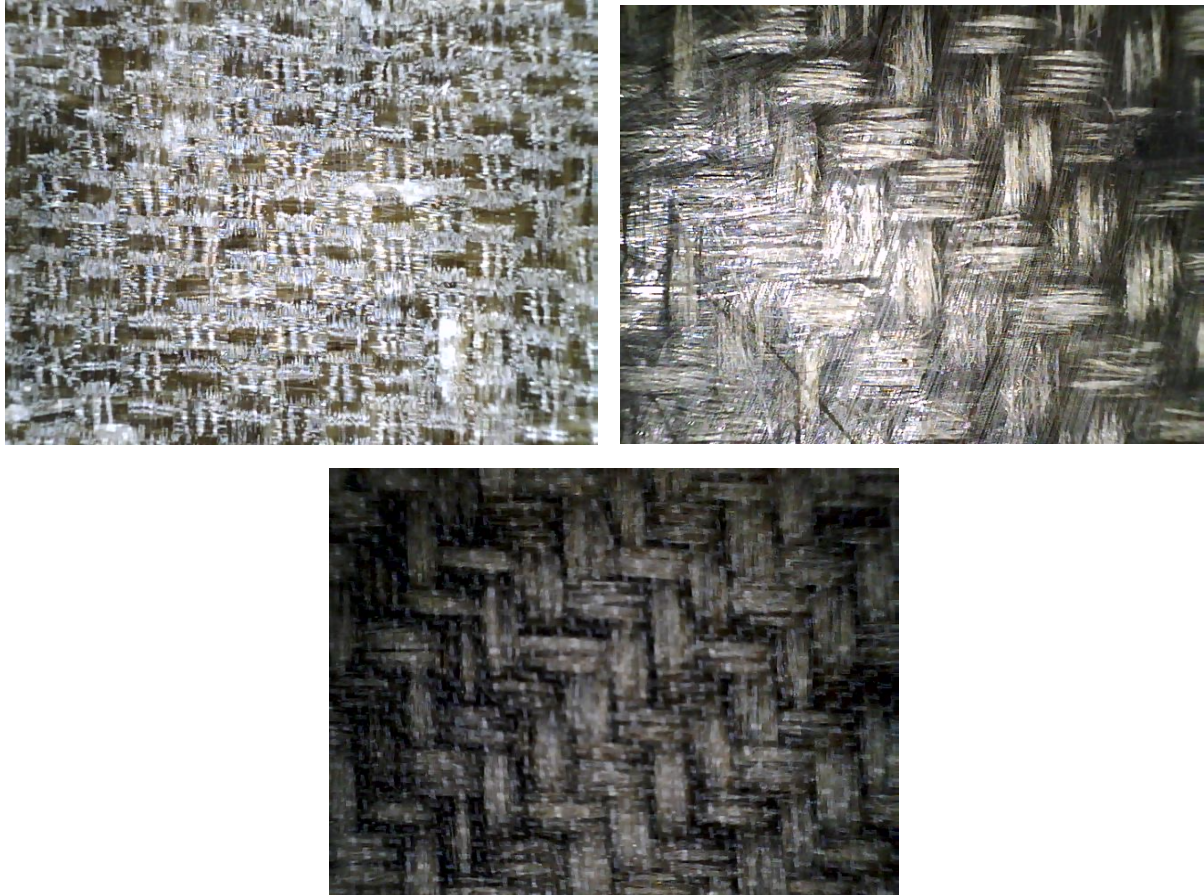


Figure 81: : flax thickness and aspect variation, conditioned (left), wet (right), reconditioned (below)

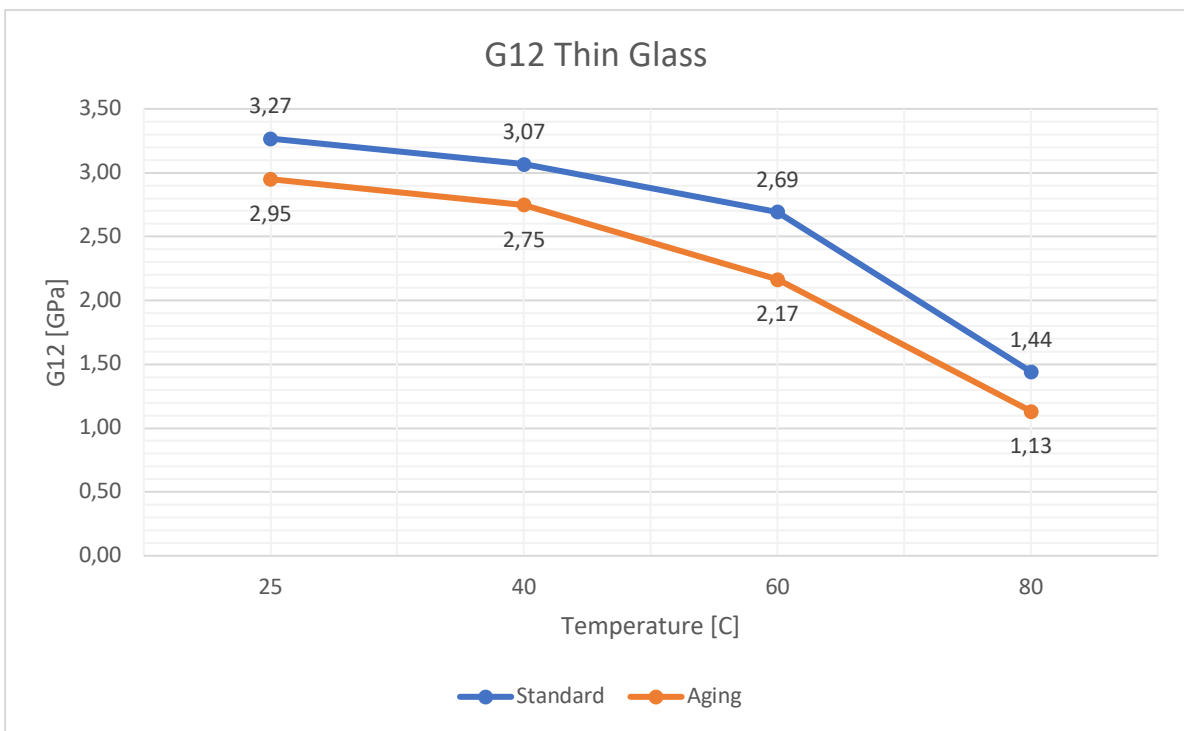
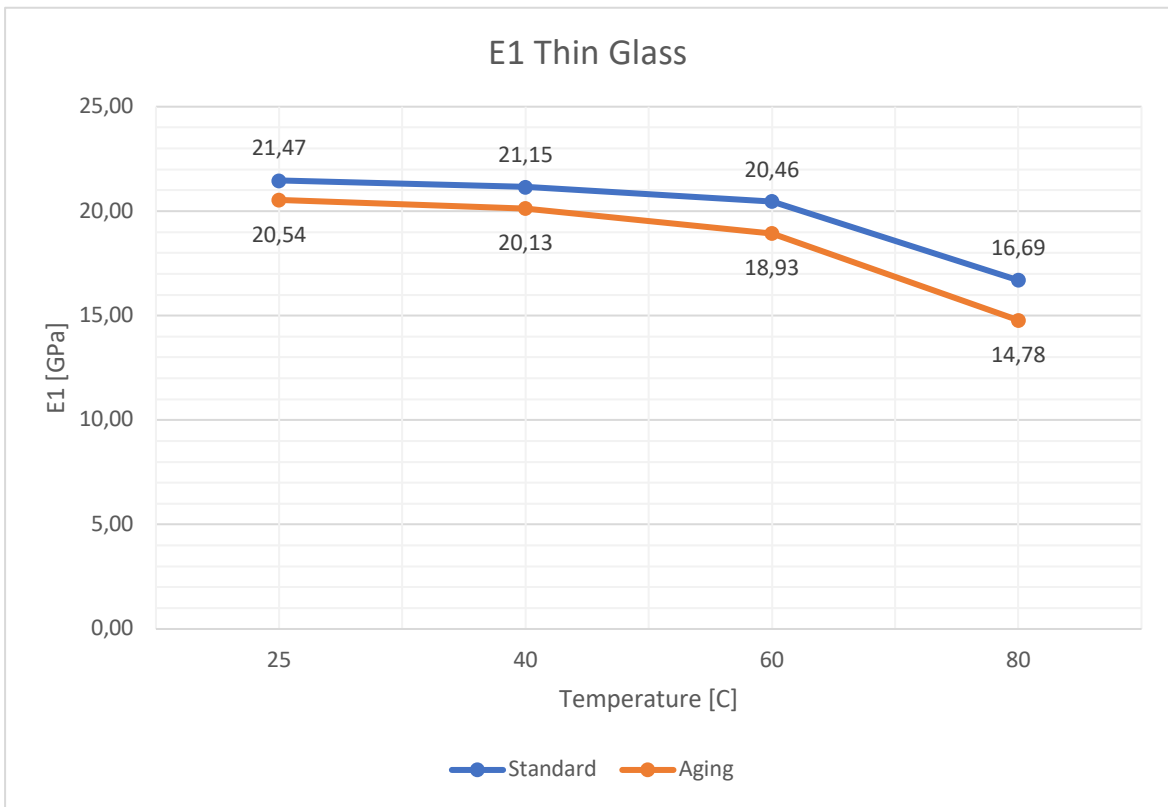


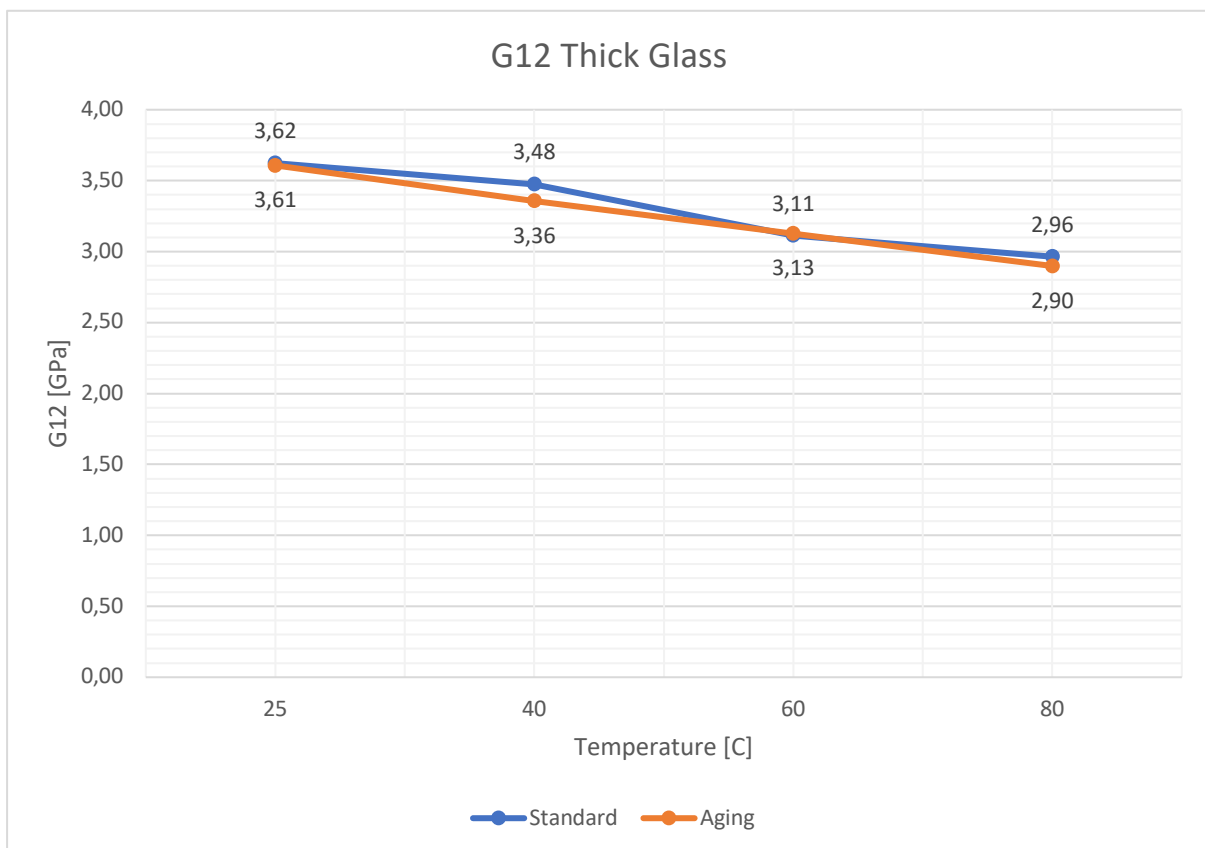
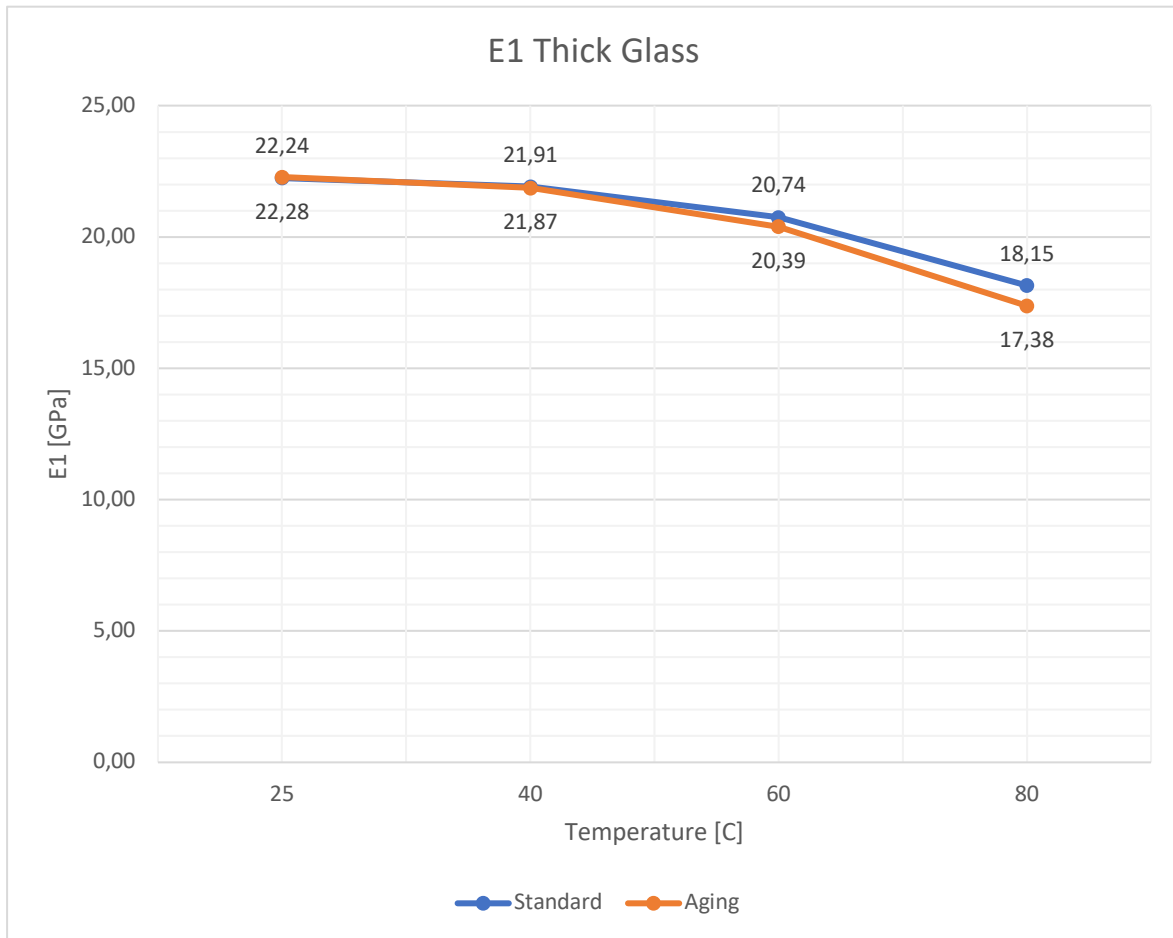
T Figure 82: flax aspect variation, conditioned (left), wet (right), reconditioned (below)

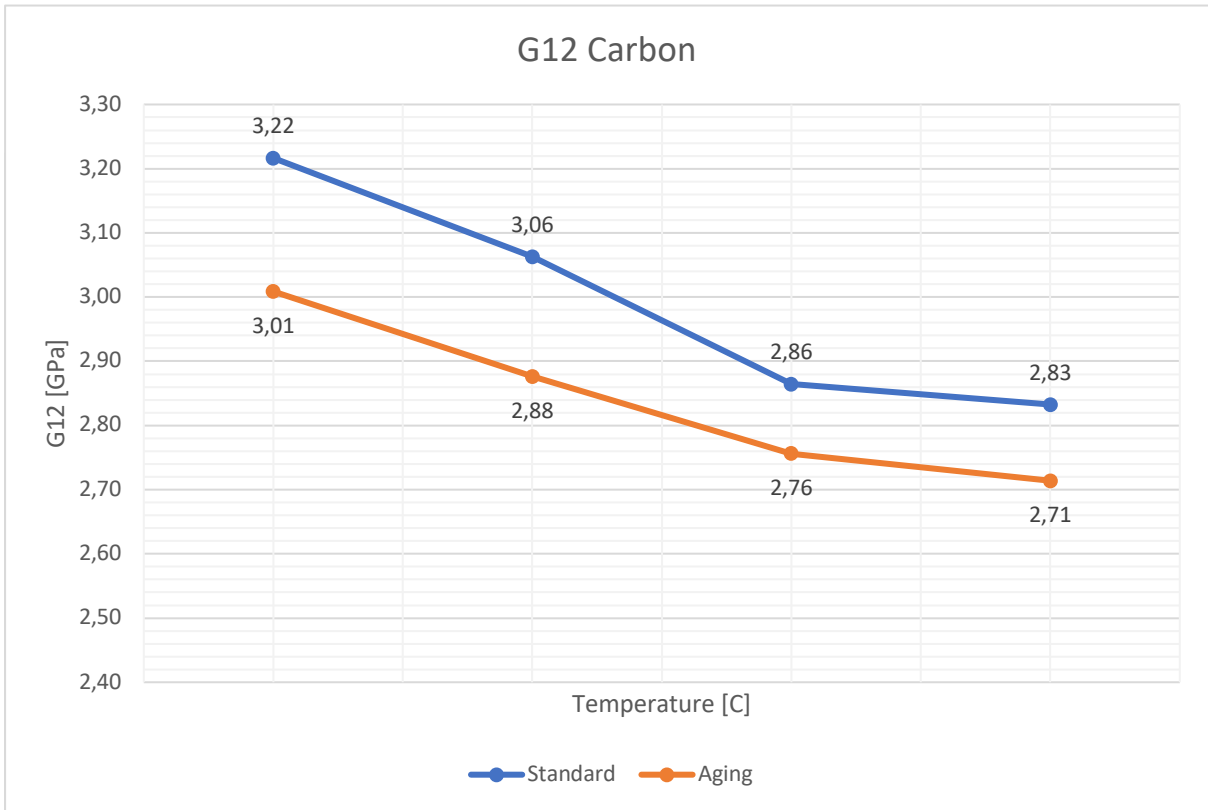
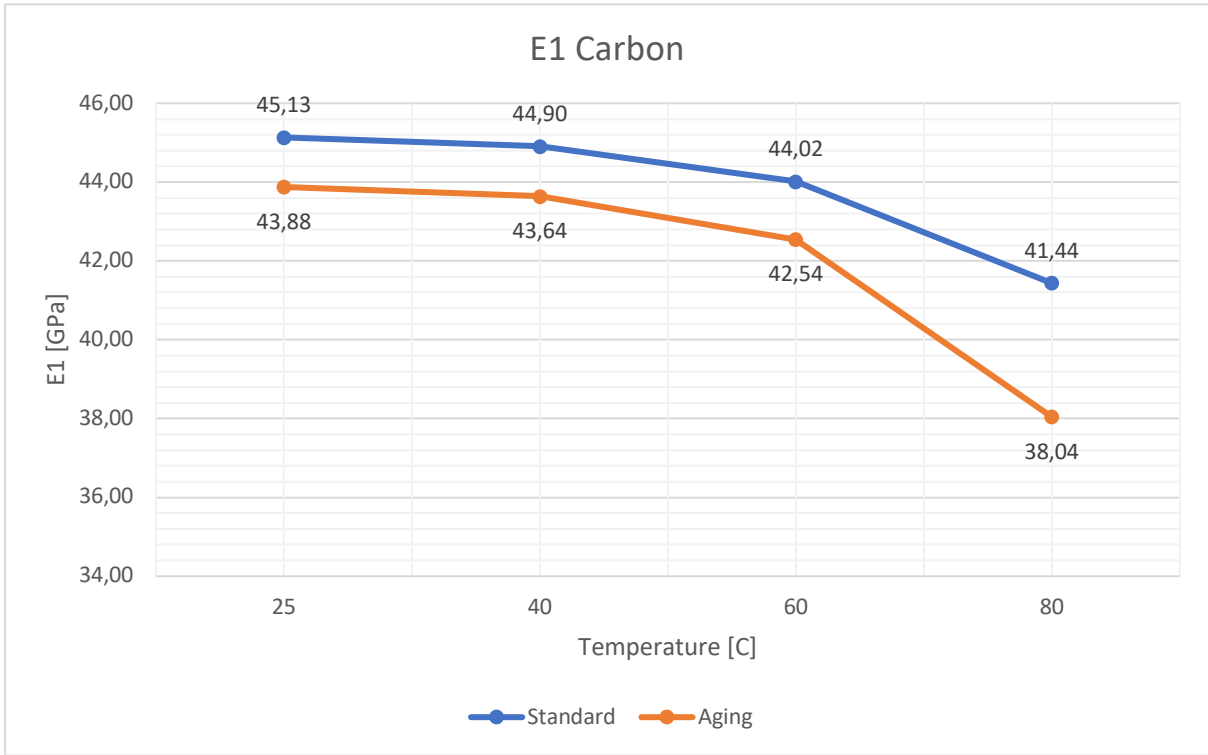
Flax Geometry				%Increase between cond. and recond.
	Conditioned	Wet	Reconditioned	
L [mm]	149.21	149.21	149.21	0%
b [mm]	29.33	29.33	29.33	0%
t [mm]	3.87	4.48	4.18	7,42%

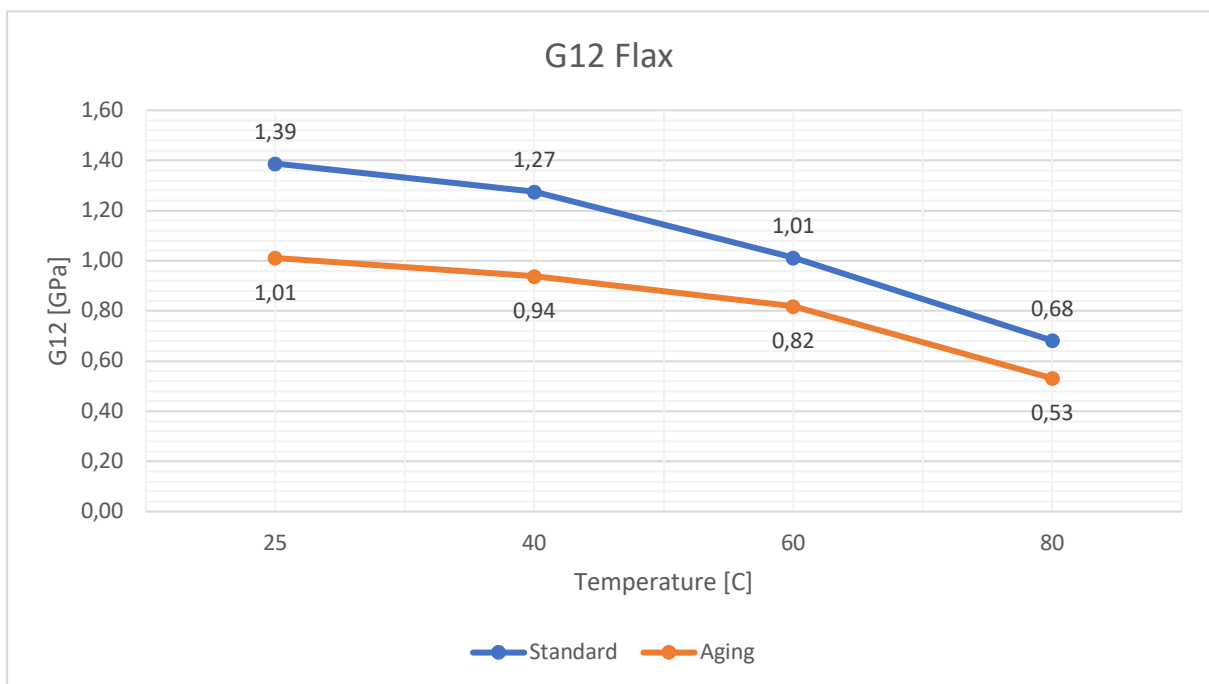
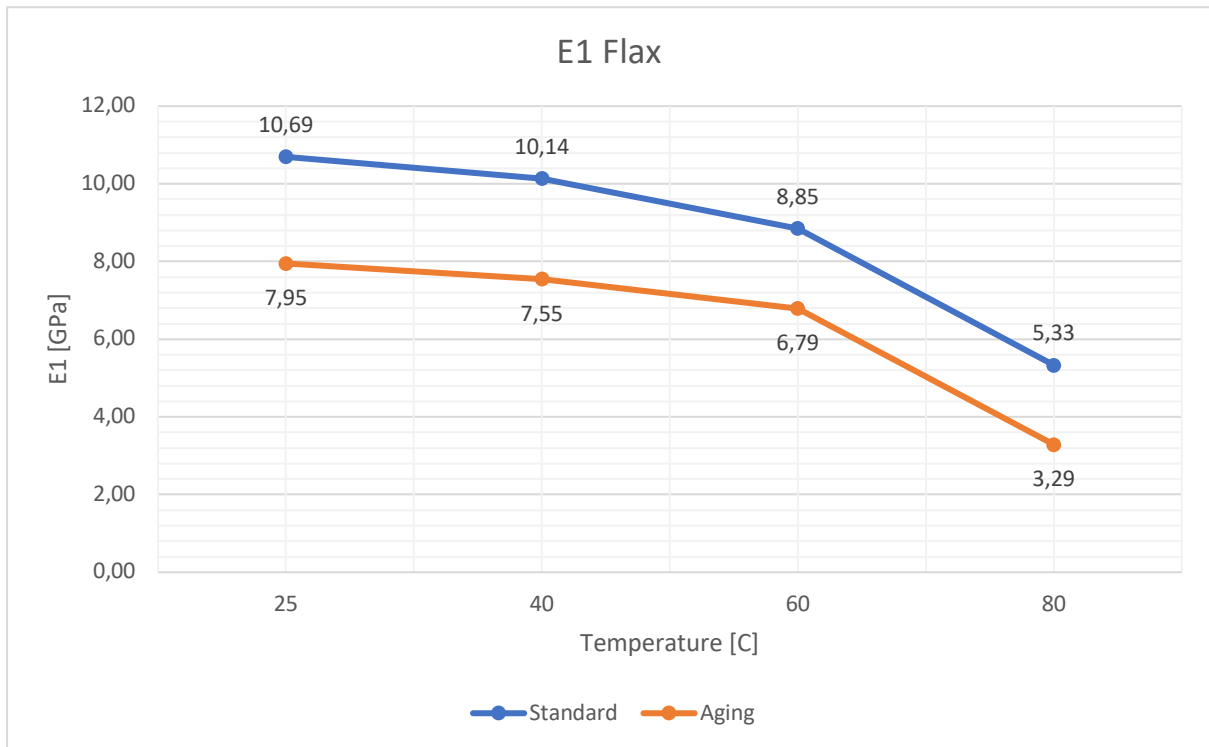
### Seven days aging – elastic moduli and damping coefficient

During this period of aging of seven days, the natural frequencies of the specimen had a reduction with respect to the standard ones (seen before) to a decrease of elastic moduli  $E_1$  and  $G_{12}$ . In the following pages, a series of graphs that compare the two conditions (standard or not aged and aged) will be presented showing how are the moduli change with temperature (25, 40, 60 ,80°C) but also how is the damping coefficient changing.

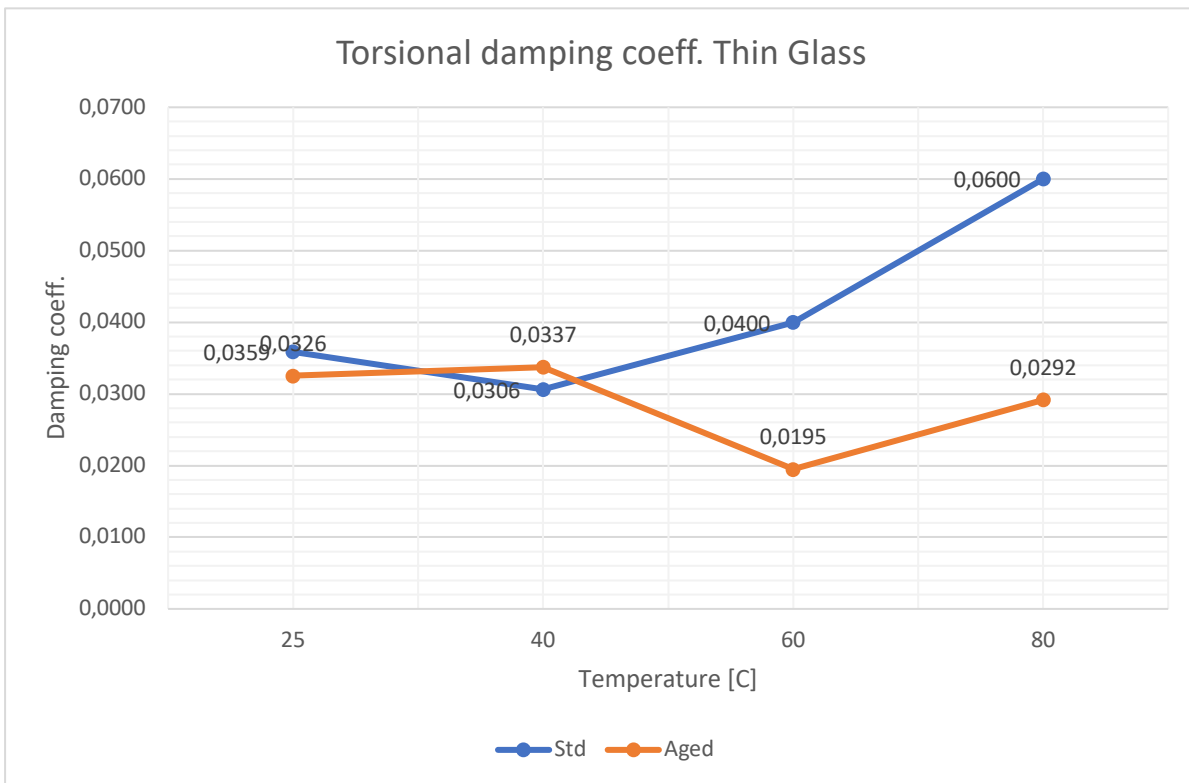
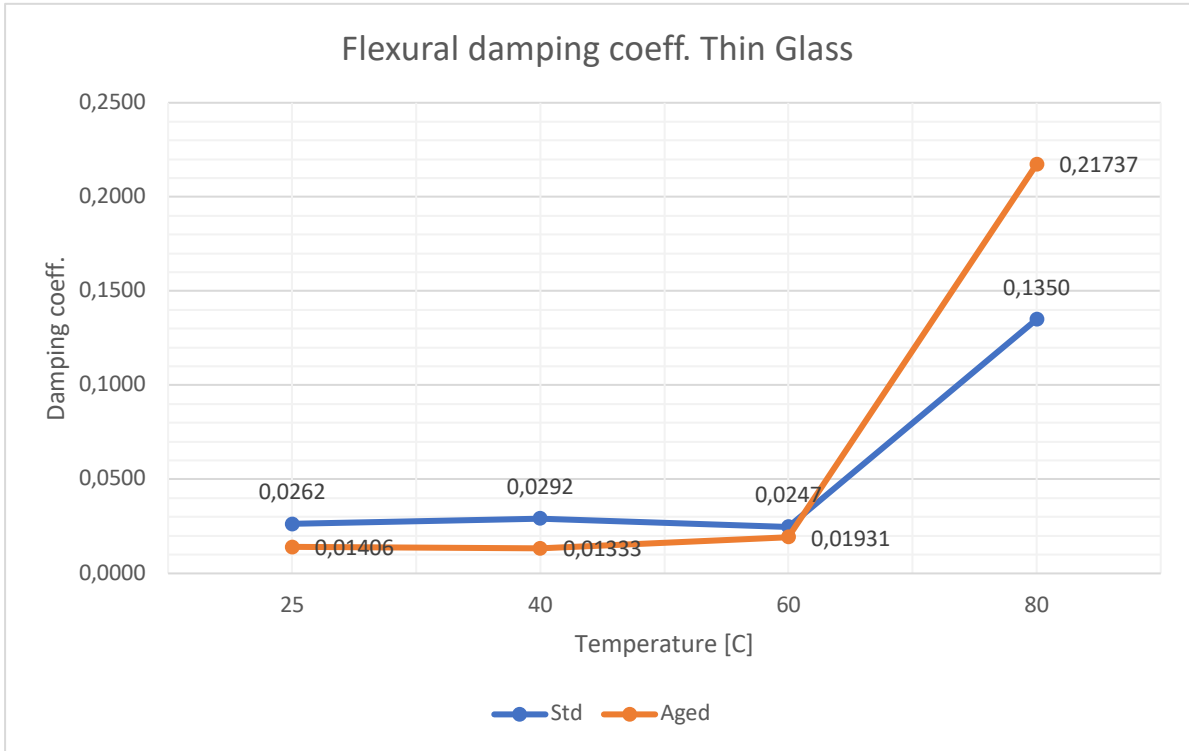


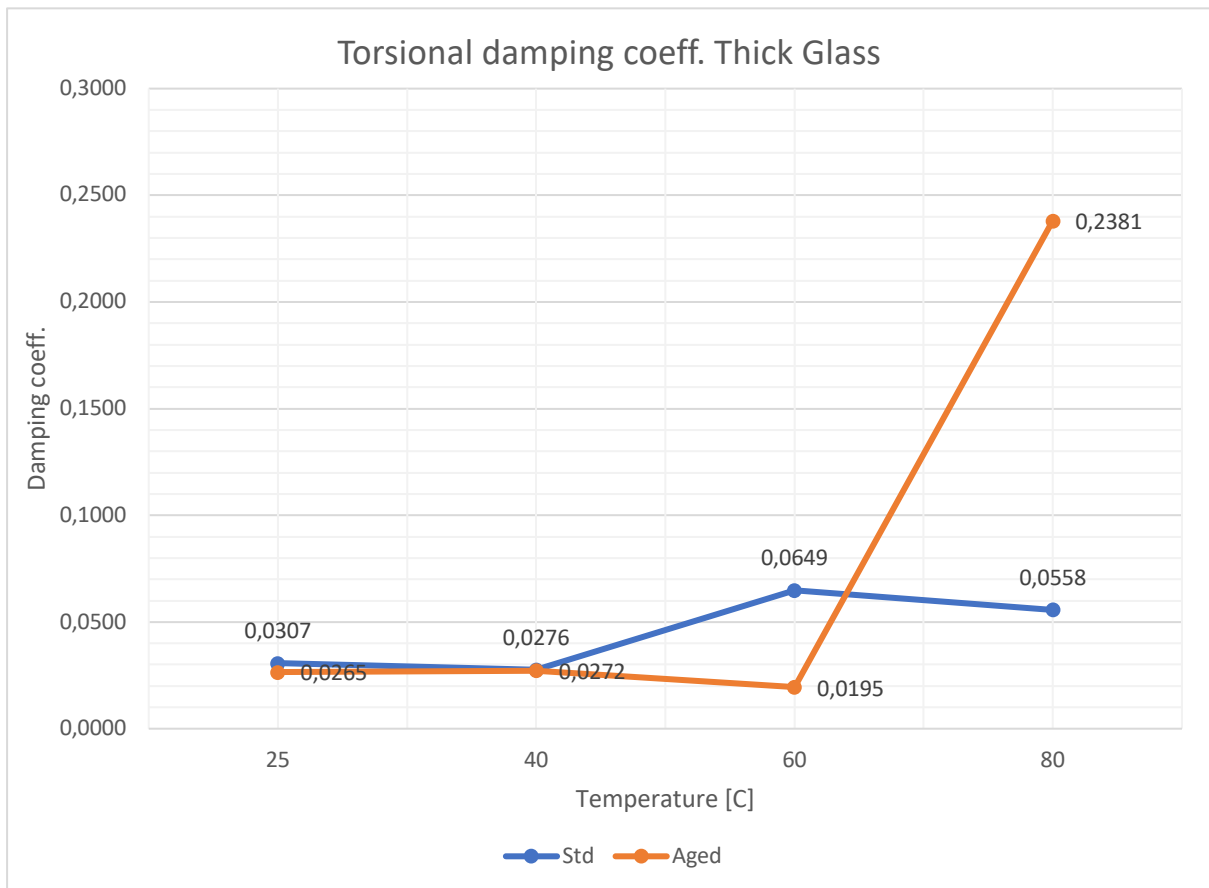
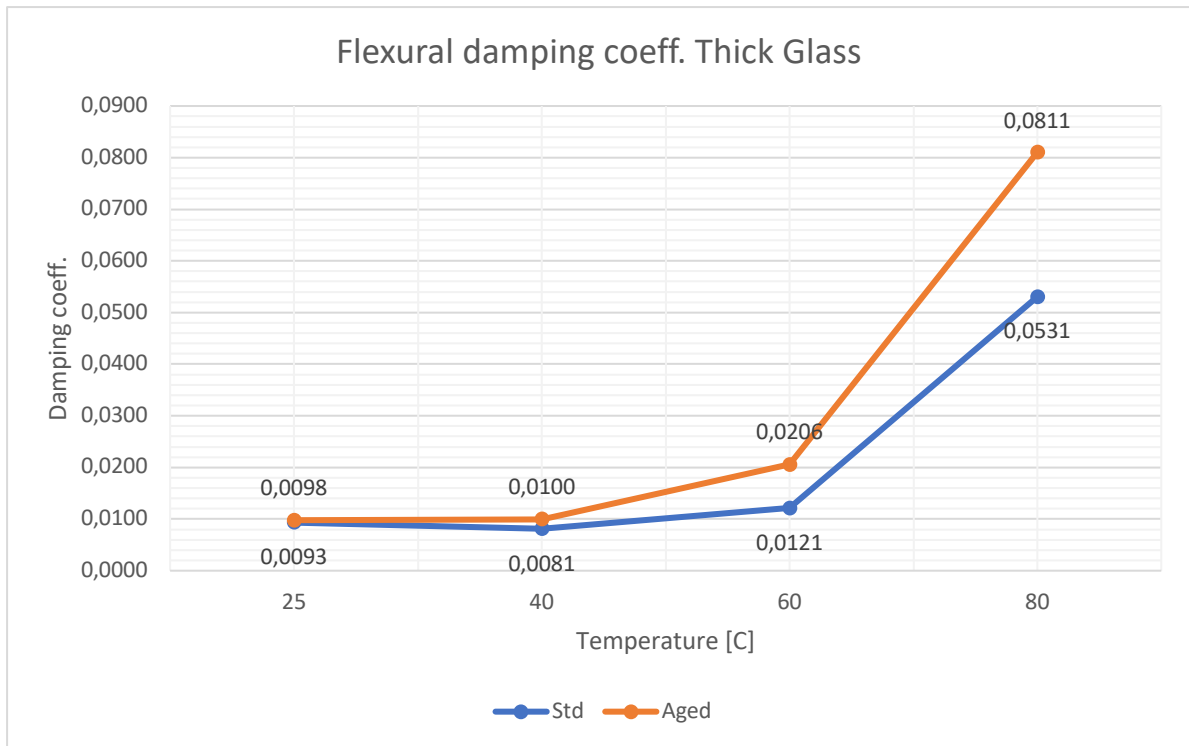




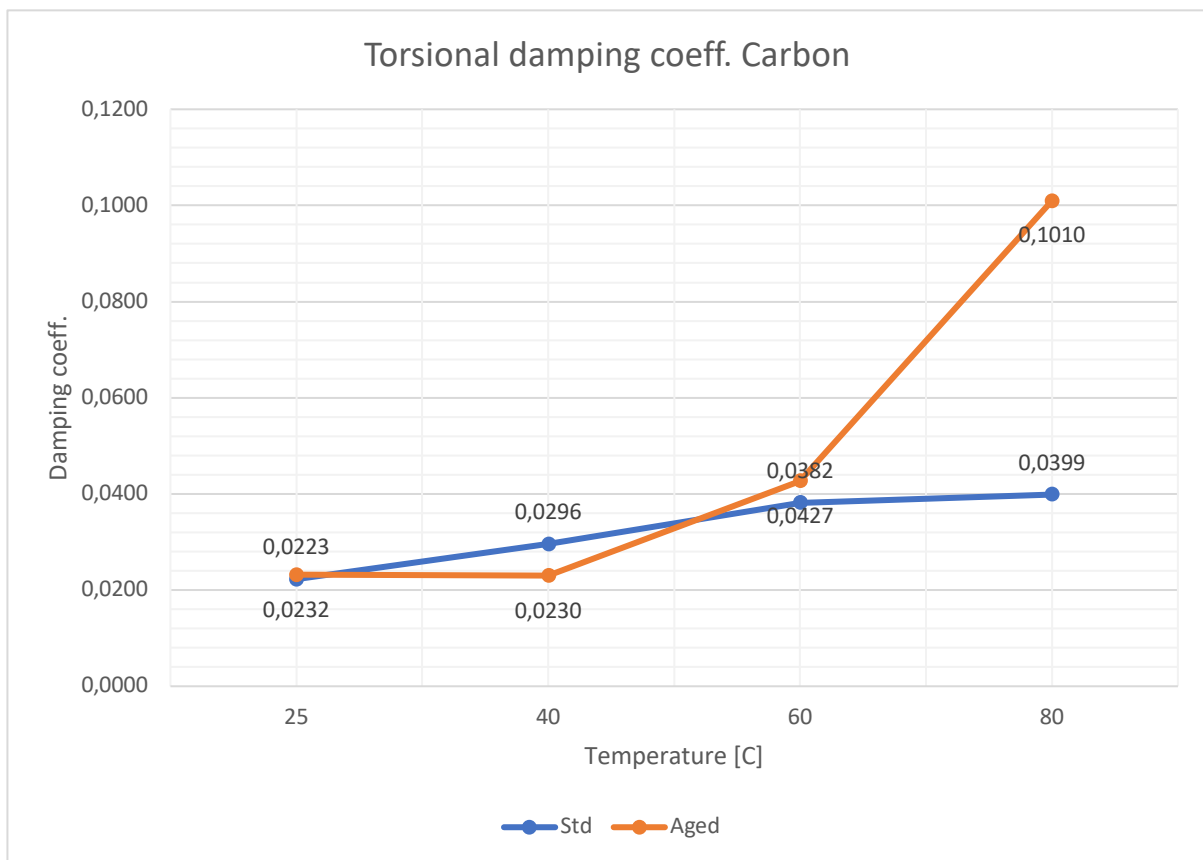
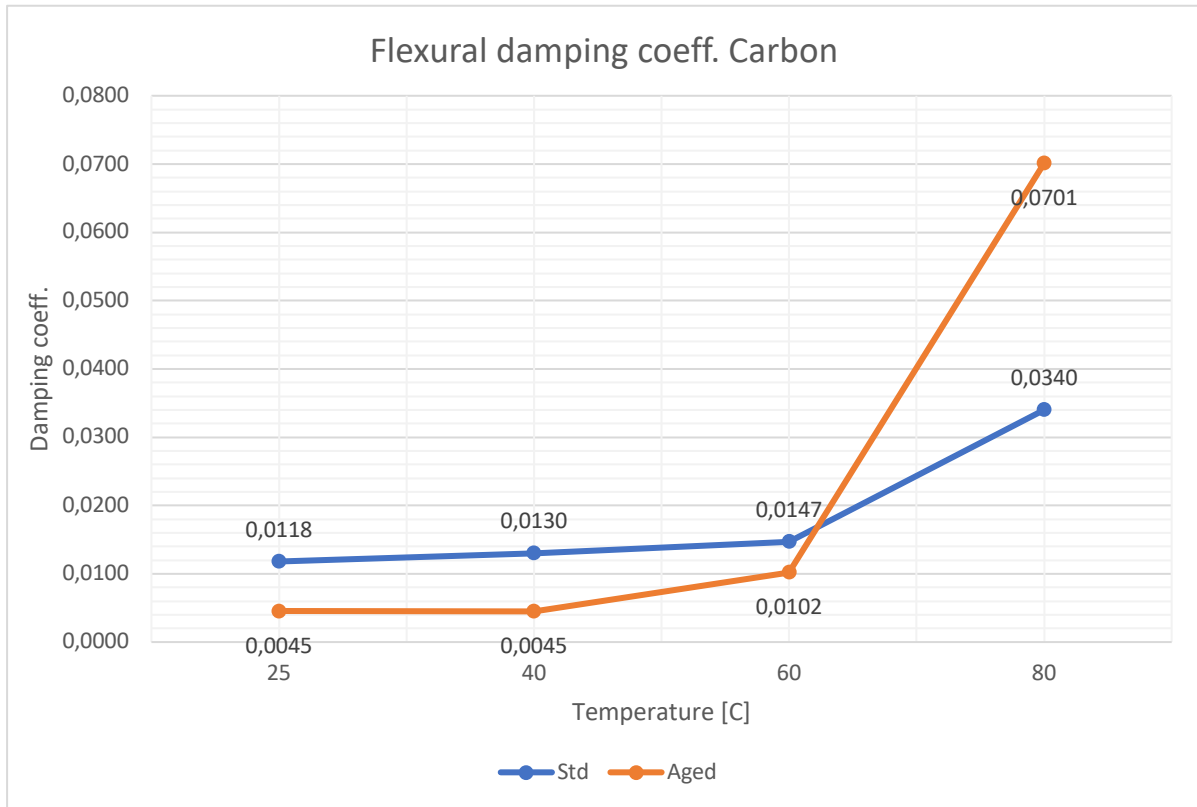


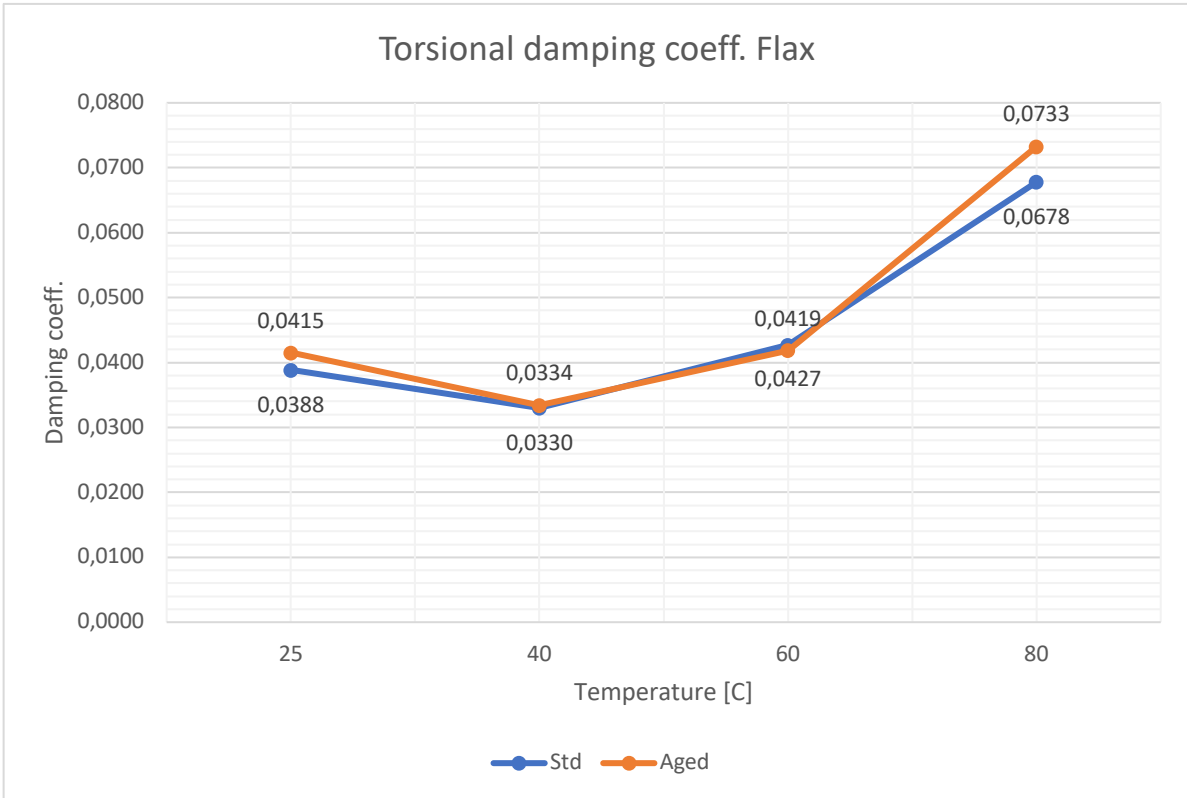
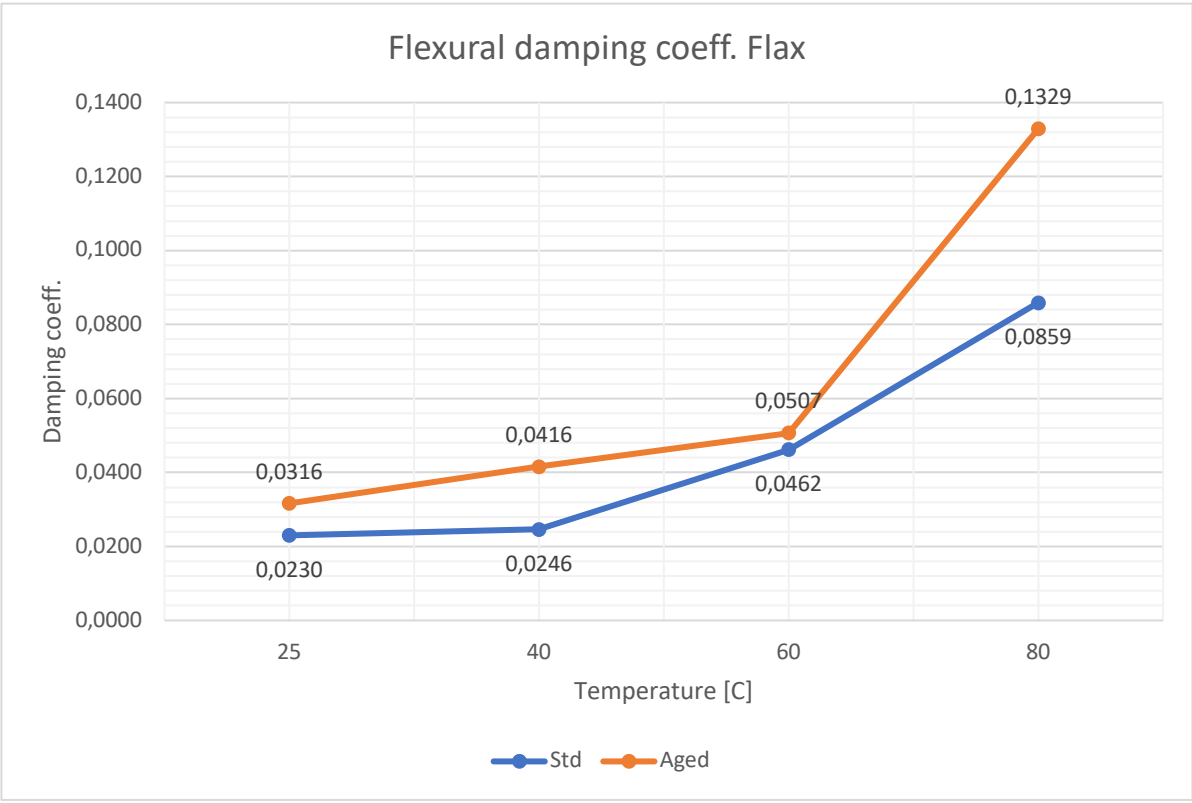
As we can see from the graphs, the most significant results in terms of reduction of moduli is present for flax and carbon, while the most stable results (meaning that this type of aging didn't affect them) are for the thick glass and thin glass.







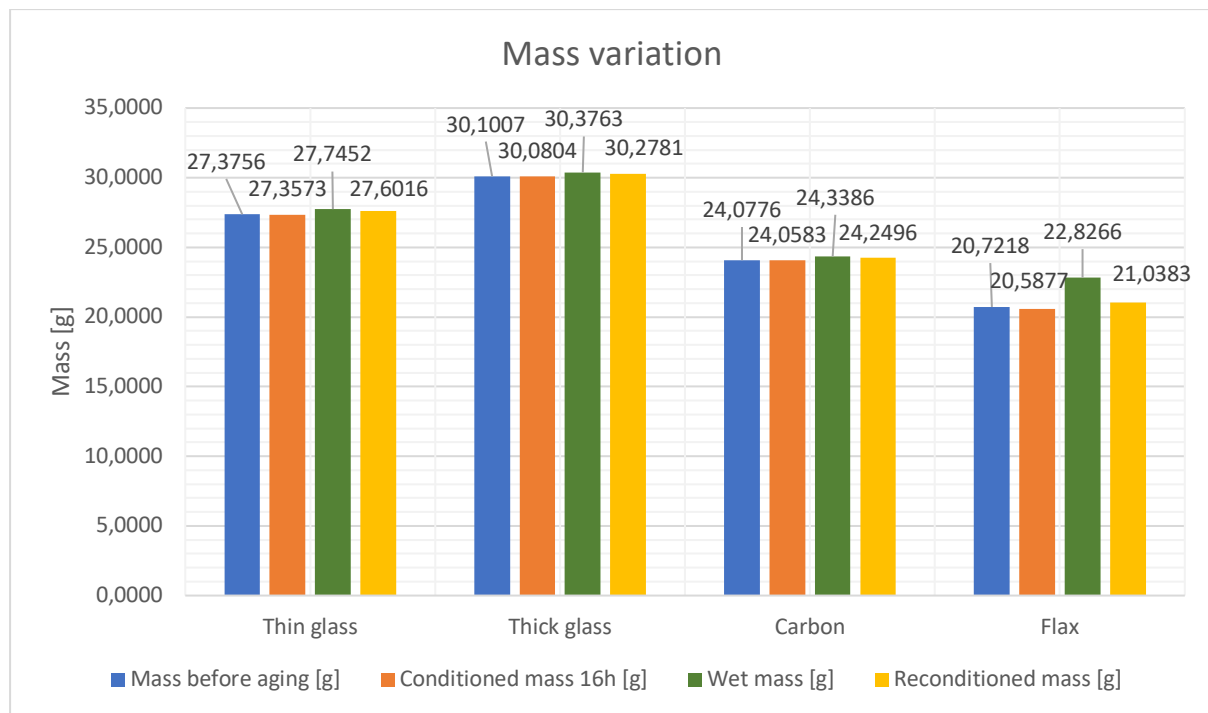




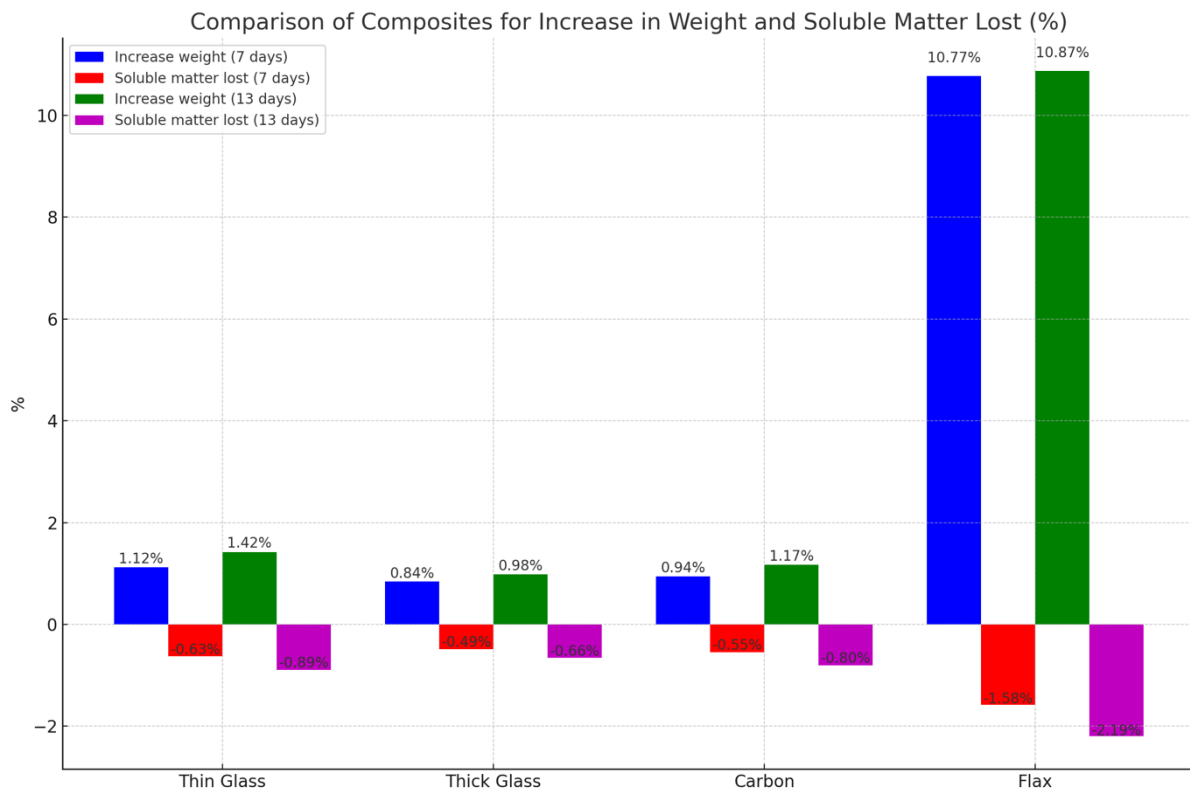
For what regards the damping coefficient, the situation as it can be seen easily from the graph is much more complicated. For some composites the damping coefficient has increased due to aging for some others exactly the opposite thing had happened. Starting from the flax, it is possible to see that in both cases, flexural and torsional, the damping has increased with respect to the non-aged case. For carbon the situations it is different, generally the aged composite exhibits a lower damping till 60°C and a higher one at 80°C. For the two types of glass it is necessary a distinction between flexural damping and torsional in terms of trends. The thick glass aged composite exhibits a higher flexural damping coefficient, with respect to the non-aged one, and also with respect to the thin glass aged composite which has a lower flexural damping coefficient, except at 80°C, with respect to its non-aged composite. For what regards the torsional damping coefficient the two glasses exhibit a very strange trend, the aged thin glass stays predominantly lower with respect to the non-aged composite while the thick glass stays lower except at 80°C [15] [16].

### Thirteen days aging – mass variation

In the following table it is shown the difference in mass of each composite (of the second set of four), before aging, after conditioning, after aging and after reconditioning.



By using the standard ASTM D570-22 and the equations suggested and seen previously (see eq. n) it is possible to calculate the percentage of increase weight between the conditioned mass and the wet mass. Moreover, it is possible to understand the percentage of soluble matter lost in the reconditioning



By adding to the table of the first set of specimens (aged seven days) the second set of composites aged thirteen days it is easy to see that the increase in weight doesn't keep the same slope when passing from seven to thirteen days, considering that after almost double the days the weight increased relatively lower. Thin glass increased in weight in the other six days of only 0.30%, the thick glass of 0.14%, the carbon of 0.23% and the flax of only 0.10%. These results may suggest that the fastest composite to age is the flax, that reaches almost its maximum of water absorption after the first seven days having in the next six the lowest increase in weight between the four types of composites.

### Thirteen days aging – external aspect and geometry

By using the same camera used for the first set of composites, it was possible to spot any external aspect variation. The geometry has been determined thanks to a digital caliper.

The first composite analyzed is as usual the thin glass. It has a small variation along the width and the thickness from conditioned to wet state. In terms of external aspect, it is basically invariant.

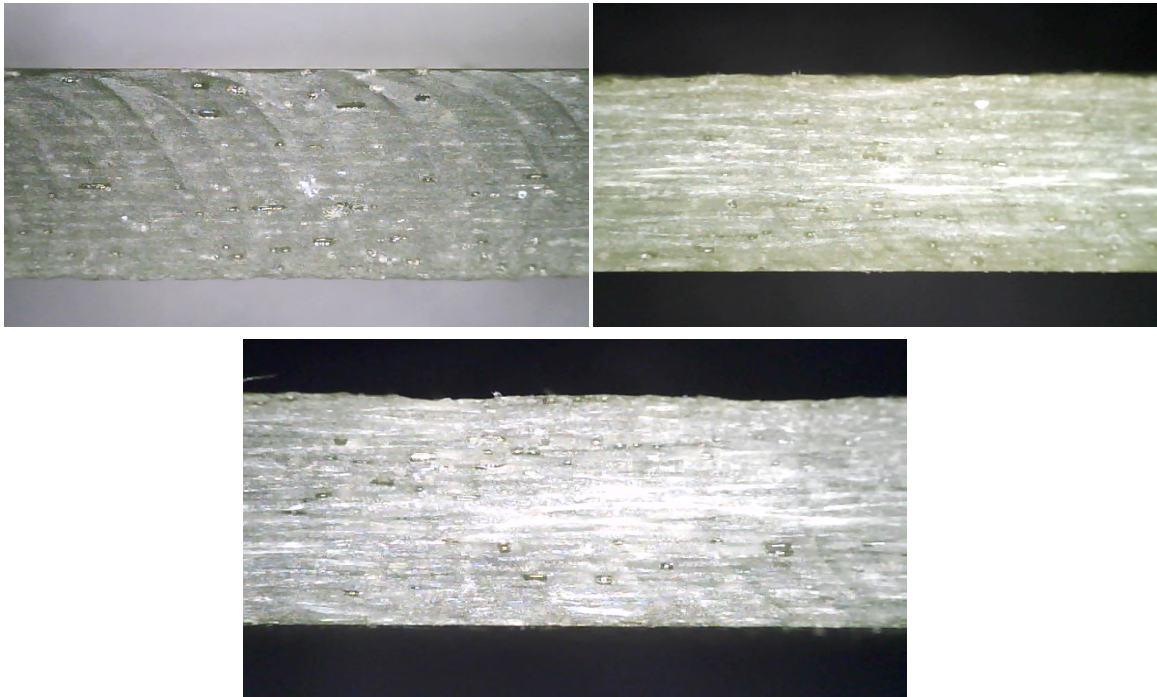


Figure 83: thin glass thickness and aspect variation, conditioned (left), wet (right), reconditioned (below)

Table 34: Geometry variation thin glass

Thin Glass Geometry				
	Conditioned	Wet	Reconditioned	%Increase between cond. and recond.
L [mm]	150.43	150.47	150.43	0%
b [mm]	30.36	30.39	30.36	0%
t [mm]	3.53	3.62	3.60	1.94%

For the thick glass composite the situation is not exactly similar as for the thin glass, it was possible to measure some geometry variations along all three dimensions. The external aspect and color remain constant during the aging.

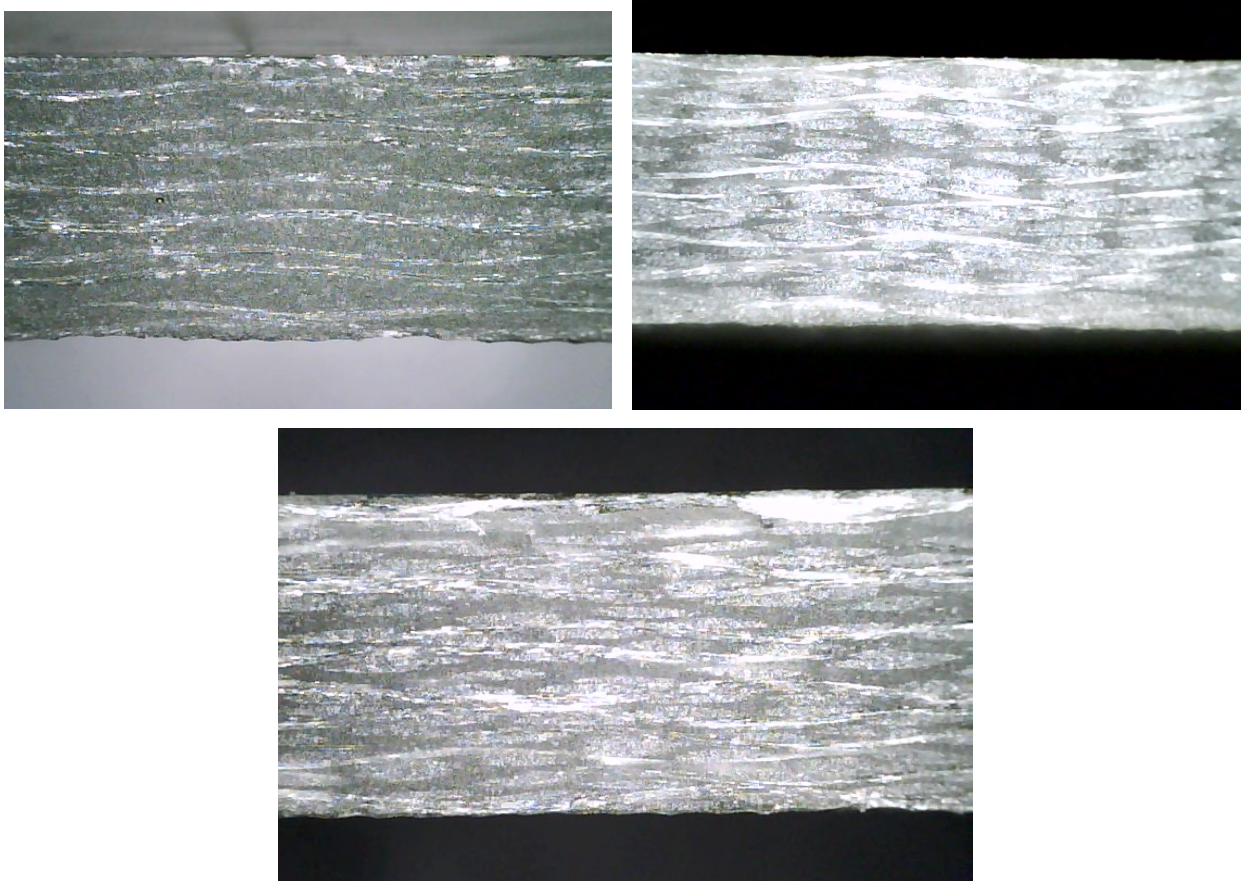


Figure 84: thick glass thickness and aspect variation, conditioned (left), wet (right), reconditioned (below)

Table 35: Geometry variation thick glass

Thick Glass Geometry				
	Conditioned	Wet	Reconditioned	%Increase between cond. and recond.
L [mm]	148.93	148.96	148.91	0%
b [mm]	29.15	29.19	29.16	0%
t [mm]	3.99	4.02	4.00	0.25%

Regarding the carbon it is possible to see from the table n, that the changes in dimensions are quite low, the thickness has the bigger influence among the three directions. From the imagines it is possible to see the small cracks present on the composites. It is in this zone that the water might get trapped.

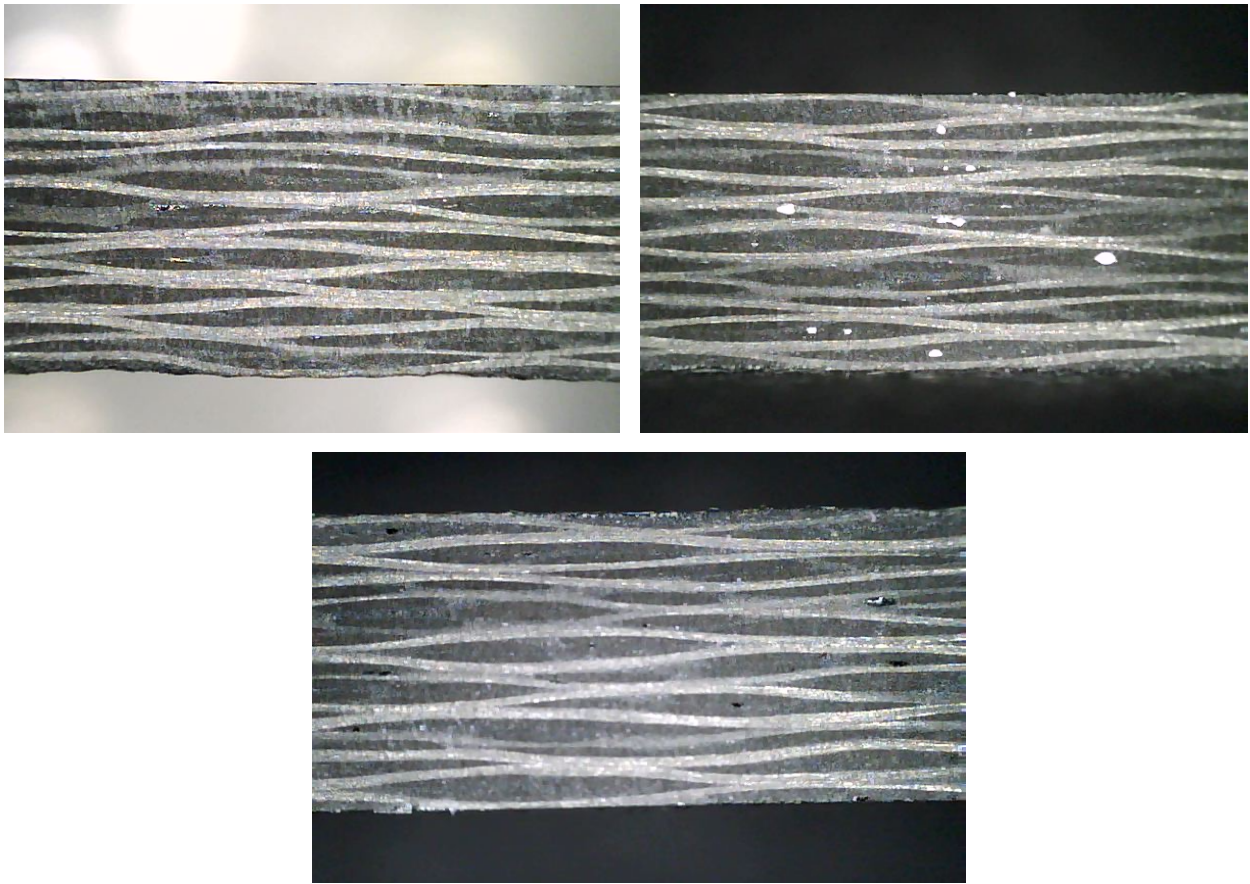
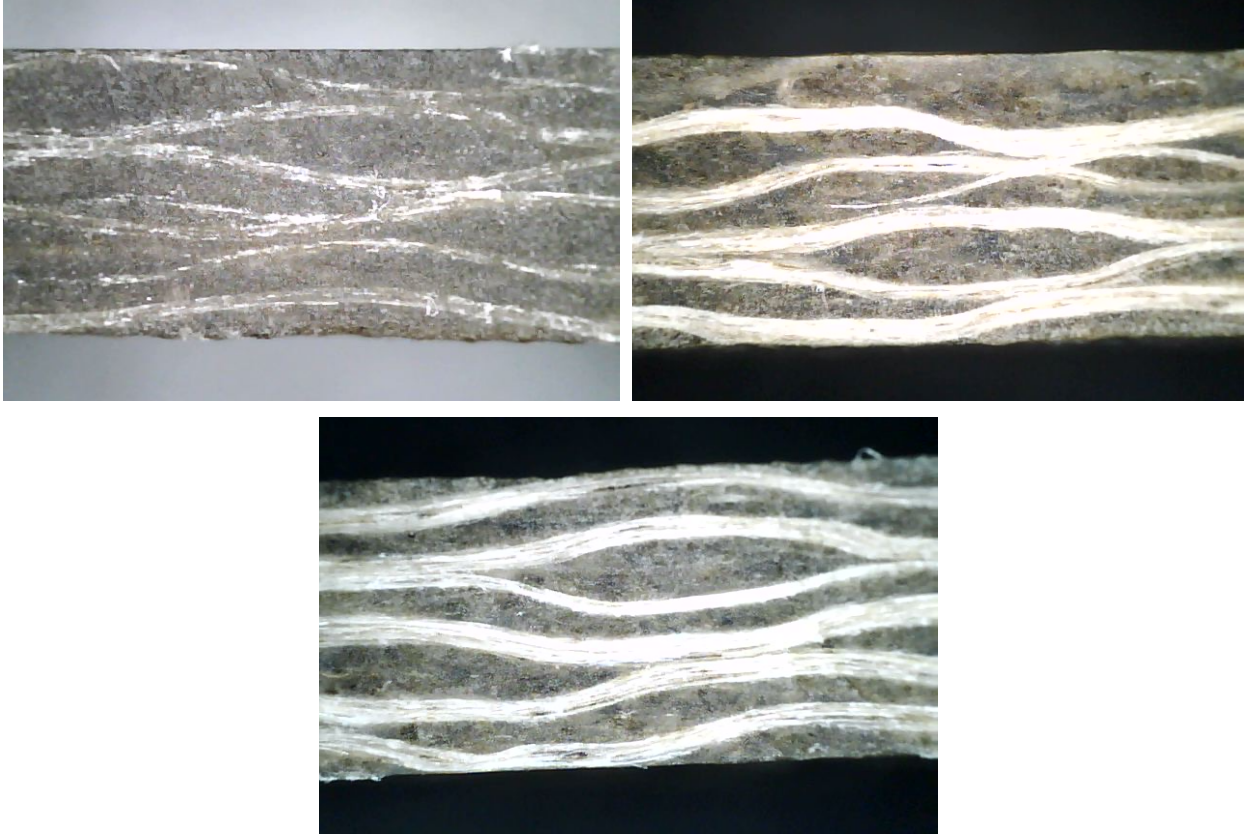


Figure 85: carbon thickness and aspect variation, conditioned (left), wet (right), reconditioned (below)

Table 36: Geometry variation of carbon

Carbon Geometry				
	Conditioned	Wet	Reconditioned	%Increase between cond. and recond.
L [mm]	149.07	149.10	149.08	0%
b [mm]	29.29	29.31	29.29	0%
t [mm]	3.98	4.05	4.01	0.75%

Last but not the least is the flax. As in the previous case is the composite that has the biggest water absorption between the four composites. This is clearly visible in the change of thickness of the fibers and in the change of geometry.



*Figure 86: flax thickness and aspect variation, conditioned (left), wet (right), reconditioned (below)*

area near the fibers due to the absorbed water.

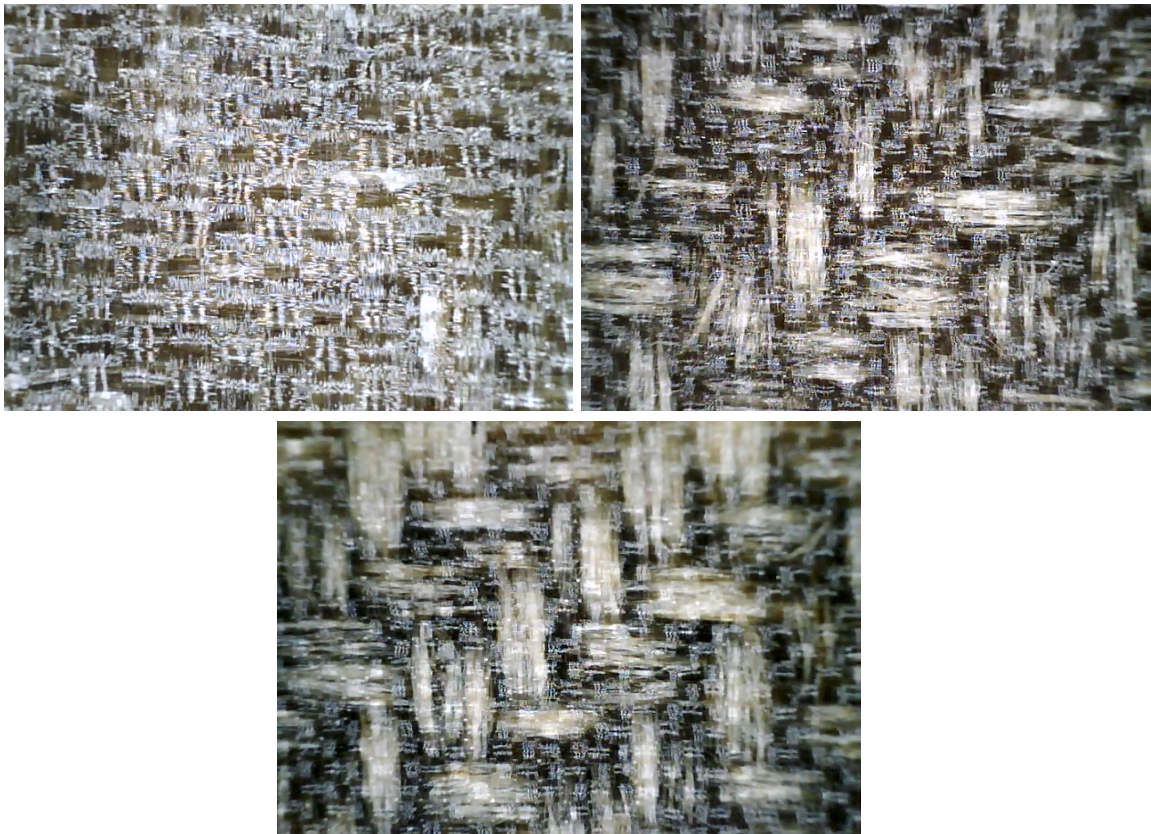


*Figure 87: flax aspect variation, conditioned (left), wet (right), reconditioned (below)*

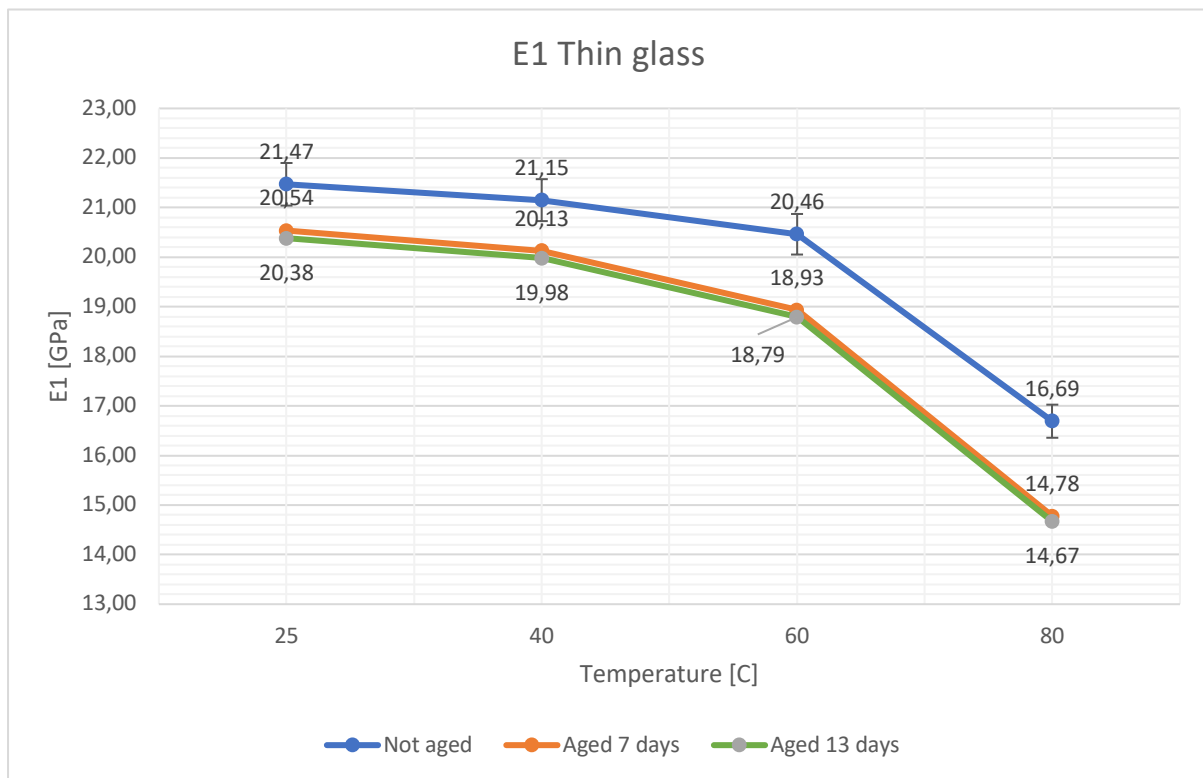


Table 37: Geometry variation of flax

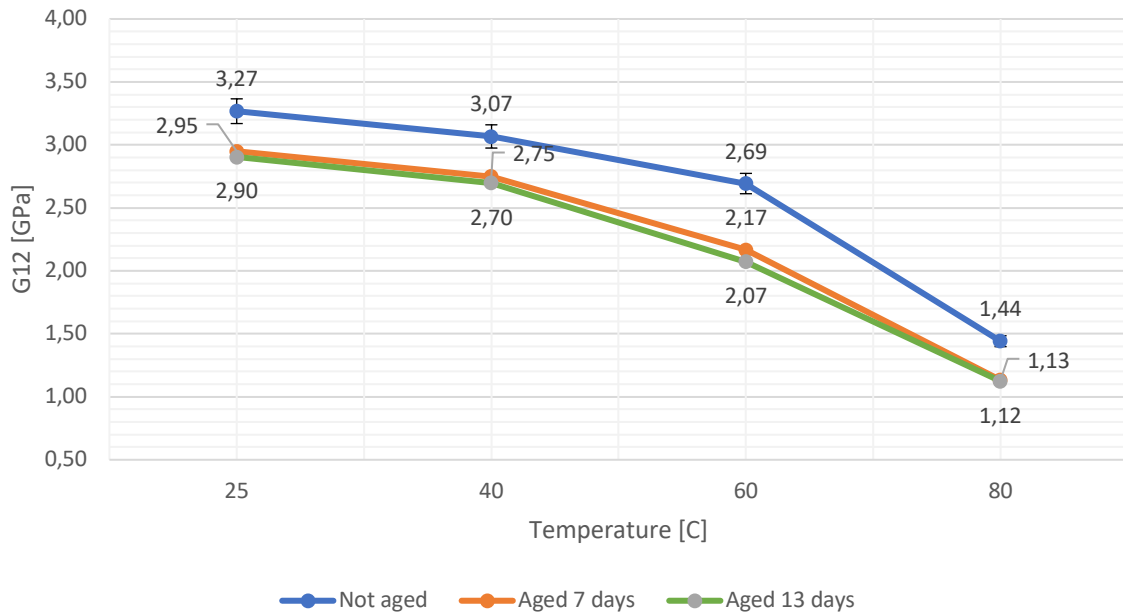
Flax Geometry				
	Conditioned	Wet	Reconditioned	%Increase between cond. and recond.
L [mm]	149.25	149.45	149.28	0%
b [mm]	29.52	29.61	29.54	0%
t [mm]	3.84	4.37	4.21	8.79%

### Thirteen days aging – elastic moduli and damping coefficient

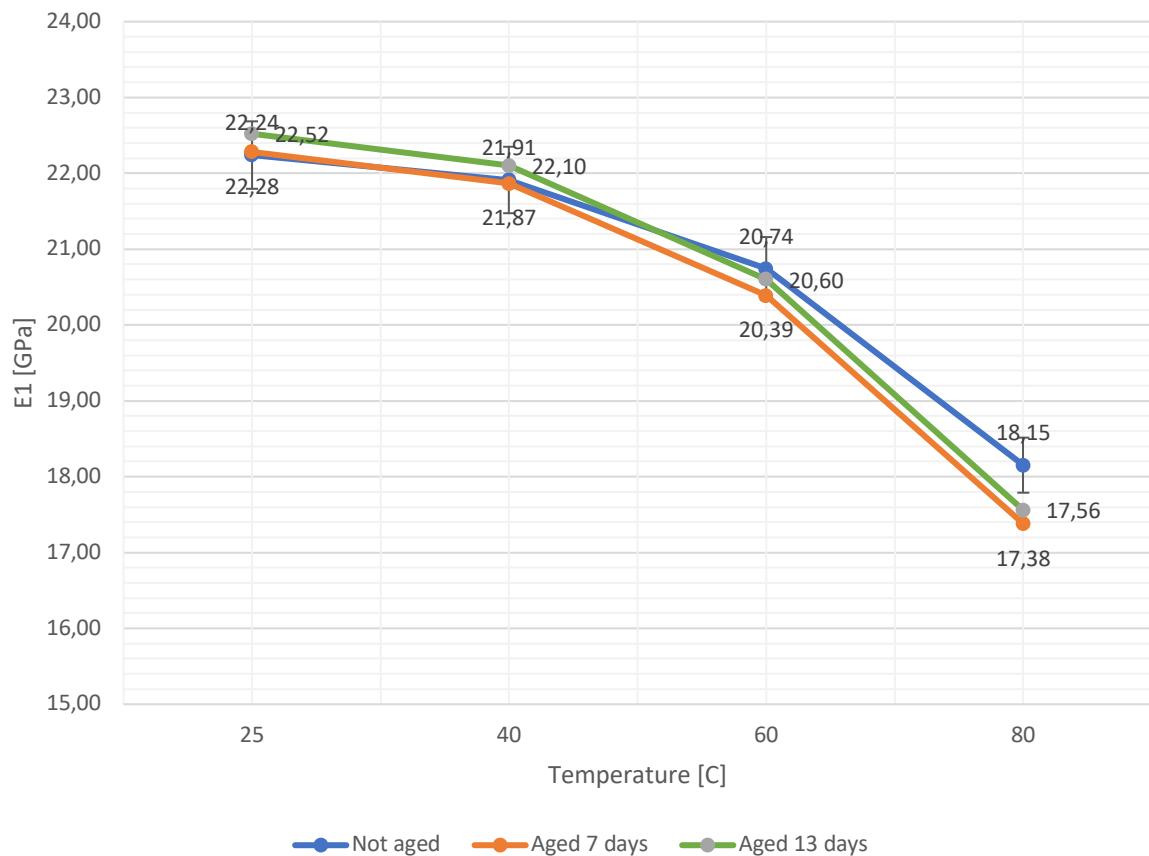
As in the previous case, a reduction of the natural frequencies from non-aged to aged composites is exhibit. The reduction is not necessary more severe with respect to the seven days aging, meaning that some composites (for example flax) reach their full aged condition already in the seven days, while others might continue aging decreasing their natural frequencies, and so the elastic moduli, slower but continually. In the following graph it will be shown the different trends of elastic moduli of the first and second set of composites on the same graph, in order to have a better view of how the aging evolved.

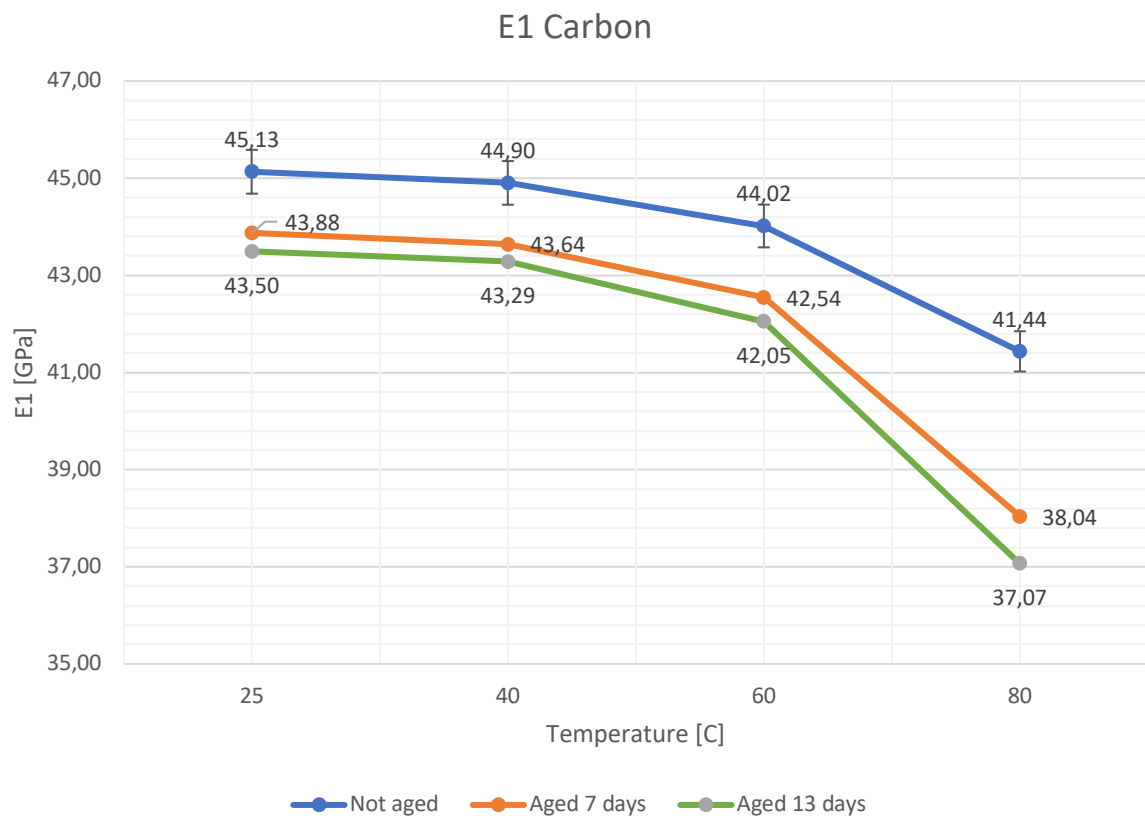
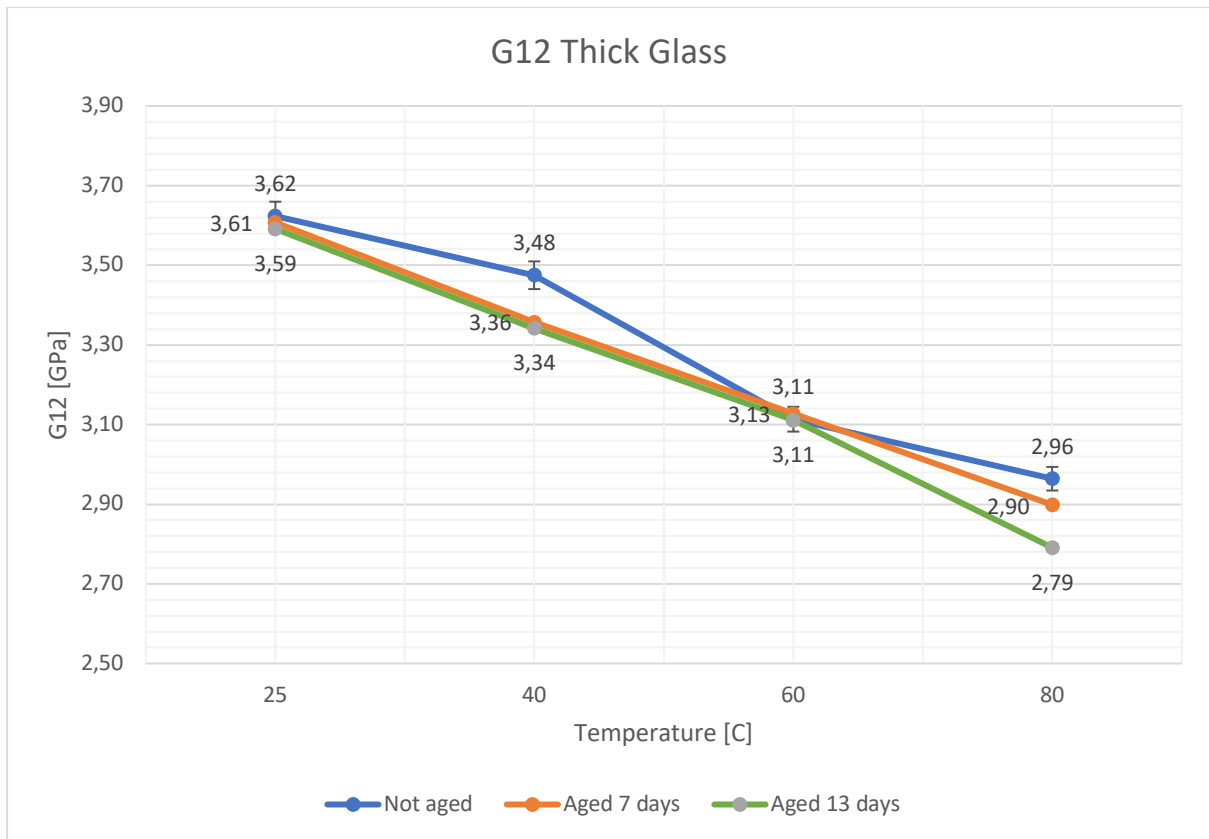


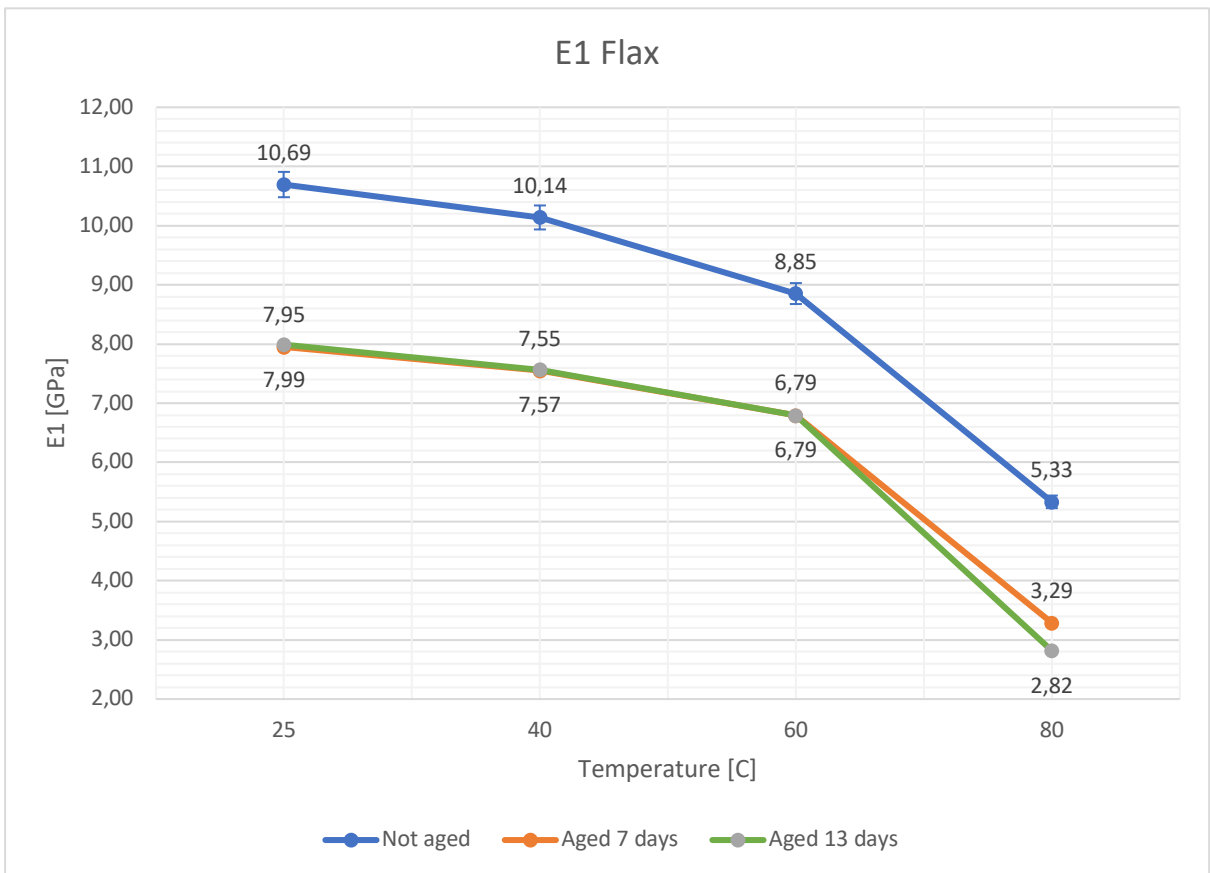
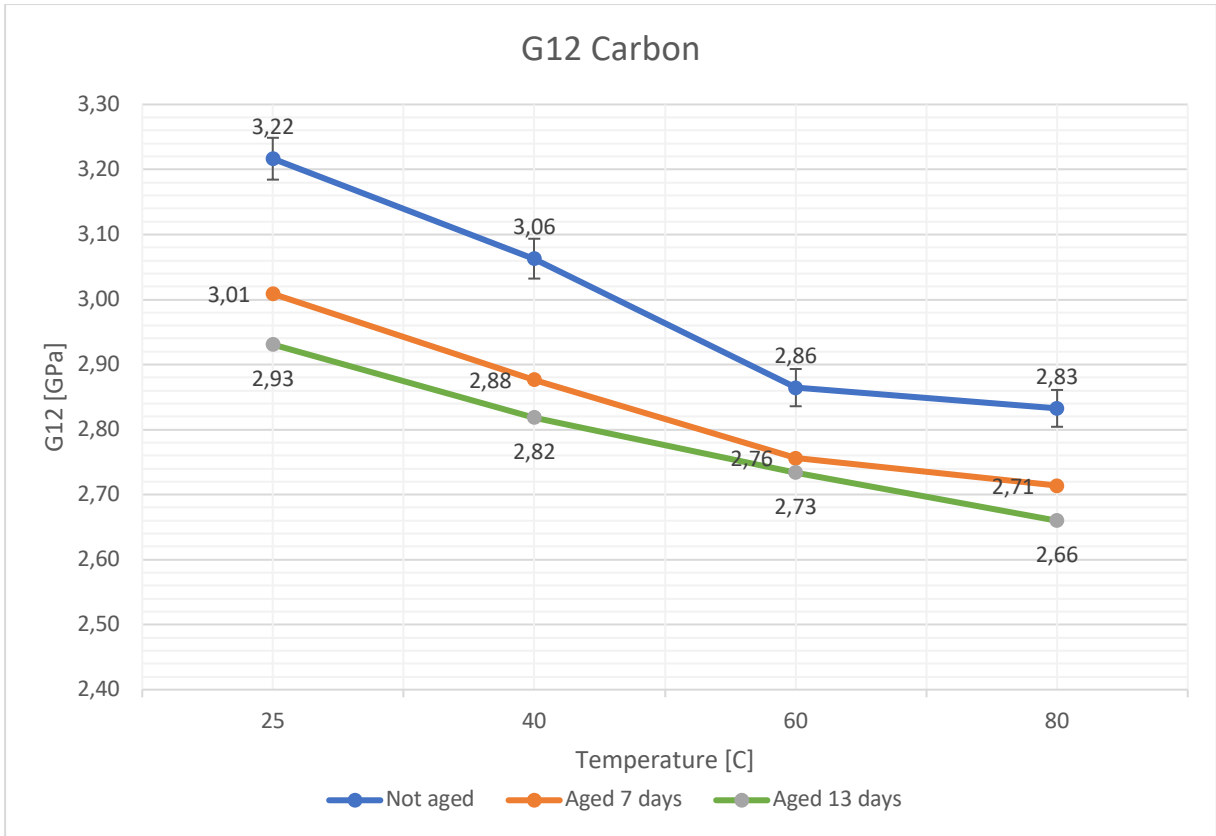
G12 Thin Glass

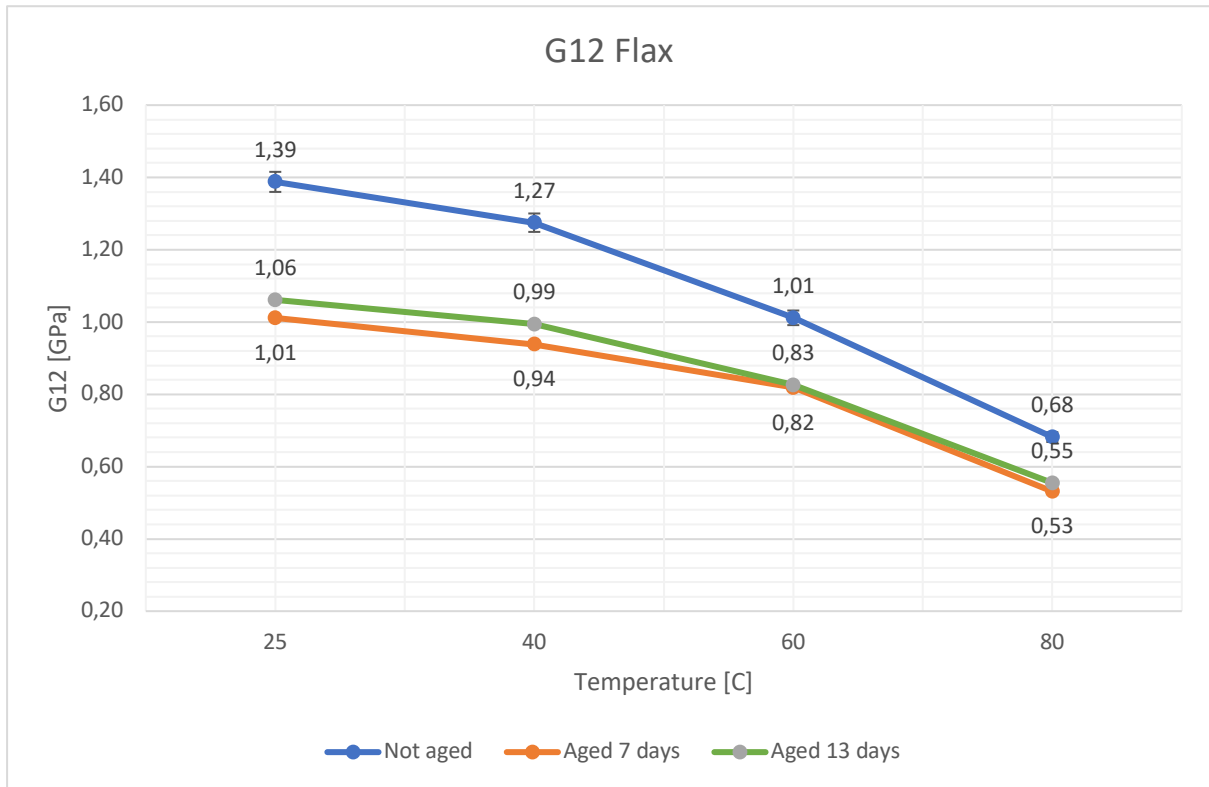


E1 Thick Glass



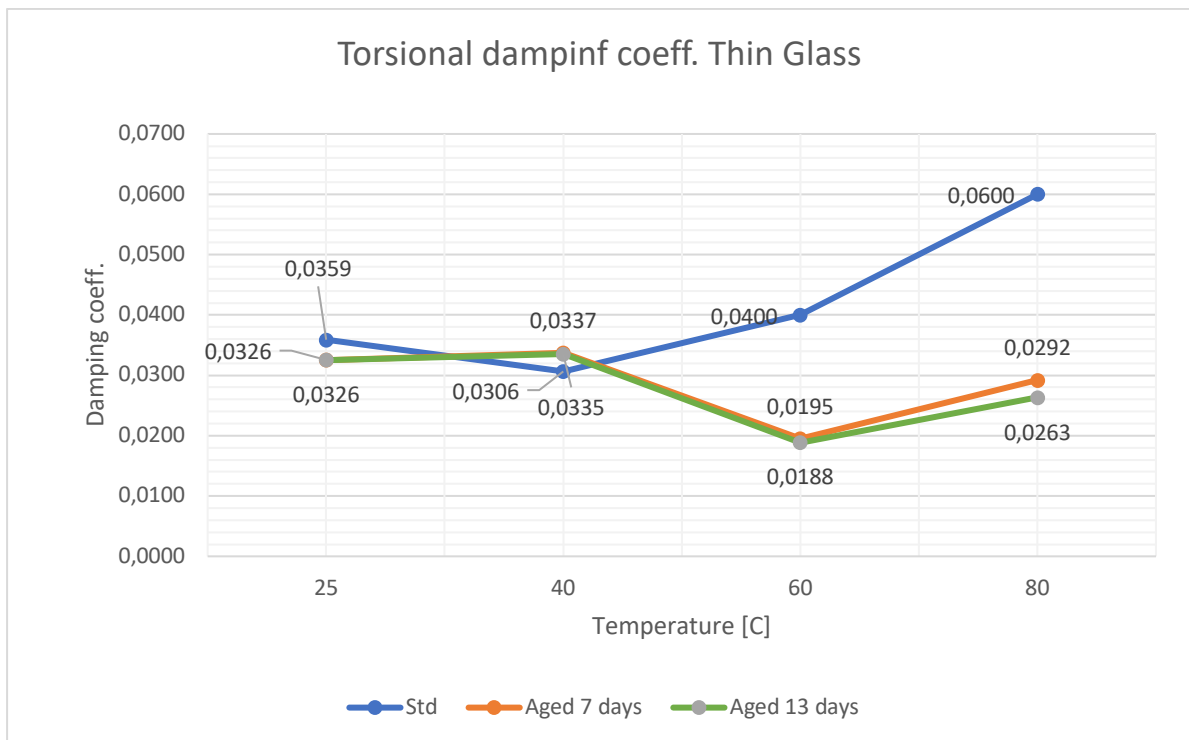
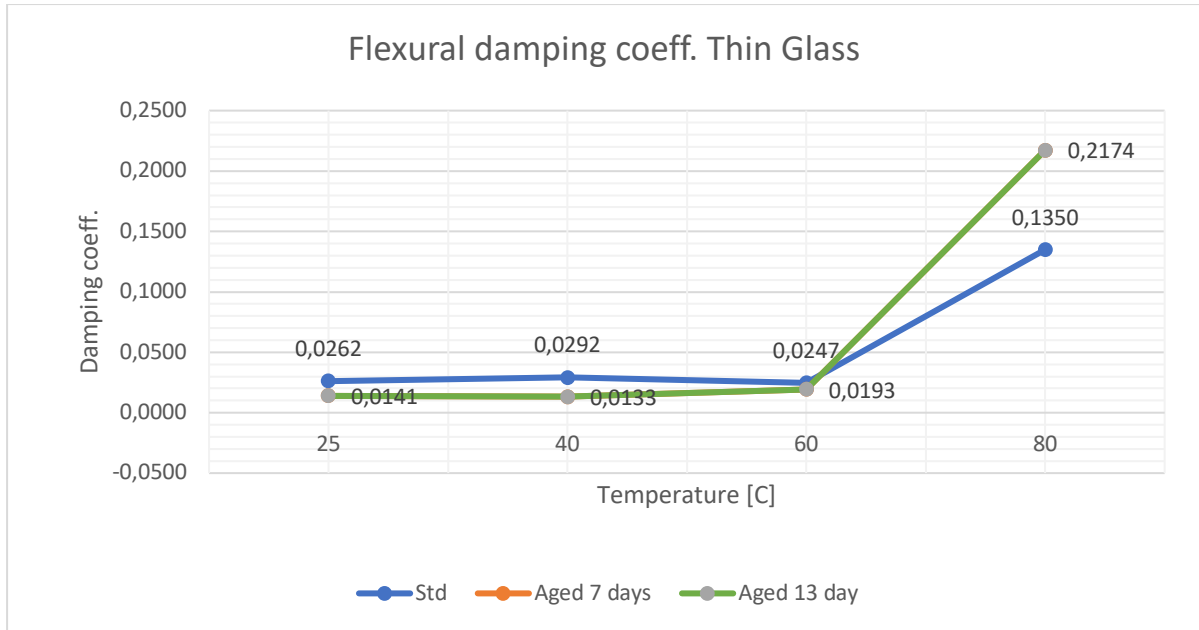


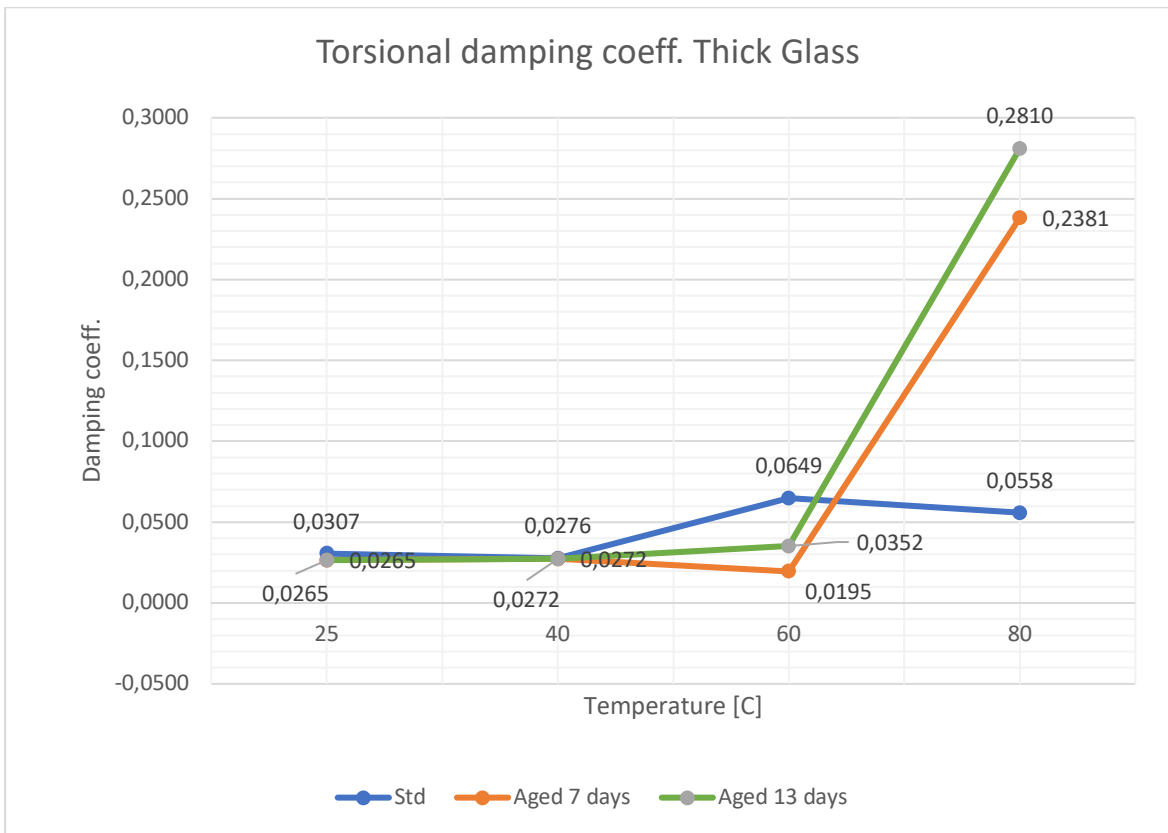




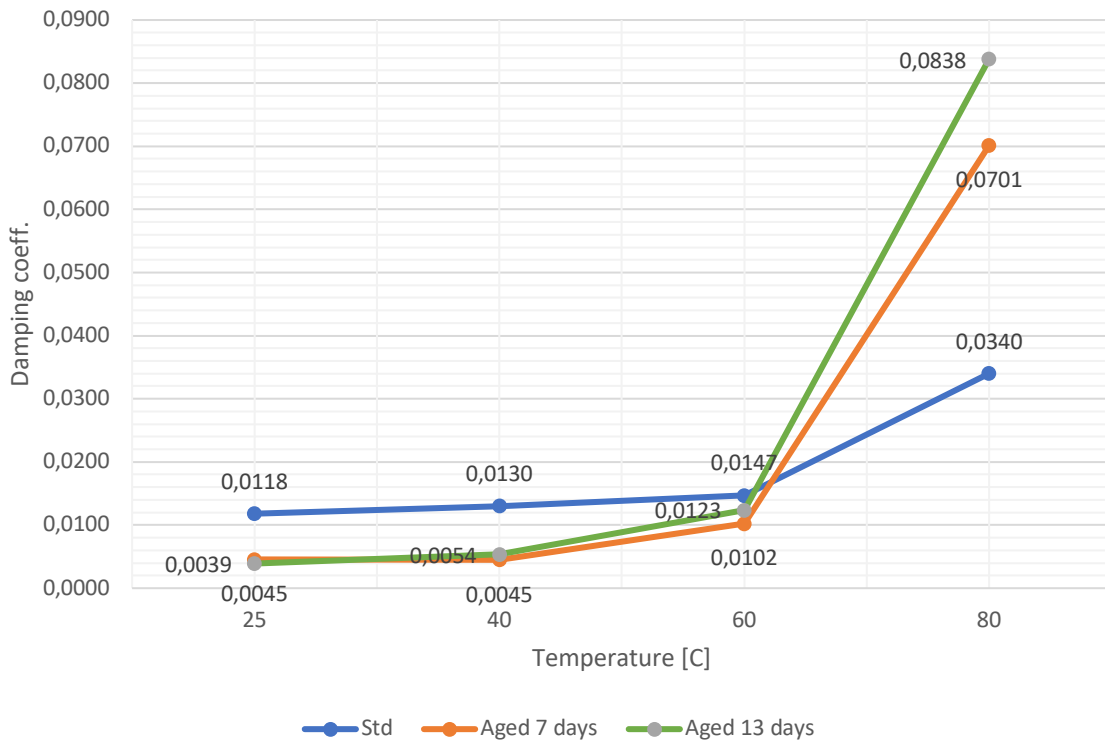
From the previous graphs can be concluded that the flax has the aging almost complete after seven days, considering that in the next six days the decrease in moduli is not so severe anymore. While for carbon for example, the situation is different, it is possible to see a continuous decrease also in the last six days of aging. For what regards the two gasses, they are affected slightly by the aging, suffering very low reductions in moduli.

Another interesting aspect to analyze and see how it did evolve with the proceeding of the aging is the damping coefficient. In the following graphs it is shown the non-aged value (called “std”), the value of the composite seven days and of the one aged thirteen days.

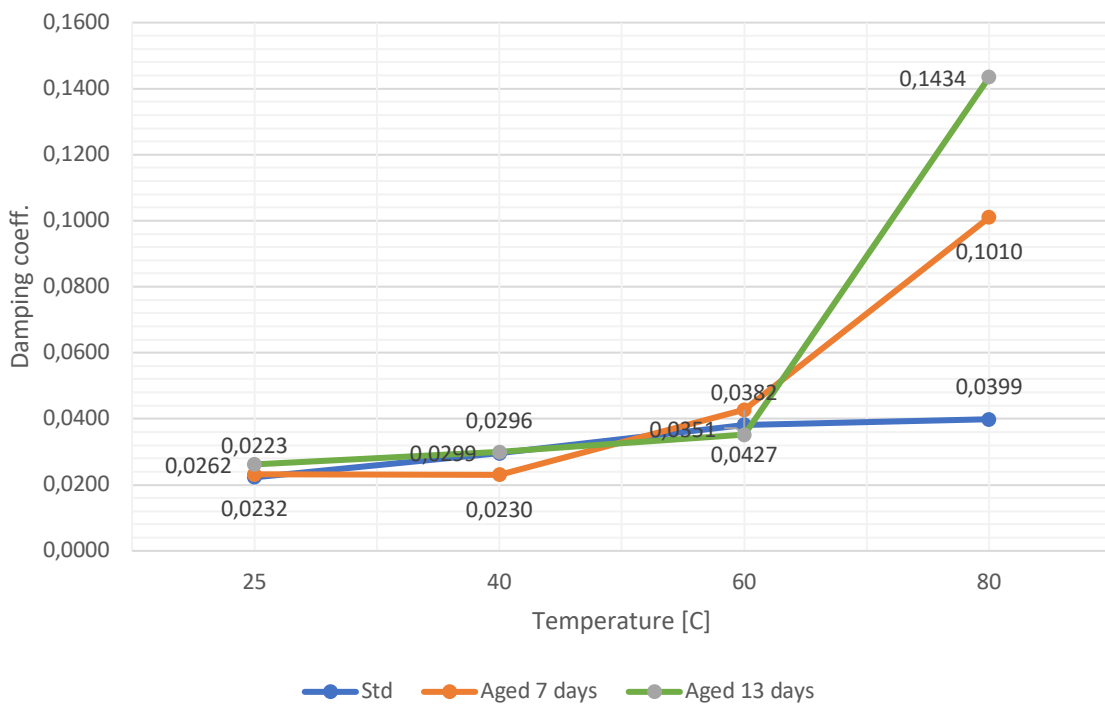




Flexural damping coeff. Carbon

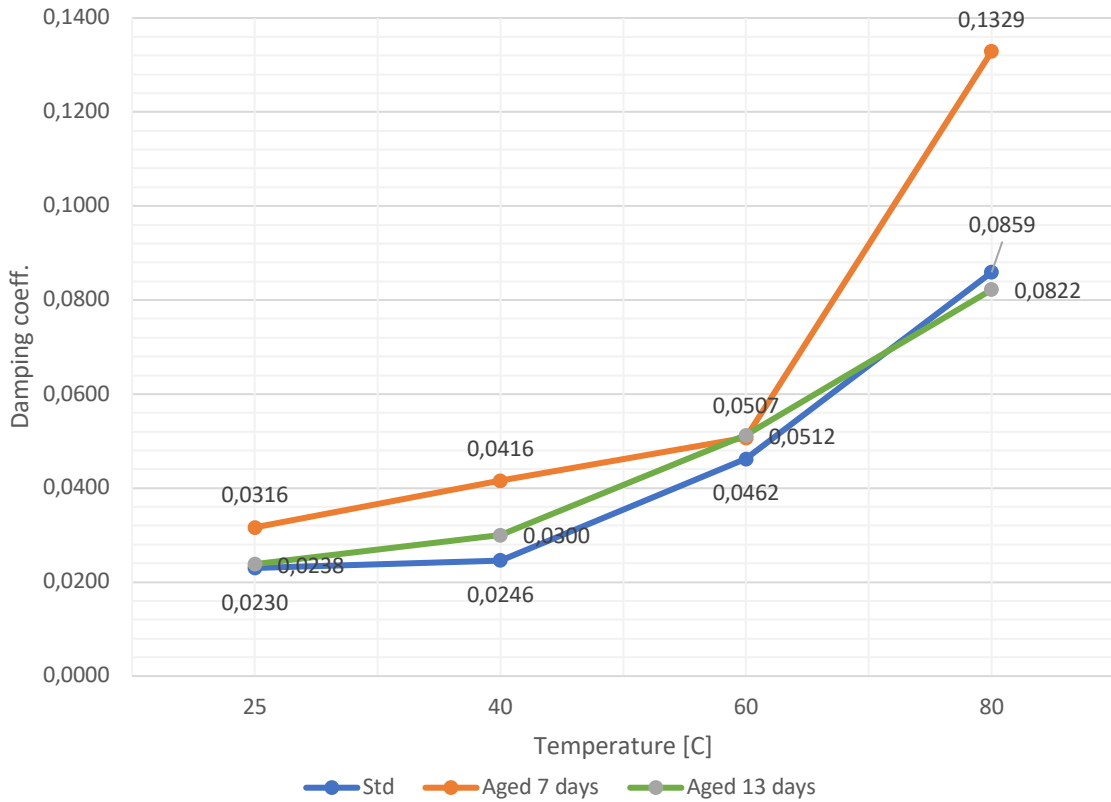


Torsional damping coeff. Carbon

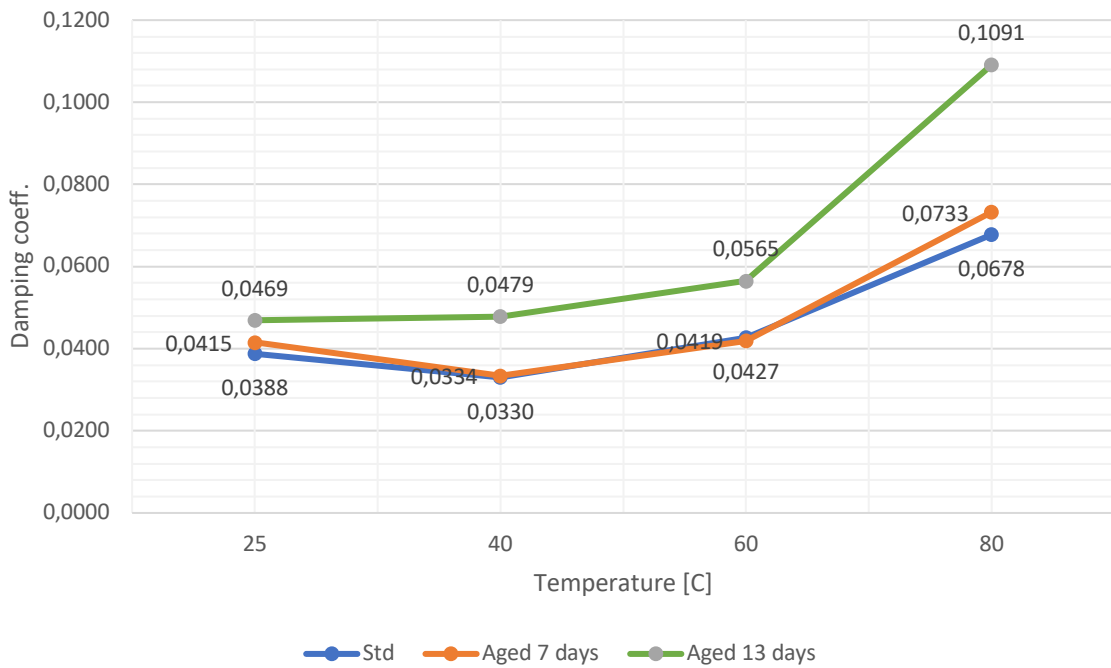




Flexural damping coeff. Flax



Torsional damping coeff. Flax



As it can be seen from the graphs, the behavior of the thirteen days aged composites damping coefficient is quite hard to predict, in some cases it just proceeds with the same trend, just more severe, as the seven days aged composites (see torsional damping of thin glass, torsional damping of thick glass, flexural damping for carbon and torsional damping for flax) in some others it is just overlapped with the seven days aged composites damping coefficient (see flexural damping for thick and thin glass), and in some others it is just exhibiting a different trend (see flexural damping for flax and torsional damping for carbon).

## 9. Conclusions

After the extensive presentation of data, tables, and graphs, it is essential to provide a well-defined conclusion. Let us revisit the aim of this study and its potential applications. The primary objective was to characterize, through the use of the Impulse Excitation Technique (IET), the elastic moduli  $E_1$  and  $G_{12}$ , and the damping coefficient at various temperatures (specifically 25°C, 40°C, 60°C, and 80°C) for four different composites: flax fiber, carbon fiber, and two types of glass fibers. These composites were combined with two distinct resin types—an inorganic epoxy resin and a 30% natural epoxy resin. The significance of this method lies in its non-destructive nature, which not only reduces the production costs (needing fewer specimen for tests) of these composites but also allows the reuse of specimens for further testing. Additionally, the IET yields reliable results comparable to those obtained through destructive methods.

For this study, three additional constants were required to ensure the reliability of the results: the coefficients of thermal expansion (CTE) for each composite. These values were calculated using strain data from three strain gauges affixed to each composite, which were tested in an oven. The inclusion of CTE enabled the division of thermal effects into two categories: changes in natural frequencies due to thermal expansion and changes due to thermal softening. A key focus of this study was on the softening effects under varying temperatures. The results of the elastic moduli and damping coefficient were calculated using the IET and following the ASTM E1976-21 standard.

As a general observation, the IET results showed that all four composites exhibited a decreasing trend in their elastic moduli and an increase in damping coefficient as temperature increased.

Another aspect of the study involved using the experimental data to create three finite element method (FEM) models. These models were then compared to the experimental results. One of the FEM models involved a modal analysis of the composite material, applying an orthotropic-elastic material card without temperature dependency. A second simulation was conducted to model the thermal expansion of the composite using an orthotropic-thermal material card. The third model sought to combine the previous two, incorporating modal analyses alongside the thermal expansion of a composite model that included temperature-dependent elastic moduli.

By comparing the experimental results with the numerical outcomes at intermediate temperatures (specifically 50°C and 70°C), it was possible to validate the FEM models, which generally demonstrated errors below 5%. Moreover, the study tested the limits of the model, concluding that in the extreme condition of providing only two points, the model was always depending a lot from the initial and final point provided, usually the two points were underestimating the stiffness of the model so also the other points interpolated by dyna where underestimating the stiffness with a linear trend in all the four cases.

Additionally, the study addressed an aging process involving immersion in distilled water at 70°C for periods of seven and thirteen days for two sets of the four composites. After the aging process, the specimens were tested again using the IET, leading to the expected conclusion when the post-aging results were compared to the standard (non-aged) values of natural frequencies and, consequently, elastic moduli. In general, water absorption by the composites resulted in a decrease in elastic moduli, and depending on the temperature, either an increase or decrease in damping coefficient. Flax fiber, due to its high affinity for moisture, absorbed

the largest amount of water among the four composites and exhibited the most pronounced aging. After seven and thirteen days of aging, the elastic moduli of flax fiber were nearly identical, indicating rapid aging. The other composites exhibited a more gradual decrease in moduli.

While this study offers significant insights, certain limitations were identified, and further research may be necessary. For instance, the IET method used in this study only characterized the elastic moduli  $E_1$  and  $G_{12}$ , as the tests were conducted in flexural and torsional configurations. Additionally, out-of-plane moduli, which are necessary for FEM analysis and differ from the in-plane moduli (as fibers in woven configurations exhibit consistent mechanical properties in directions 1 and 2), may require characterization through different tests or methods.


Furthermore, to achieve a more comprehensive understanding of the aging process in composites, a larger number of samples may be required to adopt a more statistically robust approach to the problem.

This research has potential applications in the automotive industry, where a deeper understanding of composite materials and their behavior under various conditions is crucial. The findings of this study could be used to optimize composites for enhanced performance, including improved damping properties and reduced fuel consumption.

In conclusion, this thesis presents a thorough analysis of the elastic moduli and damping properties of four different composite materials, offering novel insights and practical applications that could inform future research on the use of composites in the automotive sector, particularly regarding their damping properties and contributions to fuel efficiency together with good mechanical properties of different parts of the vehicle.

# Appendix

## Strain Gauge HBM technical data sheet



**Dehnungsmeßstreifen**  
**Strain Gauges**  
**Jauges d'extensométrie**

Bestellnummer  
Order No.  
No. de référence

1-XY11-0.6/120

Typ  
Type

0.6/120XY11

Stückzahl  
Contents  
Quantité

5

Temperaturkoeffizient  
des k-Faktors  
Temperature coefficient  
of gauge factor  
Coefficient de température  
du facteur k

93 ±10 [10<sup>-6</sup> / °C]  
(-10...+45°C)

Folienlos  
Lot  
Lot de la feuille

A390/06

Herstellungslös  
Batch  
Lot de fabrication

812047775

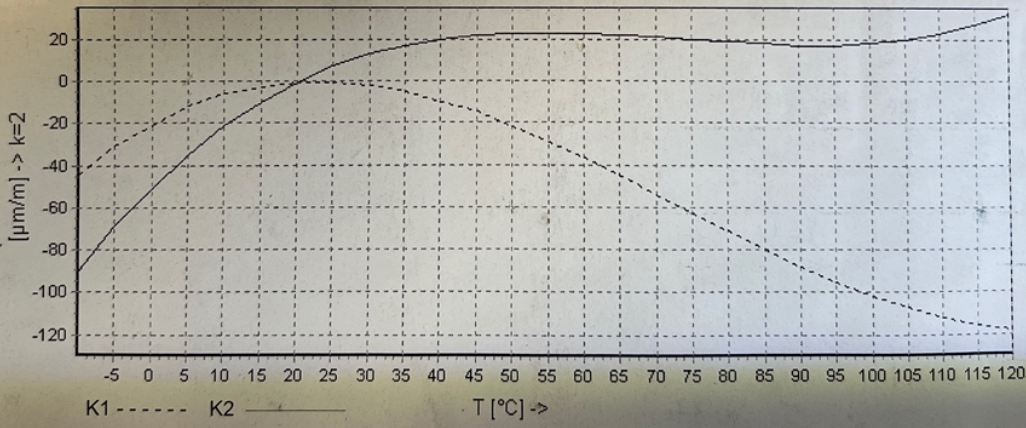
  

Widerstand Resistance Résistance	120 Ω ± 0.35 %	
k-Faktor Gauge factor Facteur k	Gitter A: 1.69 ± 1.5 % Gitter B: 1.69 ± 1.5 %	
Querempfindlichkeit Transverse Sensitivity Sensibilité transverse	Gitter A: 1.0 % Gitter B: 1.0 %	

Temperaturkompensation: Angepaßt für Temperature Compensation: Compensated for Compensation de température: Compensation pour	Ferritischen Stahl mit Steel with Acier avec	α = 10.8 [10 <sup>-6</sup> / °C]
---	--	----------------------------------



$$\epsilon_s(T) = -20.7 + 1.9 \cdot T - 4.98 \cdot 10^{-2} \cdot T^2 + 2.27 \cdot 10^{-4} \cdot T^3 + 0.0500 \cdot L \cdot (T-20) \mu\text{m/m} \pm 0.3 (\mu\text{m/m}) \text{ } ^\circ\text{C}^{-1}$$

## Bibliography

- [1] Lessons of mechanical system dynamics - Elvio Bonisoli.
- [2] Lessons of design of dynamic machines DDM - Nicola Amati.
- [3] Book: Vibration Mechanics and Control - Giancarlo Genta.
- [4] Book: Meccanica delle vibrazioni - Fasana & Marchesiello.
- [5] Book: Elementi Finiti - Antonio Gugliotta, Aurelio Somà, N. Zampieri.
- [6] Lecture Slides: Design of lightweight & composite structures - Davide S. Paolino.
- [7] Manual: RFDA HT 1600 - [www.imce.net](http://www.imce.net).
- [8] ASTM Standard 1876 - Standard Test Method for Dynamic Young's Modulus, Shear Modulus, and Poisson's Ratio by Impulse Excitation of Vibration.
- [9] Publication: Mechanical parameters identification for laminated composites based on the impulse excitation technique Wenlei Song, Yongteng Zhong, Jiawei Xiang.
- [10] Publication: Modal vibration response measurements for characterization of composite materials and structures Ronald F. Gibson.
- [11] Publication: An iterative method for identification of temperature and amplitude dependent material parameters of fiber-reinforced polymer composites Hui Lia, Tengfei Wua, Zhijiang Gaoa, Xintong Wanga, Hui Maa, Qingkai Hana, Zhaoye Qin.
- [12] Publication: Measurement of Thermal Expansion Coefficients of Composites Using Strain Gages by F. Lanza di Scalea.
- [13] Manual: LS DYNA Theory manual, Keywords user's manual Volume 1 and 2.
- [14] ASTM D570 Standard: Test Method for Water Absorption of Plastics.
- [15] Publication: Ageing of autoclaved epoxy/flax composites: Effects on water absorption, porosity and flexural behaviour Júlio César dos Santos, Lívia Ávila de Oliveira, Túlio Hallak Panzera, Chrystel D. L. Remillat, Ian Farrow, Vincent Placet.
- [16] Publication: Seawater ageing effect on the mechanical properties of composites with different fiber and matrix types E Jose-Trujillo, C Rubio-Gonzalez and JA Rodriguez-Gonzalez.